



**THE UNIVERSITY
OF ADELAIDE
AUSTRALIA**

**Department of Mechanical Engineering
THE UNIVERSITY OF ADELAIDE
Australia**

**Understanding the Influence of Alloy Additions on
Microstructure and Mechanical Properties of Weld Metal
from Gas-shielded Processes**

By

Vinay K. Tyagi
B.E.(Honours), M.E.(Honours)

A Thesis Submitted for the Degree of Doctor of Philosophy

May 2002

**This work is dedicated
to my Father
Sri Ram Kishor Tyagi.
For him education is the beginning of
better life.**

TABLE OF CONTENTS

ABSTRACT	viii
ACKNOWLEDGEMENTS	x
STATEMENT OF ORIGINALITY	xii
LIST OF FIGURES	xiii
LIST OF TABLES	xx
NOMENCLATURE	xxii
ACRONYMS	xxv
Chapter 1. Introduction	1
1.1 Background to the Project	1
1.2 Scope of the Project	2
1.3 Main Outcomes of the Literature Survey	5
Chapter 2. Literature Review	7
2.1 Introduction	7
2.2 The Gas-Shielded Arc Welding Weld Metal	8

Table of Contents

2.2.1 Solid Wire Gas Metal Arc Welding	11
2.2.2 Flux Cored Gas Metal Arc Welding	16
2.3 Development of Weld Metal Microstructure	17
2.3.1 Solid-State Transformations	23
2.4 Refining Weld Metal Structures	28
2.4.1 Alloying Additions in Weld Metal	28
2.4.1.1 Effect of Alloy Addition on Microstructure and Mechanical Properties	30
2.4.1.1.1 Effect of Carbon	32
2.4.1.1.2 Effect of Manganese	38
2.4.1.1.3 Effect of Silicon	40
2.4.1.1.4 Effect of Titanium	43
2.4.1.1.5 Effect of Aluminium	47
2.4.1.1.6 Effect of Boron	52
2.4.1.1.7 Effect of Nitrogen and Oxygen	55
2.5 Summary	62
Chapter 3. Experimental Procedure	64
3.1 Manufacture of Special Wires	64
3.2 Welding Procedure	72
3.3 Weld Composition	75

Table of Contents

3.4 Mechanical Testing	75
3.5 Metallography	76
3.6 Study of Inclusions	78

Chapter 4. Influence of Manganese and Silicon on Weld

Metal Properties	79
4.1 Introduction	79
4.2 Results	80
4.2.1 Weld Metal Compositions	80
4.2.2 Mechanical Properties	83
4.2.2.1 Tensile Properties	83
4.2.2.2 CVN Impact Results	84
4.2.3 Weld Metal Microstructure	87
4.2.4 Non-metallic Inclusions	94
4.3 Discussion	96
4.3.1 Weld Metal Tensile Properties	96
4.3.2 Weld Metal Impact Properties	96

Chapter 5. Influence of Titanium and Aluminium on Weld

Metal Properties	103
5.1 Introduction	103

Table of Contents

5.2 Results	105
5.2.1 Weld Metal Compositions	105
5.2.2 Mechanical Properties	108
5.2.2.1 Tensile Properties	108
5.2.2.2 CVN Impact Results	108
5.2.3 Weld Metal Microstructure	114
5.2.4 Non-metallic Inclusions	120
5.3 Discussion	122
5.3.1 Weld Metal Tensile Properties	122
5.3.2 Weld Metal Impact Properties	122
Chapter 6. Effect of Stress Relief on Low and High Titanium Containing Weld Metals	128
6.1 Introduction	128
6.2 Results	129
6.2.1 Heat-Treatment	129
6.2.2 Weld Metal Compositions	129
6.2.3 Mechanical Properties	131
6.2.3.1 Hardness Testing	131
6.2.3.2 CVN Impact Results	131
6.2.4 Weld Metal Microstructure	134

Table of Contents

6.3 Discussion	136
Chapter 7. Influence of Boron on Weld Metal Properties	138
7.1 Introduction	138
7.2 Results	140
7.2.1 Weld Metal Compositions	140
7.2.2 Mechanical Properties	142
7.2.2.1 Tensile Properties	142
7.2.2.2 CVN Impact Results	144
7.2.3 Weld Metal Microstructure	147
7.2.4 Non-metallic Inclusions	151
7.3 Discussion	154
7.3.1 Weld Metal Tensile Properties	154
7.3.2 Weld Metal Impact Properties	154
Chapter 8. Influence of Titanium and Boron on Weld Metal Properties	160
8.1 Introduction	160
8.2 Results	163
8.2.1 Weld Metal Compositions	163
8.2.2 Mechanical Properties	165
8.2.2.1 Tensile Properties	165

Table of Contents

8.2.2.2 CVN Impact Results	168
8.2.3 Weld Metal Microstructure	172
8.2.4 Non-metallic Inclusions	180
8.3 Discussion	183
8.3.1 Weld Metal Tensile Properties	183
8.3.2 Weld Metal Impact Properties	183
Chapter 9. Summary and Conclusions	189
9.1 Introduction	189
9.2 Influence of Manganese and Silicon on Weld Metal Properties	193
9.2.1 Conclusions	195
9.3 Influence of Titanium and Aluminium on Weld Metal Properties	195
9.3.1 Conclusions	197
9.4 Effect of Stress Relief on Low and High Titanium containing Weld Metals	197
9.4.1 Conclusions	198
9.5 Influence of Boron on Weld Metal Properties	198
9.5.1 Conclusions	200
9.6 Influence of Titanium and Boron on Weld Metal Properties	200
9.6.1 Conclusions	202
9.7 Combined Influence of Alloying Elements on Weld Metal Properties	203

Table of Contents

9.8 Recommendations for Future Work	209
References	210
Publications Originating from this Thesis Work	230
Appendix A	232
Compositions and Photomicrographs of Manganese and Silicon Series	
Appendix B	259
Compositions and Photomicrographs of Titanium Series	
Appendix C	283
Compositions and Photomicrographs of Aluminium Series	
Appendix D	301
Compositions and Photomicrographs of Boron Series	
Appendix E	316
Compositions and Photomicrographs of Titanium and Boron Series	
Appendix F	334
Example of Publications	

ABSTRACT

An investigation was undertaken to study the influence of alloying additions on weld metal from gas-shielded, metal-cored wires used for welding structural grade steel. Further it aimed to provide an understanding for these effects through detailed assessment of the as-deposited and reheated regions of weld microstructures and non-metallic inclusions.

Batches of specially formulated metal-cored wires were manufactured in which alloy additions were varied over predetermined ranges. The alloying elements investigated were manganese, silicon, titanium, aluminium and boron. From each of these wires, test plates were welded (multi-pass weld metal) under a consistent set of conditions so that weld metal tensile and low temperature impact properties could be assessed.

Results from welds in which manganese and silicon levels were varied showed that, while tensile strengths increased with alloy level, the best low temperature impact properties were observed when manganese was in the range 1.3 to 1.6wt% and silicon was in the range 0.3 to 0.6wt%. These impact properties are better than those obtained from other welding processes as Charpy-V-Notch values of 100J were achieved at temperatures lower than -40°C .

The titanium and aluminium additions had little influence on weld tensile properties but considerable influence on impact properties. Either no added titanium or levels in the weld of around 0.08wt% gave the best low temperature impact properties while aluminium additions were detrimental to impact properties over the whole range tested. Similarly to titanium,

Abstract

boron additions had a significant influence on impact properties with the best low temperature values occurring with no added boron and at levels of around 0.013wt%.

In addition to the studies on the influence of alloying, some limited work was done on the effect of stress relief heat treatment on impact properties. This was done for welds with titanium levels found to give the best impact properties and showed that heat treatment over the entire temperature range improved the impact values significantly for the optimum titanium levels.

It was found that a large volume fraction of acicular ferrite (up to 95%) could be obtained by maintaining the optimum boron and titanium contents. Addition of titanium or boron alone had very little influence on acicular ferrite formation in the weld deposits. A direct relationship between the acicular ferrite content and the low temperature impact properties of the weld deposits was established.

No single microstructural feature provided an explanation for the variation in weld metal mechanical (particularly impact) properties observed. Although a direct relationship exists in many cases with low temperature properties, it is important to understand their relationship with each other to optimise alloy composition. The proportion of fine-grained acicular ferrite in the as-deposited part of the welds did have a bearing on impact properties but was not the only or even the major factor. The number density of large non-metallic inclusions was also found to have a significant influence on impact properties and the interaction between these two factors provided some explanation for the observed behaviour. Several other microstructural factors e.g. primary ferrite, reheated weld metal region, strength levels and grain size, also appeared to influence the weld metal mechanical properties.

ACKNOWLEDGEMENTS

The work reported herein was undertaken as part of a Research Project of the Cooperative Research Centre (CRC) for Materials Welding and Joining. The Cooperative Research Centre for Materials Welding and Joining was established by and is supported under the Australian Government's Cooperative Research Centre Program. CSIRO MST, WIA and The University of Adelaide are core partners of this CRC and participated in the research project. This project was done in collaboration with the Colorado School of Mines, Colorado, USA. The author would like to thank these institutions for their participation in this work.

I would like to thank my supervisor Ian H. Brown (The University of Adelaide) for much help and support, and for all the efforts in reading this thesis. I would like to thank Ian E. French my CSIRO MST supervisor, for his supervision of all the experimental work done.

I would like to thank Glyn M. Evans for his guidance in formulating the research methodology for this research project.

Acknowledgements

The author would like to thank Glen Edwards, David LeRoy Olson and Stephen Liu of Colorado School of Mines, Colorado, USA, for their suggestion, analysis and guidance to conduct this work. I would like to thank them for their hospitality during my stay in Colorado.

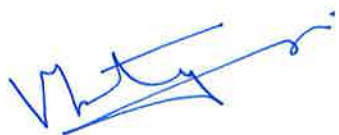
I must also thank people from CSIRO MST who have lent assistance. These include Peter Knott for making the experimental wires; Tom Gordon for welding test plates; Gellian Laughton for assistance with the literature search and Trevor Kenyon for photography.

I also appreciate the assistance of John Terlet and the staff of CEMMSA for their assistance in the SEM inclusion study.

Finally I would like to thank my father Sri Ram Kishor Tyagi and my mother Smt Champa Tyagi for their inspiration, love and support. I would also thank my wife Alka, my sons Asvin and Jay for their love and support.

STATEMENT OF ORIGINALITY

To the best of my knowledge and belief all of the material presented in this thesis, except where otherwise referenced, is my own original work and has not been presented previously for the award of any other degree or diploma in any University. If accepted for the award of the Degree of Doctor of Philosophy, I consent that this thesis be made available for loan and photocopying.



Vinay K Tyagi

List of Figures

Figure 1.1: The relationship between weld metal microstructure and mechanical properties.

Figure 2.1: Effect of the weld metal manganese-to-silicon ratio on the resulting oxygen concentrations [15].

Figure 2.2: Deoxidation equilibrium in liquid iron alloys at 1600 °C.

Figure 2.3: Schematics showing microstructure of solid-liquid interface for different modes of solidification and the temperature gradients that generate each of the different modes.

Figure 2.4: Plot of solute content versus solidification parameter to show the nature of solidification [34].

Figure 2.5: Schematic showing solute distribution at the dendrite or cell core and in the intercellular or interdendritic regions.

Figure 2.6: (a) Relationship between microstructure and cleavage resistance;
(b) Effect of alloy content on cleavage resistance as a function of heat input [88].

Figure 2.7: Variation of yield strength with the proportion of acicular ferrite for C-Mn-Nb weld metals [89].

List of Figures

Figure 2.8: Variation of fracture appearance transition temperature with the proportion of acicular ferrite for C-Mn-Nb weld metals [89].

Figure 2.9: The effect of carbon equivalent on toughness and hardenability.

Figure 2.10: The 35-J transition temperature in the coarse-grained zone as a function of the hardenability of the steels, expressed as P_{cm} .

(a) The relationship for a low heat input (1 kJ/mm FCAW).

(b) The relationship for 5 kJ/mm SAW [108].

Figure 2.11: Eutectoid composition and its temperature in steels as influenced by alloying elements [90].

Figure 2.12: Effect of manganese on Charpy V-notch toughness for multipass MMA C-Mn steel welds [7].

Figure 2.13: Relative effectiveness of alloying elements commonly used in steels to strengthen ferrite, the alpha phase (bcc) of iron [90].

Figure 2.14: Correlation between the oxygen content and the deoxidation parameter $([\%Si][\%Mn])^{-0.25}$.

Figure 2.15: Effect of titanium on the Charpy-V curve for multi-run basic flux MMA weld deposits [115].

Figure 2.16: Charpy-V curve for 100 J for multi-run basic flux MMA weld deposits:

(a) Ti-O series,

(b) Ti-N series [115].

Figure 2.17: Effect of niobium with 35 ppm titanium on the Charpy-V curve for multi-run basic flux MMA weld deposits [115].

List of Figures

Figure 2.18: Effect of aluminium on the Charpy-V curve for multi-run basic flux MMA weld deposits [115].

Figure 2.19: Effect of aluminium with 35 ppm titanium on the Charpy-V curve for multi-run basic flux MMA weld deposits [10].

Figure 2.20: Charpy transition curves for the metal-cored wire deposits, of various aluminium contents (7.5 by 10 mm Charpy specimens).

Figure 2.21: Effect of boron on the Charpy-V curve for multi-run basic flux MMA weld deposits [115].

Figure 2.22: Effect of boron with 35 ppm titanium on the Charpy-V curve for multi-run basic flux MMA weld deposits [115].

Figure 2.23: Influence of the basicity index on oxygen content.

Figure 2.24: Diagram of the derived weld microstructure as a function of the oxide-forming propensity $[O + (Si) / 4]$ and the hardenability (manganese) [142].

Figure 2.25: A plot of oxide-forming propensity vs. hardenability. Notice that either an increase in hardenability or a decrease in oxide-forming propensity will shift from an acceptable microstructure to one of aligned carbide [142].

Figure 2.26: Photomicrograph of various ferrite morphologies in weld metal.

Figure 3.1: Schematic diagram of the metal-core wire manufacturing process.

Figure 3.2: Pictures of CSIRO MST wire mill, for production of small batches of cored wires for welding.

Figure 3.3: Cross-section of a metal-core welding wire produced using CSIRO MST wire mill.

Figure 3.4: Section through a test plate showing the position of impact specimens.

List of Figures

Figure 3.5: Micrographs of grade 250 steel base material (etched in 2% nital).

Figure 3.6: International Institute of Welding scheme for the classification of microstructures in C-Mn weld metals [71].

Figure 4.1: Mean CVN impact energy as a function of temperature and manganese content at different silicon contents.

Figure 4.2: Variation of the proportions of ferrite morphologies as a function of manganese contents at different silicon levels.

Figure 4.3: Variation of the proportion of acicular ferrite (AF) with weld metal manganese content for all silicon levels.

Figure 4.4: Variation of the proportion of acicular ferrite (AF) with weld metal silicon content for all manganese levels.

Figure 4.5. Plot showing the T100J values as a function of weld metal manganese and silicon contents.

Figure 4.6: Number density of inclusions with diameter $> 1\mu\text{m}$ as a function of increase in manganese for all silicon levels in the weld metal.

Figure 5.1: Variations in yield, tensile strength and percent elongation as a function of (a) titanium and (b) aluminum content in weld metal.

Figure 5.2: Mean CVN impact energy as a function of temperature (a) and titanium levels in weld metal (b) and for aluminum levels in weld metal.

Figure 5.3: The upper CVN (J), lower CVN (J) and T100J ($^{\circ}\text{C}$) values as a function of (a) titanium and (b) aluminum contents.

Figure 5.4: Variation in the proportion ferrite morphologies as a function (a) titanium levels (b) aluminum levels.

List of Figures

- Figure 5.5:** Photomicrograph of as-deposited weld metal with (a) 0.0054wt% titanium (b) 0.0852wt% titanium in weld metal.
- Figure 5.6:** Photomicrograph of as-deposited weld metal with (a) 0.0133wt% aluminum (b) 0.0570wt% aluminum in weld metal.
- Figure 5.7:** Variation of number/mm³, mean 3D diameter and percent > 1µm diameter of non-metallic inclusions with increase in (a) titanium level (b) aluminium level.
- Figure 5.8:** Effect of proportion of AF on mean CVN impact energy corresponding to T100J, for titanium and aluminum series of weld metals.
- Figure 5.9:** Number density of inclusions with diameter > 1µm as a function of increase in (a) titanium and (b) aluminum in the weld metal.
- Figure 6.1:** Mean CVN impact energy as a function of temperature for low titanium (0.0065wt%) levels in weld metal.
- Figure 6.2:** Mean CVN impact energy as a function of temperature for high titanium (0.0656wt%) levels in weld metal.
- Figure 6.3:** Microphotograph of the top pass of 0.044wt% carbon and 1.4wt% manganese deposits in the, (a) as-welded and (b) stress-relieved conditions.
- Figure 6.4:** Microphotograph of coarse-grained regions of 0.044wt% carbon and 1.4wt% manganese deposits in the, (a) as-welded and (b) stress-relieved conditions.
- Figure 7.1:** Variations in yield, tensile strength and percent elongation as a function of boron content in the weld metal.
- Figure 7.2:** Mean CVN impact energy as a function of temperature for various boron levels in the weld metal.

List of Figures

- Figure 7.3:** The upper CVN (J), lower CVN (J) and T100J(°C) values as a function of boron content.
- Figure 7.4:** Variation in the proportions of ferrite morphologies in as-deposited weld metal as a function of boron content.
- Figure 7.5:** Photomicrograph of as-deposited weld metal with (a) 0.0005wt% boron and (b) 0.0176wt% boron content.
- Figure 7.6:** Variation of non-metallic inclusions number/mm³, mean 3D diameter and percent > 1µm diameter with boron content.
- Figure 7.7:** Number density of inclusions with diameter > 1µm as a function of boron contents in the weld metal.
- Figure 8.1:** Variation in yield, tensile strength and percent elongation as a function of titanium for (a) 0.0005wt% boron (b) 0.0100wt% boron in the weld metal.
- Figure 8.2:** Mean CVN impact energy as a function of temperature at different titanium and boron levels in the weld metal
- Figure 8.3:** The upper CVN (J), lower CVN (J) and T100J (°C) values as a function of titanium contents for (a) 0.0005wt% boron and (b) 0.0100wt% boron in the weld metal.
- Figure 8.4:** Variation in the proportions of ferrite morphologies in as-deposited weld metal as a function of titanium contents at two boron levels.
- Figure 8.5:** Photomicrographs of as-deposited and re-heated weld metal for various titanium and boron levels.
- Figure 8.6:** Variation of non-metallic inclusions number/mm³, mean 3D diameter and percent >1µm diameter with titanium level at two boron levels.

List of Figures

Figure 8.7: Summary plot of the variation in weld metal T100J ($^{\circ}\text{C}$) temperature values as a function of proportions of acicular ferrite.

Figure 8.8: Summary plot of the variation in weld metal T100J ($^{\circ}\text{C}$) temperature values as a function of grain size of reheated zone (μm).

Figure 9.1: Photomicrographs of as-deposited weld metal with (a) 0.0570wt% aluminum, (b) 0.0176wt% boron, (c) 0.0112wt% boron and 0.0228wt% titanium in weld metal.

Figure 9.2: Summary plot of the variation in acicular ferrite as a function of weld metal T100J temperature values ($^{\circ}\text{C}$).

Figure 9.3: Summary plot of the variation in ferrite with second phase as a function of weld metal T100J temperature values ($^{\circ}\text{C}$).

Figure 9.4: Summary plot of the variation in primary ferrite phase as a function of weld metal T100J temperature values ($^{\circ}\text{C}$).

Figure 9.5: Summary plot of the variation in acicular ferrite lath size (μm) as a function of weld metal T100J temperature values ($^{\circ}\text{C}$).

Figure 9.6: Summary plot of the variation in prior austenite grain size (μm) as a function of weld metal T100J temperature values ($^{\circ}\text{C}$).

Figure 9.7: Summary plot of the variation in grain size of reheated zone (μm) as a function of weld metal T100J temperature values ($^{\circ}\text{C}$).

Figure 9.8: Summary plot of the variation of percent inclusions with diameter $>1\mu\text{m}$ as a function of weld metal T100J temperature values ($^{\circ}\text{C}$).

List of Tables

Table 2.1 Elements used for alloying irons and steels, and their influence on the crystalline structure of the alloy.

Table 4.1. Weld metal compositions (wt %).

Table 4.2. Weld metal tensile properties.

Table 4.3: Acicular ferrite lath width and reheated grain sizes.

Table 4.4: Non-metallic inclusions.

Table 5.1: Weld metal compositions (wt %) with varying titanium levels.

Table 5.2: Weld metal compositions (wt %) with varying aluminum levels.

Table 5.3: Acicular ferrite lath width and reheated grain sizes for titanium series.

Table 5.4: Acicular ferrite lath width and reheated grain sizes for aluminum series.

Table 6.1: Weld metal compositions (wt %) for stress relieved titanium weld metal.

Table 6.2: Average Vickers hardness for stress relieved titanium welds.

Table 7.1: Weld metal compositions (wt %) with varying boron levels.

Table 7.2: Columnar austenite grain width, acicular ferrite lath width and reheated grain sizes for boron series.

Table 7.3. Non-metallic inclusions with varying boron levels.

List of Tables

Table 8.1: Weld metal compositions (wt %) with varying titanium and boron levels.

Table 8.2: Weld metal tensile properties with varying titanium and boron levels.

Table 8.3: Acicular ferrite lath width and reheated grain sizes for titanium and boron series.

Table 8.4: Non-metallic inclusions with varying titanium and boron levels.

Table 9.1: Optimised weld metal composition (wt%) with best low temperature properties.

Table 9.2: Weld metal properties with optimised composition (wt%) with best low temperature properties.

Nomenclature

Nomenclature

α	Ferrite
δ	Delta Ferrite
γ	Austenite
τ	Metal Transfer Coefficient
Ae_1	Eutectoid Temperature
AC	Aligned Carbide
AF	Acicular Ferrite
Al	Aluminium
Ar	Argon
B	Boron
C	Carbon
C_0	Nominal Solute Content
CO_2	Carbon dioxide
C.E.	Carbon Equivalent
3D	Three Dimensional
f	Fill Ratio

Nomenclature

FC	Ferrite Carbide Aggregate
Fe	Iron
FS	Ferrite with Second Phase
FS(A)	Ferrite with Aligned Second Phase
FS(NA)	Ferrite with Non-Aligned Second Phase
G	Thermal Gradient in the Liquid
HAZ	Heat Affected Zone
I	Current (Amps)
kJ	Kilo Joule
MAC	Martensite, Austenite, Carbide Microphase
Mn	Manganese
Mo	Molybdenum
N	Nitrogen
Nb	Niobium
O	Oxygen
ppm	Parts Per Million
PF	Primary Ferrite
PF(G)	Grain Boundary Ferrite
PF(I)	Polygonal (intragranular) Ferrite
r^2	Coefficient of Determination
R	Growth rate of the solid at a given point on the moving solid-liquid interface
Si	Silicon

Nomenclature

T	Temperature
T _{100J}	Temperature at 100J Charpy V-Notch Strength
Ti	Titanium
UTS	Ultimate Tensile Strength (MPa)
V	Volts
X _L	Distance from Solid Liquid Interface
X	wt% of Alloy X
X _{CORE}	wt% of Alloy X in Core
X _{WELD METAL}	wt% of Alloy X in Weld Metal
X _{WIRE}	wt% of Alloy X in Wire
X _{STRIP}	wt% of Alloy X in Strip
YS	Yield Strength (MPa)

Acronyms

Acronyms

AIA	Automatic Image Analysis
AC	Alternating Current
AS	Australian Standard
ASM International	The Materials Information Society
ASME	American Society of Mechanical Engineers
ASTM	American Society for Testing and Materials
AWS	American Welding Society
BCC	Body Centred Cubic (structure)
CRC-MWJ	Cooperative Research Centre for Materials Welding and Joining
C-Mn	Carbon-Manganese (steel)
CMST	CSIRO Manufacturing Science and Technology
CSIRO	Commonwealth Scientific and Industrial Research Organisation
CVN	Charpy V-Notch
DC	Direct Current
DCEN	Direct Current Electrode Negative

Acronyms

DCEP	Direct Current Electrode Positive
FCAW	Flux-Cored Arc Welding
FCC	Face Centred Cubic (structure)
FESEM	Field Emission Scanning Electron Microscope
GMAW	Gas-Metal Arc Welding
ICP-AES	Inductively Coupled Plasma Atomic Emission Spectrometry
IIW	International Institute of Welding
MAG	Metal Active Gas Welding
MMAW	Manual Metal Arc Welding
MIG	Metal Inert Gas Welding
SAW	Submerged Arc Welding
SEM	Scanning Electron Microscope
TEM	Transmission Electron Microscope
TWI	The Welding Institute
WDX	Wavelength Dispersive X-Ray Spectrometry
WIA	Welding Industries of Australia
WRC	Welding Research Council
WTIA	Welding Technology Institute of Australia

Chapter 1. Introduction

1.1 Background to the Project

A previous investigation sponsored by the Corporate Research Centre for Materials Welding and Joining (CRC for MW&J) (The Control of Weld Metal Microstructure from Gas-Shielded Arc Welding Processes in Structural Steels)[1], showed the existence of a relationship between the welding conditions - microstructure - mechanical properties for weld metal from gas-shielded wires. In that project commercially available solid and flux-cored wires were used and a great deal of practical information of benefit to users of these processes was produced [2-6].

While results of this work suggested that the levels of alloying additions were important in determining weld microstructure and hence mechanical properties, the use of commercial wires did not allow a detailed and systematic study of these effects. The extensive work of Evans on manual metal arc welding [7-11] has demonstrated that major differences in microstructure and mechanical properties (low temperature impact toughness) can be

Introduction

achieved by controlled, often low level, additions of some elements (like aluminium, titanium and boron). Comparable studies are not currently available for gas-shielded wires. However this can now be done since the Commonwealth Scientific and Industrial Research Organization - Manufacturing Science and Technology (CMST) has a facility for manufacturing small batches of well characterised experimental cored wires which are essential for such a study.

1.2 Scope of the Project

The gas-shielded continuous wire processes already accounts for the majority of structural steel welding in industry and this process sector is increasing in market share. With the growing importance of the gas-shielded processes an improved understanding of the effect of alloying addition has a high probability of leading to significant advances in weld quality and productivity via improvements in consumables.

As shown in figure 1.1, detailed knowledge of the influence of alloying and microalloying elements on the weld microstructure and mechanical properties from these processes is essential for designing optimum microalloyed consumables, resulting in best low temperature impact properties.

This current study considers the controlled additions of alloying, and/or deoxidising, elements in experimental metal-cored welding consumables for gas-shielded welding.

Introduction

The major components of the project are:

- The manufacture of a series of cored wire consumables from high purity materials;
- The welding trials using a shielding gas with argon + 5% CO₂;
- The detailed assessment of the weld metal microstructure development including:
 - The as-deposited and reheated structure.
 - The details of non-metallic inclusions.
 - The relationships between microstructure and inclusions.
- The assessment of the weld mechanical properties.

Influence of Alloying Additions on Weld Metal Structure-Property Relationships from Gas-Shielded, Continuous Wire Welding

(Using Specially Prepared Metal-Cored Arc Welding Wires and Multi-pass welds in Structural Steel)

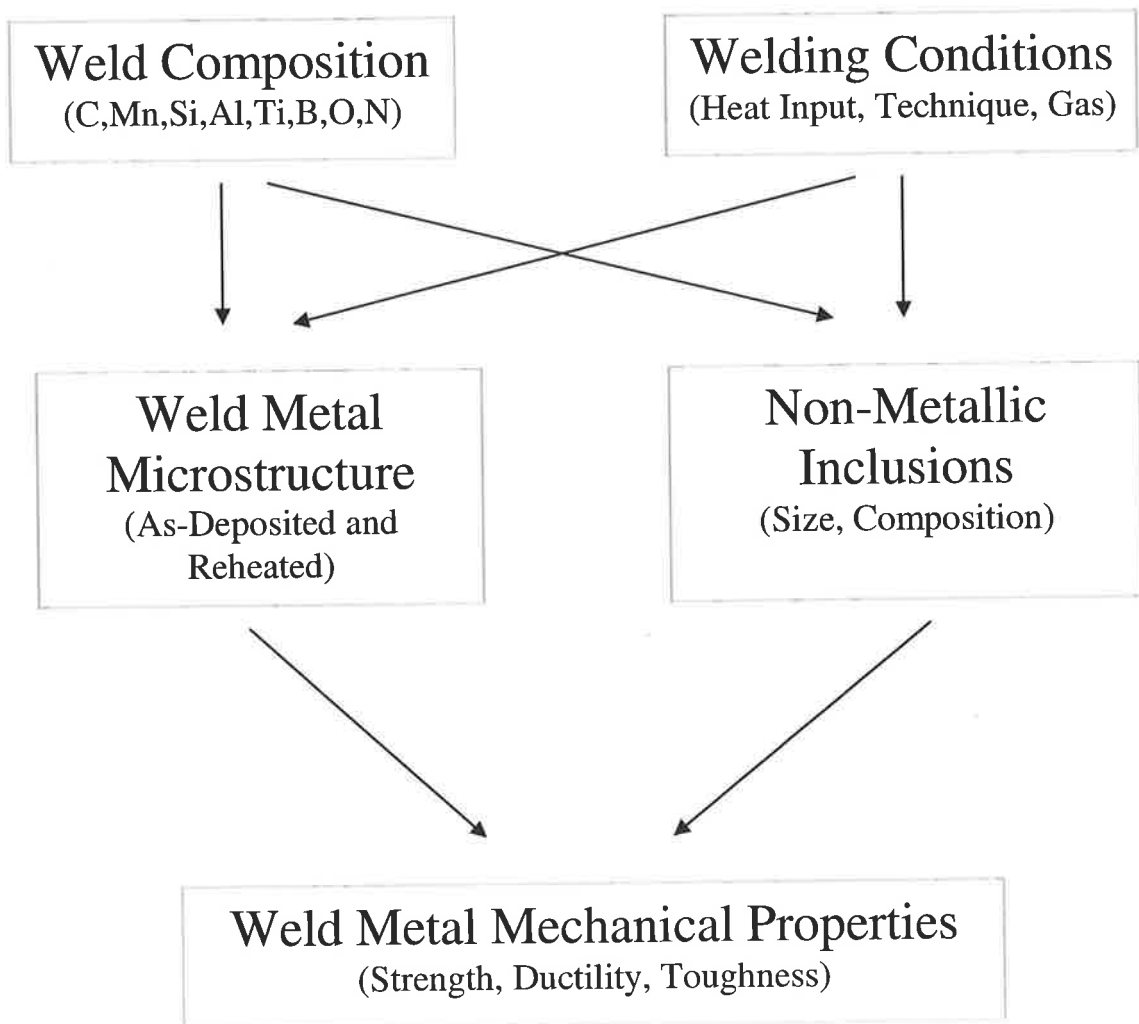


Figure 1.1: The relationship between weld metal microstructure and mechanical properties.

1.3 Main Outcomes of the Literature Survey

Published work relating to the influence of alloy additions on microstructural and mechanical properties of weld metal from gas-shielded processes was reviewed. This revealed that detailed knowledge of the influence of alloying and microalloying elements on the weld microstructure and mechanical properties from the gas shielded processes lags well behind that available for other welding processes such as manual metal arc welding and submerged arc welding.

The addition of alloying elements to iron to accomplish a desired improvement in properties may require only a few tenths of one percent of the element. Sometimes improved properties are gained by stringent control and/or reduction of an element that may have been tolerated as a residual element in welding processes. This is a relatively new approach in alloying technology which can be credited with improving the quality of welding consumables.

The austenite to α -ferrite transformation is mainly affected by non-metallic inclusions, alloy additions, cooling rate and prior austenite grain size. Acicular ferrite usually nucleates on inclusions present in the columnar austenite grains, which stimulates the sympathetic nucleation of other acicular ferrite plates. Particles of titanium oxide and titanium nitride are most likely to nucleate acicular ferrite.

Introduction

However, it is apparent that significant gaps exist in the detailed knowledge of the influence of alloying and microalloying elements on weld metal microstructure and mechanical properties for GMAW processes, and the purpose of the current study is to address this lack of information.

Chapter 2. Literature Review

2.1 Introduction

Gas-shielded continuous wire processes already account for the majority of structural steel welding in industry and are still increasing market-share [12]. These processes are often used in applications where weld metal mechanical properties are critical. For C-Mn steels, gas-metal-arc welding (GMAW) using solid wires accounts for more than 50% of the amount of weld metal deposited in Europe. In addition use of cored wire (either metal-cored or flux-cored) is also increasing rapidly in Europe. In the U.S. and Japan, the use of cored wires is more common and accounts for about 15% of all welding consumables sold in these countries.

The outer metal tube of a cored consumable is usually made from a low carbon steel strip and alloying is facilitated through the use of powder mixtures in the core. For a metal-cored wire the filling in the core is iron powder, with alloying elements and the addition of deoxidants. Flux-cored wires have a core of minerals similar to those used for the coating of covered electrodes. This provides a convenient way of changing the composition of GMAW consumables. The practical importance of the gas-shielded processes suggests that

Literature Review

an improved understanding of these aspects (core materials) has a high probability of leading to significant advances in weld quality and productivity via improvements in consumables.

The main objective of this chapter is to present a critical literature survey of the influence of alloy additions on microstructural and mechanical properties of weld metal from gas-shielded processes.

2.2 The Gas-Shielded Arc Welding Weld Metal

In GMAW, an externally supplied gas or gas mixture acts to shield the arc that is established between a consumable electrode (wire) and the molten weld pool.

Although the basic GMAW concept was introduced in the 1920s, it was not commercially available until 1948. At first, it was considered to be fundamentally a high-current-density, small-diameter, bare-metal electrode process using an inert gas for arc shielding. Its primary application was aluminium welding. As a result, it became known as metal-inert gas (MIG) welding, which is still a common nomenclature [13].

Subsequent process developments included operation at low current densities and with pulsed current, use of reactive gases (particularly carbon dioxide) leading to its application to a broader range of materials, and gas mixtures. The latter development, in which both inert and reactive gases are used, led to the formal acceptance of the term GMAW [13].

The GMAW process can be operated in semi-automatic and automatic modes. All commercially important metals, such as carbon steel, high-strength low-alloy steel,

Literature Review

stainless steel and aluminium, copper, and nickel alloys can be welded in all positions by this process if appropriate shielding gases, electrodes, and welding parameters are chosen.

The application of the process is dictated by its advantages, the most important advantages are [13]:

- Continuous wire consumables do not have the restrictions of electrode length encountered with manual metal arc welding (MMAW).
- Welding can be done in all positions, a feature not found in submerged arc welding.
- Welding speeds are higher than those of the MMAW process.
- Deposition rates are significantly higher than those obtained by the MMAW process.
- Deeper penetration than for the MMAW process is possible, which in some circumstances permits the use of smaller-sized fillet welds for equivalent strengths.
- Less operator skill is required than for other conventional processes, because the arc length is maintained constant with reasonable variations in the distance between the contact tip and the workpiece.
- Minimal postweld cleaning is required because of the absence of a heavy slag.

These advantages make the process particularly well suited to high-production and automated welding application. With the advent of robotics, GMAW has become the predominant process choice.

The chemical composition of the wire must be selected to achieve the desired properties in the weld metal. The composition can be designed with extra deoxidisers or other scavenging agents to compensate for reactions with the atmosphere and the base metal. The

Literature Review

deoxidisers most commonly used in steel electrodes are silicon and manganese. Silicon has the additional effect of increasing weld metal fluidity.

The physical characteristics (finish, straightness, etc) of wires used in the GMAW process are important to successful welding. The specifications for these wires establish manufacturing requirements to ensure that users receive a uniform product that feeds smoothly through the equipment [13] and has the following characteristics:

- Uniform winding on the spool or coil with no kinks or bends
- Smooth surface finish free of slivers, scratches, or scale
- Prescribed cast and helix
- Uniform diameter

Cast and helix refer to dimensions of a single coil of wire removed from a spool or coil and layed (that is, cast) on a flat surface. If this coil is too small in diameter (cast) or shows an excessive lift from the flat surface (helix), feeding problems during welding can be anticipated [13]. Prescribed cast and helix can be obtained by both, wire straightening and by work hardening of the wire during manufacturing by using thicker sheath material.

2.2.1 Solid Wire Gas Metal Arc Welding

The primary function of the shielding gas in most welding processes is to protect the molten metal from contact with the surrounding atmosphere. In the GMAW process, this gas plays an additional role in that it has a pronounced effect on arc characteristics, mode of metal transfer, depth of fusion, weld bead profile, welding speed, and cleaning action.

Inert gases, such as argon and helium, are commonly used, as is the active gas, CO_2 . It is also common to use mixtures of these gases with small additions of oxygen [13]. The oxygen addition improves the arc stability and bead morphology, but increases the oxygen content in the weld metal and increases the losses of alloying elements [14].

Extensive investigations of the silicon / manganese deoxidation of steel weld metal in gas metal arc welds, have clarified the mechanism controlling the separation of the precipitated oxides from the weld pool. The final weld metal oxygen content is directly related to both the total amount of silicon and manganese present and the resulting manganese to silicon ratio. A decrease was observed in the weld metal oxygen content with increasing manganese to silicon ratio until this reached a value of approximately 3.5. This is solely attributed to a reduction in the silica activity of the deoxidation product (figure 2.1) [15]. The levelling off of the oxygen content is due to separation of precipitated oxides from the weld pool. Figure 2.1 can be interpreted on the basis of the pseudo equilibrium concept [15], which postulates that the final weld metal contents of silicon, manganese and oxygen are controlled by local equilibria established between the reactants and precipitated slag at elevated temperatures in the weld pool.

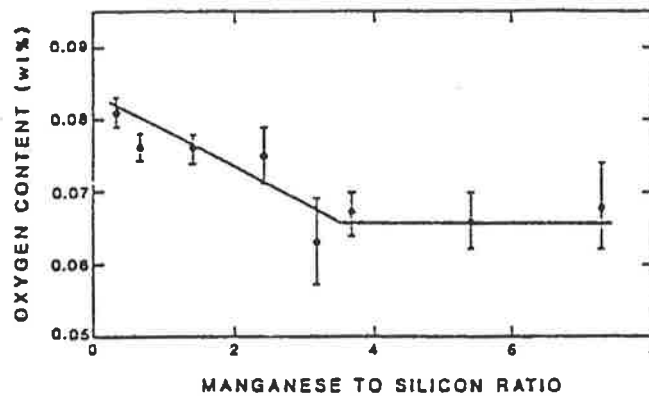


Figure 2.1: Effect of the weld metal manganese-to-silicon ratio on the resulting oxygen concentrations [15].

The weld metal oxygen level can range from 100 to 1000ppm, depending on the type of welding consumable used. At the melting point, the solubility of oxygen in pure liquid iron is approximately 1600ppm at 100kPa (1atm) pressure. During solidification, solubility decreases initially to about 860ppm at 1500⁰C in δ -iron and then further decreases with δ -iron \rightarrow γ (austenitic) \rightarrow α (ferrite) iron transformation. Most of the alloying elements present in liquid steel reduce oxygen solubility through deoxidation equilibrium [16].

Deoxidation of the weld metal occurs in two separate steps, the first being the primary deoxidation of the weld pool [17]. Secondary deoxidation occurs during solidification as solute concentrations increase within the intercellular or interdendritic regions. The secondary deoxidation will either form very small inclusions or will form a surface layer on the interdendritically trapped primary inclusions.

Figure 2.2 [18] shows experimentally measured soluble oxygen concentrations for various deoxidants (solid lines), along with deoxidation curves predicted by the solubility products

Literature Review

(broken lines). The experimental deviation is caused by interactions of the deoxidant with other alloy elements. If the oxygen and metallic element concentrations resulting from the welding process exceed the equilibrium concentration for a specific reaction, inclusions will result. The ability to form a specific inclusion will correspond directly to the position of the weld pool composition relative to the activity plot for this inclusion. Thus, the thermodynamic order for the formation of primary oxides would be $\text{Al}_2\text{O}_3 > \text{Ti}_2\text{O}_3 > \text{SiO}_2 > \text{Cr}_2\text{O}_4 > \text{MnO}$ [16].

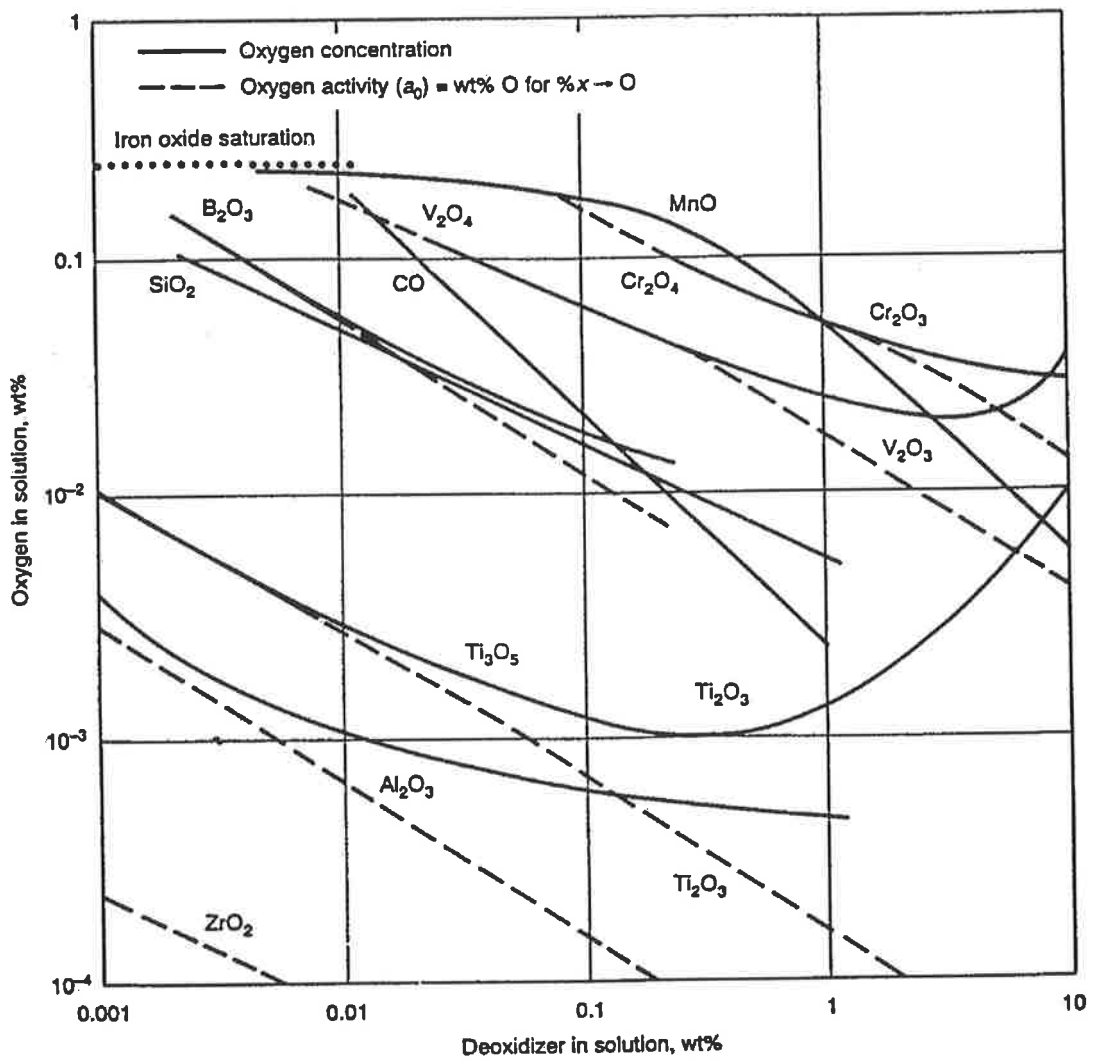


Figure 2.2: Deoxidation equilibrium in liquid iron alloys at 1600 °C [18].

The broken lines in figure 2.2 show the deoxidation equilibria predicted by solubility product calculations. The solid lines show experimentally determined soluble oxygen concentrations for various deoxidants. The experimental deviation is caused by variations in the activity coefficients with increasing deoxidant concentration [18].

The influence of oxygen on notch toughness of weld metal deposits is well known [19,20]. Watanabe et al, working with silicon-manganese-molybdenum, titanium and titanium-

Literature Review

boron weld metals deposited by GMAW with various shielding gases, observed that 200-300 ppm oxygen was associated with the lowest transition temperature in the weld metal.

The chemical reactions of the GMAW process have been studied by means of a 'melt spinning' technique in order to suppress effectively the weld pool reactions [21]. Analysis of chilled metal, of regular multi-run deposits and of collected electrode tip droplets were compared for assessment of gas/metal interactions taking place at the electrode tip, in the arc plasma and in the weld pool. Welding was performed in Ar-O₂ and Ar-CO₂ mixtures. The results indicate that the oxidation of carbon occurs at the electrode tip and to a very small extent, if at all, in the arc plasma. The most probable site for CO nucleation during droplet formation will be at the large metal/atmosphere interface. It is probable that most of the observed carbon oxidation occurs at the droplet surface, where the reaction is thermodynamically favoured [21]. At positions other than the surface the lower metal temperature which is only slightly above the melting point of the consumable at the time of detachment, together with silicon and manganese, protect the carbon from reacting [22].

Carbon oxidation gradually levels off with increasing oxygen potential of the shielding gas, which may be a result of build up of CO in the surrounding atmosphere. When the critical CO gas pressure is reached the carbon reaction is blocked, which leads to the control of the oxygen level by manganese and silicon. This critical CO gas pressure is reached much earlier in the welding cycle when welding with shielding gases Ar-O₂ than with Ar-CO₂ [21,23].

2.2.2 Flux Cored Gas Metal Arc Welding

Cored wires are filled with metal or flux powder. The filling in the core can either be iron powder with the addition of alloying elements and some deoxidants, giving a metal-cored wire, or it can contain minerals similar to those used for the coating of covered electrodes, giving a flux-cored wire. The metal tube is usually made from a low carbon steel strip. Changing filling in the core is a convenient way to change the composition of GMAW weld metal. The alternative would be to change the composition of the solid wire, which is likely to be much more expensive, and also rolling of alloyed wire is operationally more difficult. Cored wires also have an advantage over solid wires when it comes to productivity, penetration, and weld metal quality. Spatter may also be reduced when flux-cored wires are used, but this is normally a function of the shielding gas and the metal transfer mode.

Information on the effect of the slag system, shielding gas and heat input on the FCAW weld metal is very limited [24-26]. Higher amounts of aluminium found in some FCAW welds influences the $\gamma \rightarrow \alpha$ transformation kinetics which determine the final weld metal microstructure. Flux-cored arc welds are thus expected to exhibit microstructures dissimilar to submerged arc welds (SAW) or shielded metal arc welds (SMAW) [27]. This was confirmed by Huseen, et al. [28] who compared the microstructures of SMA and FCA ferritic welds. Furthermore, Mejias, et al. [29], studied the microstructure and mechanical properties of FCA welds produced with various electrode compositions and heat inputs and suggested better parameters to achieve high toughness properties. Varying the basicity of

Literature Review

the slag system in FCAW metal effects the oxygen content of the weld metal. A basic slag results in a lower oxygen level in the weld metal, as does the use of an Ar-CO₂ mixture, as it has a lower potential to oxidise weld metal than CO₂.

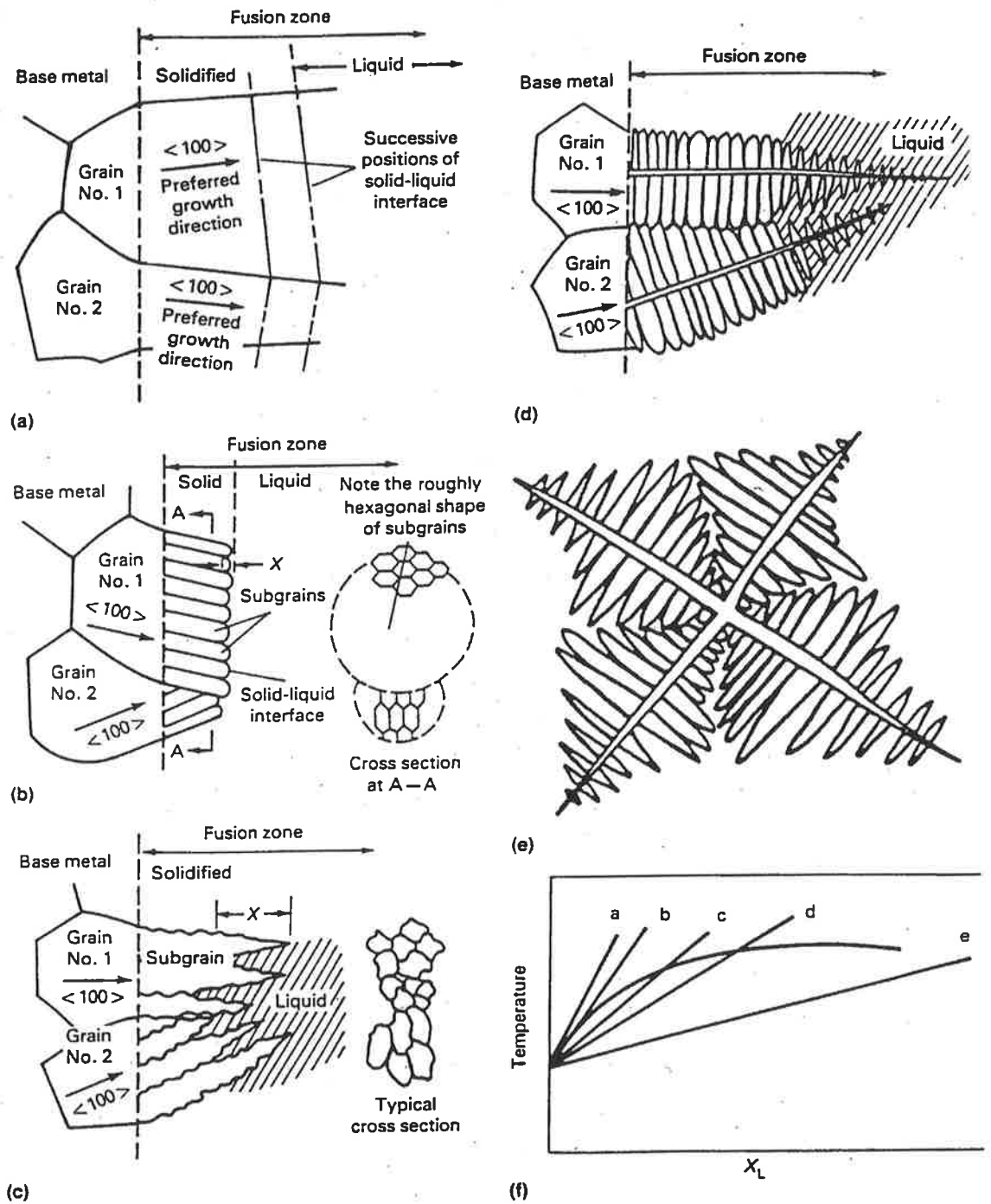
2.3 Development of Weld Metal Microstructures

In an alloy, constitutional supercooling allows non-planar solidification in a weld. The lower the temperature gradient, the greater the degree of constitutional supercooling. The effect of the degree of supercooling on the solid morphology is shown in figure 2.3 (a-e). Figure 2.3f indicates the degree of supercooling for various temperature gradients [30-35].

In general the cell size decreases as the cooling rate increases [36], and the cell and secondary dendrite arm spacings depend directly on the local solidification time [37-41]. Lanzafame et al [42] verified this effect of heat input on the dendrite arm spacing. Also, Brown et al [43] and Jarman et al [44] investigated the relationship between secondary dendrite arm spacing and heat input on aluminium-copper alloys. They predicted theoretically that the dendrite arm spacing in partial penetration welds deposited under conditions of three dimensional heat flow on relatively thick plate would be related directly to the square root of the heat input per unit length of weld.

Literature Review

Figure 2.4, which is based on experimental observations, relates the gradient $G/R^{1/2}$, (where G is temperature gradient in the liquid adjacent to the solid, and R is the rate of growth of solid), solidification rate, and composition to the type of structure developed [33-35]. The center of each cell or dendrite behaves like the initial transient, that is, the solute content is low. The regions between the cells or dendrites behave like the final transients, that is, they are enriched in solute. This is illustrated schematically in figure 2.5 [45].



Distance from solid liquid interface.

Figure 2.3: Schematic diagram showing microstructure of solid-liquid interface for different modes of solidification and the temperature gradients that generate each of the different modes. (a) Planar growth. (b) Cellular growth. (c) Cellular dendritic growth. (d) Columnar dendritic growth. (e) Equiaxed dendrite. (f) Five temperature gradients versus constitutional supercooling [34].

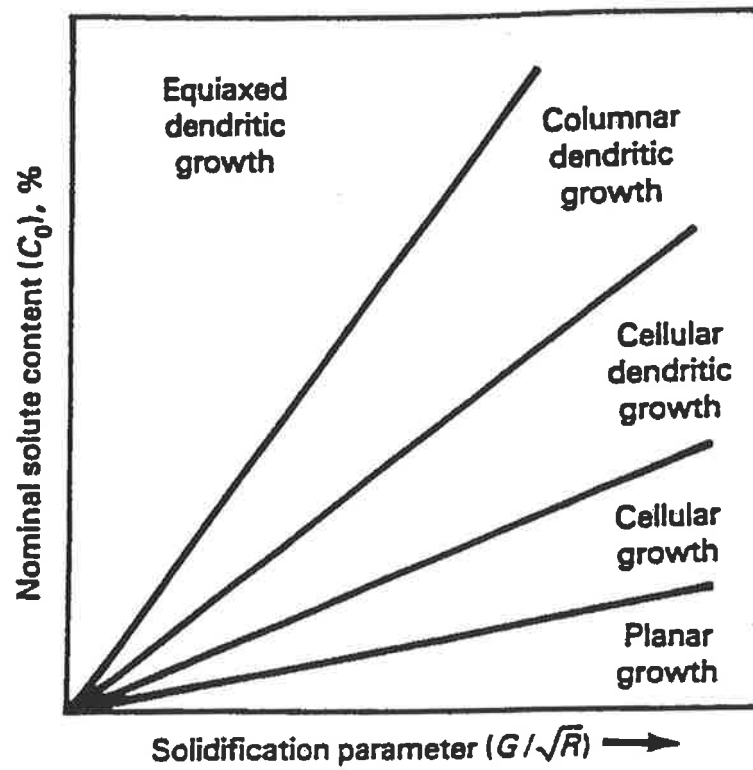


Figure 2.4: Plot of solute content versus solidification parameter to show the nature of solidification [34].

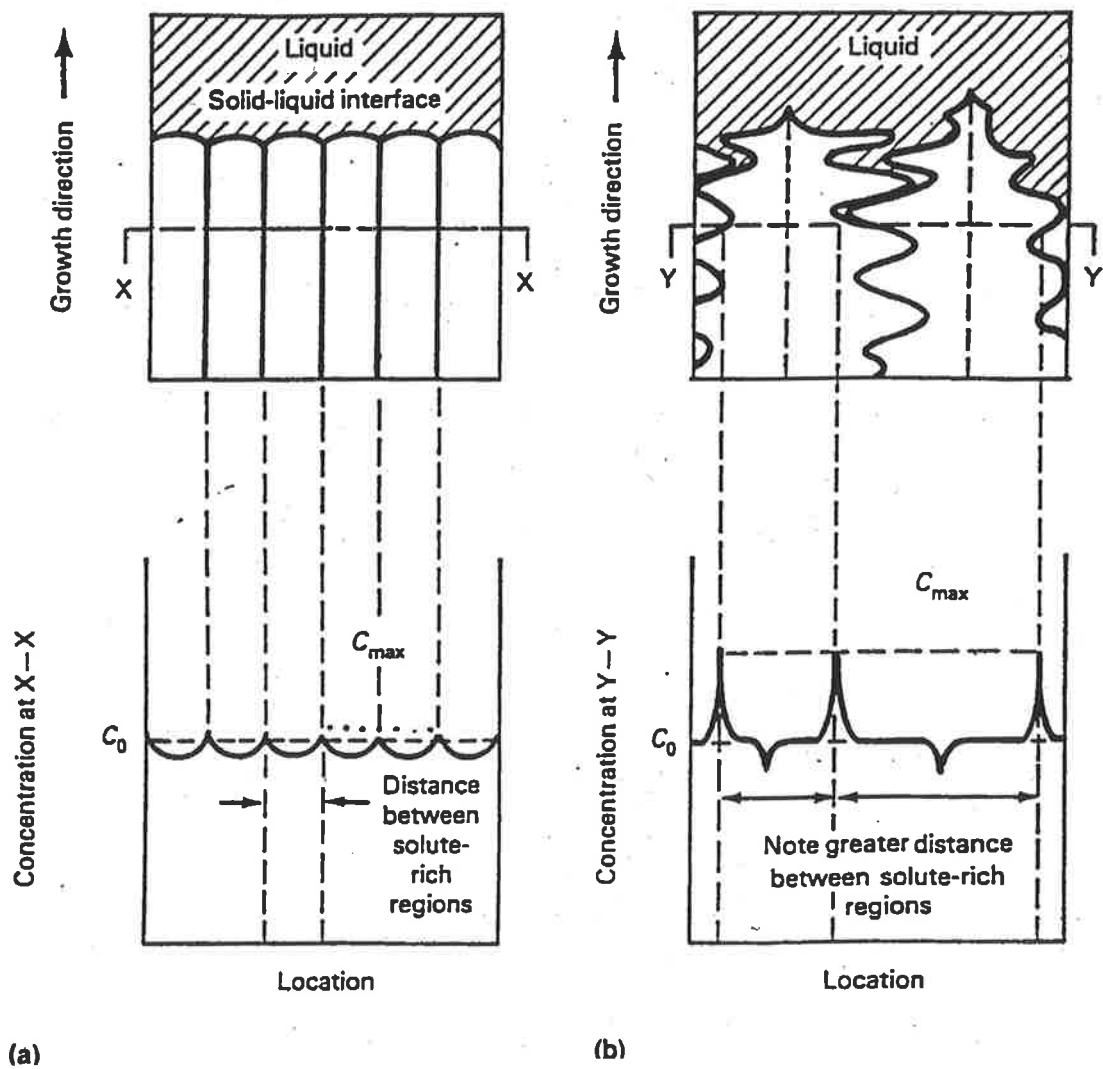


Figure 2.5: Schematic showing solute distribution at the dendrite or cell core and in the intercellular or interdendritic regions. (a) Cellular growth. (b) Dendritic growth [45].

Literature Review

Weld-pool microsegregation may lead to both a variation in mechanical properties and to solidification cracking [46]. Miller [47] has established the presence of a solute rich layer ahead of the advancing solid-liquid interface in the weld-pool and shown that the equilibrium distribution coefficient is the same for weld-pool and ingot solidification. Bell [48] found that segregation will be greater at grain boundaries than within the substructure composing the grain. The enhanced level of solute and impurity segregation at the centerline of a bead can significantly lower the toughness of a weld deposit. The causes of this low level of toughness at the weld centre line may include embrittlement due to grain boundary precipitation or non-metallic inclusions [48,49]. Also, elongated veins of pro-eutectoid ferrite are known to reduce the toughness of weldments compared to more equiaxed structures [50-60].

Generally a planar solidification structure is difficult to maintain. As the boundary layer becomes further established, the thermal gradient decreases and the solidification rate increases [61]. Due to the fact that nuclei survival is very limited [62] in the weld-pool, equiaxed weld-pool solidification tends to occur unaided only in the region of the centre line of the pool, where solidification rates are highest and the thermal gradients are lowest due to the distance from the arc. This structure is generally associated with high welding speeds [63,64] and high alloy contents [47,64]. The predominant solidification structure in many welds is a transition structure between cellular and cellular-dendritic [65,66], as the interface becomes more unstable with increasing constitutional supercooling and secondary arms grow from the primary arms [67-69]. It was found that the higher the alloy content of the weld-pool, or the lower the thermal gradient, the greater the tendency for cellular dendritic or free dendritic growth modes to form. Columnar dendrites have been reported

Literature Review

in Ti-6Mn welds [65]. A range of substructures in melt runs in a given material can be generated by varying the welding conditions [70].

2.3.1 Solid-State Transformations

During austenite decomposition a large variety of microstructures can develop, depending on cooling rates and weld metal chemical composition. With approximately decreasing order of transformation temperature these microstructures can be [71]:

- PF - primary ferrite
- PF(G) - grain boundary ferrite
- PF(I) - polygonal (intragranular) ferrite
- FS(A) - ferrite with aligned second phase
- FS(NA) - ferrite with non-aligned second phase
- AF - acicular ferrite
- FC - ferrite-carbide aggregate.

The microstructure of low-alloy steel weld metals consists of a mixture of grain boundary ferrite (PF(G)), ferrite side-plates (FS), acicular ferrite (AF) and small quantities of “microphases” [72]. It is generally accepted that the presence of substantial quantities of grain boundary ferrite can lead to poor toughness in low-alloy steel weld deposits [73-76]. The relatively large grains of ferrite offer little resistance to cleavage crack propagation.

Secondary ferrite side-plates [77] nucleate at the ferrite-austenite grain boundaries and grow as sets of parallel plates separated by thin regions of austenite. The latter

Literature Review

subsequently being retained to ambient temperature or (perhaps partially) transforming to martensite and/or pearlite. These small quantities of retained-austenite, martensite and degenerate pearlite mixtures are called “microphases” [78]. Primary ferrite side-plates can nucleate directly at γ grain boundaries which are not covered by grain boundary ferrite, although its growth mechanism is identical to that of secondary ferrite side-plates. Acicular ferrite is believed to form after ferrite side-plates during continuous cooling experiments [79].

The austenite to α -ferrite transformation behaviour is mainly affected by non-metallic inclusions, alloy additions and prior austenite grain size [80]. The influence of non-metallic inclusions on the austenite to ferrite transformation, as per classical nucleation theory, is that the nucleation of ferrite at inclusions is always thermodynamically more favourable than homogeneous nucleation. AF usually nucleates on inclusions present in the columnar austenite grains, which stimulates other AF plates to nucleate autocatalytically (sympathetic nucleation). Therefore a one to one correspondence between the number of active inclusions and the number of AF plates is not expected [81].

At same time as FS(A) forms at the austenite grain boundaries, intragranular AF may start to nucleate at inclusions. AF is a very fine grained Widmanstätten-type of ferrite and nucleates in the transformation temperature range between grain boundary ferrite and upper bainite [82-85].

Depending on the prior austenite grain size, a bainitic or ferritic structure can be generated under identical isothermal transformation conditions in an inclusion-rich steel. To generate bainite, the austenite grain size has to be small in order to ensure that most of the

Literature Review

nucleation events occur at the austenite grain surfaces. When the austenite grain size is large and the density of inclusions relatively high, AF is obtained. However the formation of AF may be completely suppressed in the absence of intragranular nucleation sites for ferrite as is the case for a very low weld metal oxygen content. Under these conditions, ferrite side plates and bainite will dominate the microstructure [86]. Depending on the transformation temperature range and the weld chemical composition, carbon-rich austenite may transform to pearlite, bainite or martensite. Occasionally intragranular islands of retained austenite are observed [87].

The schematic relationship between AF and toughness, and the effect of alloying content on heat input and toughness is shown in figure 2.6 (a) and (b). It appears that the optimum level for cleavage resistance is at about 90% AF and at lower heat input levels [88]. Both Charpy 'V' notch (CVN) toughness and yield strength show improvements with increasing AF content as shown in figures 2.7 and 2.8 [89].

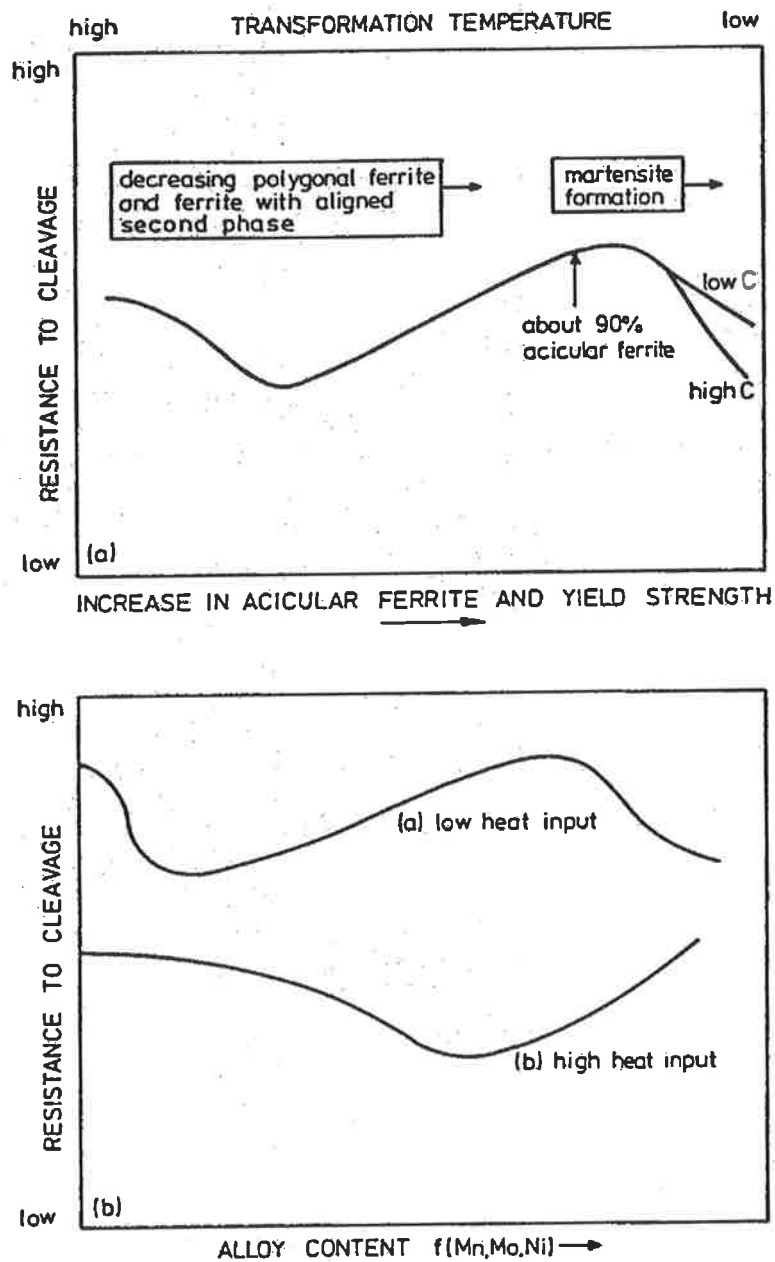


Figure 2.6: (a) Relationship between microstructure and cleavage resistance; (b) Effect of alloy content on cleavage resistance as a function of heat input [88].

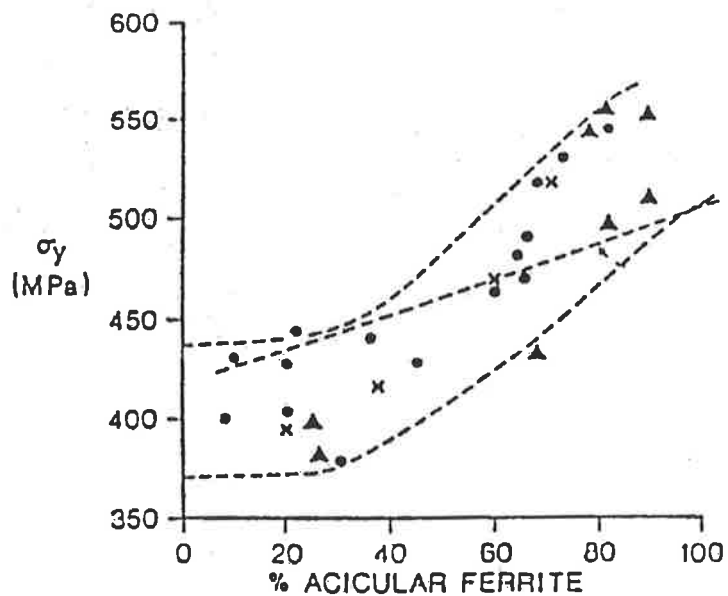


Figure 2.7: Variation of yield strength with the proportion of acicular ferrite for C-Mn-Nb weld metals [89].

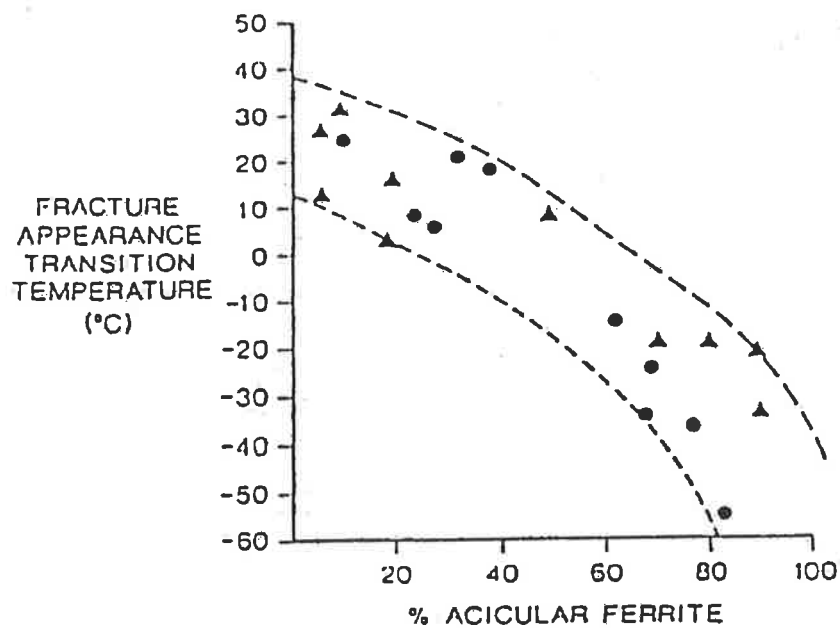


Figure 2.8: Variation of fracture appearance transition temperature with the proportion of acicular ferrite for C-Mn-Nb weld metals [89].

2.4 Refining Weld Metal Structures

2.4.1 Alloying Additions in Weld Metal

The addition of alloying elements to iron to accomplish a desired improvement in properties may require only a few tenths of one percent of the element. In fact, most alloy additions are less than 3 wt.%. Generally improved properties are obtained by stringently controlling elements that may have previously been tolerated as residual elements in wrought products. This is a relatively new approach in alloying technology which has its beginnings in welding consumables [90].

Many elements can be characterised as either a ferrite-former or an austenite-former (see table 2.1). These classifications indicate the influence of the given alloying element on the crystallographic inclination of iron in the matrix structure of the alloy. Carbon is the most important element in terms of controlling microstructure, and its major effect is to control the amount of carbides formed. Beyond that, carbon has a refining effect on the microstructure [91] and influences the solidification substructure [8]. During grain boundary transformation, the diffusion of alloying elements, mainly carbon, will occur from the grain boundary regions towards the center of the grain [92-98].

Literature Review

Table 2.1 Elements used for alloying irons and steels, and their influence on the crystalline structure of the alloy.

Ferrite Formers	Austenite Formers
Elements that favour the formation of alpha phase in iron, ie, the ferritic (bcc) crystalline form in steel.	Elements that favour the formation of gamma phase in iron, ie, the austenitic (fcc) crystalline form in steel.
Aluminium	Carbon
Chromium	Cobalt
Molybdenum	Manganese
Niobium	Nickel
Silicon	Nitrogen
Titanium	
Tungsten	
Vanadium	

When added to iron, certain elements will favour the retention of the alpha iron or ferrite crystalline structure (bcc) and in doing so will restrain the inclination for the allotropic transformation to take place to the gamma iron or austenite in steel (fcc). A sufficient quantity of one of these ferrite-formers (chromium, for example) will suppress the austenite structure form completely, and the alloy will retain the ferrite structure at all temperatures up to melting. Conversely, the addition of a sufficient amount of an austenite-former (nickel, for example) can stabilise the austenite crystalline form, for temperatures ranging from room temperature to the melting point.

Literature Review

The effects of alloying elements on the crystallographic behaviour of the iron matrix is much more complex, because these effects involve not only the expansion or contraction of the phase fields for the respective crystalline structures, but also the alloying element's valency interactions with iron. Aluminium has an fcc crystalline structure, but it is a powerful ferrite-former when added to iron. In fact, the addition of little more than 1 wt.% aluminium to iron will completely prevent the allotropic transformation of alpha iron to gamma iron. Silicon, is such a profound ferrite-former that a stable or permanent ferrite structure is formed when this element is added to iron in an amount approaching about 3 wt.%. It seems that the crystalline structure of the alloying elements has no influence on whether it will be a ferrite- former or austenite-former. Whether a significant ferrite-forming or austenite-forming effect will be observed in iron alloyed with multiple elements will depend on the balance between the totals of the two classes of alloying elements [90,99-101].

2.4.1.1 Effect of Alloy Additions on Microstructure and Mechanical Properties

Alloying not only allows control over the basic crystalline structure, but it is even more effective in manipulating the nature of the matrix on an atomic scale [90]. When iron is alloyed to form steel, the effects involve the dissolution of phases and compounds in the microstructure by heating above a particular temperature. This effect is followed by either (1) retention of the elements in solid solution via cooling at some predetermined rate, or (2) if not held in this manner, their dispersal in some form in the microstructure. A final important point concerning microstructure is that the rate of cooling from the solution-

Literature Review

treating temperature can have a profound influence on many microstructural features, such as grain size; formation of phases; and the distribution of phases, compounds, and dislocations in the matrix structure [90].

Mechanical properties are generally discussed in terms of hardness, ductility and toughness. At least five different mechanisms may act in an alloy to increase its mechanical (tensile) properties. These mechanisms are:

1. solid-solution hardening,
2. order-disorder hardening,
3. precipitation hardening,
4. dispersion hardening,
5. work hardening,
6. grain refinement, and
7. transformation hardening.

It is often desirable to have a fine grain size, because this can increase both strength and toughness. The most efficient way to decrease the effective grain size is to have many nucleation sites to initiate transformation. The most effective nucleation sites are grain boundaries, but impurity particles and deformation bands may also act as nucleants[102].

It is often found that microstructures containing large proportions of fine acicular ferrite have good cleavage resistance, whereas those containing regions of coarse grain boundary ferrite, or ferrite with aligned second phase (each colony of which behaves as one grain during cleavage) tend to have poorer toughness [102].

2.4.1.1.1 Effect of Carbon

Small amounts of carbon, less than 0.1wt% by weight, can cause significant changes in metallurgical behaviour and mechanical properties. An appreciable amount of carbon can dissolve in gamma iron, where it forms an interstitial solid solution. However, the solubility of carbon in ferrite (alpha iron) is very much lower, and the maximum that can be held in interstitial solid solution is 0.0218 wt.% at 727⁰C [90]. At room temperature, solid solubility is only about 0.008 wt.%. The carbon that cannot remain in solid solution in ferrite generally forms a compound rather than existing as some form of free carbon. This compound is iron carbide (Fe₃C, also called cementite) and it is a material of very high hardness. Microstructural evidence suggests that the strengthening of ferrous alloys by carbon is principally due to morphology and distribution of the carbides which are formed, although there will be a slight effect due to grain refinement. Studies on bead-in-groove CO₂ welds, found that carbon had a much smaller influence on yield stress than on tensile strength of weld metal [103-106]. A martensitic microstructure with low carbon content has appreciable toughness, whereas high carbon martensite is brittle. The low carbon martensite will be autotempered during cooling, improving toughness. This is shown in the schematic diagram, figure 2.9, where at high heat inputs steels with lower hardenability are generally softer and thus have better toughness. The reduction in the carbon content of steels that has taken place during the 1980s, probably has been the largest single factor responsible for the improvement in toughness in the HAZ of welds [107]. However, this relationship is not entirely straightforward. As shown by Harrison and Hart [108], low heat input welding (1 kJ/mm) gives better toughness in steels with higher hardenability, while high heat inputs (5kJ/mm) give the opposite result (figure 2.10).

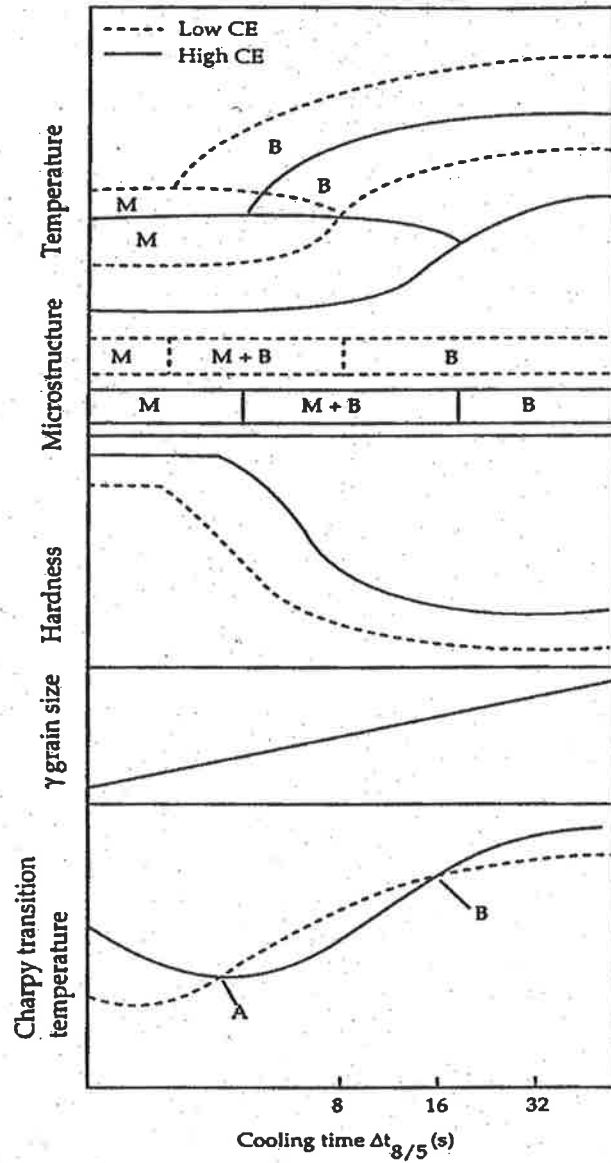


Figure 2.9: The effect of carbon equivalent on toughness and hardenability [108].

Literature Review

Figure 2.9 is an explanation for the toughness-hardenability results shown in figure 2.10.

Hardenability of steels, expressed as P_{cm} (also known as the carbon equivalent) is given by:

$$P_{cm} = C + (Mn + Cr + Cu)/20 + Si/30 + V/10 + Mo/15 + Ni/60 + 5B$$

Steels with high hardenability will have an autotempered martensite when welded with low heat input (because the bainite nose is moved to the left and the M_s temperature is relatively high), as can be deduced from the schematic CCT diagram. The low hardenability steels will have a bainitic structure. Cross-over point A corresponds to such low heat input that in the low hardenability steels autotempered martensite is also formed. The critical value of heat input is below 1 kJ/mm. Point B corresponds to the point where the microstructures of all steels are bainitic and the steels with lower hardenability will then be softer, which should give them a better toughness [108].

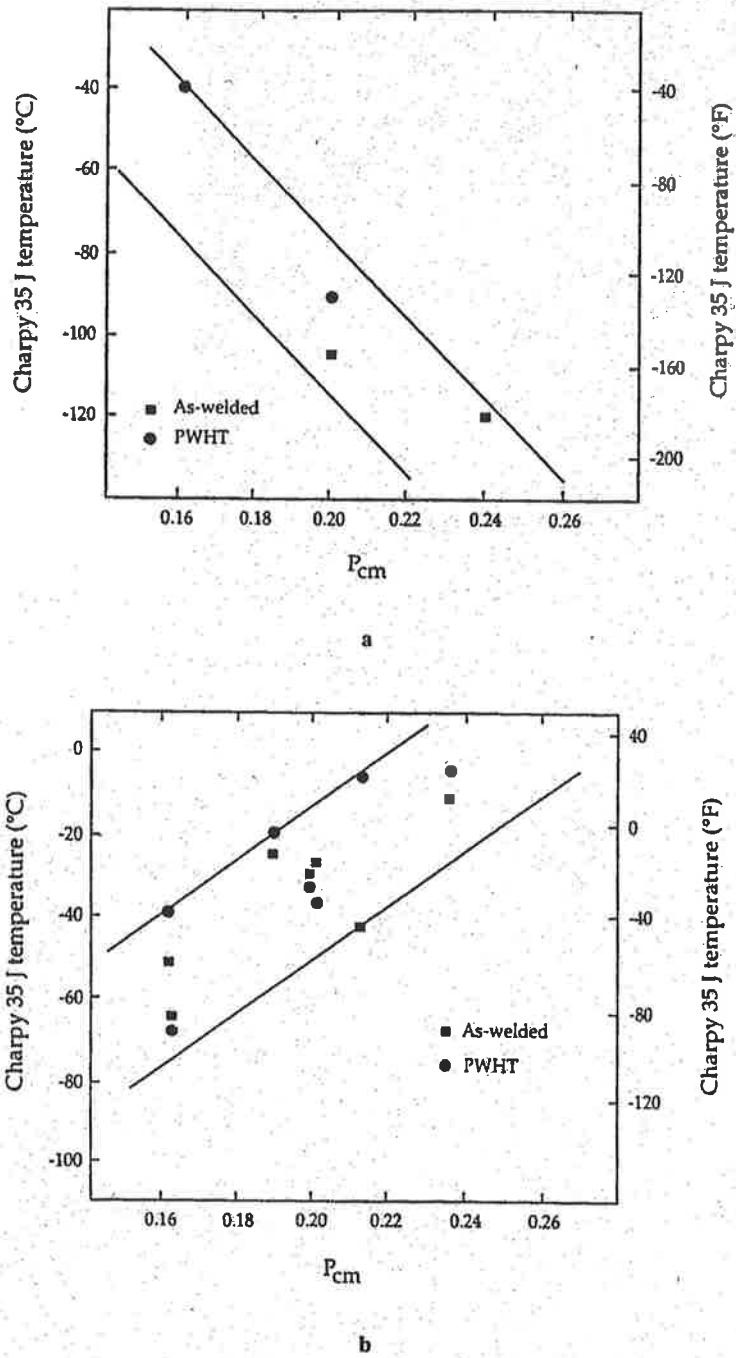


Figure 2.10: The 35-J transition temperature in the coarse-grained zone as a function of the hardenability of the steels, expressed as P_{cm} . (a) The relationship for a low heat input (1kJ/mm FCAW). (b) The relationship for 5 kJ/mm SAW [108].

Literature Review

The presence of additional alloying elements, as commonly found in steels, has a profound influence on the critical temperatures, even when heating or cooling through the transformation range is performed at the very slow rates employed for establishing equilibrium temperature levels. Manganese and nickel additions shift the eutectoid temperature (A_{e1}) temperature downward from the 727°C level, while the elements chromium, molybdenum, silicon, titanium, and tungsten raise the A_{e1} temperature. The presence of other alloying elements can also cause a significant shift in the eutectoid carbon content, which 0.77 wt.% carbon in alloys consisting of only iron and carbon. As shown by the lower graph in figure 2.11, the addition of two percent chromium to an iron-carbon alloy would lower the eutectoid composition to approximately 0.60wt% carbon. Additions of manganese, nickel, molybdenum, silicon, titanium, and tungsten act in a similar fashion and will shift the eutectoid composition to lower carbon contents.

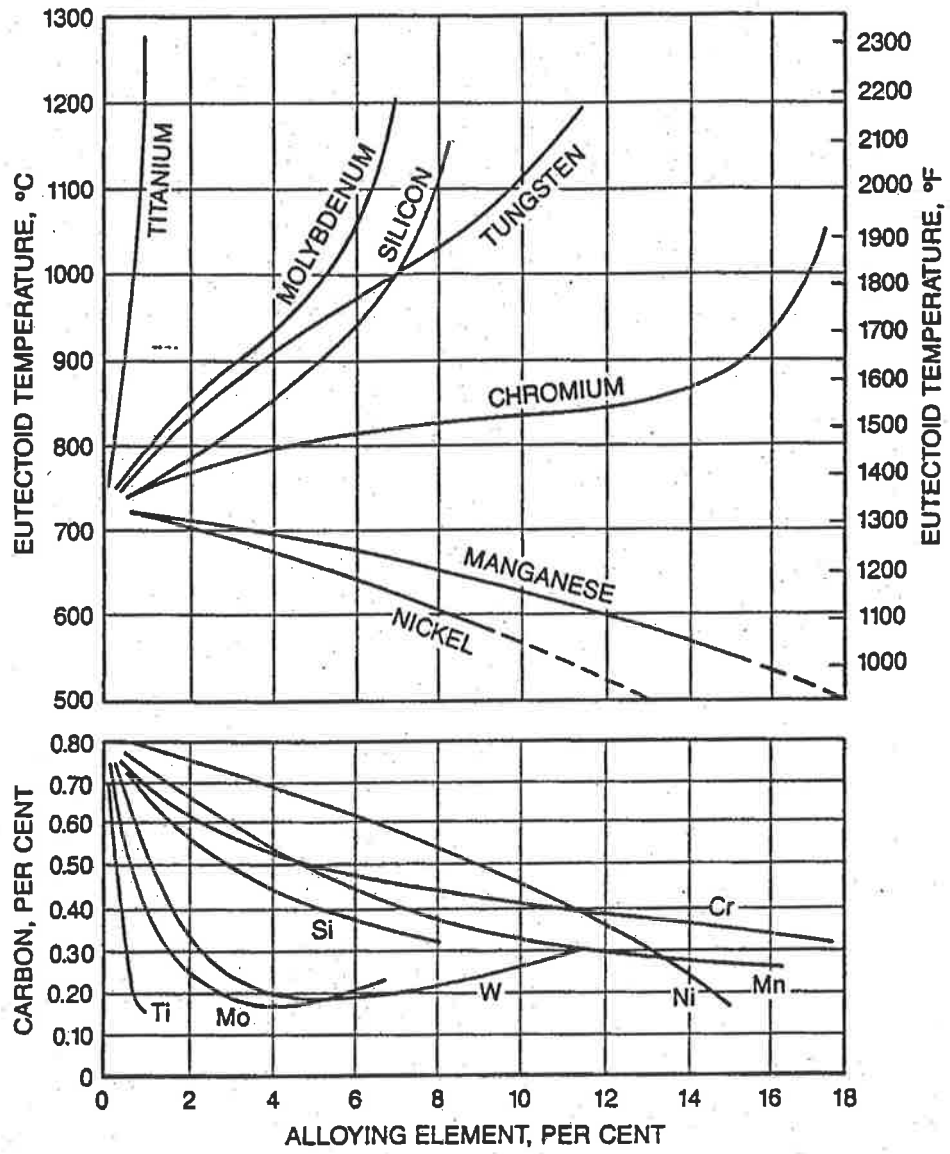


Figure 2.11: Eutectoid composition and its temperature in steels as influenced by alloying elements [90].

Literature Review

It is generally accepted that the addition of carbon to low strength ferritic weld metal causes the yield and tensile strengths to increase and ductility to decrease. Furthermore, the hardness increases and, at a constant grain size, the yield-to-tensile strength ratio decreases [109-111]. The effect of 0.05 to 0.15wt% carbon on the microstructure and properties of MMAW welds containing 0.6 to 1.8wt% manganese has been investigated for basic iron powder electrodes. It was found that carbon promoted acicular ferrite, at the expense of grain boundary polygonal ferrite, and caused grain refinement of the reheated regions. With regard to impact properties, it was found that carbon substantially reduced the degree of scattering. Optimum toughness was achieved at a manganese level of 1.4wt% when the carbon content was in the intermediate range, ie 0.07 to 0.09wt% [8].

2.4.1.1.2 Effect of Manganese

The chemical properties and metallurgical characteristics of manganese enable it to perform several helpful functions when alloyed in iron. As compared with iron, manganese has a stronger affinity for oxygen, sulphur and carbon. When added to molten iron, manganese reacts with oxygen contained in the melt to form manganese oxide (MnO). This reaction does not go to completion to take up all of the oxygen present, but proceeds to a point of balance or equilibrium. Therefore, although manganese is a deoxidiser, it is not as powerful in this respect as some other elements, like aluminium and silicon. The manganese in the melt also will combine preferentially with any sulphur present to form manganese sulphide (MnS), a compound which has only limited solubility in the molten iron and rises to escape in the slag if conditions permit. Manganese sulphide also is virtually insoluble in the solid metal, where it appears as non-metallic inclusions. Any

Literature Review

manganese, beyond the amount required to combine with all of the sulphur present, will combine with the carbon in the steel to form manganese carbide, Mn_3C , as the steel cools through the Ar_1 critical point, this phase is isomorphous with cementite and the actual carbides which develop are complex $(Fe,Mn)_3C$. The properties of manganese carbide and the appearance of particles of $(Fe,Mn)_3C$ in the microstructure are indistinguishable from iron carbide.

Evans [7] investigated the effect of manganese in basic flux MMA welds and found that increasing the manganese level from 0.6 to 1.8 wt % progressively increased the acicular ferrite (AF) content while reducing intragranular polygonal ferrite (PF(I)) and grain boundary ferrite (PF(G)). Increasing the manganese level also refined the acicular ferrite grain size. Another effect of manganese is the reduction of the austenite-to-ferrite transformation temperature at almost all cooling rates for MMA weld metals, with the start temperature of polygonal ferrite being depressed to a greater extent than the acicular ferrite start temperature [112,113]. For MMA multilayer steel welds, the best impact properties are attained at a manganese content of 1.5 wt.% as shown in figure 2.12. The recorded peak in toughness arises from a balance between the formation of a more favourable microstructure on the one hand, and higher yield strength on the other [7].

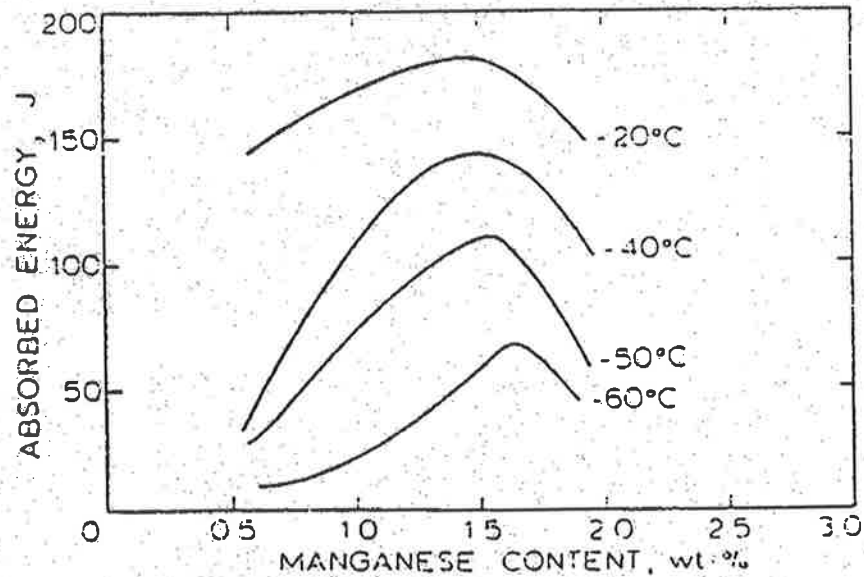


Figure 2.12: Effect of manganese on Charpy V-notch toughness for multipass MMA C-Mn steel welds [7].

2.4.1.1.3 Effect of Silicon

Silicon is used mainly in steels as a deoxidising agent. Not only is it sufficiently strong as an oxygen-getter to remove unwanted amounts of oxygen, but the oxide formed as inclusions in the metal ordinarily can be tolerated without significant adverse effects. The general effect of dissolved silicon is to lower the delta-to-gamma transformation range in iron, and to raise the gamma-to-alpha transformation range. In addition silicon is a strong ferrite former.

Silicon offers benefits as an alloying addition that have been utilised in certain steels, usually with silicon contents exceeding 0.3 wt.%. Silicon is a ferrite strengthener, and it is stronger in this respect than most other commonly used alloying elements (see figure 2.13).

Literature Review

Also, silicon is a strong promoter of hardenability, and additions as high as 2 wt.% have been added to heat-treatable alloy steels for this reason.

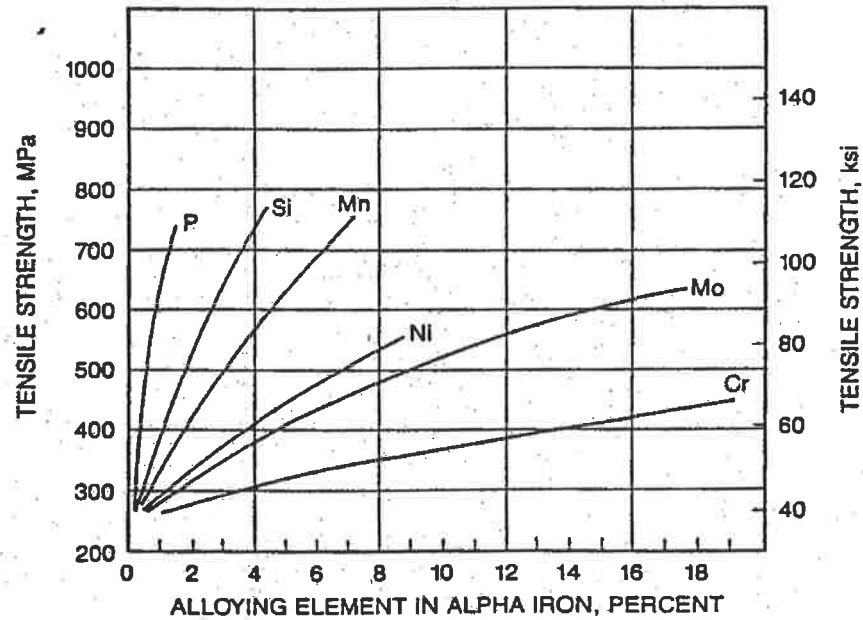


Figure 2.13: Relative effectiveness of alloying elements commonly used in steels to strengthen ferrite, the alpha phase (bcc) of iron [90].

Evans [9] also reviewed the role of silicon in weld metal from basic flux MMA electrodes in the range of 0.2 to 0.94 wt.% and found that increased silicon encourages the formation of acicular ferrite, particularly when the manganese levels are below 1 wt.%, but results in lower values of upper shelf Charpy toughness. Court [114] noted that increasing the silicon level led to a decreased acicularity of the acicular ferrite and a transformation from lath-like micro-phases to twinned martensite in intergranular regions of the microstructure. Therefore silicon is considered detrimental to toughness even in small concentrations [80].

Literature Review

The final weld metal oxygen content is related directly to both the total amount of silicon and manganese present and the resulting manganese-to-silicon ratio. The combined effect of these two contributions (see figure 2.14) has been included in a new deoxidation parameter $([\%Si][\%Mn])^{-0.25}$. The small, negative exponent in the deoxidation parameter indicates that control of the weld metal oxygen level through addition of deoxidants is limited [15]. Silicon has a powerful solid solution hardening effect, but the basic reason for adding silicon is to kill (remove oxygen from) the steel. A positive factor with silicon killed steels is that they have a lower oxygen and nitrogen content.

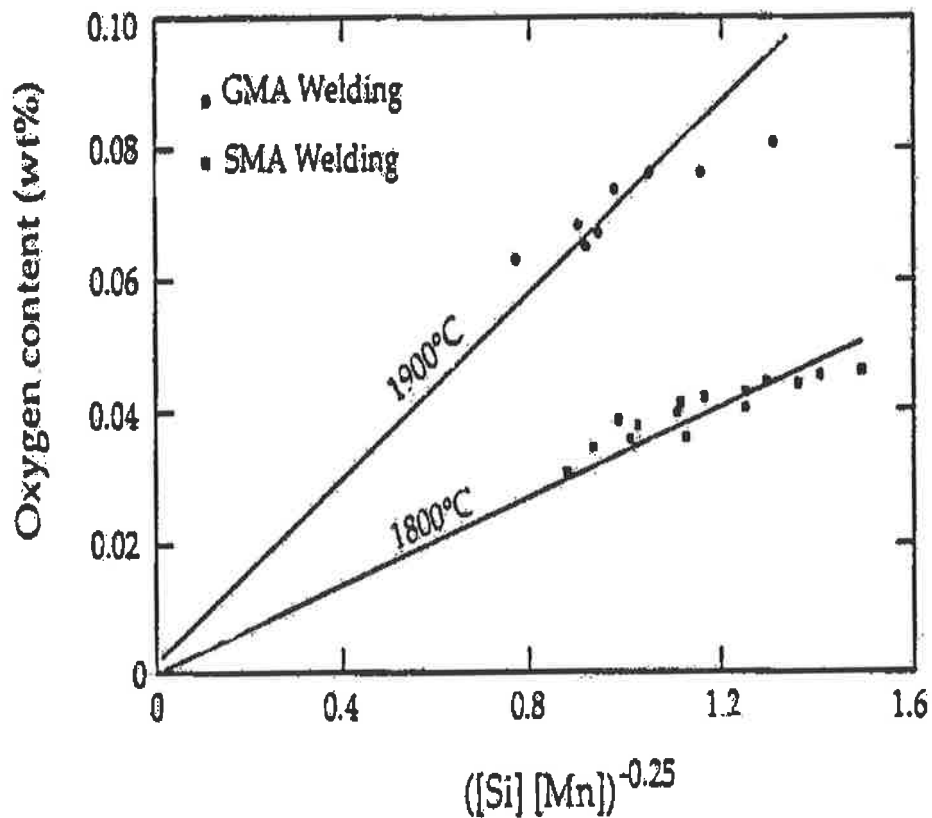


Figure 2.14: Correlation between the oxygen content and the deoxidation parameter $([\%Si][\%Mn])^{-0.25}$. The points represent measurements, while the solid lines represent thermodynamical calculations. Data for both GMAW and SMAW are shown [15].

2.4.1.1.4 Effect of Titanium

Unique effects are obtained by adding very small percentages of titanium to selected steels in wrought form, in castings, and also as weld metal. To date, the benefits of titanium additions in the range of only 0.005 to 0.06 wt.% are impressive. The effects of its use are complex, and much research is continuing on the metallurgical mechanisms involved [90].

When titanium is added to molten steel, a complex interplay takes place with the oxygen, nitrogen and carbon that is commonly present, because titanium has a strong affinity for all three of these elements. Therefore, it is difficult to confine the activity of titanium to only one function, that is, only deoxidising, only nitride-forming, or only carbide-forming. Because of titanium's strong affinity for oxygen, much of a small titanium addition to molten steel would be relegated to the formation of titanium oxide unless the melt has low oxygen content; for instance, approximately 0.01 wt.%. A suitable dispersion of very small titanium oxide particles in the melt can serve to nucleate finer grains during solidification and during subsequent microstructural transformations. Titanium treatment of molten steel to produce very small oxide inclusions that remain dispersed in the solid steel is being pursued as a steelmaking technique for steels that are resistant to excessive HAZ grain coarsening by welds made with very high heat input [90].

A very small percentage of titanium can have profound beneficial effects on the mechanical properties and the metallurgical behaviour of steel providing the proper technology is applied in (1) making the titanium addition, (2) controlling the association of the titanium with other minor elements that may be present, and (3) manipulating by hot working and/or heat treatments the form of titaniferrous constituents that appear in the final microstructure.

Literature Review

Evans [115] investigated the effects of micro-alloying elements on toughness for multi-run basic flux MMA weld deposits [95-97]. Titanium was found to be the most effective element for enhancing the toughness of as-welded deposits. Its effect on toughness is significant (Figure 2.15) and a titanium content of about 30 ppm is considered optimal [11]. Abson [116] developed a formula for the optimisation of the titanium content,

$$Ti = (S + O) / 15$$

which was confirmed by reducing the weld metal oxygen by 150 ppm. This was also observed by Evans [11] illustrated in figure 2.16 (a) at the optimum titanium content of 20 ppm. Adding nitrogen by nitrated-manganese leads to slightly higher optimal titanium levels figure 2.16 (b). An important role of titanium is to protect boron from nitrogen (and oxygen) and reduce the level of free nitrogen in the weld metal. The optimum content of titanium will be a function of the weld concentration of nitrogen and nitride formers (V, Nb, Al, and Ti). With low levels of titanium, niobium additions led to a significant decrease in toughness (figure 2.17), and acicular ferrite was replaced by aligned ferrite in as-deposited and reheated regions [117]. These facts led to the conclusion that niobium should be as low as possible in micro-alloyed C-Mn weld deposits.

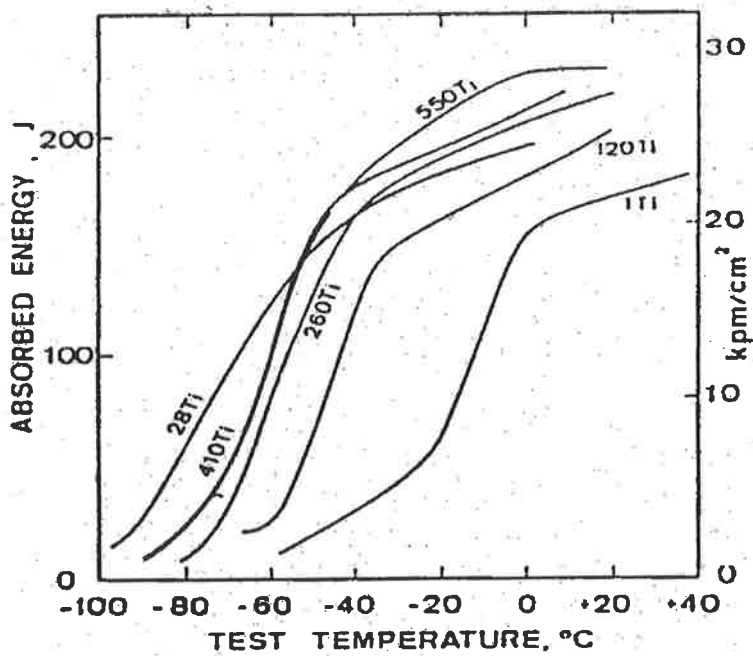


Figure 2.15: Effect of titanium ppm on the Charpy-V curve for multi-run basic flux MMA weld deposits [115].

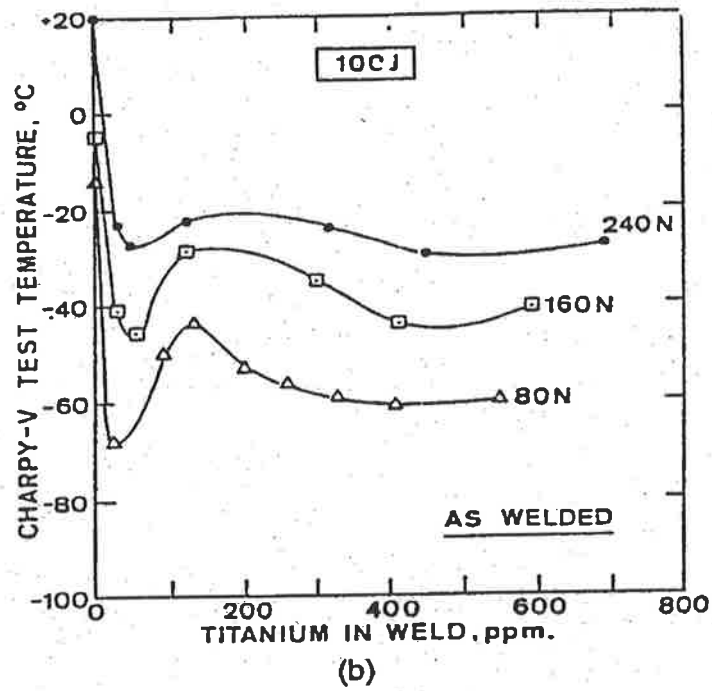
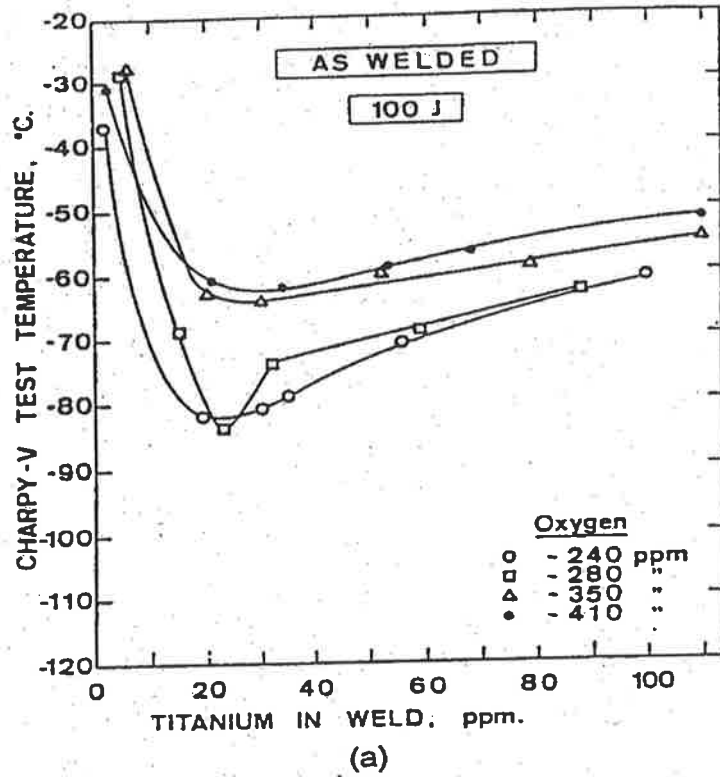


Figure 2.16: Charpy-V curve for 100 J for multi-run basic flux MMA weld deposits:
 (a) Ti-O series, (b) Ti-N series [115].

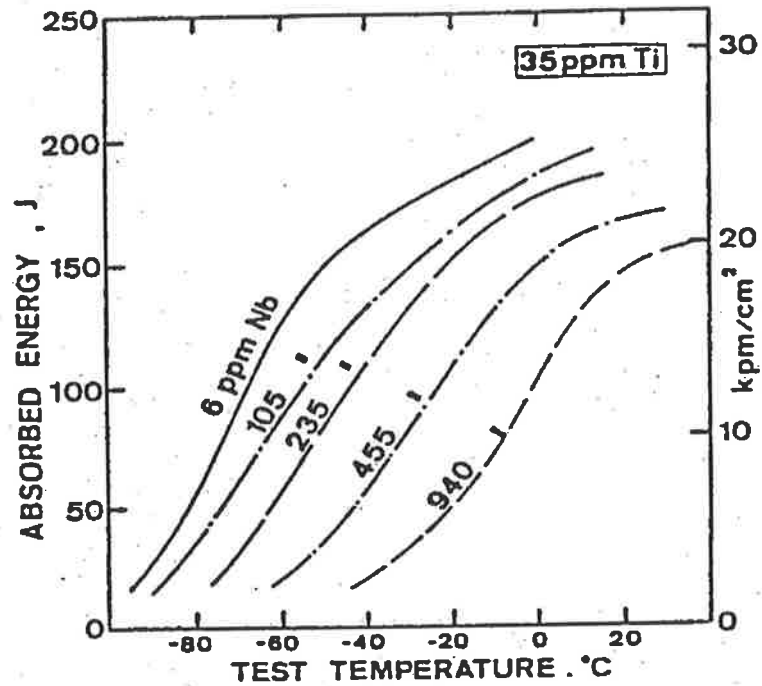


Figure 2.17: Effect of niobium with 35 ppm titanium on the Charpy-V curve for multi-run basic flux MMA weld deposits [115].

2.4.1.1.5 Effect of Aluminium

Aluminium plays important roles in steel as a deoxidising agent, as a nitrogen fixation agent, and as a grain-refining additive. These functions require only very small additions of aluminium.

The amount of acicular ferrite increases with increasing amounts of aluminium in SAW weld metal [118]. However, when all of the available oxygen was tied up by aluminium to form γ -alumina (when the Al:O ratio was 1:1.13), there was an abrupt decrease in the acicular ferrite content. This behaviour probably occurs because at low aluminium

Literature Review

concentrations, the aluminium oxide is in the form of galaxite ($\text{MnO} \cdot \text{Al}_2\text{O}_3$) rather than γ -alumina, the former being very effective as a nucleant of acicular ferrite according to lattice matching theory. The observations of Terashima and Hart [119] on the effect of small variations of aluminium on impact toughness in SAW weld metals are however an indication that there is a practical problem associated with obtaining the correct type of particles to act as nucleation sites for acicular ferrite.

Adding aluminium powder at low titanium levels in basic flux MMA welds results in an increase of the lower shelf energy (figure 2.18), but an optimum level was not observed and the microstructural changes were insignificant [115]. When titanium was present (figure 2.19) degradation in toughness was observed at 80 ppm aluminium and at higher levels. The acicularity of the initial microstructure was modified and the non-metallic inclusions contained increased amounts of aluminium indicating that aluminium modified the role of titanium [10].

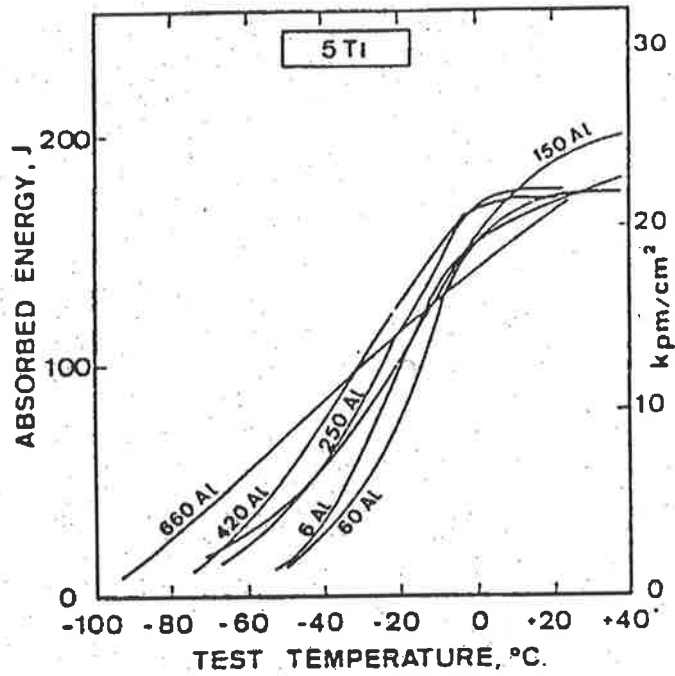


Figure 2.18: Effect of aluminium on the Charpy-V curve for multi-run basic flux MMA weld deposits [115].

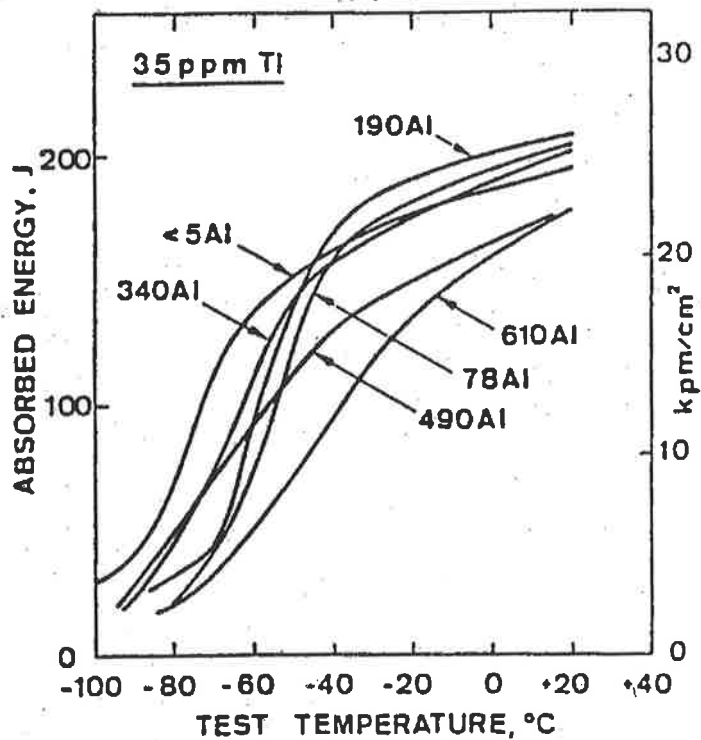


Figure 2.19: Effect of aluminium with 35 ppm titanium on the Charpy-V curve for multi-run basic flux MMA weld deposits [10].

Literature Review

Abson [120] studied the effect of aluminium (Al) and alumina (Al_2O_3) on the microstructure and mechanical properties of metal-cored and basic-flux FCA weld metals using the metal-active-gas (MAG) process. In the metal-cored deposits, aluminium gave a substantial increase (approximately 15%) in the strength accompanied by a similar increase in the proportion of acicular ferrite. Cleavage resistance changed little with the lowest aluminium additions, before decreasing with the higher levels (see figure 2.20).

The Al_2O_3 additions to the metal-cored wires produced a modest microstructural improvement, but the inclusion content increased substantially, and many of the inclusions were large. The detrimental influence of large inclusions on resistance to cleavage fracture is well known, the mechanism being that cleavage fracture is initiated at or immediately adjacent to inclusions. However, the fractographic evidence did not support inclusion initiation of cleavage in all instances, and this indicates a probable change in the microphases with increasing aluminium. The decrease in upper shelf toughness with increasing aluminium additions, and with the Al_2O_3 addition, at least in weld W33 (figure 2.20), in the metal-cored wires is associated with an increase in the mean inclusion diameter.

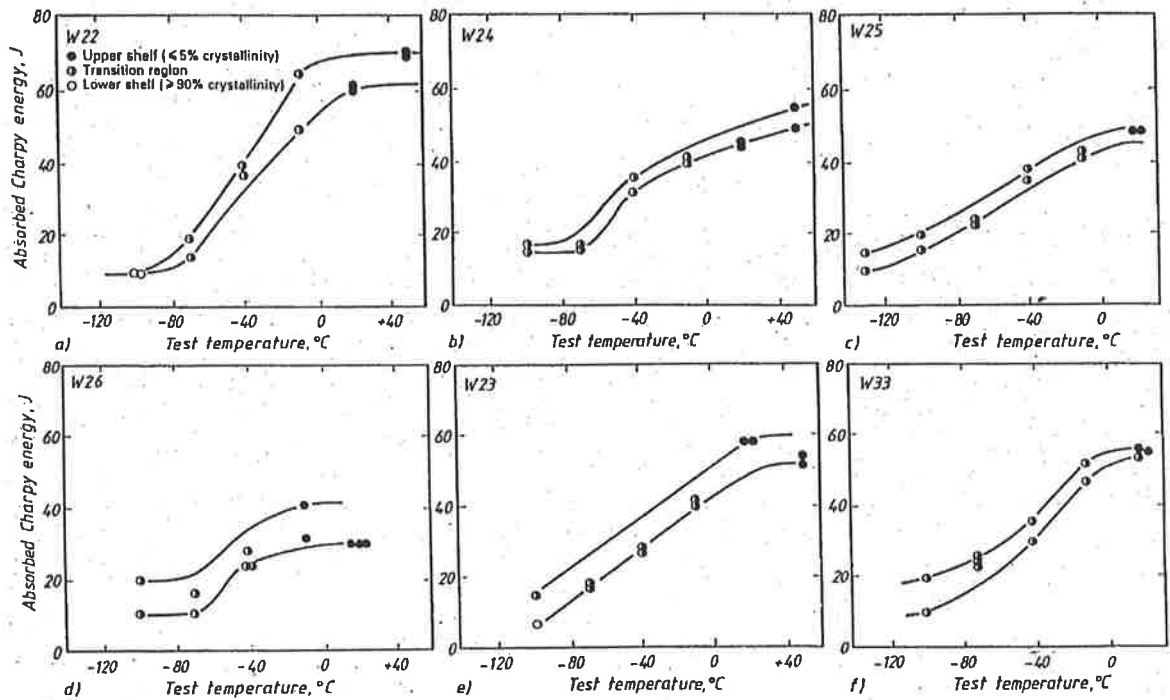


Figure 2.20: Charpy transition curves for metal-cored wire deposits, of various aluminium and Al₂O₃ weld metals (7.5 by 10 mm Charpy specimens)

- (a) Weld W22 FeAl addition (0.007 % Al);
- (b) Weld W24 FeAl addition (0.039 % Al);
- (c) Weld W25 FeAl addition (0.075 % Al);
- (d) Weld W26 FeAl addition (0.117 % Al);
- (e) Weld W23 Al₂O₃ addition (0.039 % Al);
- (f) Weld W33 Al₂O₃ addition (0.021 % Al) [120].

Literature Review

In the basic flux-cored deposits, the strength increase accompanying the increase in weld aluminium content was less pronounced, in spite of a higher total aluminium addition. Cleavage resistance improved as the proportion of acicular ferrite was increased by the lowest aluminium addition; further increases in aluminium content had a deleterious effect on both microstructure and cleavage resistance. The lower aluminium addition also improved upper shelf toughness, but the highest aluminium addition was slightly detrimental. The addition of Al_2O_3 gave a weld with a lower proportion of acicular ferrite than that with a comparable aluminium level produced with an aluminium addition, probably because of an associated lower recovery of titanium in the inclusions; there was a consequent reduction in cleavage resistance. The Al_2O_3 addition had minimal influence on upper shelf toughness [120].

Powell [121] investigated the effect of metallic-aluminium and alpha-alumina additions on the microstructure and mechanical properties of a microalloyed rutile weld metal and found that toughness depends on the form in which aluminium is added to the flux cored wire. In this case (micro-alloyed rutile) the alpha alumina additions significantly increased the amount of acicular ferrite and therefore the toughness compared with metallic-aluminium additions.

2.4.1.1.6 Effect of Boron

Boron is added to alloy steels in very small amounts, perhaps as little as 0.003 wt.%, to increase hardenability. Boron is a very powerful promoter of hardenability on a weight percentage basis, but this effect is gained only with amounts of boron below approximately

Literature Review

0.010 wt.%. Any boron above this level is ineffective. Therefore, it has become a common practice to “needle” some alloy steels with a very small addition of boron to obtain increased hardenability. The benefit derived from this element is often measured and controlled by means of hardenability testing. Chemical analyses reveal such low levels of boron in the steel that the correlation between hardenability and boron level is not always clear.

Adding boron to high purity basic flux MMA electrodes [115] caused a substantial lateral shift of the Charpy-V curves to lower temperatures as shown in figure 2.21. Boron additions of about 140 ppm were considered optimal. When 35 ppm titanium was present the addition of boron generally resulted in the displacement of Charpy-V curves to lower temperatures (figure 2.22) and caused the elimination of grain boundary ferrite and a change to a bainitic type structure. Several authors have reported that the formation of grain boundary ferrite can nearly be eliminated by balanced alloying with boron and titanium [122-127]. The mechanism for the hardenability of boron was based on the fact that boron segregates extensively to the prior austenite grain boundaries, where it reduces the grain boundary energy [128]. The reduction in grain boundary energy will then increase the energy barrier to nucleation by lowering the surface free energy ratio and therefore suppress the formation of grain boundary ferrite facilitating nucleation on oxide inclusions [2,129].

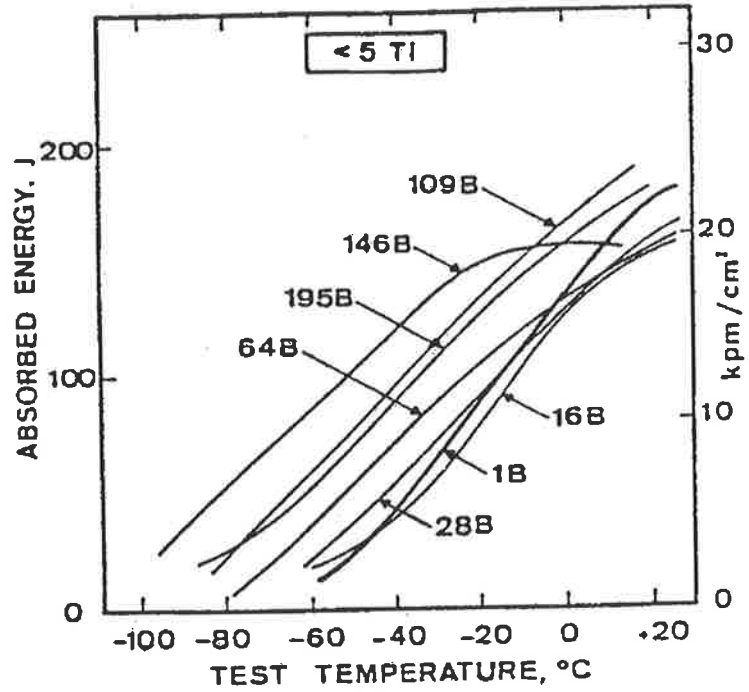


Figure 2.21: Effect of boron on the Charpy-V curve for multi-run basic flux MMA weld deposits [115].

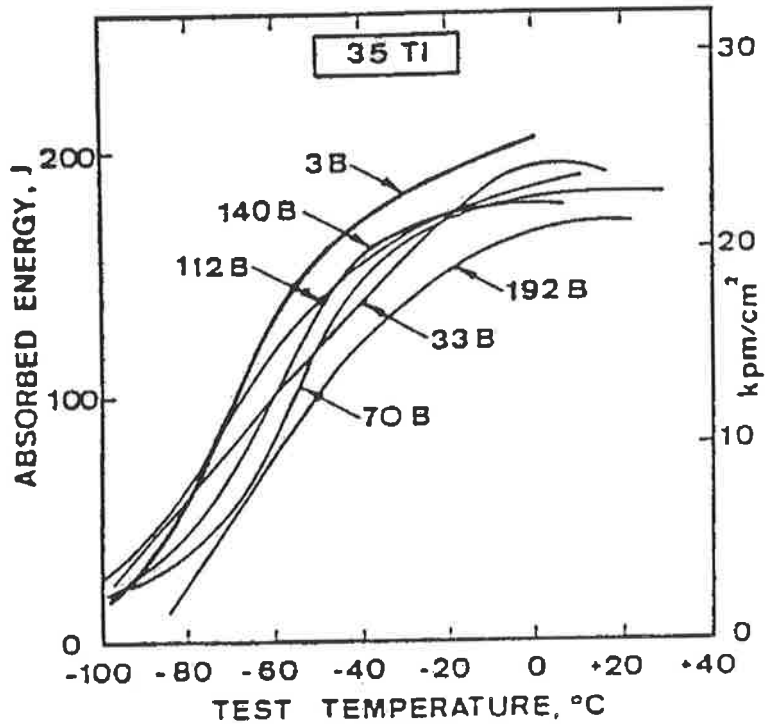


Figure 2.22: Effect of boron with 35 ppm titanium on the Charpy-V curve for multi-run basic flux MMA weld deposits [115].

Literature Review

The influence of boron on increasing the proportion of acicular ferrite in weld metal is minor without a sufficient titanium addition. The influence of titanium was also very small without sufficient levels of boron. A large volume fraction of acicular ferrite (up to 95%) can be obtained by maintaining boron and titanium contents between 40-45 ppm and 400-500ppm, respectively. This is based on a 2.23kJ/mm heat input on 25 mm thick microalloyed steel plate. The decrease in low-temperature toughness with excess boron and titanium contents can be explained by an increased volume content of upper bainite [130].

Optimum concentrations of boron and zirconium additions to low carbon steel weld metals produced predominantly acicular ferrite microstructures. Boron in weld metal is protected from oxygen and nitrogen by both zirconium and titanium. Elemental boron hinders the formation of grain boundary ferrite resulting in increased undercooling of weld metal austenite, and this promotes the nucleation of fine intragranular acicular ferrite. The inclusion size distribution in zirconium-containing weld metal was similar to or finer than that for titanium-containing weld metal. The specific inclusion concentration and size distribution, with proper protection of weld metal boron, are the primary factors in achieving high intragranular acicular ferrite contents [131].

2.4.1.1.7 Effect of Nitrogen and Oxygen

Although the reactions with oxygen are the most important from the aspect of properties of the weld metal, nitrogen also has significant effects on the weld metal properties.

Literature Review

The solubility of nitrogen in solid steel undergoes sharp changes as the metal cools, particularly as the crystalline structure undergoes allotropic transformations. The bcc ferrite form of steel just below the A_{r1} (approximately 727 °C) critical temperature is able to hold only about 0.10 % nitrogen in interstitial solid solution. Excess nitrogen forms iron nitride and other complex nitride particles. These particular particles exert only a minimal influence on mechanical properties. Also, the presence of other alloying elements will influence the amount of nitrogen that actually is retained in solid solution. Carbon, silicon and oxygen decrease nitrogen solubility in ferrite; whereas a number of alloying elements, including chromium, manganese, titanium, zirconium, and vanadium, increase solubility [90].

Weld metals from rutile MMAW electrodes usually have high contents of both oxygen and nitrogen, with nitrogen levels around 200 ppm. This is probably due to comparatively low amounts of shielding gas generated by this type of coating. Basic-type coatings give nitrogen contents of around 50 to 100 ppm. In SAW welds, the nitrogen content is the same as that in the wire [108].

As stated by Kotecki [132,133], nitrogen additions are intentionally made to austenitic and duplex austenitic - ferritic stainless steel deposits, where it has a strong effect on the phase balance. However, in the case of C-Mn steel deposits, nitrogen is often, but not always, detrimental to properties. Excess nitrogen usually causes porosity, and shielding efficiency is known to be dependent on electrode type, polarity, coating thickness and the baking temperature. The lowest nitrogen levels down to 35 ppm have been achieved experimentally by combining argon protection with a short arc length [134,135].

Literature Review

The effect of oxygen on weld metal microstructure has been discussed by many researchers [136-140]. The impact toughness is especially dependent on the oxygen content of the weld metal. Rutile type welds having higher oxygen contents (600 to 1000 ppm by weight) generally produce welds of lower impact toughness. They are usually tested at 0°C. As a consequence of the high oxygen content, rutile-type electrodes have quite a low manganese content (around 0.5 wt%), because this gives a lower strain hardening. With variants that are slightly more basic (ie, rutile-basic), acceptable impact toughness at -20°C can be achieved. Basic electrodes (oxygen content around 300 to 400 ppm) usually have good impact toughness down to at least -40°C and sometimes even lower temperatures. In these types of electrodes higher manganese contents can be used [99].

Oxygen combines with elements such as silicon and manganese to form slag particles. These may serve as initiation points for cleavage fracture if retained in the weld metal. The slag particle content also affects the ductile fracture energy, in that higher amounts lead to decreased toughness. Oxygen often coprecipitates with sulphur to form oxysulphides. It is important to prevent sulphur from combining with iron, leading to liquid phase embrittlement. The oxygen content decreases with an increased basicity index (see figure 2.23) and this is of the utmost importance, because it creates the possibility of improving the toughness of weld metals [141]. The most accepted basicity index (BI) is given below:

$$BI = \frac{[CaO+CaF_2+MgO+K_2O+Na_2O+Li_2O+BaO+SrO+1/2(MnO+FeO)]}{[SiO_2+1/2(Al_2O_3+TiO_2+ZrO_2)]}$$

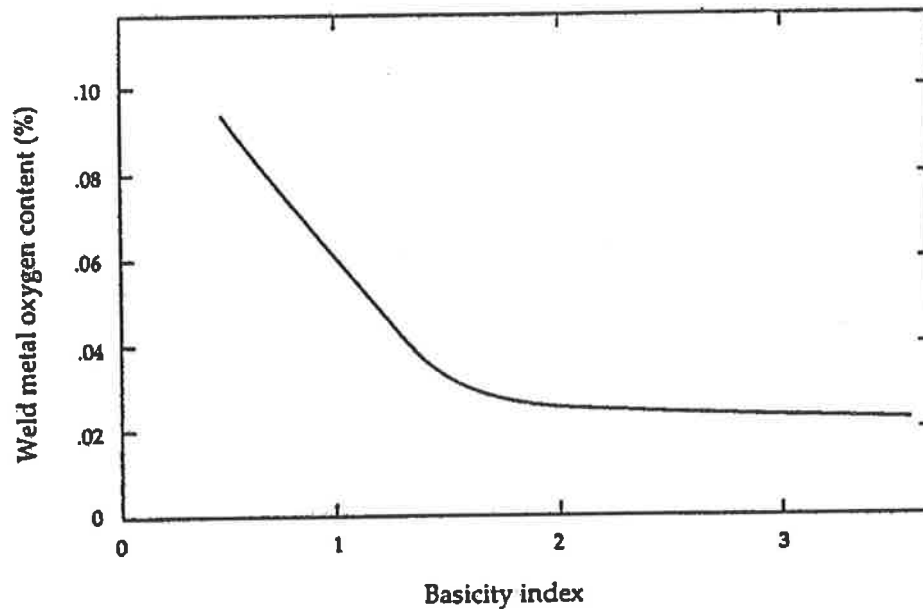


Figure 2.23: Influence of the basicity index on oxygen content [141].

The oxygen content of the weld metal decreases rapidly when going from an acid to a medium basic slag. When all SiO_2 is used, no further reduction of the oxygen content occurs [141].

For C-Mn steel weld metals, the analytical oxygen content normally falls within the range calculated for equilibrium with silicon and manganese at 1800 to 1900 °C (see figure 2.14). In this range the oxygen concentration arises from the fact that the separation of deoxidation products from the pool is strongly influenced by the operational conditions applied. Any change in welding parameters or flux or shielding gas composition, which alters the fluid flow-field in the weld pool, directly affects the oxygen level. This is done by moving the zone for possible inclusion removal towards either higher or lower metal temperatures. Thus, the choice of operational conditions finally determines the degree of deoxidation that can be achieved [15].

Literature Review

Plots of inclusion-forming agent vs. hardenability agent can be used to predict the microstructure of GMA weld metal. For a particular cooling rate that crosses into the grain boundary ferrite region, changes in composition, which result in an increase in the manganese or a decrease in the oxide content, will shift the initiation curve as illustrated in figure 2.24. This can result in the formation of acicular ferrite. Likewise, an acceptable microstructure from a particular cooling curve can be lost by shifting out of that acceptable (acicular ferrite) region by either increasing the manganese or decreasing the oxide content into the aligned ferrite or bainite region (figure 2.25). The volume fraction of acicular ferrite is influenced by the oxygen and carbon dioxide content in the argon cover gas (figure 2.26) [142].

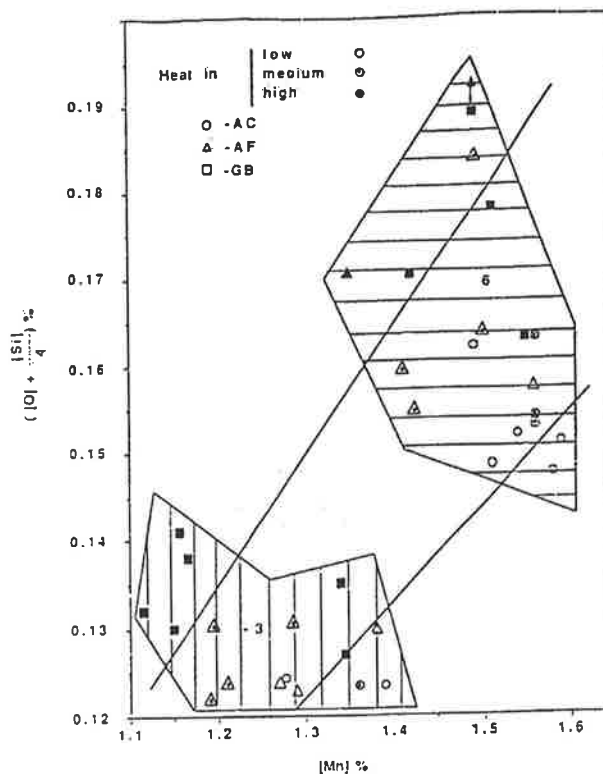


Figure 2.24: Diagram of the derived weld microstructure as a function of the oxide-forming propensity $[O + Si / 4]$ and the hardenability (manganese) [142].

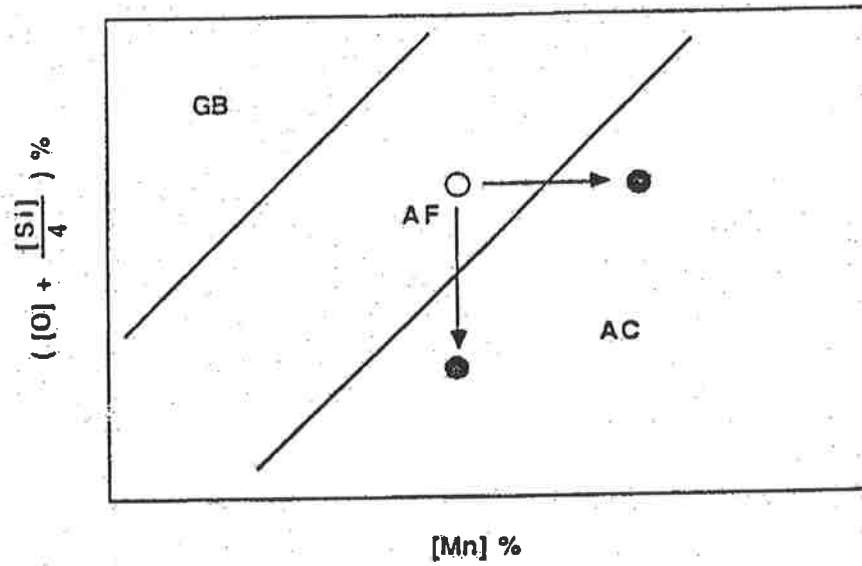


Figure 2.25: A plot of oxide-forming propensity vs. hardenability [142].

It should be noted from the above figure that either an increase in hardenability or a decrease in oxide-forming propensity will shift from an acceptable microstructure to one of aligned carbide [142].

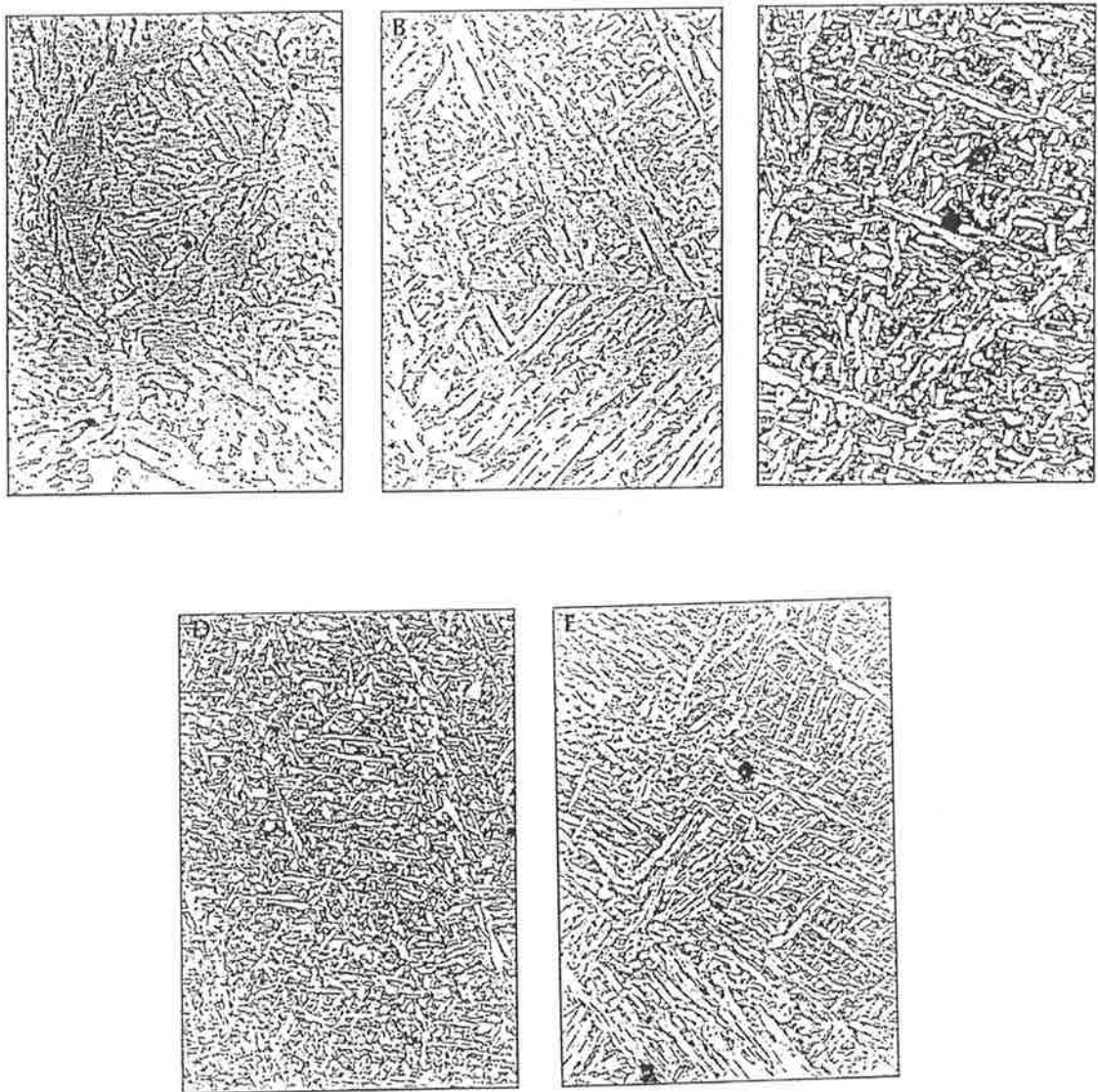


Figure 2.26: Photomicrographs of various ferrite morphologies in weld metal [142].

The figure 2.26 shows (a) photomicrograph showing blocky, grain boundary ferrite weld metal. This weld was made at 25V and 390A using argon plus 75% carbon dioxide, ER70S-6 welding wire and a 7.5- in./min travel speed. (b) Photomicrograph showing Widmanstätten side plates growing from the prior austenite grain boundary. This

Literature Review

microstructure was produced by welding at 25V, 380A and using ER70S-6 weld wire, argon plus 3% oxygen cover gas and 7.5 in./min travel speed. (c) and (d) Photomicrographs showing coarse and fine acicular ferrite weld metal. Both welds were produced using 25V and 380A. Weld C was produced using argon plus 3% oxygen, ER70S-3 welding wire and 15 in./min travel speed. The fine structure in weld D was produced using argon plus 23% carbon dioxide, ER70S-6 welding wire and 30in./min travel speed. (e) Photomicrograph showing the microstructure described as aligned carbide or upper bainite. The weld was made at 25V and 390A using argon plus 23% carbon dioxide and ER70S-3 welding wire. The travel speed was 15 in./min [142].

2.5 Summary

The addition of alloying elements to iron to accomplish a desired improvement in properties may require only a few tenths of one percent of the element. Sometimes improved properties are gained by a stringent reduction of a harmful element that may have previously been tolerated as a residual element. This is a relatively new approach in alloying technology, which can be credited with improving welding consumables.

The austenite to α -ferrite transformation behaviour is mainly affected by non-metallic inclusions, alloy additions, cooling rate and prior austenite grain size. Acicular ferrite usually nucleates on inclusions present in the columnar austenite grains, which stimulates other acicular ferrite plates to nucleate autocatalytically. Particles of titanium oxides and nitrides are most likely to nucleate acicular ferrite.

Literature Review

Published work relating to the influence of alloy additions on microstructural and mechanical properties of weld metal from gas-shielded welding processes has been reviewed. This revealed that detailed knowledge of the influence of alloying and microalloying elements on the weld microstructure and mechanical properties from these processes lags well behind that available for other welding processes, such as manual metal arc welding and submerged arc welding.

From this literature review, it is apparent that significant gaps exist in the detailed knowledge of the influence of alloying and microalloying on weld metal microstructure and mechanical properties for these processes. The purpose of the current investigation is to address this lack of information.

Chapter 3. Experimental Procedure

3.1 Manufacture of Special Wires

For the present investigation, special metal-cored wires were manufactured. Figure 3.1 shows the schematic diagram of the metal-core wire manufacturing process, while figure 3.2 shows the CSIRO MST wire mill, capable of producing small batches of cored wires for welding. Figure 3.3 shows the cross-section of a metal-core welding wire produced using the CSIRO MST wire mill.

The sheath material was cold-rolled mild steel of approximate composition 0.05% carbon, 0.22% manganese, 0.01% silicon and 0.015% aluminium. Core ingredients used included iron powder, silico-manganese, ferro-silicon, electrolytic manganese, titanium metal, aluminium metal and ferro-boron powders. All of these were commercial powders normally used for arc welding consumable manufacture. The wires were manufactured with a nominal core weight to total wire weight of 21% and were drawn to a final diameter of 1.6 mm.

Experimental Procedure

To calculate the final chemical composition of the weld metal for a given welding condition, the following procedure was used:

- (a) The metal transfer coefficient for each metal was determined using;

$$X_{\text{WELD METAL}} = \tau X_{\text{WIRE}} \quad (3.1)$$

τ = Metal Transfer Coefficient

X= wt % of alloy

- (b) The core composition of each alloying element was determined using;

$$X_{\text{WIRE}} = f X_{\text{CORE}} + (1-f) X_{\text{STRIP}} \quad (3.2)$$

f= Fill Ratio (21%)

After calculating the wt% alloy needed in the core for each alloy, the wire was manufactured, the weld metal deposited and its chemical composition checked. When the desired composition had been achieved a test plate was welded to confirm the analysis.

The content of the cores in the initial series of wires was varied to yield deposited weld metals containing nominally 0.35, 0.6 and 0.8 wt.% silicon. At each of these silicon levels different amounts of manganese were added to the core to produce three nominal levels of manganese in the deposited weld metals, 1.1, 1.4 and 1.6 wt.% manganese. In addition, the weld metal carbon content was maintained at a nominal level of 0.05 wt.%, for all wires.

Experimental Procedure

Whilst maintaining the manganese and silicon content of the wires constant to yield weld metal containing nominally 0.60 wt.% silicon and 1.34 wt.% manganese, different amounts of titanium, aluminium and boron were added to the core to produce eight levels of titanium, in the ranges 0.005 to 0.095 wt.%, six levels of aluminium, 0.013 to 0.065 wt.% and six levels of boron, 0.0005 to 0.018 wt.%, in the deposited weld metals.

Finally to study the combined effect of titanium and boron, a titanium-boron series of wires was manufactured. In this series, three levels of titanium 0.0054, 0.0230 and 0.0458 wt.% were studied. For each level of titanium two levels of boron 0.0005 and 0.0100% were used. Carbon, manganese and silicon levels were nominally constant at 0.04 to 0.05 wt.%, 1.26 to 1.49 wt.% and 0.58 to 0.68 wt.% respectively. The levels of the remaining metallic elements were relatively low and constant throughout the series.

Experimental Procedure

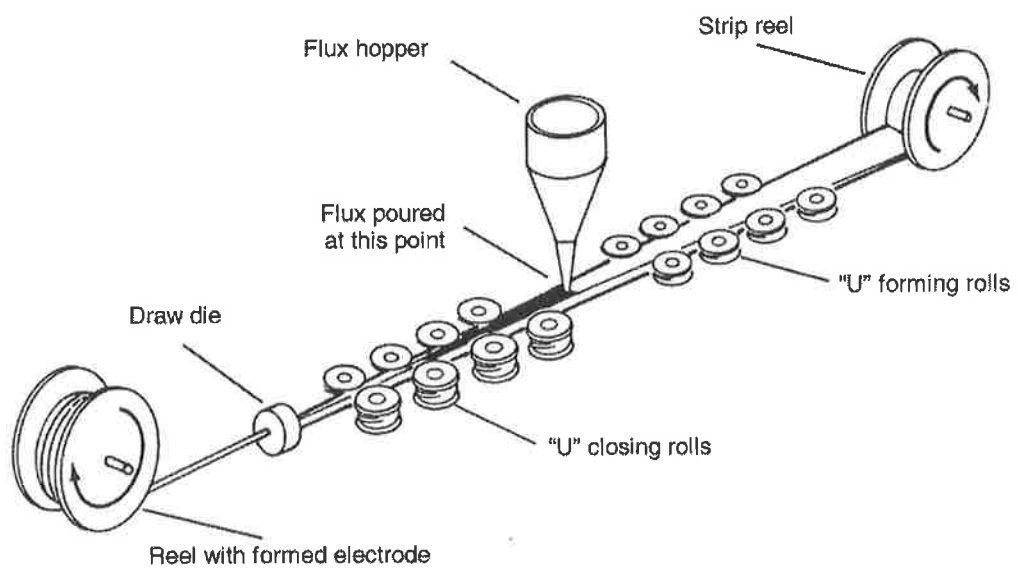


Figure 3.1: Schematic diagram of the metal-core wire manufacturing process.

Experimental Procedure

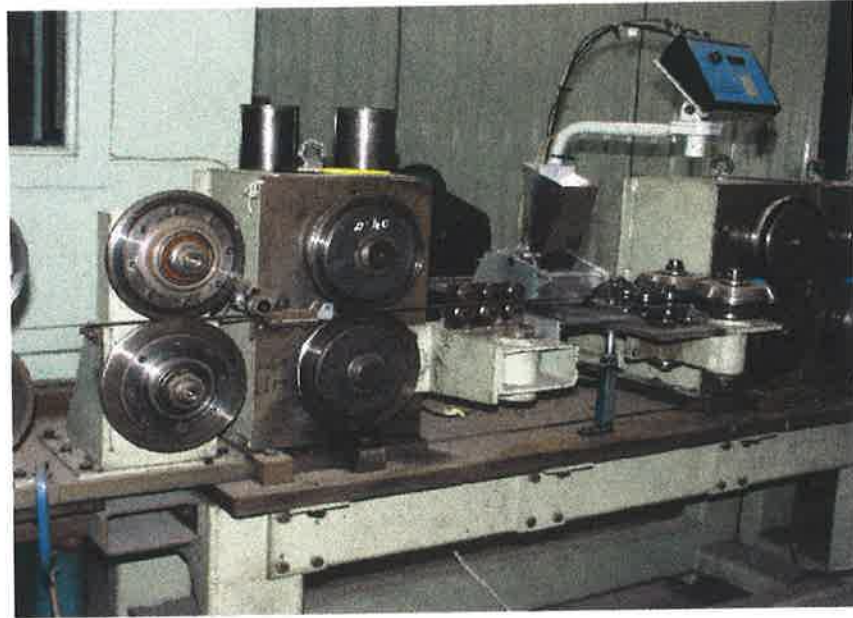


Figure 3.2(a) Sheath forming rolls.



Figure 3.2(b) Core metal powder feeder with electronic feed controller.

Experimental Procedure

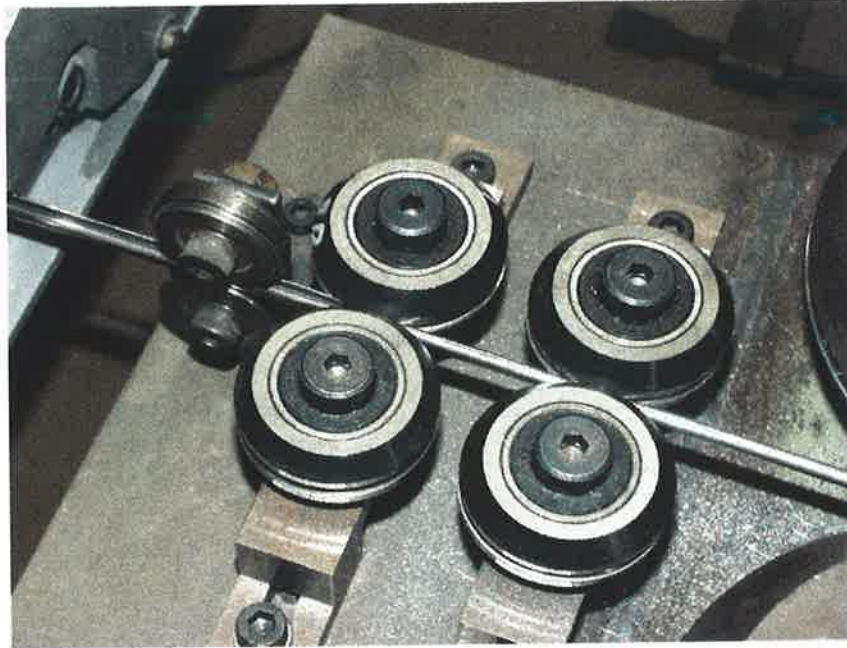


Figure 3.2(c) Closing rolls.

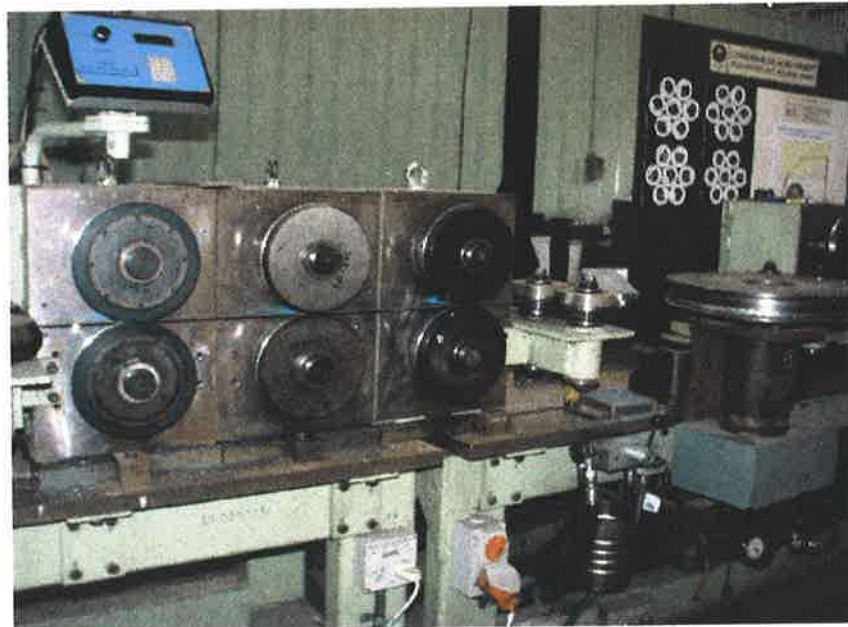


Figure 3.2(d) Reducing rolls.

Experimental Procedure



Figure 3.2(e) Three hydraulic power rollers to pull the wire.

Figures 3.2: Photographs (a)-(e) of CSIRO MST wire mill, for production of small batches of cored wires for welding.

Experimental Procedure

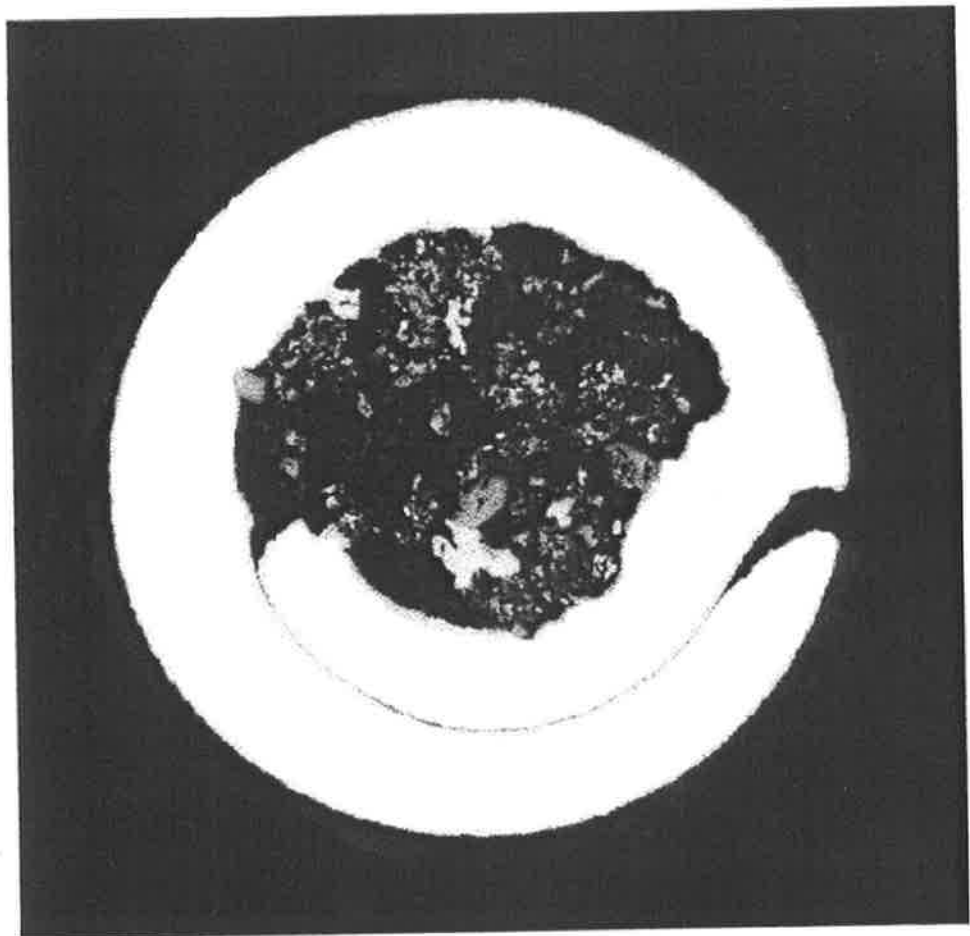


Figure 3.3: Cross-section of a metal-core welding wire produced using the CSIRO MST wire mill.

Experimental Procedure

3.2 Welding Procedure

The joint geometry shown in figure 3.4 (b) was used for all test-plates as this allowed a welding sequence comprising of three beads per layer to be used, as shown in the macrograph (figure 3.4 (a)). This permitted the placement of the notch in the impact specimens at the centre of the middle bead where there was approximately 60% as-welded and 40% reheated weld metal. The parent plate material was AS Grade 250 steel. Figure 3.5 shows micrographs of the base material used for all trials (etched in 2% nital) [143].

Welding was done in the flat position (1G) under mechanised conditions. The total number of passes required to fill the individual joints was 15. Direct current electrode positive was used with a welding current of 300A and a welding voltage of 30V. Heat-input was nominally 1.5 kJ/mm. The shielding gas used was argon with 5% CO₂. The inter-pass temperature was standardised at 150 °C.

Experimental Procedure

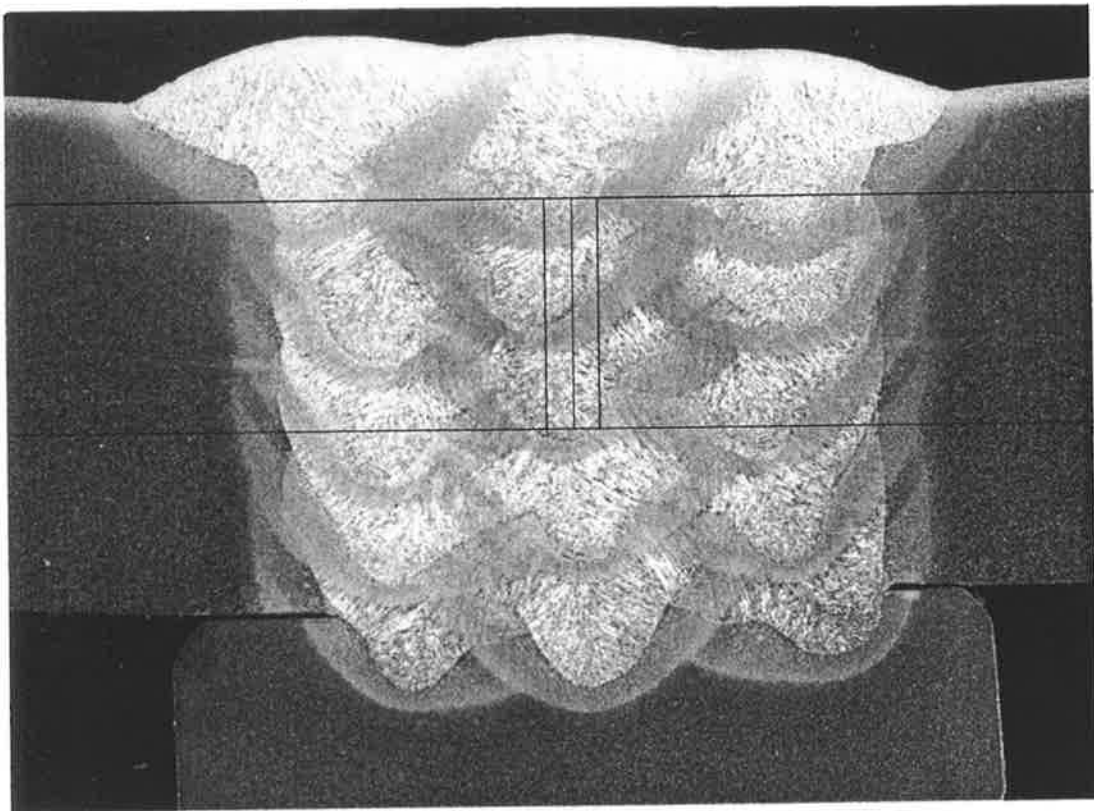
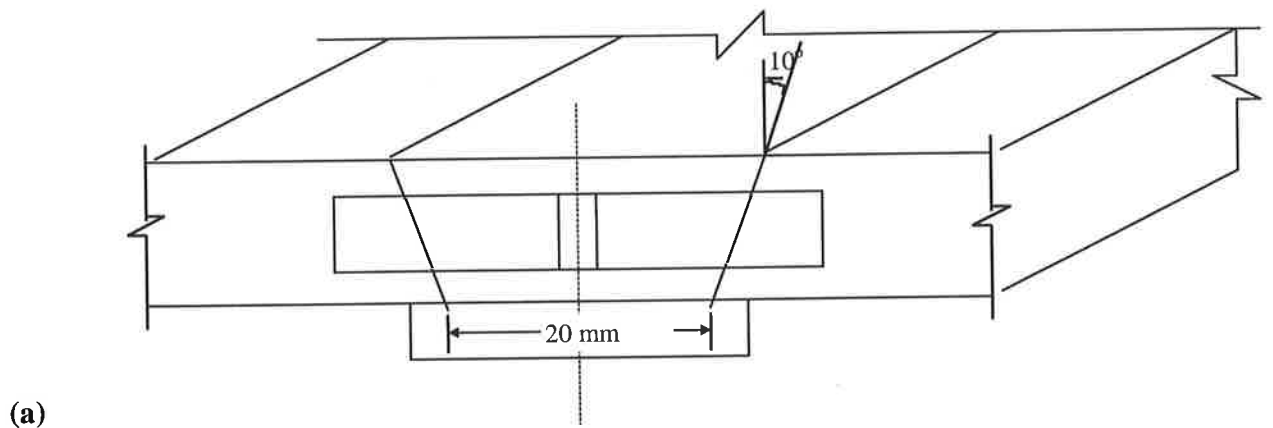
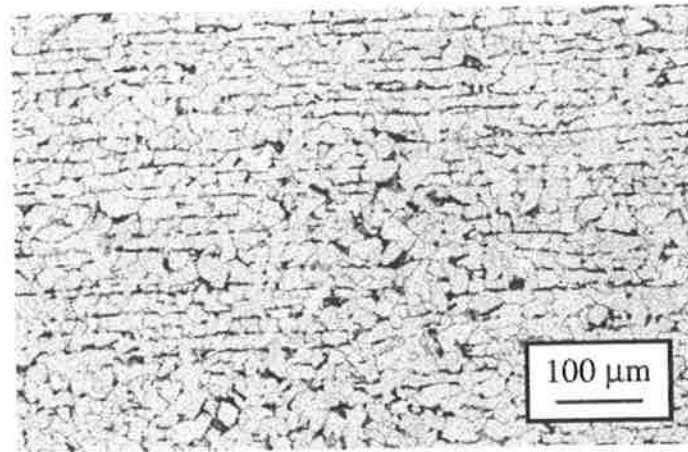
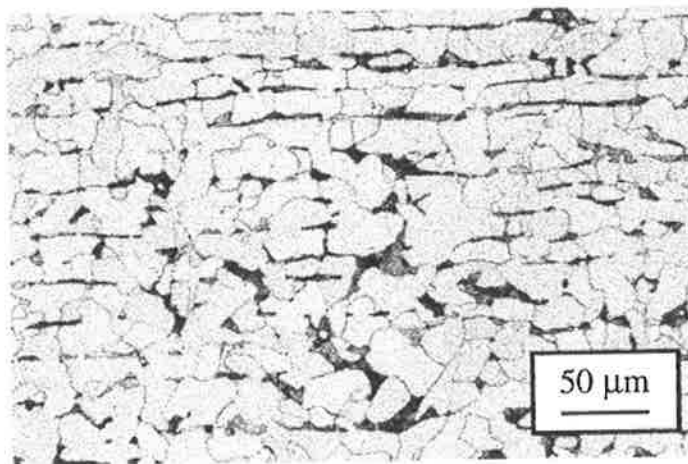


Figure 3.4: (a) Schematic diagram of a test-plate section showing the position of impact specimens and (b) macrograph of test-plate section showing bead placement and showing location of the impact specimen and the notch. Point count shows approximately 60% as-welded and 40% reheated weld metal exists in the notch area.

Experimental Procedure



(a) low magnification



(b) higher magnification

Figure 3.5: Micrographs of AS Grade 250 steel base material (etched in 2% nital).

Experimental Procedure

3.3 Weld Composition

Chemical analyses of the all-weld-metal deposits were carried out with an optical emission spectrometer. The vanadium, titanium, aluminium and boron contents of the experimental welds were determined to four decimal places so that small variations could be detected. Oxygen and nitrogen levels in the weld metal were determined using a Leco TC136 analyser.

3.4 Mechanical Testing

The impact toughness of each weld metal was assessed by the Charpy V-notch (CVN) test (as per AS1544.2 and AS2205.7.1). The (10×10mm) CVN specimens were orientated transverse to the welding direction and notched on the weld centre line with the notch axis perpendicular to the plate surface. Tests were carried out at -60, -40, -20, 0, and 20°C in order to obtain a transition curve for each weld. Three specimens were tested at each temperature and the mean absorbed energy calculated.

An all-weld metal tensile test was carried out (as per AS2205.2.2) on a tensile specimen of 10mm gauge diameter and 60mm gauge length extracted from each weld with the longitudinal axis of the specimen parallel to the longitudinal axis of the weld. These specimens were aged at 250 °C for 16 hours for hydrogen removal, prior to testing.

Experimental Procedure

3.5 Metallography

Transverse sections were prepared and detailed examination was carried out on the top beads and on the adjacent reheated zones. The specimens were mechanically polished to a 1 μ m diamond finish and weld metal microstructure revealed by etching in a 2% nital solution. The volume fraction of the different micro-constituents in each sample was obtained from point counts on more than 1000 points, using the IIW Guidelines (see figure 3.6) [71]. The prior austenite grain sizes were determined (as per AS1733-1976) by means of the mean linear intercept technique for all welds as were the lath widths of the acicular ferrite.

Experimental Procedure

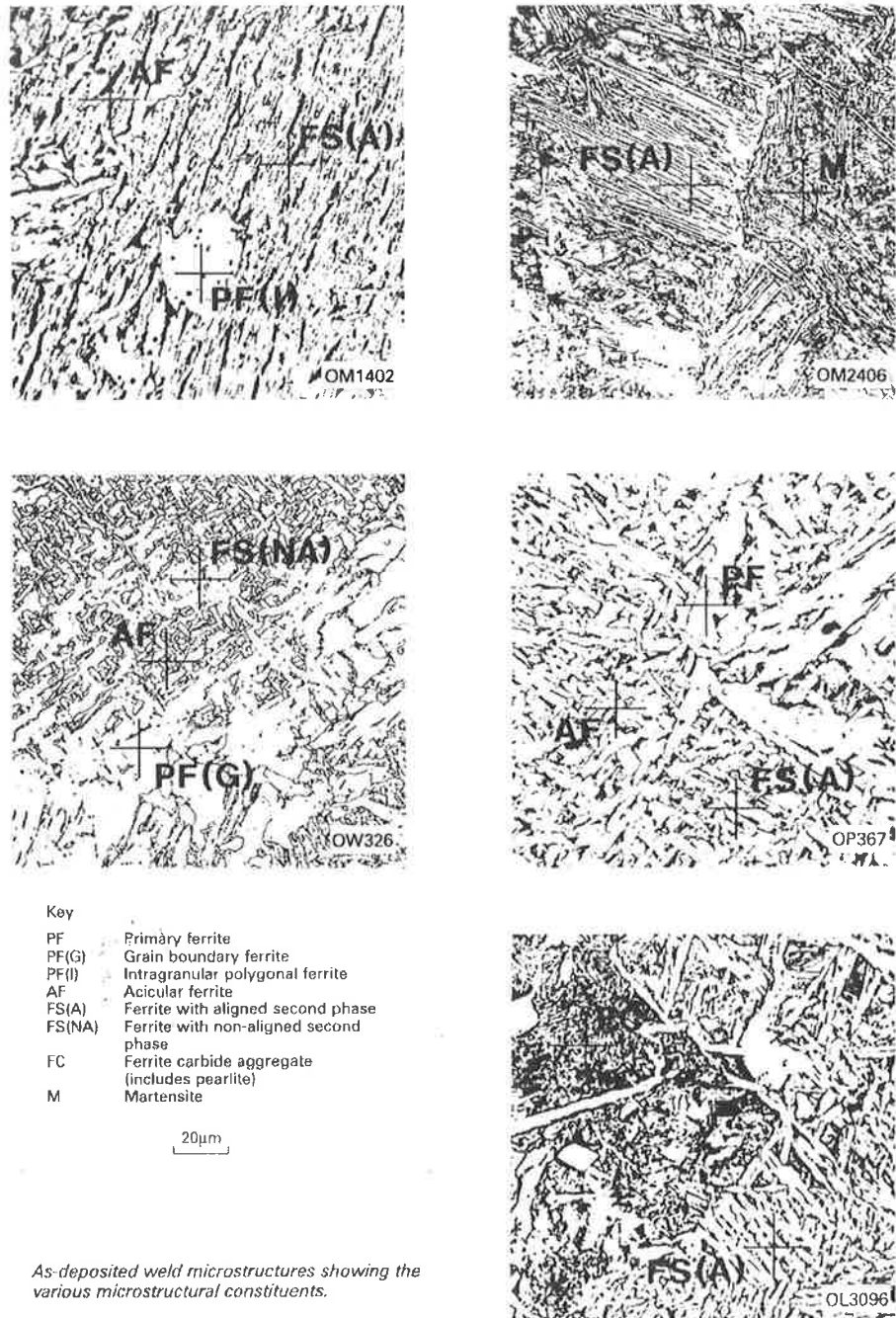


Figure 3.6: International Institute of Welding scheme for the classification of microstructures in C-Mn weld metals [71].

Experimental Procedure

3.6 Study of Inclusions

The size distribution and composition of non-metallic inclusions in polished specimens of the as-deposited weld metal were examined, using an SEM-based automatic image analyser. Inclusion size distributions were measured with a PHILIPS XL20 scanning electron microscope, with facilities for automatic image analysis (AIA), particle sizing and chemical analysis. The methods used were in line with those detailed in [144]. The AIA unit incorporates a computer interfaced digital beam control system and a software-based energy dispersive X-ray analysis system (EDAX) for micro-analysis. In the present investigation, a magnification of 10,000X, an accelerating voltage of 15kV, a grid point spacing of 0.02 μm and a working distance between 8 and 10 mm were used.

Chapter 4. Influence of Manganese and Silicon on Weld Metal Properties

4.1 Introduction

Gas-shielded flux cored arc welding (FCAW-G) is a widely used welding process because of its ease of use, high productivity and versatility. The main types of gas-shielded FCAW-G wires available are rutile-flux, basic-flux and metal-cored. Of these, metal-cored wires are popular for joining steels of thickness greater than about 3 mm because they offer a high deposition rate with semi-automatic or mechanised processes and give weld beads of good shape and minimal slag formation [145]. The core ingredients of metal-cored wires essentially consist of the required alloying powders (often present as ferro-alloys) and iron powder.

The applications for which metal-cored wires are suited often require premium weld metal mechanical properties in multi-pass welds. It is therefore important that the influence of alloying additions on mechanical properties of welds from such wires should be well understood so optimum wires can be produced for this high productivity process.

There is however only limited information available in the literature regarding the influence of alloy additions in the metal-cored arc welding system. That information which is available deals mainly with the influence of low levels of single elements, such as aluminium [120]. This is in contrast to the detailed information available for other arc welding systems, such as manual metal arc welding (MMAW) and submerged arc welding [146].

This chapter reports on a study of the influence of the major alloying/deoxidising elements, manganese and silicon, on the mechanical properties of weld metal from specially prepared metal-cored wires. The microstructural features of the welds have also been examined in order to better understand the relationship between alloy level and mechanical properties. The results are not only applicable to the metal-cored system but also have some applicability to the solid wire gas metal arc welding (GMAW) process since only metallic additions were made to the wires.

4.2 Results

4.2.1 Weld Metal Compositions

The chemical compositions of the all-weld-metal deposits studied are given in table 4.1. Carbon was essentially maintained at a constant level between 0.04 to 0.05wt%. Manganese and silicon levels were varied between 0.98 and 1.66wt% and 0.34 and 0.84wt% respectively. The levels of the remaining metallic elements were relatively low

Influence of Manganese and Silicon on Weld Metal Properties

and constant throughout the series with titanium being 0.004 to 0.006wt% and aluminium being 0.012 to 0.016wt%. The oxygen levels in the welds were relatively constant and were all in the range 0.042 to 0.057wt%. Oxygen level did not appear to be strongly dependent on manganese and silicon in the ranges tested although the highest oxygen did correspond to the lowest manganese and silicon.

Only the nitrogen level found in the welds appeared to vary unexpectedly between the test-plates. Most of the nitrogen values were in the range 0.004 to 0.01wt% which is considered normal for this type of weld and process. Three nitrogen values however were above 0.01wt% and are considered high for this process.

Influence of Manganese and Silicon on Weld Metal Properties

Table 4.1. Weld metal compositions (wt %).

Si	Mn	C	S	P	Ni	Cr	Mo	Cu	V	Nb	Ti	Al	B	O	N
0.34	0.98	0.05	0.009	0.018	0.02	0.01	<0.01	0.01	0.0100	<0.01	0.0040	0.0120	<0.0005	0.0570	0.0160
0.34	1.4	0.05	0.009	0.017	0.02	0.01	<0.01	0.01	0.0100	<0.01	0.0051	0.0139	<0.0005	0.0430	0.0041
0.39	1.50	0.04	0.012	0.014	0.03	0.01	<0.01	0.01	0.0067	<0.01	0.0050	0.0123	<0.0005	0.0550	0.0063
0.34	1.62	0.05	0.016	0.014	0.02	0.01	<0.01	0.01	0.0100	<0.01	0.0066	0.0162	<0.0005	0.0500	0.0090
0.57	1	0.04	0.007	0.016	0.02	0.01	<0.01	0.01	0.0063	<0.01	0.0045	0.0134	<0.0005	0.0470	0.0057
0.67	1.27	0.04	0.007	0.016	0.02	0.01	<0.01	0.01	0.0100	<0.01	0.005	0.0140	<0.0005	0.0420	0.0106
0.64	1.34	0.04	0.012	0.014	0.02	0.01	<0.01	0.01	0.0058	<0.01	0.0054	0.0133	<0.0005	0.0530	0.0047
0.57	1.64	0.04	0.007	0.016	0.02	0.01	<0.01	0.01	0.0100	<0.01	0.0060	0.0148	<0.0005	0.0480	0.0098
0.8	1.21	0.05	0.009	0.017	0.02	0.01	<0.01	0.01	0.0100	<0.01	0.0059	0.0158	<0.0005	0.0440	0.0080
0.84	1.66	0.05	0.014	0.017	0.02	0.01	<0.01	0.01	0.0080	<0.01	0.0060	0.0130	<0.0005	0.0480	0.0116

4.2.2 Mechanical Properties

4.2.2.1 Tensile Properties

The tensile test data are presented in table 4.2. The measured yield strengths varied between 460 and 550 MPa while tensile strengths varied between 500 and 600 MPa and elongations were between 14 and 30%.

Table 4.2. Weld metal tensile properties.

Silicon %	Manganese %	Yield Strength (MPa)	Tensile Strength (MPa)	Elongation (%)
0.34	0.98	469	523	21
0.34	1.4	473	525	26
0.39	1.50	499	541	29
0.34	1.62	519	573	28
0.57	1	459	504	30
0.67	1.27	521	574	14
0.64	1.34	507	557	29
0.57	1.64	549	588	28
0.8	1.21	510	574	18
0.84	1.66	531	601	27

A comparison of the weld compositions with strength levels in the 3x3 matrix of manganese and silicon, suggests the highest and lowest strengths generally correspond to

Influence of Manganese and Silicon on Weld Metal Properties

the highest and lowest manganese and silicon values in the matrix. This is borne out by conducting multiple linear regression analyses on the variation of yield strength (YS) and tensile strength (TS) with manganese and silicon levels in the welds. The analysis gave the following equations

$$YS = 82Mn + 67Si + 355 \quad (\text{MPa}) \quad (4.1)$$

$$TS = 77Mn + 101Si + 395 \quad (\text{MPa}). \quad (4.2)$$

The Coefficients of Determination (r^2 values) were 0.76 and 0.82 respectively indicating that the fit between strength values and manganese and silicon levels was reasonable. This fit was only improved marginally if weld metal nitrogen level was included in the regression.

Table 4.2 also shows that most of the elongation results are above 25% and are thus quite high. Three elongation values are however in the range 14 to 21%. These low values do not appear to be related to either alloy level or strength level of the deposits and may be caused by chance local defects like slag inclusion or porosity within the gauge length of the tensile specimens.

4.2.2.2 CVN Impact Results

The variations of mean CVN energy with test temperature for the various weld manganese levels at weld silicon levels of nominally 0.35wt%, 0.6wt% and 0.8wt% are plotted in

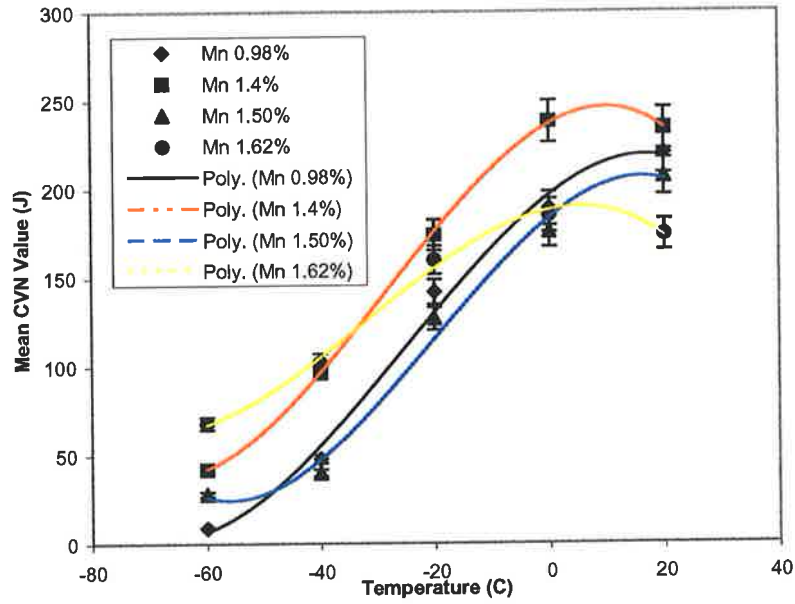
Influence of Manganese and Silicon on Weld Metal Properties

figure 4.1 (a), (b) and (c) respectively. At the lowest silicon level (figure 4.1 (a)) the upper shelf CVN energies are relatively insensitive to manganese content except for the highest manganese weld where this value is significantly lower. The temperatures at which 100J CVN values are achieved (T100J values) were best, at around -40°C , for welds with 1.4 and 1.62wt% manganese and slightly worse, at approximately -30°C , for the welds with 0.98 and 1.45wt% manganese. The lower shelf energy, or at least the energy at -60°C , was lowest for the weld with 0.98wt% manganese and highest for the weld with 1.62wt% manganese. Overall, the best impact properties at this silicon level were achieved with a weld manganese content of 1.4wt% although the differences were not large.

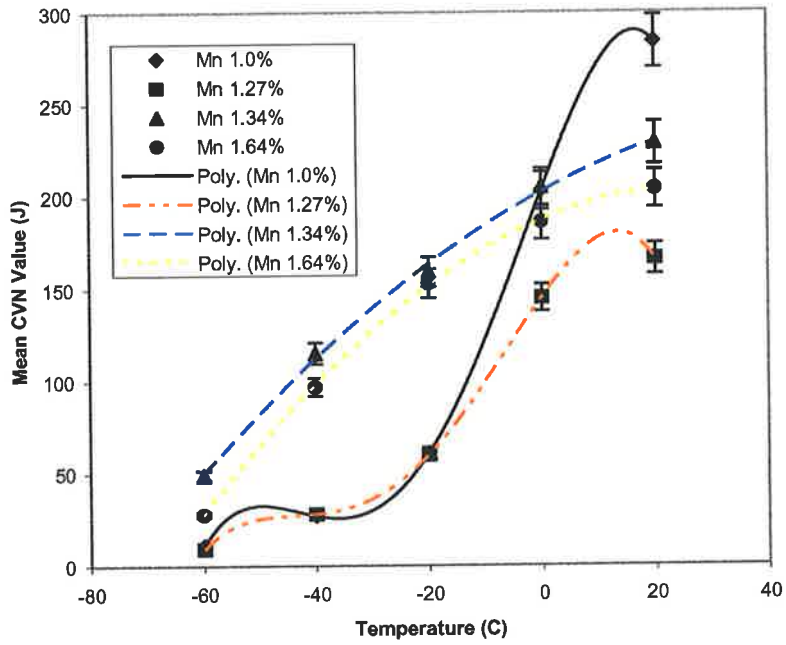
Differences in CVN properties with weld manganese are more distinct at weld silicon levels of nominally 0.6wt% (see figure 4.1 (b)). The highest upper shelf energy occurred with the lowest weld manganese value. The T100J values were considerably better for the welds containing 1.34 and 1.64wt% manganese compared to those for the welds with lower manganese (-45 to -40°C compared to -15 to -10°C). The best overall impact properties at this silicon level were achieved with 1.34wt% manganese.

Figure 4.1 (c) shows the impact properties recorded for weld silicon values of nominally 0.8wt%. In this case the impact energies for the weld with the lower manganese level were clearly improved over the whole temperature range compared to those from the high manganese weld. The T100J values, for example, were -30 and $+10^{\circ}\text{C}$ for the two welds. It should be noted however that, even for the lower manganese level, the upper shelf energy was not as high and the T100J was not as low as those achieved at lower silicon level.

Influence of Manganese and Silicon on Weld Metal Properties

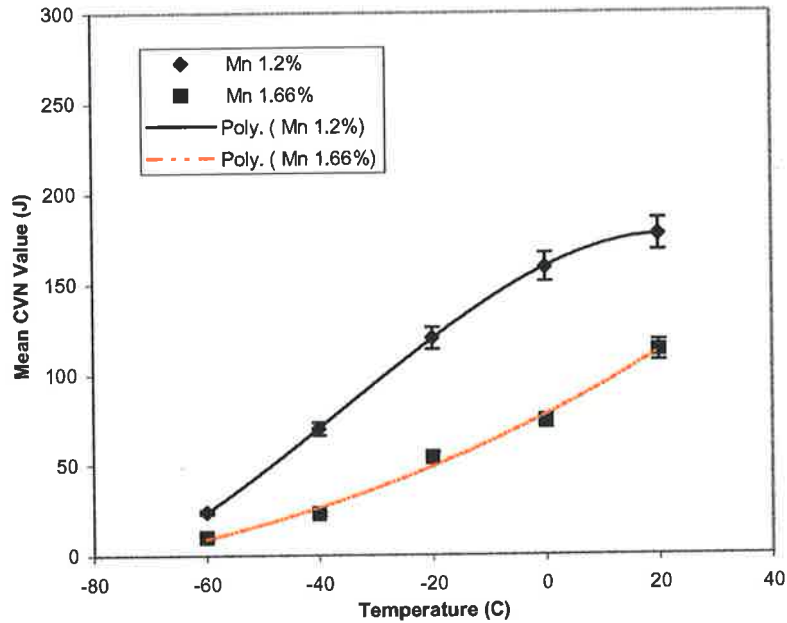


(a) 0.35wt% silicon



(b) 0.6wt% silicon

Influence of Manganese and Silicon on Weld Metal Properties



(c) 0.8wt% silicon.

Figure 4.1: Mean CVN impact energy as a function of temperature and manganese content for weld metals at different silicon contents.

4.2.3 Weld Metal Microstructure

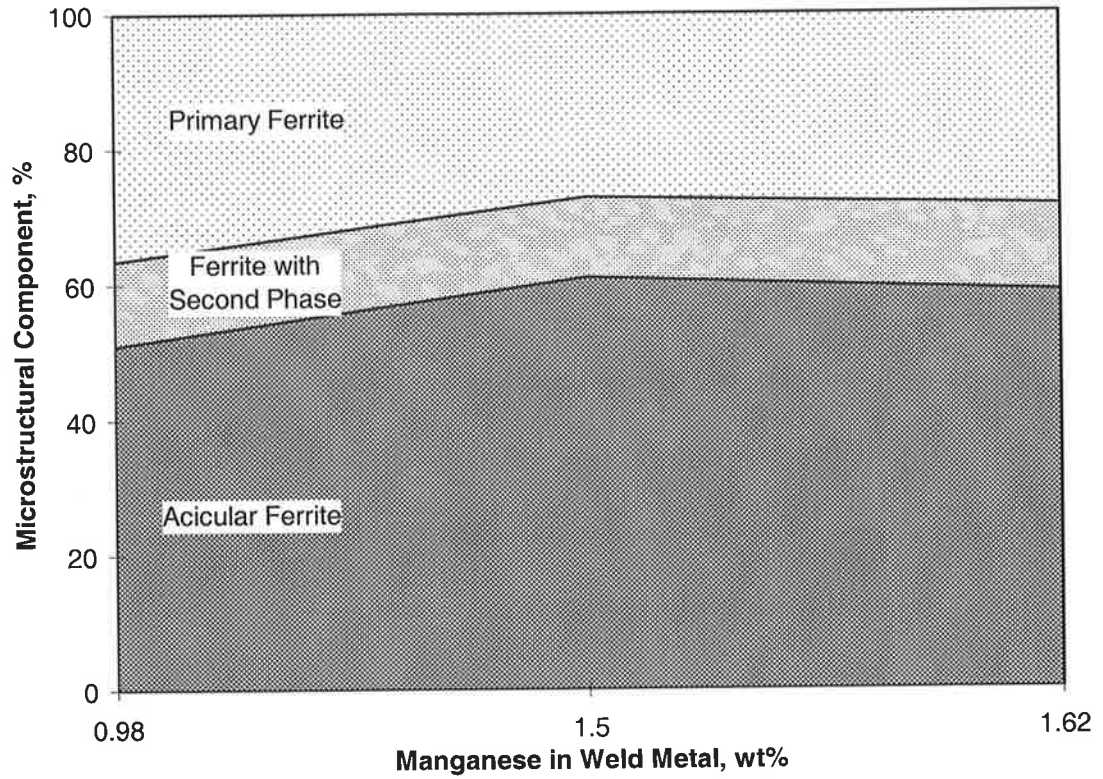
Area measurements from cross-sections of welds such as figure 3.4(a) indicated that the region of the weld from which mechanical test specimens (particularly CVN specimens) were extracted contained approximately 60% as-deposited and 40% reheated weld metal. Area fractions of acicular ferrite (AF), ferrite with second phase (FS) and grain boundary ferrite (PF(G)) were determined in as-deposited regions of the top layer from each weld.

Influence of Manganese and Silicon on Weld Metal Properties

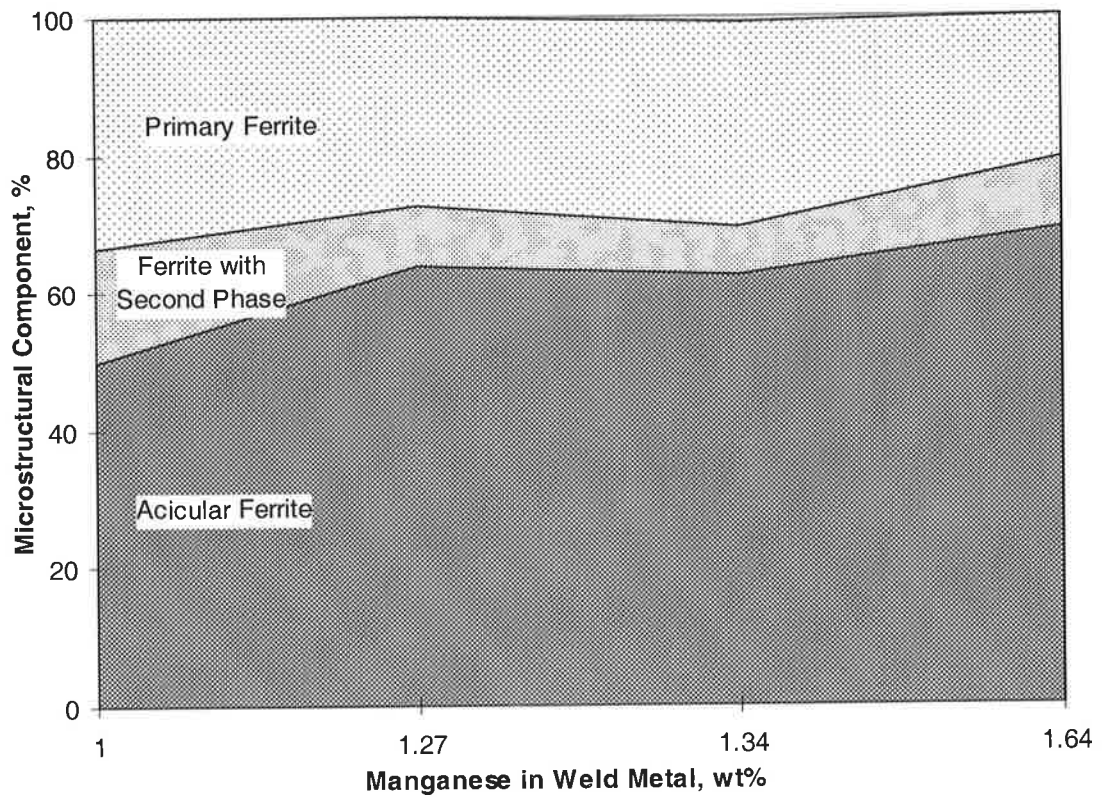
While reheated region below the top bead were used for comparing the grain size of reheated region.

Plots of the variation of percentage area of AF, FS and PF with weld manganese level for weld silicon levels of 0.35, 0.6 and 0.8wt% are shown in figure 4.2 (a), (b) and (c) respectively. These graphs show that area of AF tends to increase with manganese level in each case. The increase in AF with manganese level was more noticeable at higher silicon levels (0.6 and 0.8wt% silicon) where it increased from 50% to 68% as the manganese level increased from 1.0 to 1.8wt%. Across all welds the amount of AF only varied between 50 and 68% so the effect was relatively small. However, when the area of AF is plotted against weld manganese value, as shown in figure 4.3 the area of AF increases relatively linearly with manganese for all of the welds. The increase in area of AF with manganese appeared to be largely independent of silicon level (as shown in figure 4.4).

Influence of Manganese and Silicon on Weld Metal Properties

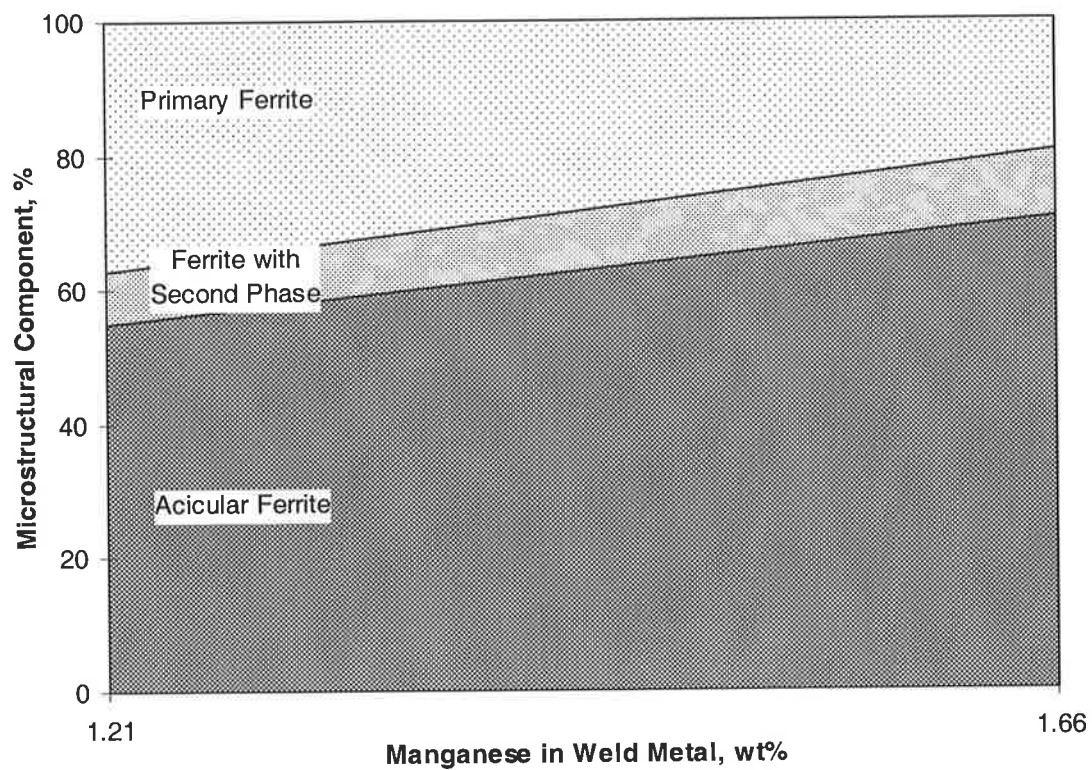


(a) 0.4wt% silicon.



(b) 0.6wt% silicon.

Influence of Manganese and Silicon on Weld Metal Properties



(c) 0.8wt% silicon.

Figure 4.2: Variation of the proportions of ferrite morphologies as a function of manganese contents in as-deposited weld metal at different silicon levels.

Influence of Manganese and Silicon on Weld Metal Properties

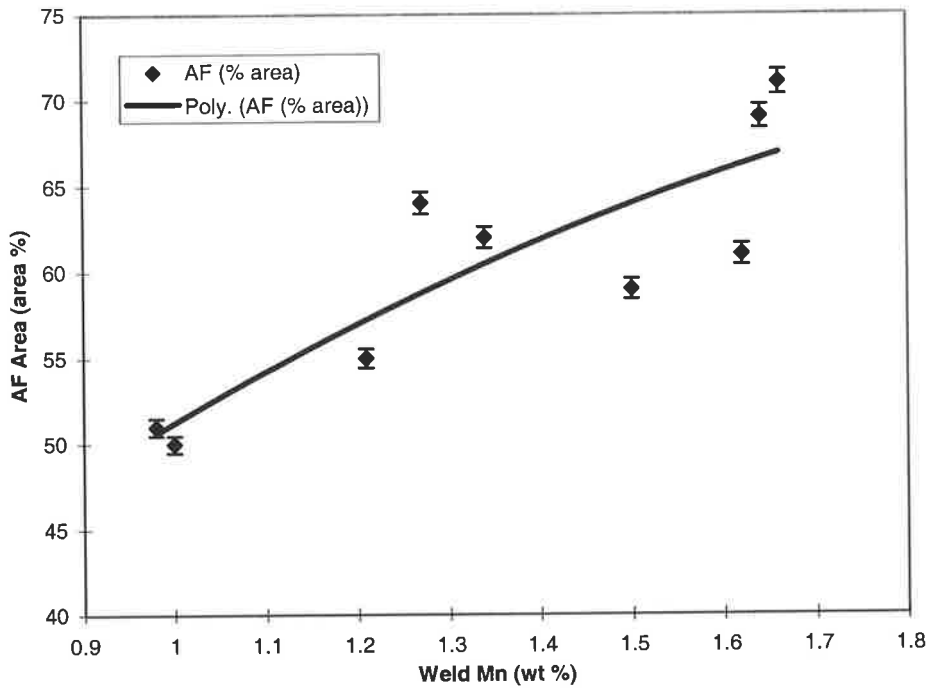


Figure 4.3: Variation of the proportion of acicular ferrite (AF) with weld metal manganese content across all silicon levels.

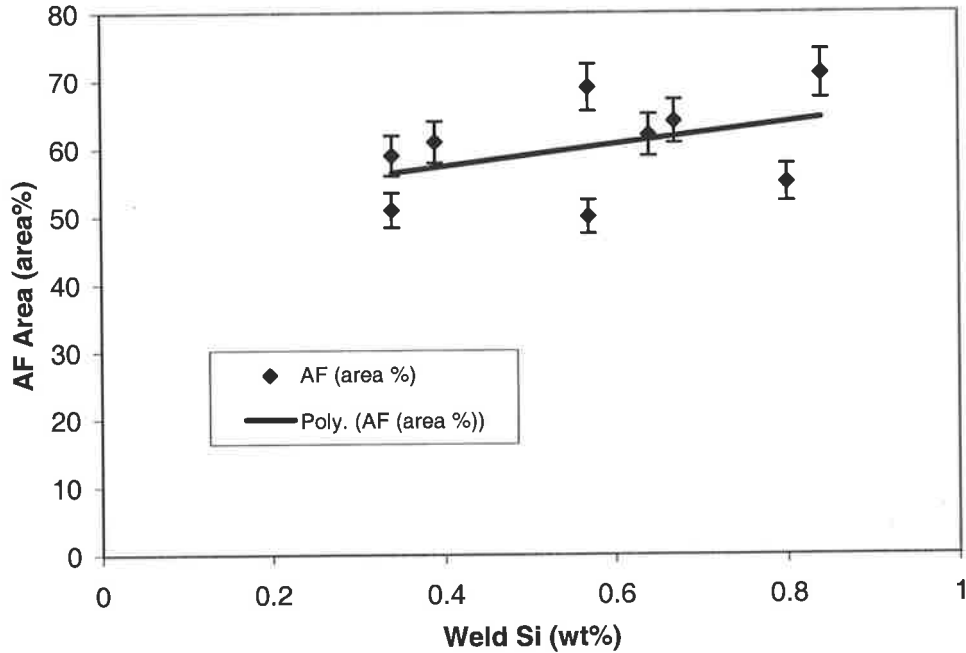


Figure 4.4: Variation of the proportion of acicular ferrite (AF) with weld metal silicon content across all manganese levels.

Influence of Manganese and Silicon on Weld Metal Properties

Figure 4.2 also shows that at all silicon levels the area of FS is relatively constant, ranging from 10 to 15wt% regardless of manganese level. The area of PF therefore decreases with manganese level over the approximate range 35 to 20wt% at all silicon levels.

In addition to these measurements of the area of the ferrite morphologies, measurements were also made of the prior austenite grain size and of the mean lath width of acicular ferrite. Prior austenite grain size was found to vary little over the manganese and silicon range tested as all of the measurements were in the range 135 to 150 μm . The lower values in this range did however tend to correspond with higher silicon levels. The values of AF lath width obtained together with the corresponding weld silicon and manganese values are listed in table 4.3. These show that AF lath width generally decreases with manganese level, although this decrease is not regular, and shows little dependence on silicon level.

Regions which had been reheated to above the upper critical temperature consisted essentially of equiaxed ferrite. Table 4.3 lists the mean grain size measurements made in these reheated regions. This suggests that the reheated grain size generally decreases as both the manganese and silicon levels increase.

Influence of Manganese and Silicon on Weld Metal Properties

Table 4.3: Acicular ferrite lath width and reheated grain sizes.

Si %	Mn %	Acicular Ferrite Lath Width (μm)	Grain Size of Reheated Zone (μm)
0.34	0.98	3.03	10.00
0.34	1.4	2.17	5.71
0.39	1.50	2.70	5.71
0.34	1.62	2.56	7.35
0.57	1	3.45	7.15
0.67	1.27	2.34	5.56
0.64	1.34	2.86	5.13
0.57	1.64	2.22	4.88
0.8	1.21	2.34	6.06
0.84	1.66	2.22	4.55

4.2.4 Non-metallic Inclusions

Table 4.4 lists the details of the non-metallic inclusions, including number per unit volume, mean three dimensional diameters and percentage with diameter equal or larger than $1\mu\text{m}$ for each weld, as measured using the SEM with automated image analyser. The number of inclusions per mm^3 and the mean diameter only vary over small ranges for the manganese and silicon levels tested and there is little dependence of these parameters on manganese or silicon values. The percentage of larger inclusions, although varying between 1 and 3.5%, appears to be independent of manganese or silicon level.

Mean non-metallic inclusion compositions, as measured using energy dispersive X-ray analysis in an SEM, are also listed in table 4.4. Inclusions in this wire, with varying manganese and silicon contents, have at least four major components MnO , SiO_2 , Al_2O_3 and TiO_2 . Mean non-metallic inclusion compositions indicate that there are no major changes in composition of inclusions with weld metal manganese or silicon level. The level of MnO in $(\text{MnO}.\text{SiO}_2)$ inclusion increase slightly with an increase in weld manganese at the expense of inclusion SiO_2 level but the changes are small. There is little evidence of any change in Al_2O_3 or TiO_2 level.

Influence of Manganese and Silicon on Weld Metal Properties

Table 4.4: Non-metallic inclusions.

Weld Si Contents wt%	Weld Mn Contents wt%	Number/ Cubic mm (x 10 ⁷)	Mean 3D Dia (μm)	Percent > 1μm Dia	Composition of Inclusions (wt%)			
					SiO ₂	MnO	Al ₂ O ₃	TiO ₂
0.34	0.98	7.98	0.46	1.25	35.8	43.7	12.2	3.6
0.34	1.5	9.89	0.39	1.25	29.6	45.8	15.3	3.7
0.39	1.62	8.8	0.46	3	32.1	54	9.1	4.4
0.57	1	5.39	0.54	1	35.7	35.3	21.2	4.4
0.67	1.27	8.91	0.43	1.25	32.6	41.1	17.7	4.7
0.64	1.34	4.86	0.58	3.5	34.5	46.7	14.1	3.8
0.57	1.64	6.77	0.51	2	31.4	45.3	15.2	3.8
0.8	1.21	7.56	0.49	1	33	39.3	18.2	5.5
0.84	1.66	7.4	0.49	2	33.9	40.6	17	3.6

4.3 Discussion

4.3.1 Weld Metal Tensile Properties

Both yield strength and tensile strength increase in a regular manner with weld manganese and silicon levels as indicated by equations (4.1) and (4.2). This essentially linear increase in weld strength levels with manganese and silicon has been observed previously for other arc welding processes such as MMAW [7,9].

The most likely explanation of the behaviour of yield and tensile strengths lies in the general decrease in effective grain size, over both as-deposited and reheated regions, with an increase in manganese and silicon. In the as-deposited weld metal not only does the proportion of the fine grained AF increase, particularly with manganese level (see figure 4.2) but the lath size of this AF also decreases with manganese and silicon levels as shown in table 4.3. In addition, the grain size of the reheated regions was also found to decrease with manganese and silicon (see table 4.3).

4.3.2 Weld Metal Impact Properties

In order to gain an overall view of the influence of weld manganese and silicon levels on the low temperature impact properties, the T100J values obtained from figure 4.1 have been plotted against manganese and silicon values (figure 4.5). Figure 4.5 shows that

Influence of Manganese and Silicon on Weld Metal Properties

although there is some variability in the results, a pattern is apparent. A zone of manganese and silicon values exists between approximately 0.3 to 0.65wt% silicon and 1.3 to 1.6wt% manganese in which the premium impact properties are obtained with the best T100J value occurring at around 0.6wt% silicon and 1.3wt% manganese. A zone of intermediate level impact properties occurs at manganese values less than 1.3wt% over the whole range of silicon values while the worst impact values occur in the high silicon - high manganese corner of the diagram. This information is valuable for the design of consumables as it defines a weld composition zone for optimum impact properties. It is also worth commenting that the impact properties obtained from these special metal cored wires with weld compositions in this zone are generally better than those from commercial metal cored wires of similar strength level [9].

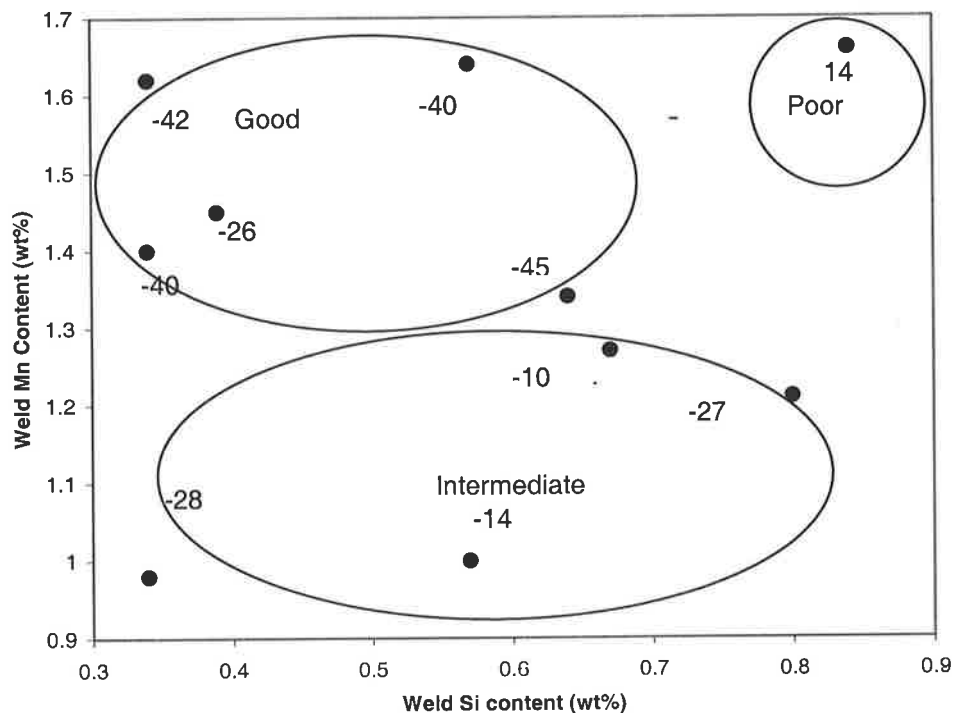


Figure 4.5. Plot showing the T100J values as a function of weld metal manganese and silicon contents

Influence of Manganese and Silicon on Weld Metal Properties

An explanation of these impact results in terms of the microstructural, or non-metallic inclusion observations is more complex. The microstructural features which are most frequently said to be related to low temperature impact properties include the proportion of AF in as-deposited regions [89]; the lath size of the AF [147]; the proportion of reheated material and the grain size in the reheated regions. In terms of inclusions, those features which are frequently said to relate to impact properties include indirectly, inclusions suitable for the nucleation of AF [116], and directly, the size distribution of inclusions as larger ones tend to initiate cleavage fracture [148].

In the present case, the proportion of AF can only partly account for the observed impact properties. The AF proportion tends to increase with manganese level (see figure 4.3) so there is some correlation with T100J. However AF only changes within a narrow range and the highest AF values are obtained at the highest manganese and silicon values where impact properties are poorest. Such observations have been made previously [9, 149] where it has been suggested that silicon in particular increases the amount of microphases present in both as-deposited and reheated regions leading to a decrease in cleavage resistance.

Lath size in the AF was found to generally decrease with alloy, particularly manganese level (see table 4.3), so that again the correlation with T100J value is at best partial since the smallest lath size occurs at the highest manganese and silicon contents where impact properties are poorest.

The proportion of reheated material is nominally constant for this series of trials so this should not influence the impact results. As shown in table 4.3 the grain size in reheated

Influence of Manganese and Silicon on Weld Metal Properties

zones did decrease with manganese and silicon levels. This grain size does not show a good correlation with impact properties however as the finest grain size corresponds with the poorest impact properties.

Another factor which can influence impact properties in some instances is the weld metal nitrogen level [150]. There were significant differences in this level between welds in these trials (see table 4.2). Comparison of the weld nitrogen values with the weld impact properties as summarised in figure 4.4 gives mixed signals regarding the significance of the affect. For example, two welds with silicon levels of about 0.35wt% and manganese levels of about 1.4wt% gave very similar T100J values (-40 and -42°C) even though the nitrogen levels are 0.004 and 0.009wt%. On the other hand, two welds with similar silicon and manganese values of approximately 0.65% and 1.3wt%, and nitrogen levels of 0.005 and 0.011wt%, gave T100J values of -45 and -10°C respectively. The question of the importance of nitrogen level on impact properties in this instance is therefore not fully answered and should be further investigated.

The data on non-metallic inclusion populations within the welds, as listed in table 4.4, do not appear to show any trends which indicate an effect on impact properties as the values obtained appear to vary randomly within small ranges. Similarly, the composition of these inclusions does not appear to provide a relationship to the impact properties since these also appear to vary randomly within tight ranges. Except for the number density of inclusions with diameter >1µm, which shows an increase with increasing manganese content for all silicon levels in the weld metal as shown in figure 4.6. The N>1µm values

Influence of Manganese and Silicon on Weld Metal Properties

were calculated from the product of overall number density and the percentage with diameter greater than $1\mu\text{m}$ values.

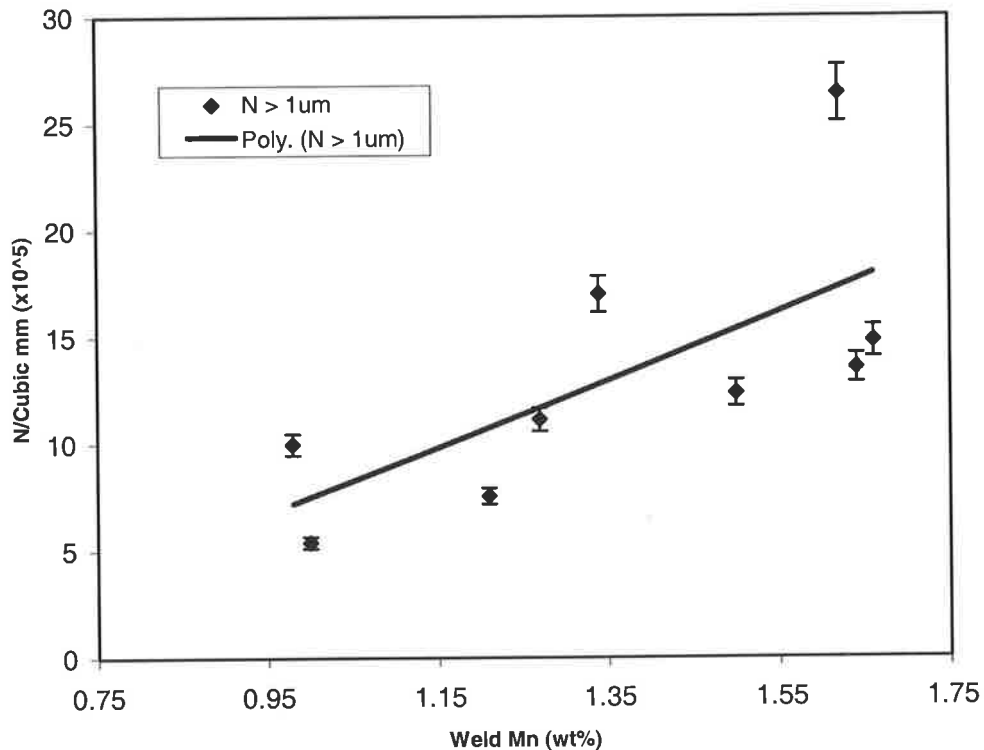


Figure 4.6: Number density of inclusions with diameter $> 1\mu\text{m}$ as a function of increase in manganese for all silicon levels in the weld metal.

It is known that non-metallic inclusions play two distinct roles in weld metals. Smaller inclusions, of around $0.4\mu\text{m}$ in diameter, have been identified as efficient nucleation sites for AF [151]. Larger inclusions, of $1\mu\text{m}$ or greater diameter, have been shown to be initiation sites for cleavage fracture [152] which is the main fracture mode for impact at low temperatures.

Influence of Manganese and Silicon on Weld Metal Properties

The premium low temperature impact properties were obtained with manganese contents between 1.3 and 1.6wt%, provided the silicon level was less than about 0.7wt% while poorer impact properties were found with manganese contents less than 1.3wt% and high manganese and silicon contents. The main features of the observed low temperature impact behaviour may, to a reasonable extent in the case of manganese and silicon, be explained on the basis of the interaction between following factors:

1. increase in both yield strength and tensile strength with weld manganese and silicon levels;
2. the proportion of PF decreasing;
3. the proportion of AF increasing;
4. decrease in AF lath size;
5. decrease in re-heated grain size; and,
6. the number density of large inclusions increasing.

With decrease in the proportion of PF associated with increase in the proportion of AF with increase in manganese and silicon in weld metal and also continuous refinement of AF lath size and re-heated grain size with increase in alloying, the low temperature impact properties may be expected to be continually improved over the range of alloying.

The inclusions with diameter greater than $1\mu\text{m}$ ($N > 1\mu\text{m}$) at all manganese and silicon level will also be present in the 40% reheated region and could adversely affect the T100J temperature. Another factor that undoubtedly influence weld metal impact properties is

Influence of Manganese and Silicon on Weld Metal Properties

increasing weld metal strength, which generally has a deleterious effect on impact properties.

Consequently, while low temperature impact properties may be expected to be continually improved by lower proportion of PF, higher levels of AF and refinement of AF lath size and re-heated grain size, this effect is offset by an increase in both yield strength and tensile strength and the increased number of the large inclusions in the weld metal available to nucleate and propagate the cleavage fracture.

These observations suggest that low manganese contents did not result in sufficient AF and grain refinement to give optimum low temperature impact properties. High manganese and silicon contents resulted in high values of both inclusions ($N > 1\mu\text{m}$) and weld strength thus degrading the impact properties. The optimum levels as shown in figure 4.5 occur at manganese contents between 1.3 and 1.6wt%, and the silicon level less than about 0.7wt%.

Chapter 5. Influence of Titanium and Aluminium on Weld Metal Properties

5.1 Introduction

In the previous chapter the influence of manganese and silicon levels on weld metal properties in this metal-cored system concluded that the low temperature impact properties are optimum when manganese is between 1.3wt% and 1.6wt% and silicon is between 0.3wt% and 0.6wt%. Abson [120] studied the effect of aluminum on metal-cored wires and observed changes in strength and microstructure. In this instance cleavage resistance changed little with the lowest aluminum additions, before decreasing with the highest aluminum addition, aluminum additions were generally detrimental to upper-shelf fracture toughness.

Observations from other arc welding processes indicate that acicular ferrite in as-deposited regions has a major influence on weld mechanical properties and that the formation of acicular ferrite depends on micro-alloy/de-oxidant additions, most notably aluminum and titanium [153]. Evans [115] investigated the effects of titanium and aluminum micro-alloying on toughness for multi-pass basic flux MMA weld deposits.

Influence of Titanium and Aluminum on Weld Metal Properties

Titanium was found to be the most effective element for enhancing the toughness of as-welded deposits. However adding aluminum powder when 0.0035wt% titanium was present degraded toughness at all aluminium levels higher than 0.008wt%.

Non-metallic inclusions can have either a beneficial or detrimental effect on the microstructure and mechanical properties of the weld metal [154]. The major beneficial effect of inclusions is the nucleation of acicular ferrite. However larger inclusions may promote fracture by providing nucleation sites for cleavage cracking in the weld metal [148,155,156].

This chapter reports a study of the influence of titanium and aluminum on the mechanical properties of weld metal from specially prepared metal-cored wires in which the major alloying/deoxidising elements, manganese and silicon, were kept nominally constant at the optimum level for this system as found in the previous chapter. The microstructural features of the welds have been examined to provide a better understanding of the relationship between alloy level and mechanical properties. The results are not only applicable to the metal-cored system but also have some applicability to the solid wire gas metal arc welding (GMAW) process since only metallic additions were made to the wires.

5.2 Results

5.2.1 Weld Metal Compositions

The chemical compositions of the all-weld-metal deposits studied are given in table 5.1 for the titanium series and in table 5.2 for the aluminum series. Carbon, manganese and silicon levels were nominally constant at 0.04wt% to 0.06wt%, 1.15wt% to 1.38wt% and 0.52wt% to 0.77wt% respectively. The levels of the remaining metallic elements were relatively low and constant throughout the series. In the titanium series, titanium was varied between 0.005wt% and 0.094wt% while in the aluminum series, aluminum was varied between 0.013wt% and 0.064wt%. For the titanium series, the oxygen levels in the welds decreased from 0.053wt% to 0.038wt% as the titanium level increased, while for the aluminum series oxygen level was relatively constant and were all in the range 0.053wt% and 0.065wt%.

The nitrogen levels found in the welds of both the titanium and aluminum series were essentially constant. Most of the nitrogen values were in the range 0.004wt% to 0.008wt% which is considered normal for this type of weld and process. One nitrogen value however was above 0.01wt% and is considered high for the process.

Influence of Titanium and Aluminum on Weld Metal Properties

Table 5.1: Weld metal compositions (wt %) with varying titanium levels.

Si	Mn	C	S	P	Ni	Cr	Mo	Cu	V	Nb	Ti	Al	B	O	N
0.64	1.34	0.04	0.012	0.014	0.02	0.01	<0.01	0.01	0.0058	<0.01	0.0054	0.0133	<0.0005	0.0530	0.0047
0.55	1.30	0.05	0.008	0.015	0.02	0.01	0.01	0.010	0.0059	<0.01	0.0124	0.0132	<0.0005	0.0450	0.0040
0.58	1.26	0.05	0.011	0.013	0.02	0.01	0.01	0.01	0.0058	<0.01	0.0273	0.0142	<0.0005	0.0420	0.0054
0.66	1.38	0.05	0.011	0.013	0.02	0.01	0.01	0.01	0.0066	<0.01	0.0458	0.0111	<0.0005	0.0380	0.0037
0.56	1.24	0.05	0.010	0.012	0.02	0.01	<0.01	0.02	0.01	<0.01	0.0588	0.0161	<0.0005	0.0380	0.0070
0.60	1.32	0.05	0.013	0.014	0.02	0.01	0.01	0.01	0.01	<0.01	0.0852	0.0147	<0.0005	0.0400	0.0038
0.63	1.27	0.05	0.012	0.012	0.02	0.01	0.01	0.02	0.01	<0.01	0.0910	0.0164	<0.0005	0.0400	0.0080
0.63	1.27	0.06	0.011	0.012	0.02	0.01	<0.01	0.02	0.01	<0.01	0.0940	0.0132	<0.0005	0.0430	0.0130

Influence of Titanium and Aluminum on Weld Metal Properties

Table 5.2: Weld metal compositions (wt %) with varying aluminum levels.

Si	Mn	C	S	P	Ni	Cr	Mo	Cu	V	Nb	Ti	Al	B	O	N
0.64	1.34	0.04	0.012	0.014	0.02	0.01	<0.01	0.01	0.0058	<0.01	0.0054	0.0133	<0.0005	0.0530	0.0047
0.61	1.32	0.06	0.024	0.015	0.05	0.03	0.02	0.01	0.0055	<0.01	0.0060	0.0190	<0.0005	0.0580	0.0048
0.60	1.29	0.05	0.020	0.017	0.05	0.03	0.03	0.01	0.0057	<0.01	0.0049	0.0320	<0.0005	0.0650	0.0065
0.77	1.38	0.05	0.020	0.018	0.05	0.03	0.02	0.01	0.0067	<0.01	0.0058	0.0495	<0.0005	0.0530	0.0054
0.52	1.15	0.06	0.016	0.018	0.05	0.03	0.02	0.01	0.0053	<0.01	0.0050	0.0570	<0.0005	0.0580	0.0045
0.68	1.35	0.05	0.013	0.018	0.05	0.03	0.01	0.01	0.0065	<0.01	0.0058	0.0642	<0.0005	0.0580	0.0068

5.2.2 Mechanical Properties

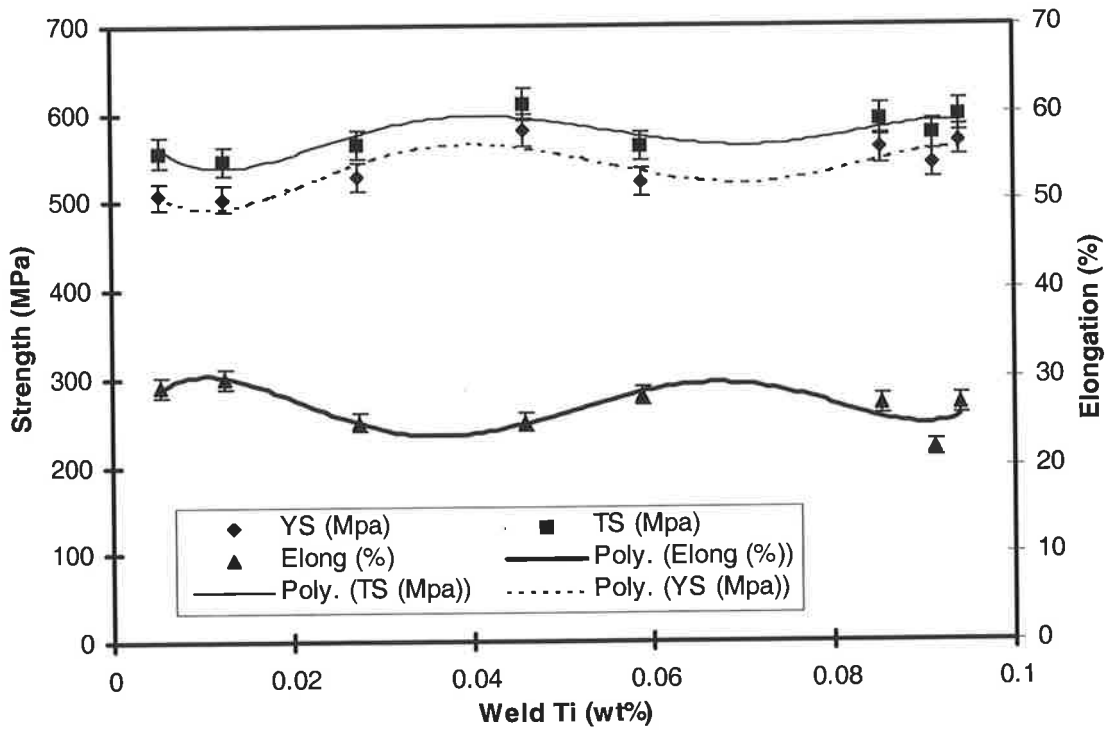
5.2.2.1 Tensile Properties

The tensile test data are presented in figure 5.1 (a) and (b). For the titanium series, the measured yield strengths varied between 504MPa and 581MPa, while tensile strengths varied between 547MPa and 610MPa and elongations were between 22% and 30%. For the aluminum series, yield strengths varied between 475MPa and 531MPa, while tensile strengths varied between 522MPa and 565MPa and elongations were between 16% and 29%. figure 5.1(a) shows that both yield and tensile strength increase approximately linearly with titanium content by about 50MPa over the range of titanium values, while elongation tended to decrease. For the aluminum series, figure 5.1(b) suggests yield and tensile strengths are independent of aluminum content over the range tested although elongation tended to decrease.

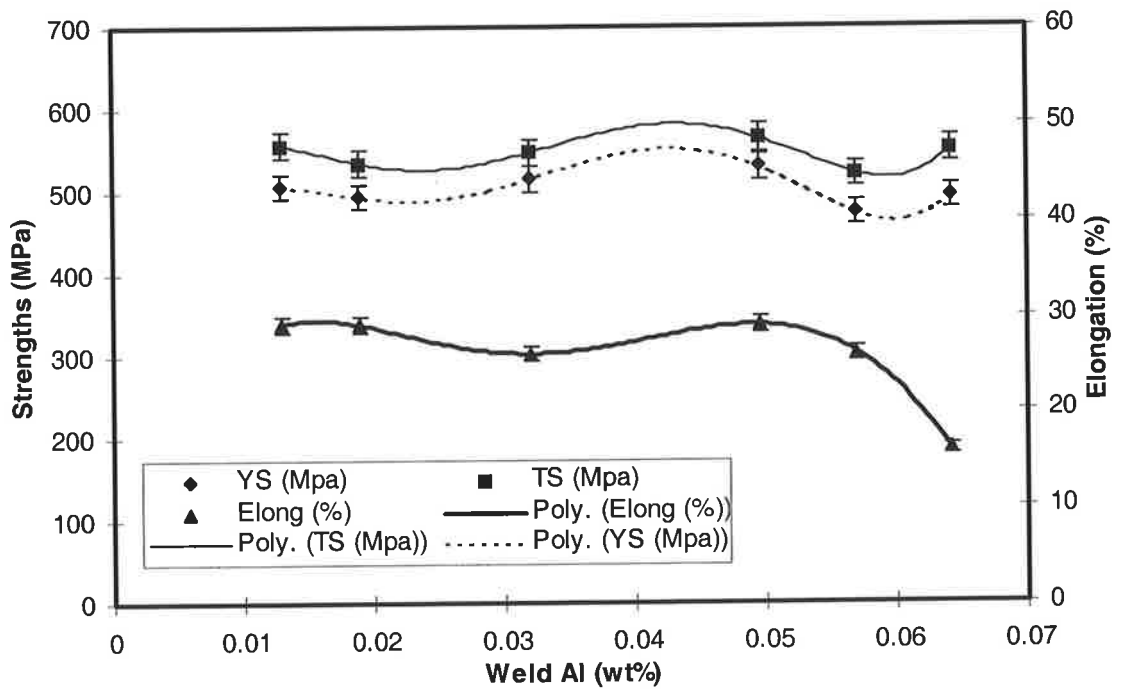
5.2.2.2 CVN Impact Results

The variations of mean CVN energy with test temperature for the various weld titanium and aluminum levels are plotted in figure 5.2(a) and (b) respectively. For the titanium series, mean CVN energies at lower temperatures appear best at 0.005wt% and 0.085wt% titanium levels. For the aluminum series mean CVN energies across the temperature range are best at 0.0133wt% aluminum level.

Influence of Titanium and Aluminum on Weld Metal Properties



(a) titanium content in weld metal.



(b) aluminum content in weld metal.

Figure 5.1: Variations in yield, tensile strength and percent elongation as a function of (a) titanium and (b) aluminum content in weld metal.

Influence of Titanium and Aluminum on Weld Metal Properties

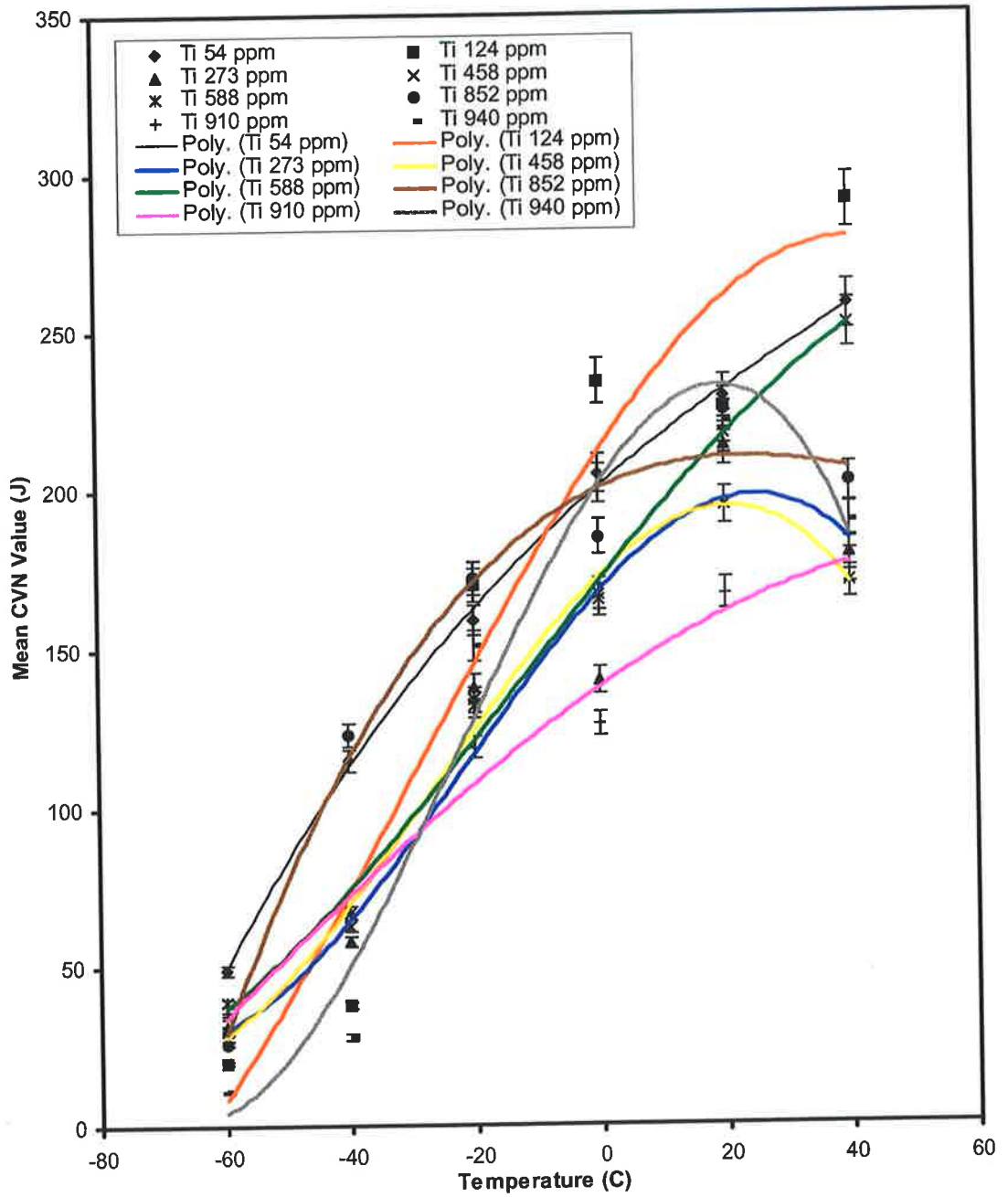


Figure 5.2(a): Mean CVN impact energy as a function of temperature for the various titanium levels in weld metal.

Influence of Titanium and Aluminum on Weld Metal Properties

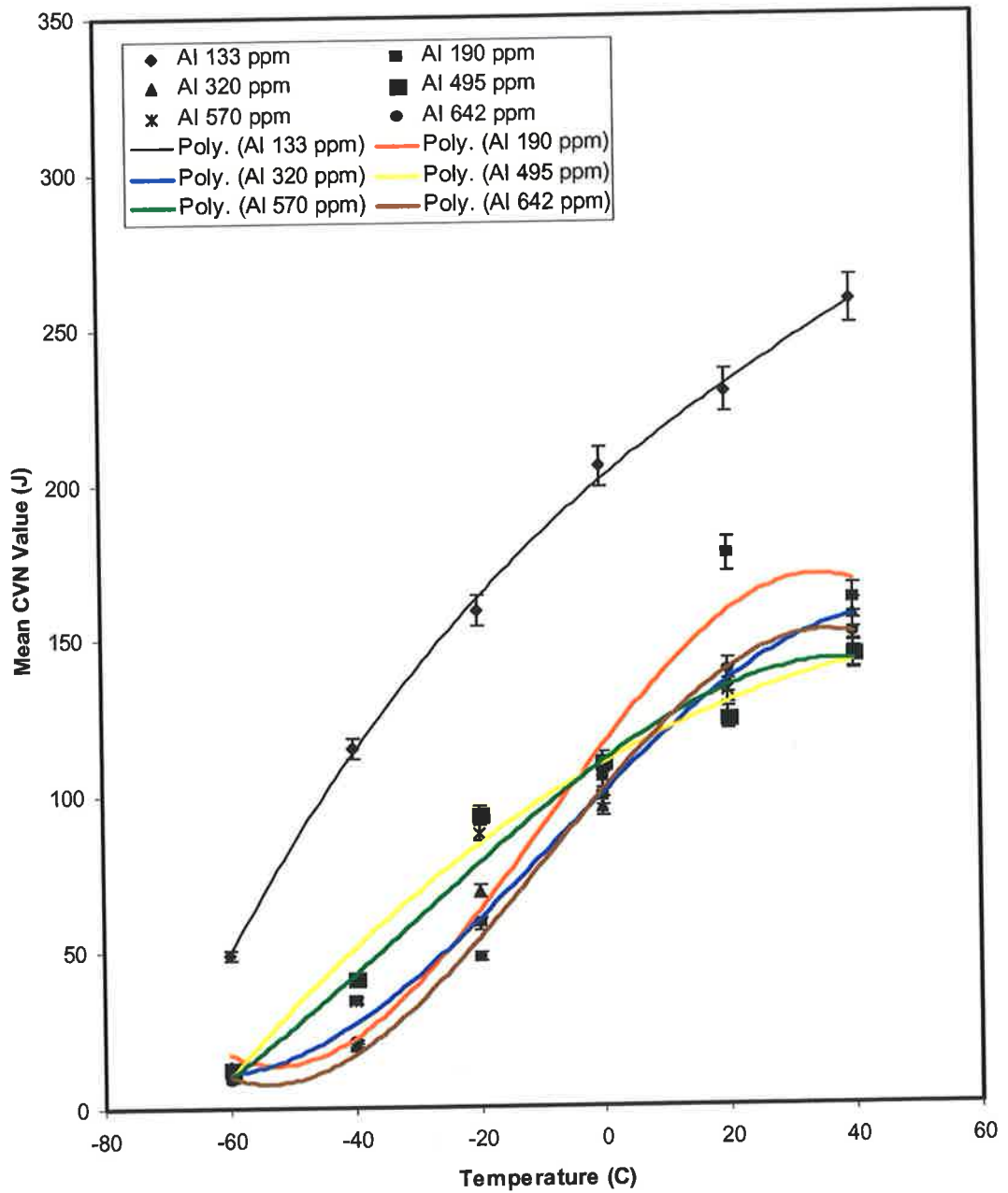


Figure 5.2(b): Mean CVN impact energy as a function of temperature for the various aluminum levels in weld metal.

Influence of Titanium and Aluminum on Weld Metal Properties

For each case the upper-shelf energy (at +40°C), the lower-shelf energy (at -60°C) and the temperature corresponding to CVN energy of 100J (T100J) were found. These values are plotted in figure 5.3(a) and (b) against weld titanium and aluminium contents respectively.

Figure 5.3 (a) shows that the upper-shelf values tend to decrease with titanium level while the lower-shelf values, except at the lowest and highest titanium levels, are independent of titanium. The T100J values, while not showing large variations with titanium level, do show a minimum value of about -45°C at titanium contents of approximately 0.005wt% and 0.085wt%.

The variations with aluminum level, as plotted in figure 5.3 (b) show that the highest upper and lower-shelf values occur at the lowest aluminum content, while the impact values are largely independent of aluminum content at all higher aluminum levels. Similarly the lowest T100J value occurs at the lowest aluminum level while T100J is independent of aluminum at higher aluminum levels. The variation of T100J is considerably larger with the weld aluminum level than with titanium.

Influence of Titanium and Aluminum on Weld Metal Properties

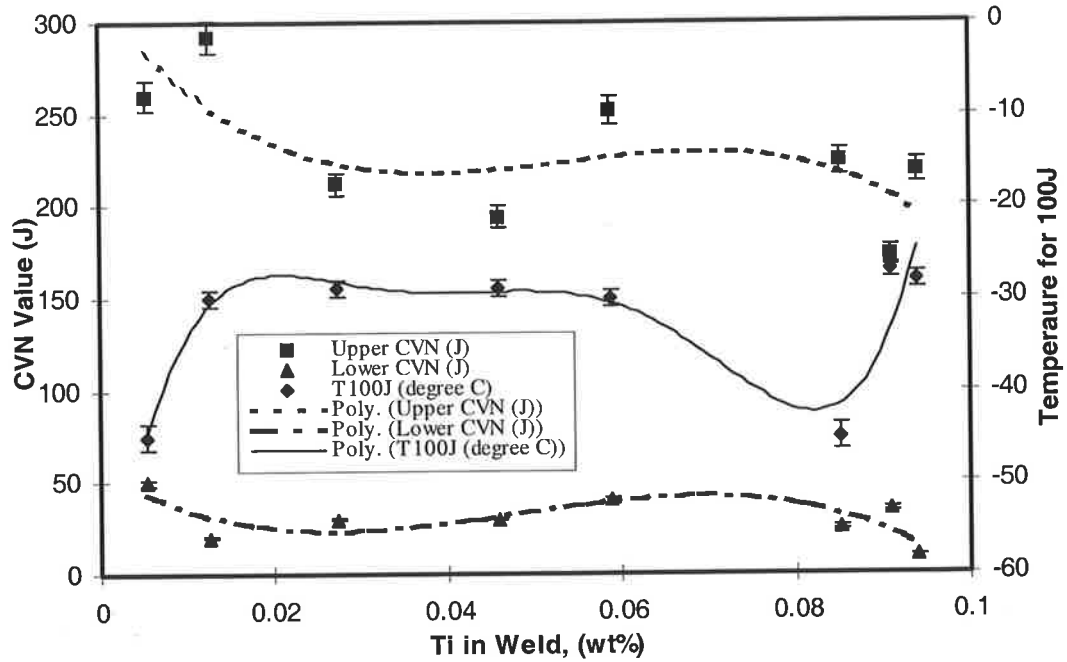


Figure 5.3(a): The upper CVN (J), lower CVN (J) and T100J ($^{\circ}\text{C}$) values as a function of titanium contents.

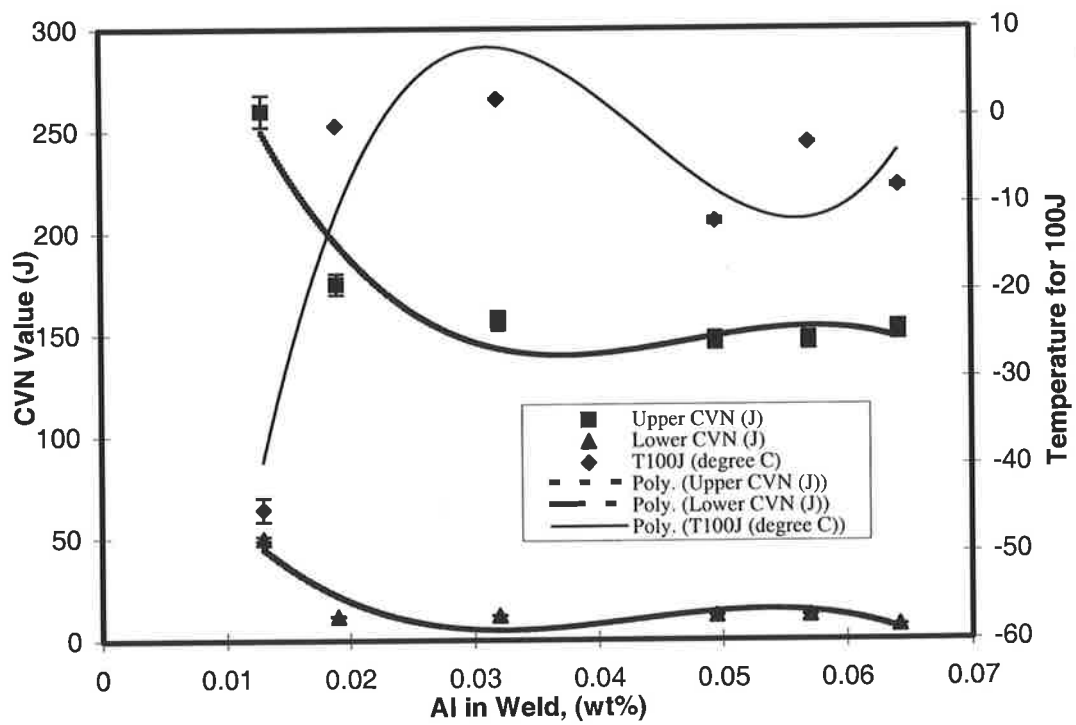


Figure 5.3(b): The upper CVN (J), lower CVN (J) and T100J ($^{\circ}\text{C}$) values as a function of aluminum contents.

5.2.3 Weld Metal Microstructure

Area measurements from cross-sections of welds indicated that the region of the weld from which all mechanical test specimens (including CVN specimens) were extracted contained approximately 60% as-deposited and 40% reheated weld metal (as mentioned in chapter 3). Area fractions of acicular ferrite (AF), ferrite with second phase (FS) and primary ferrite (PF) were determined in as-deposited regions of the top layer from each weld.

Plots of the variation of percentage area of AF, FS and PF with weld titanium and aluminum levels are shown in figure 5.4 (a) and (b) respectively. These graphs show that the area of AF tends to decrease from 60% to 20% with increasing titanium level. A corresponding increase in FS is seen, and the PF stayed relatively unchanged. The extent of this change in as-deposited microstructure with titanium level is illustrated in figures 5.5(a)&(b) which shows micrographs of the welds containing 0.0054wt% and 0.0852wt% titanium with 62% and 43% AF respectively.

As the aluminum levels are increased, AF also decreases from 60% to 20%. The decrease was somewhat irregular in that AF appeared to decrease rapidly with the initial increase in weld aluminum from the base level of 0.013wt%. As shown by figure 5.4(b), this decrease in AF is accompanied by an increase in area of FS whilst observed PF remains constant at 30%.

Influence of Titanium and Aluminum on Weld Metal Properties

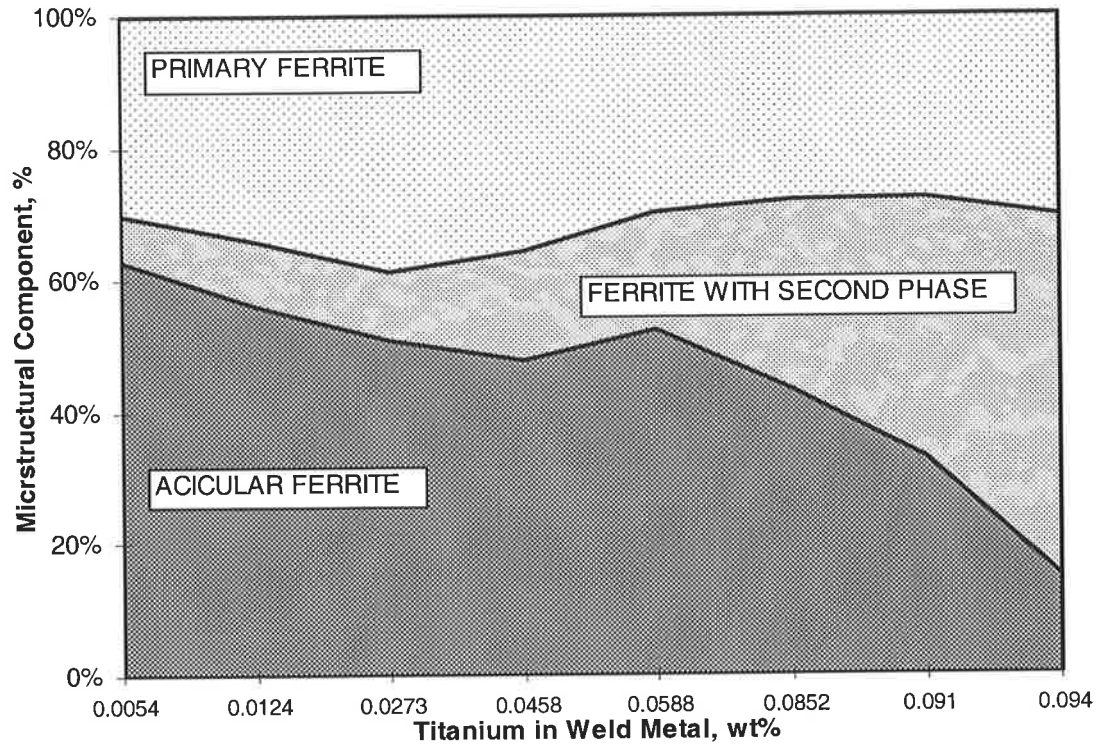


Figure 5.4(a): Variation in the proportion ferrite morphologies as a function titanium levels.

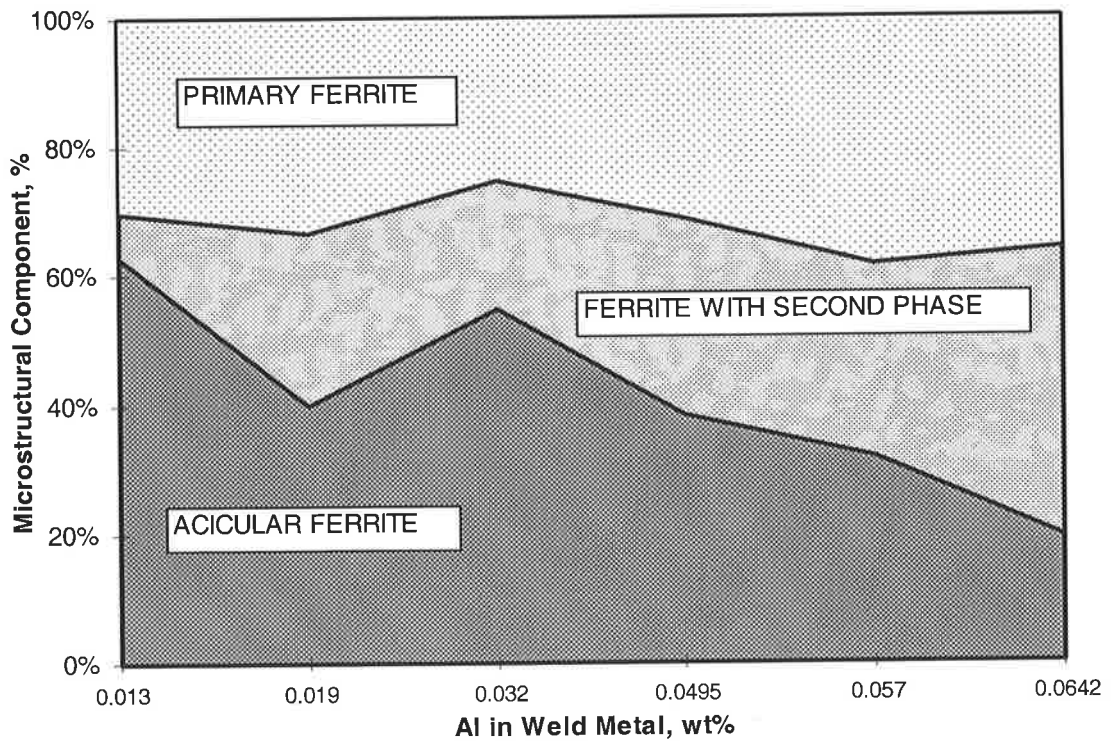


Figure 5.4(b): Variation in the proportion ferrite morphologies as a function aluminum levels.

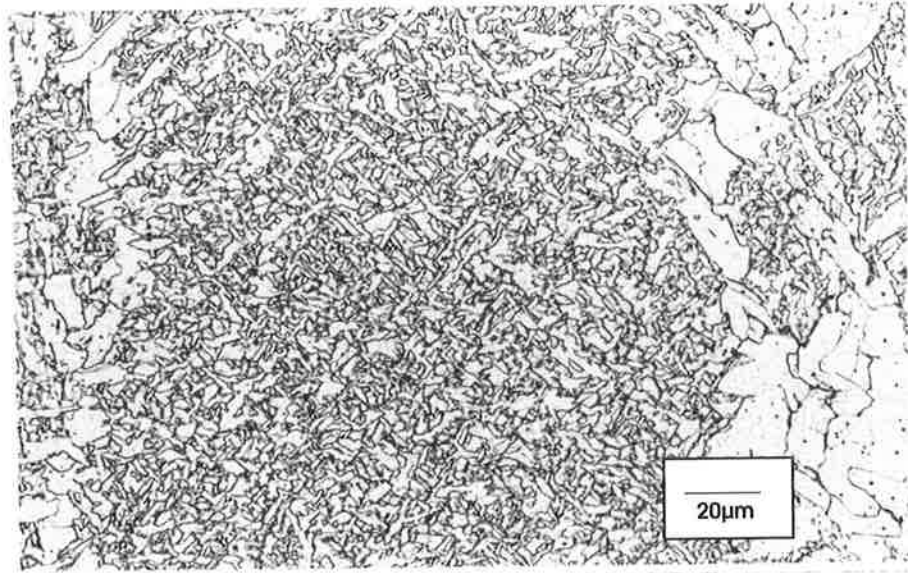


Figure 5.5(a): Photomicrograph of as-deposited weld metal with 0.0054wt% titanium.

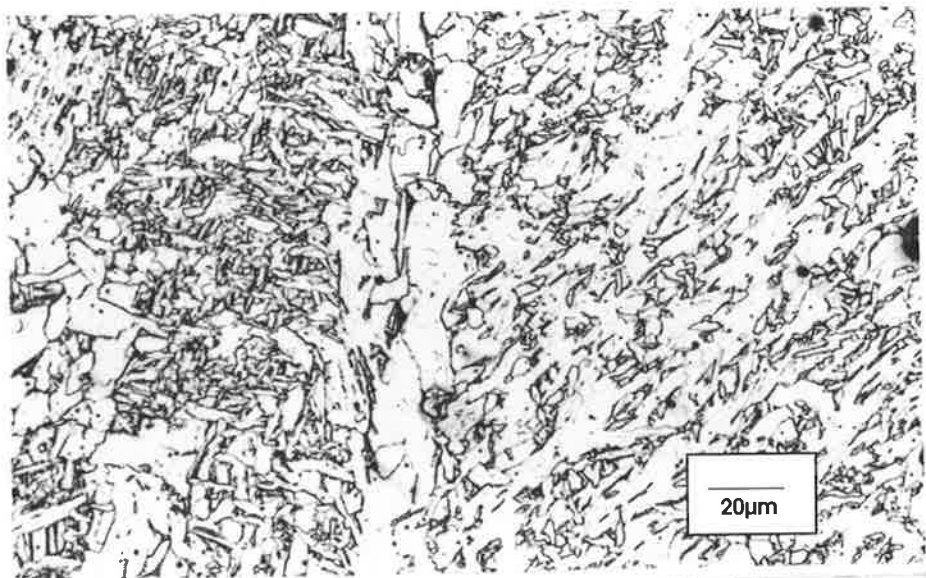


Figure 5.5(b): Photomicrograph of as-deposited weld metal with 0.0852wt% titanium in weld metal.

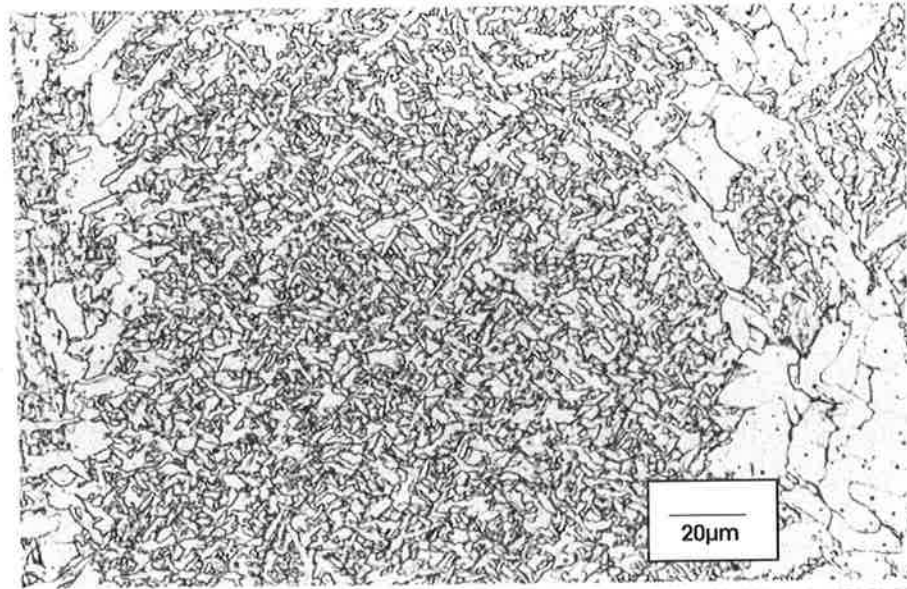


Figure 5.6(a): Photomicrograph of as-deposited weld metal with 0.0133wt% aluminum.



Figure 5.6(b): Photomicrograph of as-deposited weld metal with 0.0570wt% aluminum in weld metal.

Influence of Titanium and Aluminum on Weld Metal Properties

In addition to these measurements of the area of the ferrite morphologies, measurements were also made of the prior austenite grain size, the grain size of the equiaxed reheated zone and of the mean lath width of acicular ferrite (see Tables 5.3 & 5.4). For the titanium series, the prior austenite grain size tended to decrease slightly with titanium level as did the acicular ferrite lath width while the grain size in the reheated zone was largely independent of titanium except perhaps at the highest titanium levels. For the aluminum series, both prior austenite grain size and acicular ferrite lath width were largely independent of aluminum level while the grain size in the reheated zone tended to increase with aluminum except for the highest aluminum level.

Table 5.3: Acicular ferrite lath width and reheated grain sizes for titanium series.

Titanium %	Columnar Austenite Grain Width (μm)	Acicular Ferrite Lath Width (μm)	Grain Size of Reheated Zone (μm)
0.0054	135	2.86	5.13
0.0124	135	2.22	5.17
0.0273	150	2.44	5.56
0.0458	130	2.44	5.13
0.0588	135	2.78	5.26
0.0852	95	2.08 *	5.41
0.0910	115	1.92 *	5.00
0.0940	110	--- **	4.76

* --- Small patches of continuous AF limited the AF count.

** --- In-sufficient, continuous areas of AF, for measurements.

Table 5.4: Acicular ferrite lath width and reheated grain sizes for aluminum series.

Aluminum %	Columnar Austenite Grain Width (μm)	Acicular Ferrite Lath Width (μm)	Grain Size of Reheated Zone (μm)
0.0133	135	2.86	5.13
0.0190	105	2.17	6.06
0.0320	125	2.38	6.25
0.0495	140	2.44	6.67
0.0570	125	--- **	6.89
0.0642	120	2.63	5.13

** --- In-sufficient, continuous areas of AF, for measurements.

5.2.4 Non-metallic Inclusions

Figure 5.7(a) & (b), show the details of the non-metallic inclusions, including number per unit volume, mean three dimensional (3D) diameter and percentage of diameter equal to or larger than $1\mu\text{m}$ for each weld, as measured using the SEM with automated image analyser. For the titanium series, both the mean 3D inclusion diameter and the percentage of inclusions with diameters greater than $1\mu\text{m}$ decreased with increase in weld metal titanium content. The number density of inclusions measured tends to increase with weld titanium, with the exception of a maximum of $16 \times 10^7 / \text{mm}^3$ at about 0.08wt% titanium.

The inclusion data for the aluminum series (figure 5.7(b)) indicates that the mean 3D inclusion diameter and the percentage of inclusions with diameter greater than $1\mu\text{m}$ tend to decrease with aluminum level. The number density of the inclusions, while showing some variability, appears to increase with increase in weld aluminum level.

Influence of Titanium and Aluminum on Weld Metal Properties

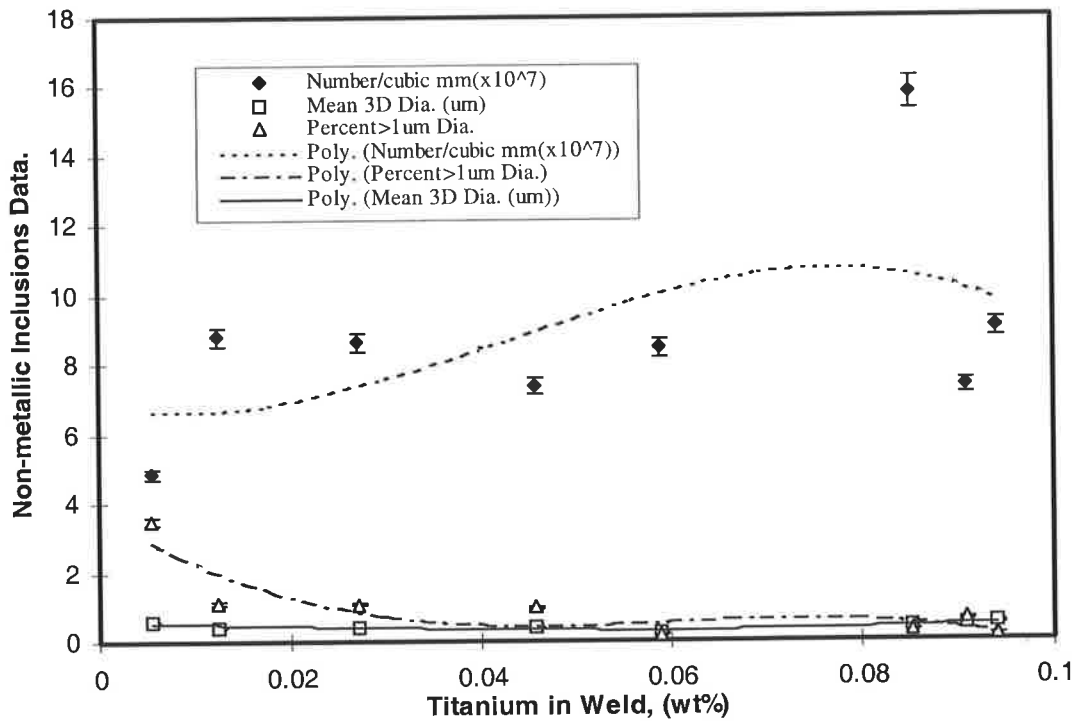


Figure 5.7(a): Variation of non-metallic inclusions number/mm³, mean 3D diameter and percent > 1µm diameter with increase in weld titanium level.

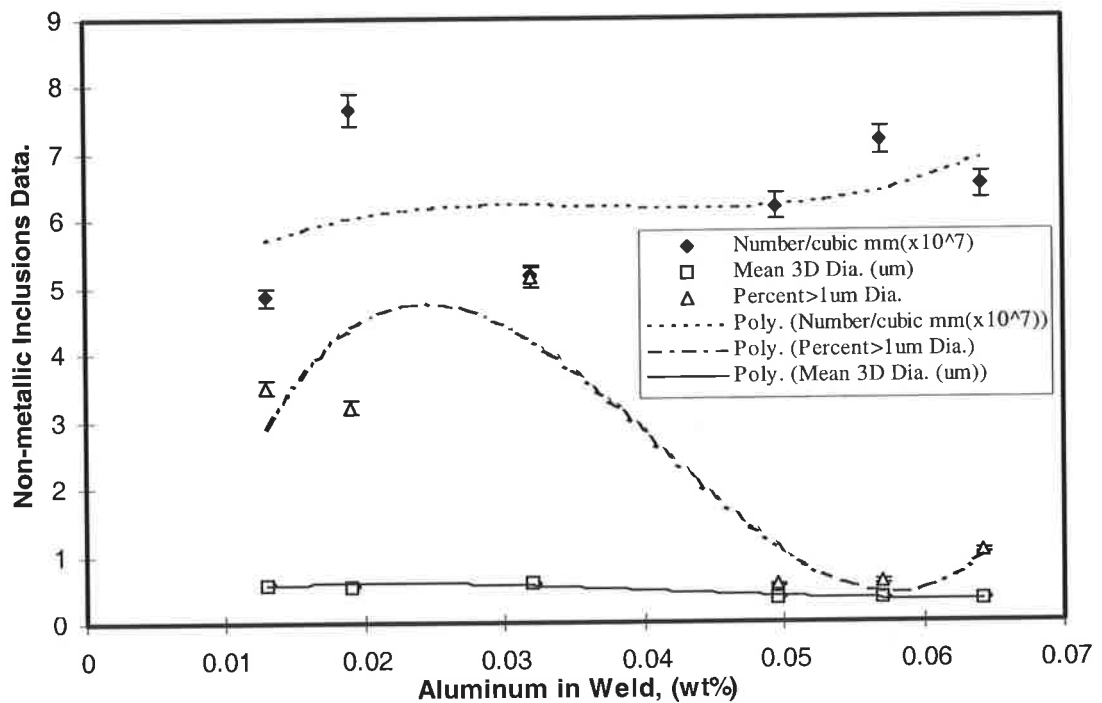


Figure 5.7(b): Variation of non-metallic inclusions number/mm³, mean 3D diameter and percent > 1µm diameter with increase in weld aluminium level.

5.3 Discussion

5.3.1 Weld Metal Tensile Properties

While some scatter existed in the measurements, the results generally showed that both yield and tensile strength increased by about 50MPa as weld titanium increased from 0.005wt% to 0.095wt% but were approximately constant as weld aluminum increased from 0.013wt% to 0.065wt%. The tensile properties are consistent with those for MMAW [157] for which it was shown that the tensile properties increased by approximately 60MPa as weld titanium increased from essentially zero to 0.055wt% but by only about 30MPa as weld aluminum increased from zero to 0.061wt%.

5.3.2 Weld Metal Impact Properties

In general it was found that the major microstructural features present in the weld metal that may influence the impact properties are the as-deposited regions, the reheated regions and the size and number of non-metallic inclusions present. In addition, the strength level of the weld metal and grain size were found to affect impact properties.

Across the present series of trials with varying weld titanium and aluminum contents the proportion of as-deposited to reheated region was nominally constant at approximately 60:40. This is because both heat input and run placement were held constant. It was observed that there was little apparent difference in either the appearance of the reheated zones or in the measured grain sizes of the equiaxed portions of these zones for trial welds

Influence of Titanium and Aluminum on Weld Metal Properties

(see table 5.3 & 5.4). This is in agreement with other investigators and it can be concluded that the reheated regions play a minor part in determining weld impact properties [148,158]. This is because the largely equiaxed, fine-grained structure gives a more difficult cleavage path than the coarser parts of the as-deposited regions. Attention will therefore be concentrated on the influence of the other factors on weld impact properties.

The as-deposited regions of welds have been characterised as consisting of acicular ferrite (AF), ferrite with second phase (FS) and primary ferrite (PF). Of these ferrite types, AF is widely considered to be the most beneficial to impact properties. This is because it consists of small non-aligned grains with high angle boundaries and therefore provides a difficult path for cleavage.

The present results show, in the ranges tested, that the proportion of AF present generally decreases with the addition of either titanium or aluminum. It is shown that maximum AF occurs at total aluminum and titanium of around 0.02wt% with ratio of aluminum to titanium around 2.4:1, this is consistent with earlier studies which tended to concentrate on other welding processes [157,159,160]. The present results do demonstrate some correlation between low temperature impact, as measured by the T100J value, and AF proportion at relatively low titanium or aluminum additions where the AF proportions are relatively high. As shown in figure 5.8, this correlation occurs down to around 50%AF for titanium addition and 55%AF for aluminum addition, these correspond to titanium and aluminum levels in the welds of about 0.06wt% and 0.02wt% respectively. However, while AF decreases continually with alloy addition, the T100J values tend to be insensitive to further alloy addition or, in the case of titanium addition, to improve at some higher alloy level. This suggests that other factors are becoming important at higher alloy levels.

Influence of Titanium and Aluminum on Weld Metal Properties

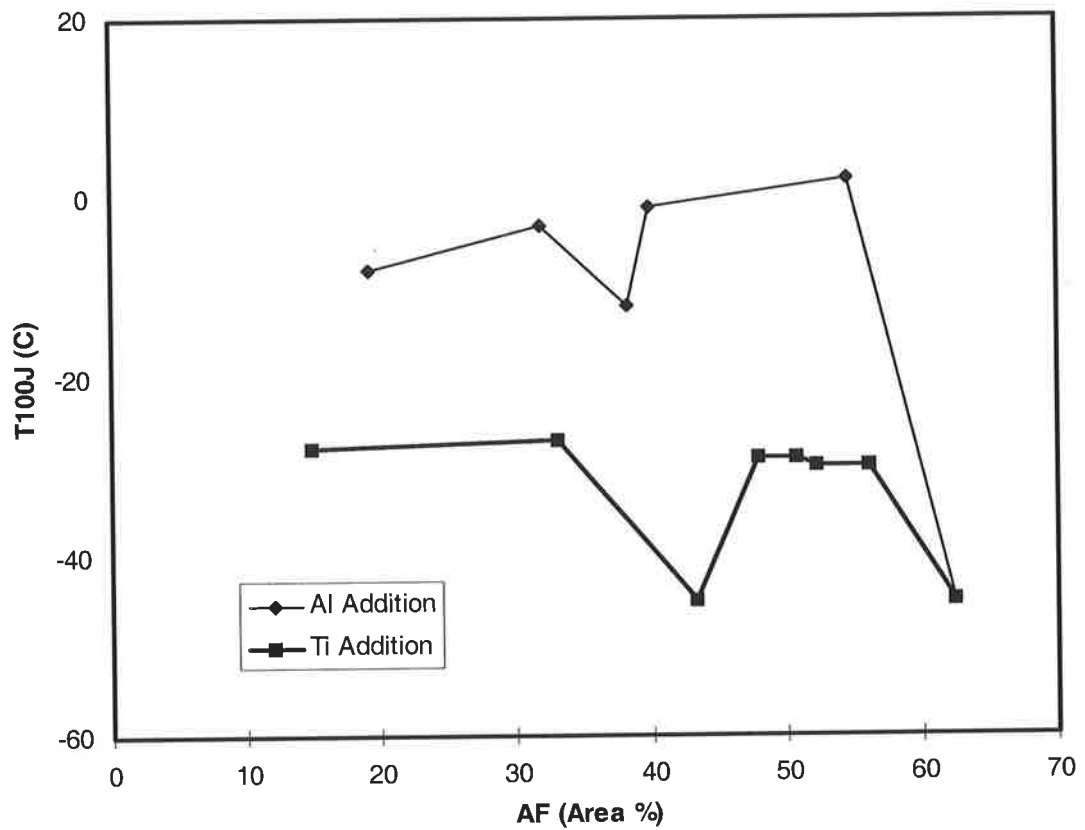


Figure 5.8: Effect of AF on mean CVN impact energy corresponding to T100J, for titanium and aluminum series of weld metal.

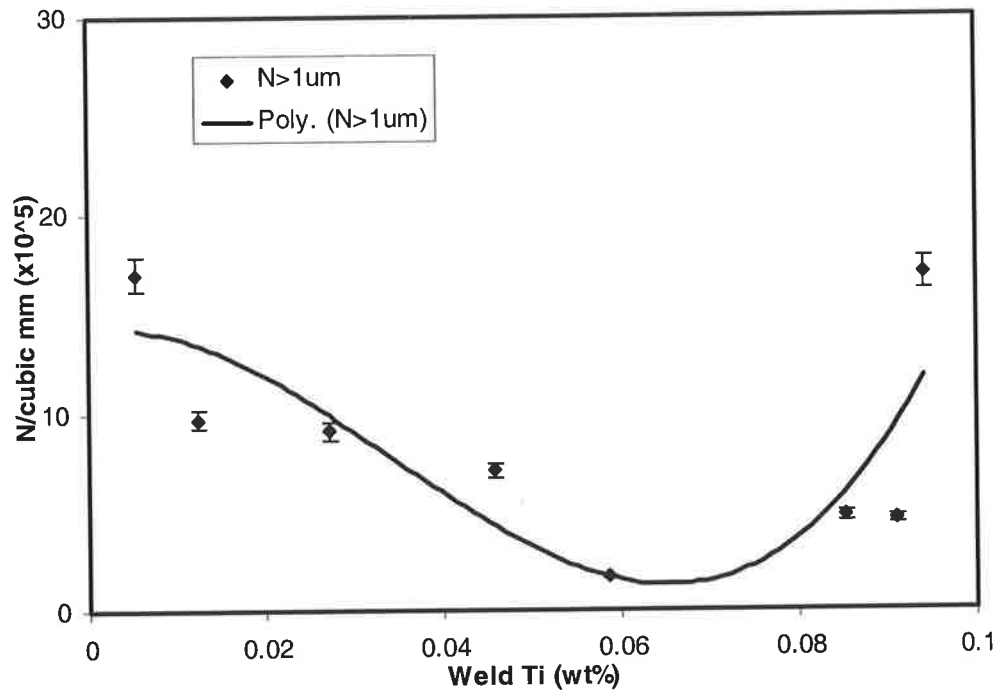
It is known that non-metallic inclusions play two distinct roles in weld metals. Smaller inclusions, of around $0.4 \mu\text{m}$ in diameter, have been identified as efficient nucleation sites for AF [151]. Larger inclusions, of $1 \mu\text{m}$ or greater diameter, have been shown to be

Influence of Titanium and Aluminum on Weld Metal Properties

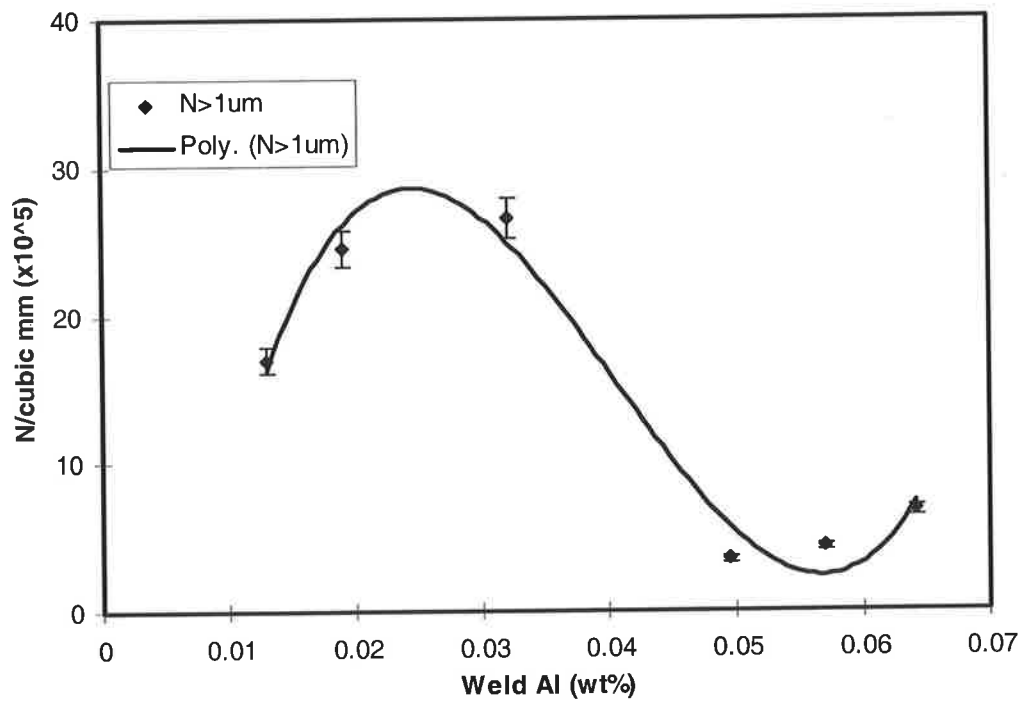
initiation sites for cleavage fracture [152] which is the main fracture mode for impact at low temperatures.

Figure 5.9 shows the variation in number density of inclusions with diameter greater than $1\mu\text{m}$ ($N > 1\mu\text{m}$) with titanium and aluminum level. The $N > 1\mu\text{m}$ values were calculated from the product of overall number density and the percentage with diameter greater than $1\mu\text{m}$ values. This shows that $N > 1\mu\text{m}$ tends to decrease with alloy level to reach relatively low values at titanium levels between about 0.04 and 0.09wt% and aluminum levels greater than about 0.04wt%. It has been observed that the aluminium content affects the size distribution of the inclusions. Probably as a result of a higher temperature of nucleation of aluminium slags (due to the higher aluminium concentration), the inclusions will have longer time to coalesce before solidification of the weld metal, resulting in larger entrapped inclusions. An earlier nucleation will also favour the removal of inclusions by the top slag (given by Stoke's equation). As the aluminium content increases in the weld metal the size of the inclusions start to increase by coalescence as shown in figure 5.9 b. Further increasing the aluminium contents inclusion size increases further until they reach a critical size, at which point they are large enough to float to the surface. The smaller inclusions remain in the weld metal. Through this process the number of large inclusions in the weld metal is reduced.

Influence of Titanium and Aluminum on Weld Metal Properties



(a)



(b)

Figure 5.9: Number density of inclusions with diameter $> 1\mu\text{m}$ as a function of increase in (a) titanium and (b) aluminum in the weld metal.

Influence of Titanium and Aluminum on Weld Metal Properties

The inclusions with diameter greater than $1\mu\text{m}$ ($N > 1\mu\text{m}$) at low titanium and aluminum level will also be present in the 40% reheated region and could adversely affect T100J temperature despite the high AF content in weld metal which has not been re-austenitised. The total AF seems to vary from about 60% to 20% in the as solidified weld metal, but taking into account that as solidified weld metal is about 60% of total weld metal, the variation in AF as a proportion of the total weld metal is 36% to 12%.

The main features of the observed low temperature impact behaviour may, to a reasonable extent, be explained on the basis of the interaction between two factors: the proportion of AF present and the number density of large inclusions. This is because, although AF tends to decrease continually with alloy addition, the number density of large inclusions also tends to decrease with alloy addition. Consequently, while low temperature impact properties may be expected to be continually degraded by lower AF levels, this effect is offset by the smaller number of the large inclusions available to nucleate the cleavage fracture.

Other factors can undoubtedly influence weld metal impact properties. Increase in weld metal strength, for example, generally has a deleterious effect on impact properties. This does not appear to be a major factor in the present case since, while the changes in impact properties are considerable, the changes in strength level are small (about 50MPa) for the titanium addition and negligible for the aluminum addition.

Chapter 6. Effect of Stress Relief on Low and High Titanium Containing Weld Metals

6.1 Introduction

During stress relief three mechanisms are likely. The first, giving an improvement in toughness, is softening of ferrite and tempering of any martensite in the martensite/austenite (M/A) constituent. In addition, grain boundary carbide films, particularly in the fine-grained HAZ regions, will change into discrete carbides. These beneficial mechanisms are opposed by the formation of relatively brittle carbides from residual austenite and coarsening of carbides in pearlite and elsewhere. Welds containing the highest manganese content, containing the most prior austenite, should give the greatest reduction in toughness. Finally, a decrease in dislocation density will contribute to a reduction in strength and, hence, an improvement in toughness [157].

6.2 Results

6.2.1 Heat-Treatment

This investigation was done to evaluate the effect of stress relief heat treatment on the mechanical properties of C-Mn steel, with two levels of titanium addition. For direct comparison between as-welded and stress-relieved weld metal, a large test plate was welded and one half was subjected to a stress-relief treatment of 2 hours at 580 °C prior to analysis and the other half of the plate tested in the as welded condition.

6.2.2 Weld Metal Compositions

The chemical compositions of the all-weld-metal deposits studied are given in table 6.1 for the as-welded and reheated low and high titanium weld metals. This indicates that the principal difference in composition was a factor of 10 in titanium level from 0.0065wt% to 0.065wt%. Carbon, manganese and silicon levels were nominally constant at 0.05wt%, 1.32wt% to 1.37wt% and 0.62wt% to 0.67wt% respectively. The levels of the remaining metallic elements were relatively low and constant throughout the series. The oxygen and nitrogen levels found in the welds were essentially constant. The oxygen levels were all in the range 0.048wt% and 0.053wt%, and the nitrogen values were in the range 0.0052wt% and 0.0082wt%.

Affect of Stress Relief on Low and High Titanium containing Weld Metal

Table 6.1: Weld metal compositions (wt %) for stress relieved titanium weld metal.

Si	Mn	C	S	P	Ni	Cr	Mo	Cu	V	Nb	Ti	Al	B	O	N
0.62	1.32	0.05	0.013	0.015	0.02	0.02	<0.01	0.01	0.0065	<0.01	0.0065	0.0156	<0.0005	0.0530	0.0052
0.67	1.37	0.05	0.012	0.015	0.02	0.02	<0.01	0.01	0.0086	<0.01	0.0656	0.0123	<0.0005	0.0480	0.0082

Table 6.2: Average Vickers hardness for stress relieved titanium welds.

Ti		Average Vickers hardness without stress relief treatment	Average Vickers hardness with stress relief treatment
0.0065	As-Welded	208	183
	Re-heated	168	158
0.0656	As-Welded	207	194
	Re-heated	182	172

6.2.3 Mechanical Properties

6.2.3.1 Hardness Testing

Average hardness values for as-welded and reheated, low and high titanium levels with and without stress relief treatment are given in table 6.2. It is seen that, stress relieving resulted in a reduction of hardness throughout the bulk of the all-weld-metal deposits studied. For the low titanium weld deposit the reduction was between 6% and 12%, while for higher titanium weld deposit a reduction of 6% in hardness is seen.

6.2.3.2 CVN Impact Results

The variations of mean CVN energy with test temperature for as-welded and reheated, low and high titanium levels are plotted in figures 6.1 & 6.2. For both low and high titanium levels, mean CVN energies for all temperatures tested showed an increase after heat treatment. For low titanium an increase of about 30 to 50J over the whole temperature range (-60 to +20°C) was found while, for the higher titanium, this increase was between ie 20J to 50J.

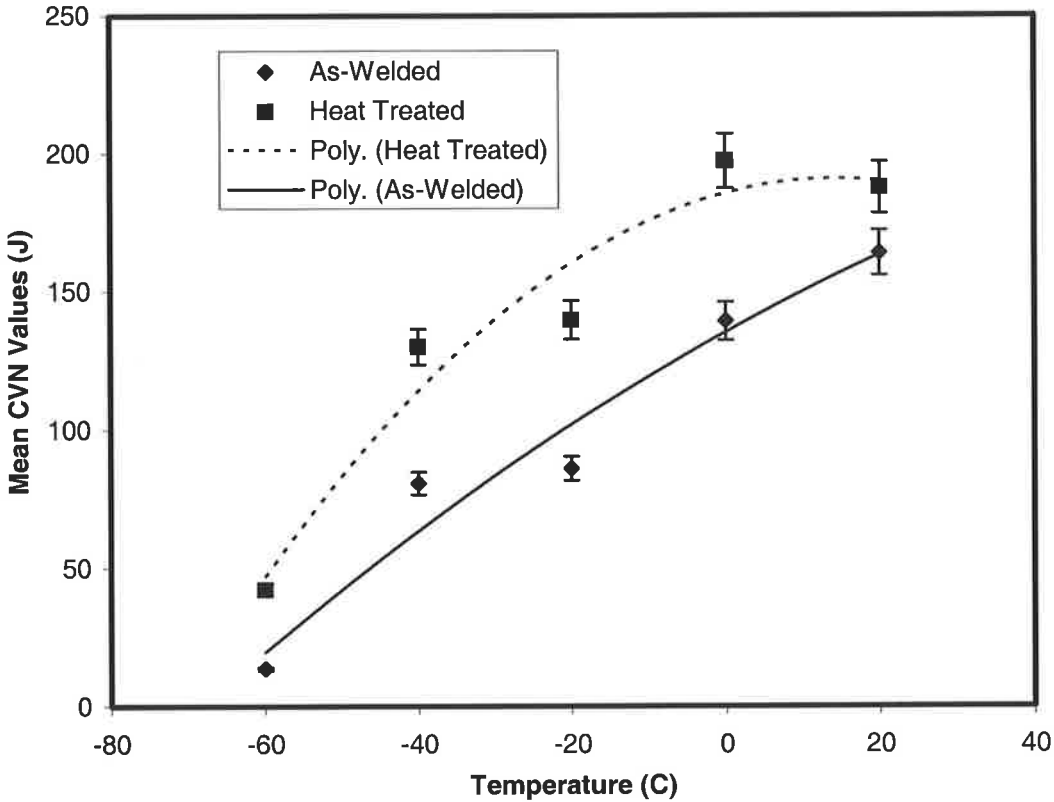


Figure 6.1: Mean CVN impact energy as a function of temperature for low titanium (0.0065wt%) levels in weld metal.

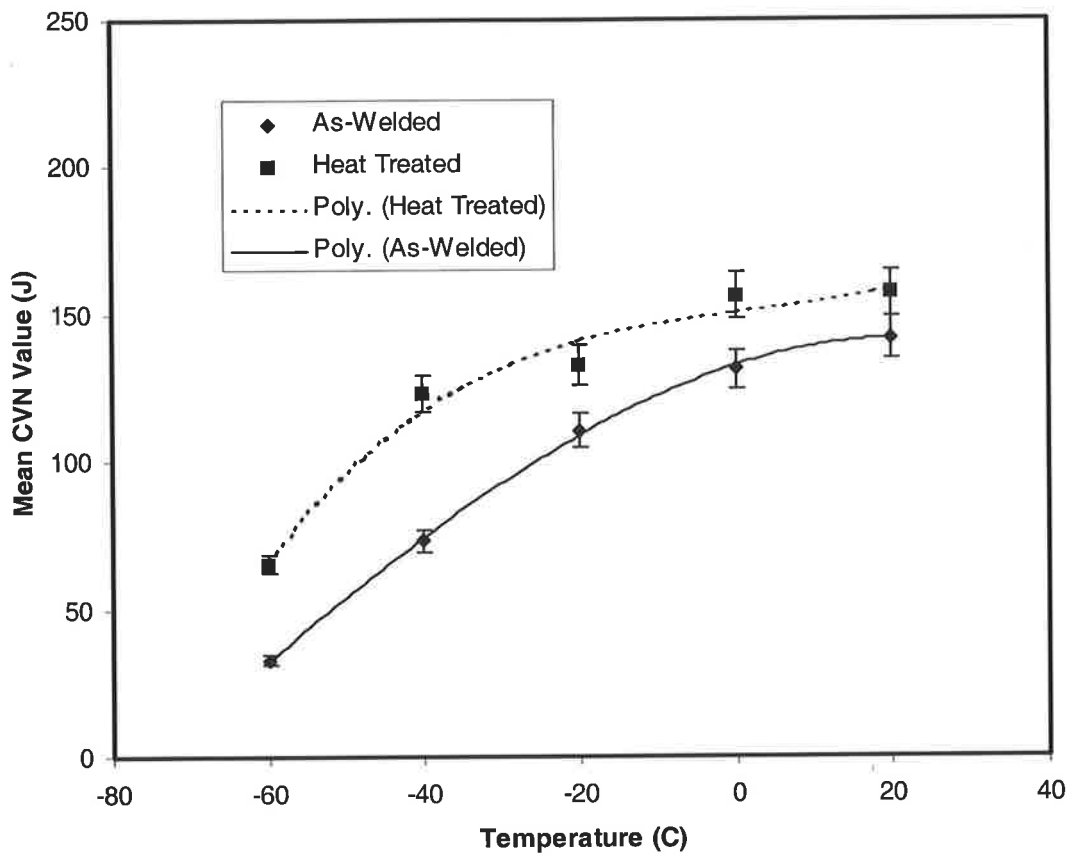


Figure 6.2: Mean CVN impact energy as a function of temperature for high titanium (0.0656wt%) levels in weld metal.

For each case the temperature corresponding to CVN energy of 100J (T100J) was found. For low titanium, the T100J values were -20 and -47°C, a lowering of the DBTT by 27°C after heat treatment. Similarly for high titanium, T100J values were -25 and -48°C, a lowering of the DBTT by 23°C after heat treatment. The T100J temperatures for as-welded weld metal were consistent with earlier results [157].

6.2.4 Weld Metal Microstructure

A comparison, using optical microscopy, of microstructures with and without stress relief heat treatment showed no variation of percentage area of AF, FS and PF for both low and high titanium levels, as expected. Also examination of the prior austenite grain size, the grain size of the equiaxed reheated zone and of the mean lath width of acicular ferrite, showed no change.

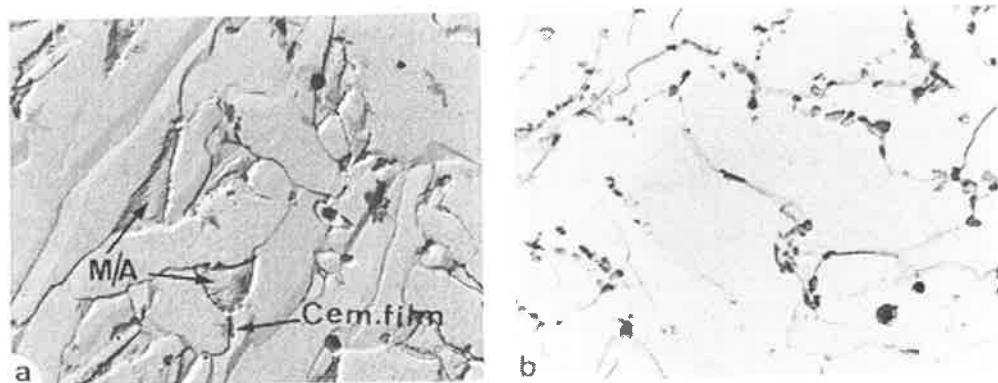


Figure 6.3: Microphotograph (x5000) of the top pass of 0.044wt% carbon and 1.4wt% manganese deposits in the, (a) as-welded and (b) stress-relieved conditions.

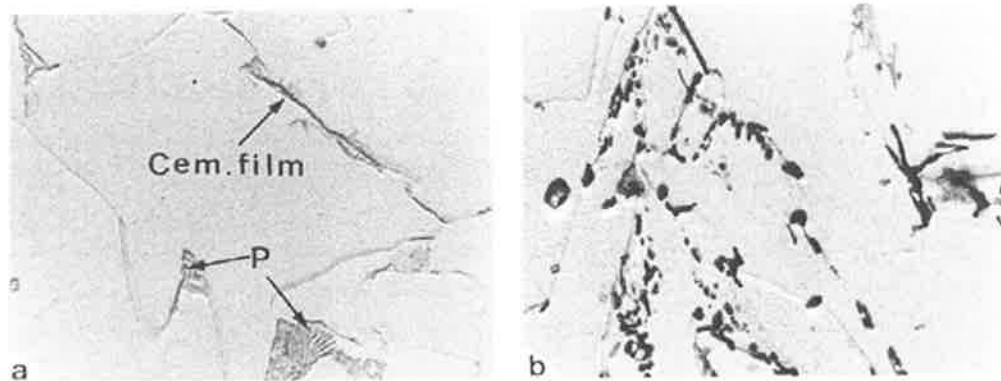


Figure 6.4: Microphotograph (x5000) of coarse-grained regions of 0.044wt% carbon and 1.4wt% manganese deposits in the, (a) as-welded and (b) stress-relieved conditions.

Improvement in toughness is due to the softening of ferrite and the tempering of any martensite in the M/A constituent. The as-welded top beads contain acicular ferrite with small regions of retained austenite partially transformed to martensite and a little cementite (figure 6.3 a), stress relief led to discrete grain boundary carbides (figure 6.3 b). Stress relieving of the coarse-grained reheated region, spheroidised the carbide in the pearlite and the cementite films and tempered the martensite/austenite constituent to form a ferrite/carbide aggregate (figure 6.4 a & b) [157].

6.3 Discussion

The metallographic studies have confirmed that stress relieving has a pronounced effect on the microstructure, causing precipitation and spheroidisation of second phase particles. The phenomenon has been documented by Cochrane [161], for plate steel, by Farrar et al [162], for submerged-arc weld metal, and by Evans [163], for MMAW. Farrar et al suggested that two significant microstructural changes occur, namely:

1. a coarsening and/or spheroidisation of pearlite and carbides,
2. a development of carbides at grain boundaries and as a fine matrix dispersion.

These two mechanisms have opposite effects on fracture toughness. When coarsening or spheroidisation of the carbides, especially pearlite, takes place, the fracture process becomes more difficult. But as time proceeds, embrittlement develops due to grain boundary cementite acting as a crack initiator. According to Cochrane, a correlation exists between the cementite particle size, particularly thickness, and the rise in impact transition temperature.

Hardness levels were reduced by stress relieving throughout the bulk of the all-weld-metal deposits studied. For low titanium weld deposit the reduction was between 6 and 12%, while for higher titanium weld deposit, about 6% reduction in hardness is seen. This agrees with the results obtained by Evans [163]. Bush and Kelly [164] also found that hardness and tensile strength decrease during tempering, this behaviour is also found during tempering of martensite (Leslie) [165].

Affect of Stress Relief on Low and High Titanium containing Weld Metal

The main consequence of stress relieving was to affect the shift in the transition range, this depends on the levels of carbon and manganese[163]. For both low and high titanium levels with carbon 0.05wt% and manganese 1.35wt%, mean notch toughness for all temperatures tested has shown an increase after heat treatment. For low titanium an increase of about 30 to 50J over the whole temperature range was found, while for the higher titanium, this increase was in the range of 20 to 50J. This positive shift of the system after heat treatment is clearly a positive feature and the optimised carbon, manganese, silicon and titanium weld metal composition is not compromised by post weld heat treatment, but shows improved mechanical properties.

Chapter 7. Influence of Boron on Weld Metal Properties

7.1 Introduction

Boron is added to alloy steels in very small amounts, perhaps as little as 0.003wt%, to increase toughness. Boron is a very powerful promoter of toughness on a weight percentage basis, but this effect is gained only with amounts of boron below approximately 0.010wt%. Any boron above this level is ineffective or may even be extremely deleterious. Therefore, it has become a common practice to “needle” some alloy steels with a very small addition of boron to obtain increased toughness. This increase in bainitic toughness of steels is due to retarding the heterogeneous nucleation of ferrite at the austenite grain boundaries [166]. It is probable that this effect is due to the reduction in interfacial energy as the boron segregates to the boundaries. This in turn makes grain boundaries less effective as heterogeneous nucleation sites. Ohmori and Yamanaka [167] have found evidence of grain boundary enrichment with high sensitivity ion microprobe analysis. The mechanism for the influence of boron was based on the fact that boron segregates extensively to the prior austenite grain boundaries, where it reduces the grain boundary

Influence of Boron on Weld Metal Properties

energy [128]. The reduction in grain boundary energy will then increase the energy barrier to nucleation by lowering the surface free energy ratio and therefore suppress the formation of grain boundary ferrite facilitating the nucleation on oxide inclusions [2,129].

Also optimum concentrations of boron and zirconium additions to low carbon steel weld metals produced predominantly acicular ferrite microstructures. Boron in weld metal is protected from oxygen and nitrogen by both zirconium and titanium. Elemental boron hinders the formation of grain boundary ferrite resulting in increased undercooling of weld metal austenite which promotes the nucleation of fine intergranular acicular ferrite. The inclusion size distribution in zirconium-containing weld metal was similar to or finer than that for titanium-containing weld metal. The specific inclusion concentration and size distribution, with proper protection of weld metal boron, are the primary factors to achieve high intragranular acicular ferrite contents [131].

Adding boron to high purity basic flux MMA electrodes [115] caused a substantial lateral shift of the Charpy-V curves to lower temperatures. Boron additions of about 140ppm were considered optimal. When 35ppm titanium was present the addition of boron generally resulted in the displacement of Charpy-V curves to higher temperatures and caused the elimination of grain boundary ferrite and a change to a bainitic type structure.

The interaction of boron and titanium is discussed in the next chapter. In this chapter the affect of boron alone has been analysed. Small amounts of boron in terms of normal weight percentage (or ppm) can have a large influence on microstructure and mechanical properties. This chapter deals with the influence of boron itself on weld metal containing

Influence of Boron on Weld Metal Properties

nominal contents carbon, manganese and silicon. Boron was added via the core as ferro-boron.

7.2 Results

7.2.1 Weld Metal Compositions

The chemical compositions of the all-weld-metal deposits studied are given in table 7.1 for the boron series. In this series, boron was varied between 0.0005wt% and 0.0176wt%. Carbon, manganese and silicon levels were nominally constant at 0.04wt% to 0.06wt%, 1.13wt% to 1.41wt% and 0.46wt% to 0.66wt% respectively. The levels of the remaining metallic elements were relatively low and constant throughout the series. The oxygen and nitrogen levels found in the welds were also essentially constant. The oxygen levels were all in the range 0.050wt% and 0.054wt%, and the nitrogen values were in the range 0.0043wt% and 0.0073wt% which is considered normal for this type of welding and process.

Influence of Boron on Weld Metal Properties

Table 7.1: Weld metal compositions (wt %) with varying boron levels.

Si	Mn	C	S	P	Ni	Cr	Mo	Cu	V	Nb	Ti	Al	B	O	N
0.64	1.34	0.04	0.012	0.014	0.02	0.01	<0.01	<0.01	<0.01	<0.01	0.0054	0.0133	<0.0005	0.0530	0.0047
0.46	1.13	0.06	0.012	0.011	0.03	0.01	<0.01	<0.01	<0.01	<0.01	0.0058	0.0149	0.0050	0.0530	0.0073
0.63	1.35	0.05	0.011	0.011	0.02	0.01	<0.01	<0.01	<0.01	<0.01	0.0057	0.0153	0.0088	0.0540	0.0067
0.66	1.41	0.04	0.011	0.012	0.02	0.01	<0.01	<0.01	<0.01	<0.01	0.0057	0.0161	0.0134	0.0500	0.0063
0.62	1.33	0.04	0.013	0.012	0.03	0.01	<0.01	0.02	<0.01	<0.01	0.0059	0.0150	0.0176	0.0500	0.0043

7.2.2 Mechanical Properties

7.2.2.1 Tensile Properties

The tensile test data is presented in figure 7.1 for the boron series. The measured yield strengths varied between 479MPa and 539MPa, while tensile strengths varied between 511MPa and 567MPa and elongations were between 20% and 29%. Figure 7.1 shows that both yield and tensile strength were largely independent of boron content over the range tested. While elongation tended to decrease by about 30%.

Influence of Boron on Weld Metal Properties

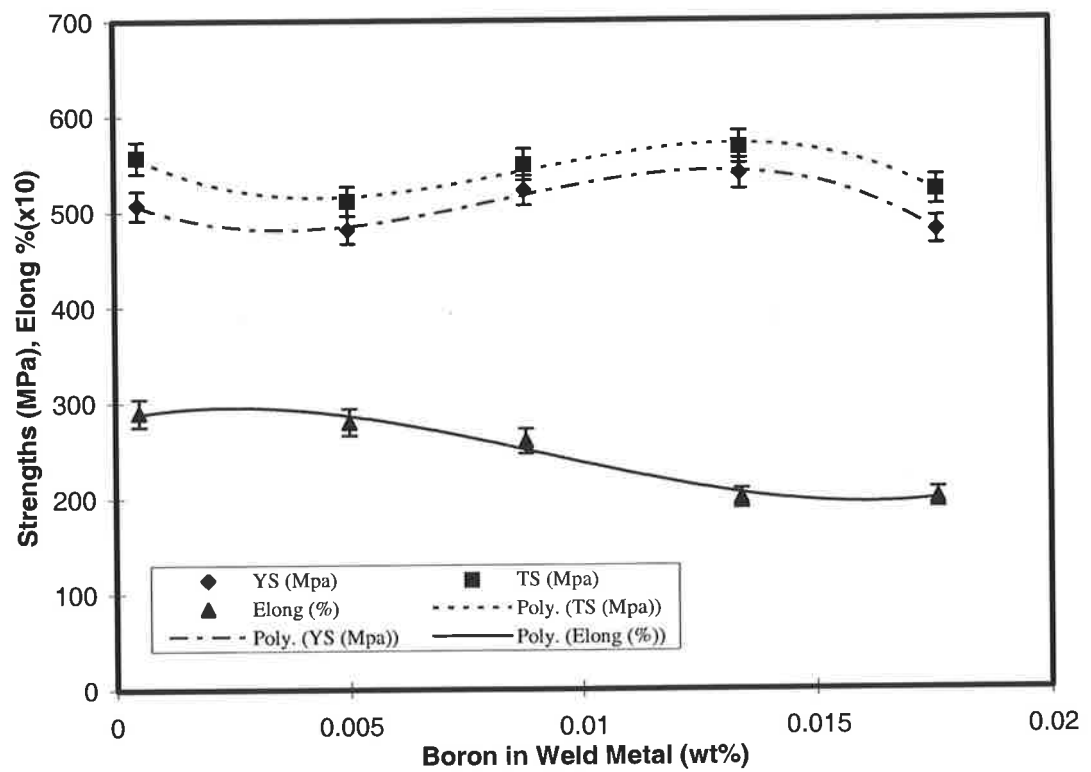


Figure 7.1: Variations in yield, tensile strength and percent elongation as a function of boron content in the weld metal.

7.2.2.2 CVN Impact Results

The variations of mean CVN energy with test temperature for the various weld metal boron levels are plotted in figure 7.2. For each case the upper-shelf energy (at +20°C), the lower-shelf energy (at -60°C) and the temperature corresponding to CVN energy of 100J (T100J) were found. These values are plotted in figure 7.3 against weld metal boron contents.

Figure 7.3 shows that the upper-shelf values have considerable scatter but tend to decrease with boron level while the lower-shelf values are independent of boron. The T100J values, while not showing large variations with boron level, do show minimum values of about -45°C and -41°C at boron contents of approximately 0.0005wt% and 0.0134wt%.

Influence of Boron on Weld Metal Properties

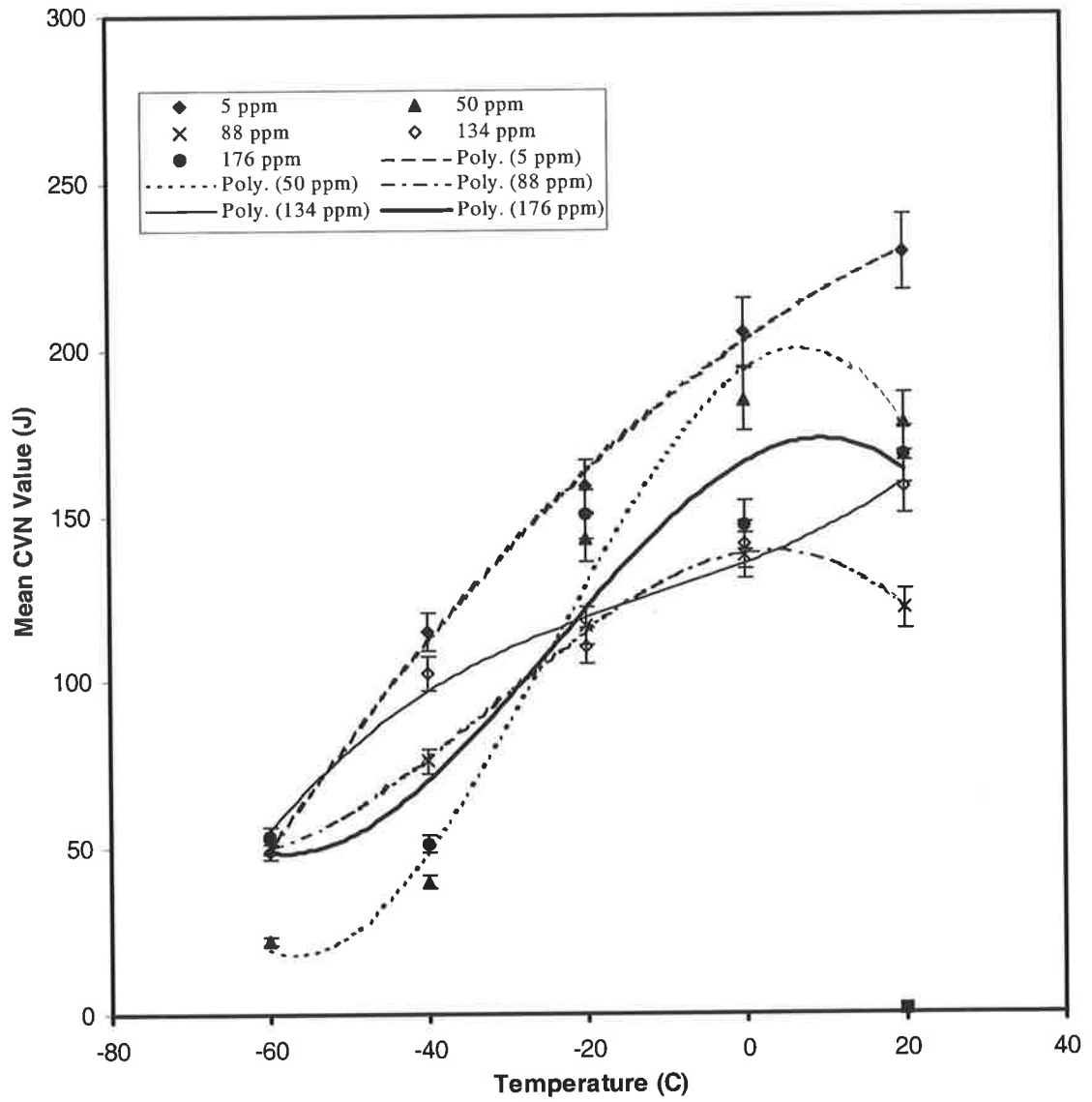


Figure 7.2: Mean CVN impact energy as a function of temperature for various boron levels in the weld metal.

Influence of Boron on Weld Metal Properties

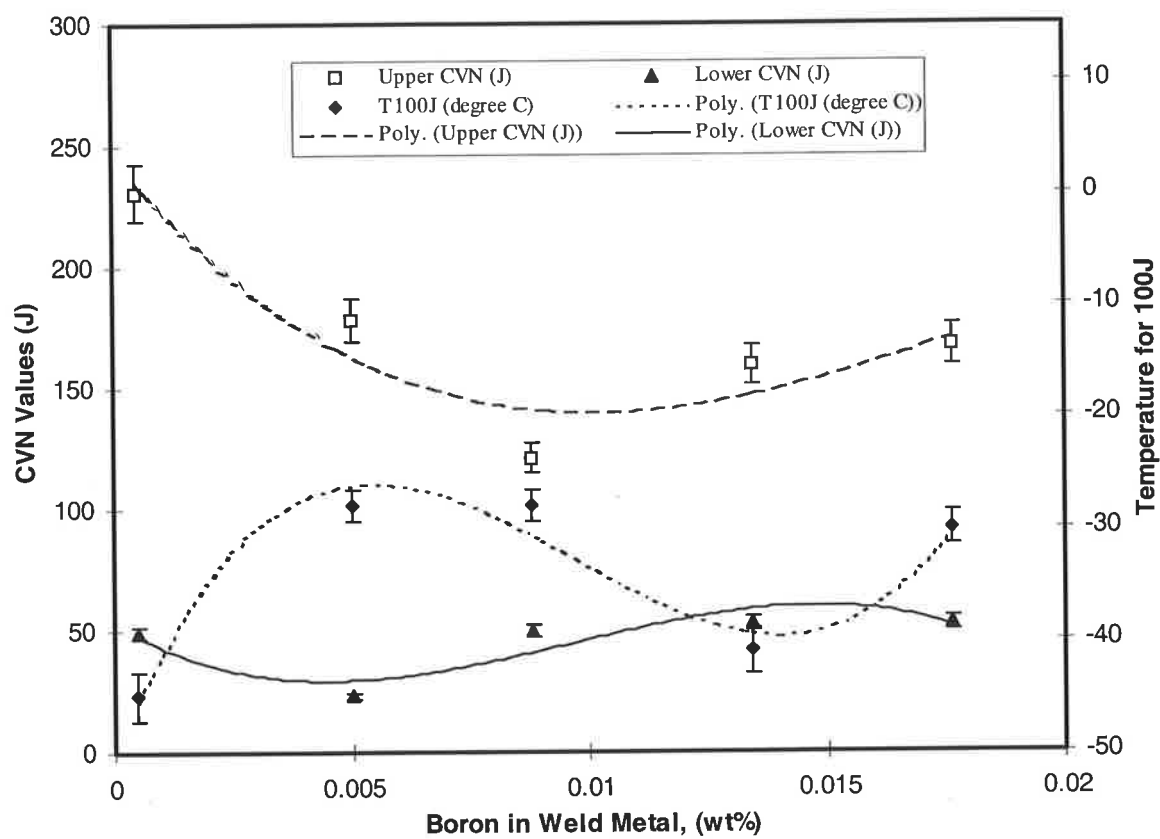


Figure 7.3: The upper CVN (J), lower CVN (J) and T100J($^{\circ}$ C) values as a function of boron contents.

7.2.3 Weld Metal Microstructure

Plots of the variation of percentage area of AF, FS and PF with weld metal boron levels are shown in figure 7.4. This graph shows that area of the AF tends to decrease from 60% to 8% with increase in boron level. A corresponding increase in FS is seen, while PF tends to decrease in the range from 30% to 10% with increase in boron level. The extent of this change in as-deposited microstructure with boron level is illustrated in figure 7.5 which shows micrographs of the welds containing 0.0005wt% and 0.0176wt% boron with 62% and 8% AF respectively.

Influence of Boron on Weld Metal Properties

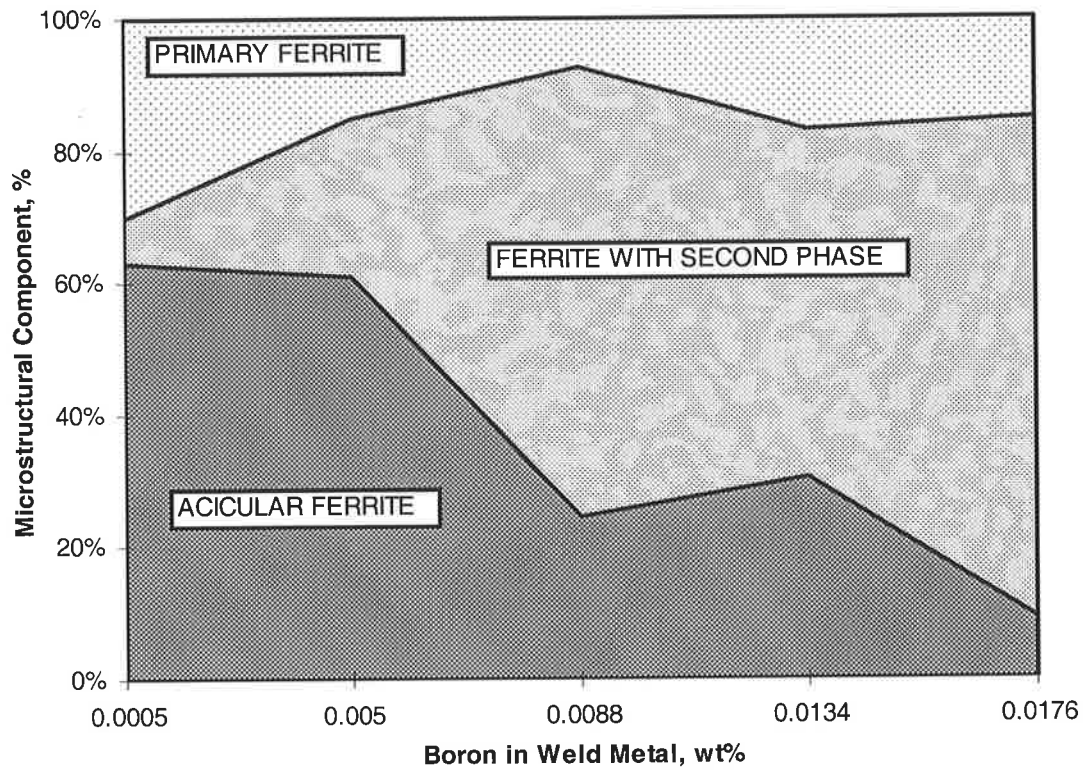
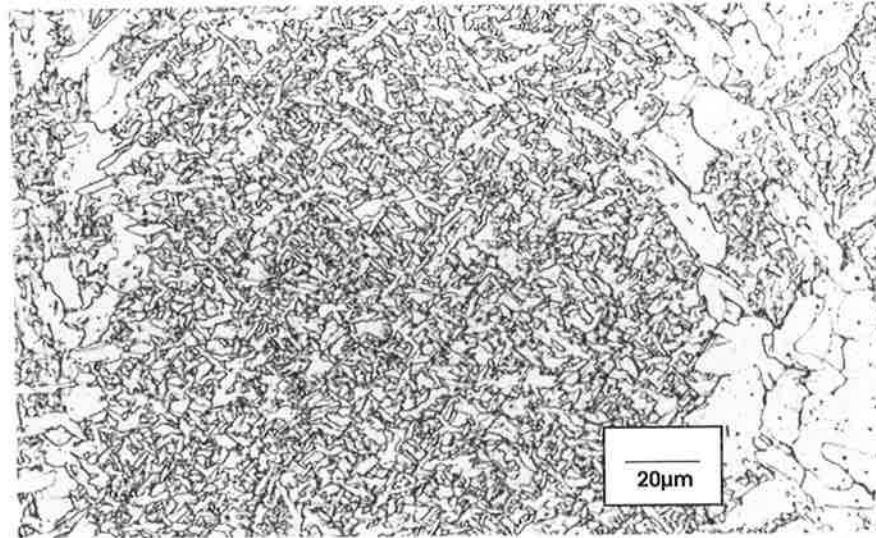
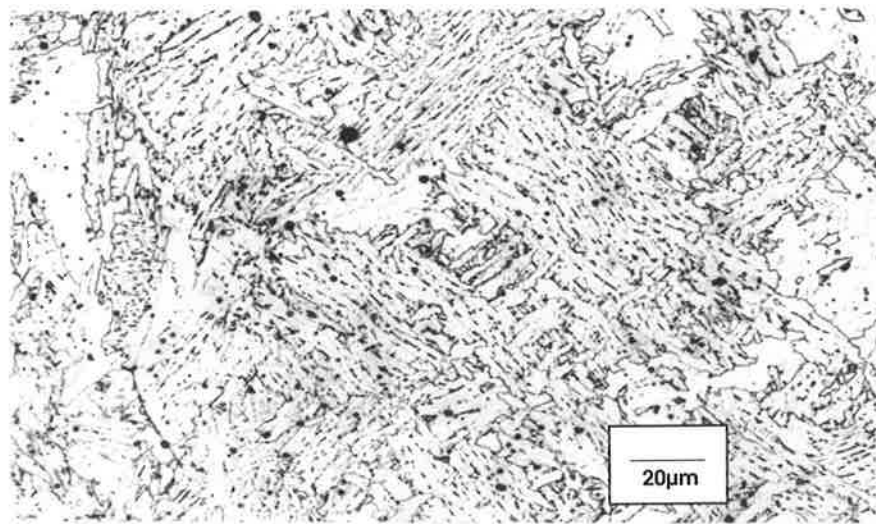


Figure 7.4: Variation in the proportions of ferrite morphologies in as-deposited weld metal as a function of boron content.

Influence of Boron on Weld Metal Properties



(a)



(b)

Figure 7.5: Photomicrograph of as-deposited weld metal with (a) 0.0005wt% boron and (b) 0.0176wt% boron content.

Influence of Boron on Weld Metal Properties

In addition to these measurements of area of the ferrite morphologies, measurements were also made of the prior austenite grain size, the grain size of the equiaxed reheated zone and of the mean lath width of acicular ferrite (see table 7.2). The prior austenite grain size tended to increase significantly with boron level while the acicular ferrite lath width and the grain size in the reheated zone was largely independent of boron except perhaps at the lowest boron level.

Table 7.2: Columnar austenite grain width, acicular ferrite lath width and reheated grain sizes for boron series.

Boron %	Columnar Austenite Grain Width (μm)	Acicular Ferrite Lath Width (μm)	Grain Size of Reheated Zone (μm)
<0.0005	135	2.86	5.13
0.0050	238	3.33	7.14
0.0088	324	3.33	7.41
0.0134	426	**	6.67
0.0176	500	**	6.06

** --- In-sufficient, continuous areas of AF, for measurements.

7.2.4 Non-metallic Inclusions

Figure 7.6, shows the details of the non-metallic inclusion population, including number per unit volume, mean three dimensional (3D) diameter and percentage with diameter equal or larger than $1\mu\text{m}$ for each weld, as measured using the SEM with an automated image analyser. For this boron series, mean 3D inclusion diameter is independent of boron level while percentage of inclusions with diameter greater than $1\mu\text{m}$ decreased with increase in boron and number density of inclusions tends to increase with weld metal boron, at 0.0088wt% boron number density of inclusions jumped significantly and does not represent the trend.

Influence of Boron on Weld Metal Properties

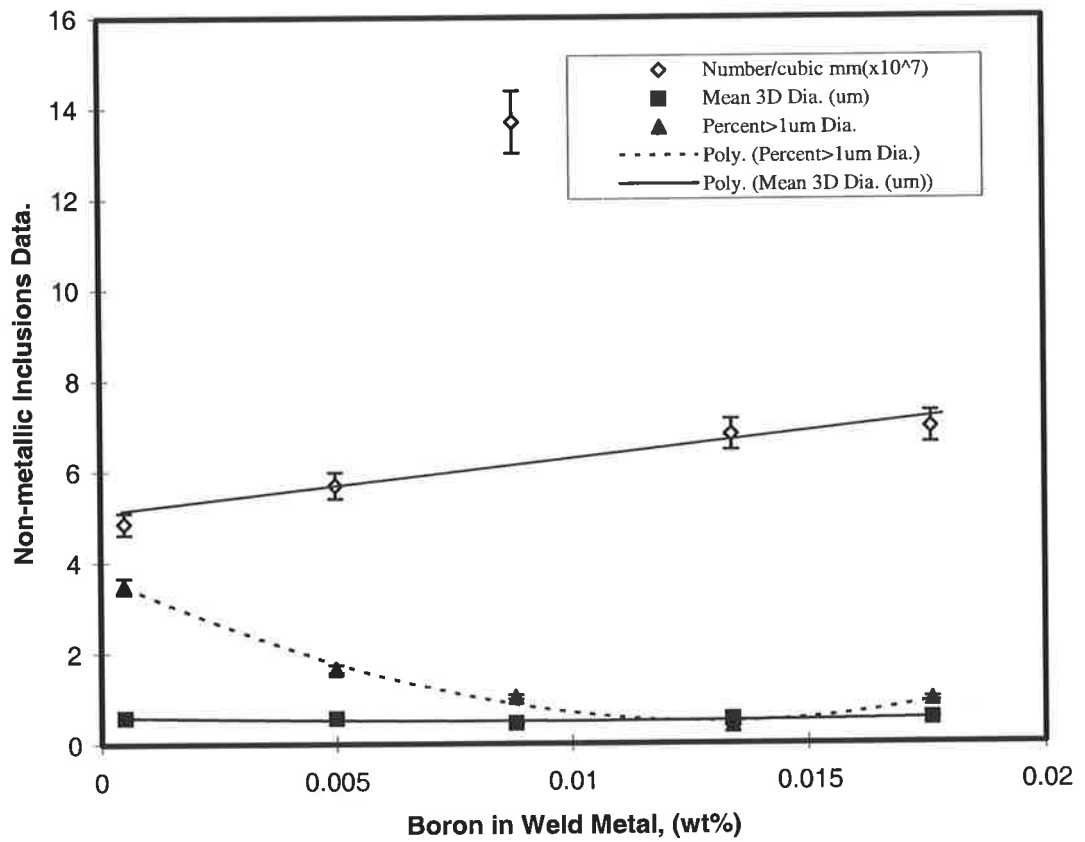


Figure 7.6: Variation of non-metallic inclusions number/mm³, mean 3D diameter and percent >1µm diameter with boron content.

Influence of Boron on Weld Metal Properties

Mean non-metallic inclusion compositions, as measured using energy dispersive X-ray analysis in an SEM, are listed in Table 7.3. These values indicate that there are no major changes in composition of the non-metallic inclusions with weld metal boron level. Note that any boron present in the inclusions does not appear in the energy dispersive analysis.

Table 7.3. Non-metallic inclusions with varying boron levels.

Weld Boron (%)	Number/ Cubic mm ($\times 10^7$)	Mean 3D Dia (μm)	Percent > $1\mu\text{m}$ Dia	Composition of Inclusions (wt%)			
				SiO ₂	MnO	Al ₂ O ₃	TiO ₂
<0.0005	4.86	0.58	3.5	34.50	46.70	14.10	3.80
0.0050	5.69	0.56	1.67	24.86	54.40	16.03	4.69
0.0088	13.70	0.45	1.02	20.91	58.24	14.69	6.16
0.0134	6.80	0.54	0.39	17.89	56.26	19.63	6.23
0.0176	6.95	0.54	0.96	23.24	44.12	27.76	4.88

7.3 Discussion

7.3.1 Weld Metal Tensile Properties

The tensile test data for the boron series shows that both yield and tensile strength were largely independent of boron content over the range tested ie from 0.0005wt% to 0.0176wt%. While elongation tended to decrease by about 30%. This is in agreement with results using other arc welding processes such as MMAW and SAW [123,168].

7.3.2 Weld Metal Impact Properties

The effect of boron in steel transformation kinetics has been a subject of research for many years. A number of toughness mechanisms have been proposed to explain the behaviour of boron in steels [169]. All assume that boron influences toughness by increasing the energy barrier against ferrite nucleation at austenite grain boundaries. It is not thought to influence the thermodynamic properties of the austenite and ferrite phases, ie reduce the A_{e3} -temperature of the steel. The toughness effect of boron is sensitive to variations in steel deoxidation and alloying practice. If the steel contains small amounts of dissolved oxygen and nitrogen, these elements may combine with boron to reduce the free, diffusible boron content [170].

The present results show, in the range tested, that the proportion of AF present generally decreases with the addition of boron. A corresponding increase in FS is seen, while PF tends

Influence of Boron on Weld Metal Properties

to decrease in the range from 30% to 10% with increase in boron level. The extent of this change in as-deposited microstructure with boron level is consistent with earlier studies, which were mostly concerned with other welding processes [130,131,168,170].

Three main factors controlling the toughness of boron-treated steels are:

1. The austenite grain size;
2. The segregation of boron atoms to austenite grain boundaries; and
3. The numbers of transformation nuclei such as non-metallic inclusions or coarse precipitates at austenite grain boundaries.

Generally with increasing austenite grain size, the number of nucleation sites for diffusion-controlled transformation decreases, resulting in the increase in toughness. The austenite grain size increases with raising the austenitising temperature. This is especially marked in the temperature range between 900 and 1000°C [171]. It is interesting to note here that the austenite grain coarsening takes place with increasing boron content. Liu and Olsen [140] showed that the prior austenite grain size increases with a decrease in the number of grain boundary pinning sites, and that grain boundary ferrite thickness is independent of the austenite grain size. The grain boundary ferrite thickness can be predicted using a modified Avrami equation. Increasing the prior austenite grain size was found to decrease the amount of grain boundary ferrite and to increase the amount of acicular ferrite in the final microstructure [140,172]. Large austenite grains allow greater undercooling in the centre of the austenite grain and produce finer intragranular ferrite.

Influence of Boron on Weld Metal Properties

In the as-deposited regions of welds, measurements were made of the prior austenite grain size, the grain size of the equiaxed reheated zone and of the mean lath width of acicular ferrite (see table 7.2). The acicular ferrite lath width and the grain size in the reheated zone were largely independent of boron except perhaps at the lowest boron level. The prior austenite grain size tended to increase significantly with boron level but the proportion of AF present generally decreases with the addition of boron. A corresponding increase in FS is also seen. This suggests that other factors are becoming important as the boron level increases.

Figure 7.3 shows that the upper-shelf values have considerable scatter but tend to decrease with boron level while the lower-shelf values are less dependent on boron. The T100J values show minimum values of about -45°C and -41°C at boron contents of approximately 0.0005wt% and 0.0134wt%, for all other boron levels T100J values tend to be insensitive to boron content and suggests that factors other than area of the ferrite morphologies are becoming important.

With boron additions the nucleation and growth of grain boundary ferrite is hindered and the weld metal intragranular inclusions will become the primary ferrite nucleation sites. Ohkita et al. [173] measured the inclusion size distributions for weld metal containing oxygen from 100ppm to 300ppm. They showed that the most frequent inclusion size is in the range of 0.3-0.7 microns, and that the average size of non-metallic inclusions increases as the oxygen content of titanium and boron-containing weld metal increases. This observation suggests that there is a specific range of weld metal oxygen content or inclusion size distribution, which is most favourable for acicular ferrite nucleation. Liu and Olsen [140] studied submerged arc

Influence of Boron on Weld Metal Properties

welds containing 250-350ppm oxygen. Their results showed that the welds which had an inclusion size distribution in the range of 0.2-0.4 microns had the largest volume fraction of acicular ferrite. It is also acknowledged that larger inclusions, of 1 μm or greater diameter, have been shown to be initiation sites for cleavage fracture [152,171,172,173] which is the main fracture mode for impact at low temperatures.

Figure 7.7 shows the variation in number density of inclusions with diameter greater than 1 μm ($N>1\mu\text{m}$) with increase in boron level. The $N>1\mu\text{m}$ values were calculated from the product of overall number density and the percentage with diameter greater than 1 μm values. This shows that $N>1\mu\text{m}$ tends to decrease with alloy level to reach relatively low values at boron levels greater than about 0.012wt%.

Influence of Boron on Weld Metal Properties

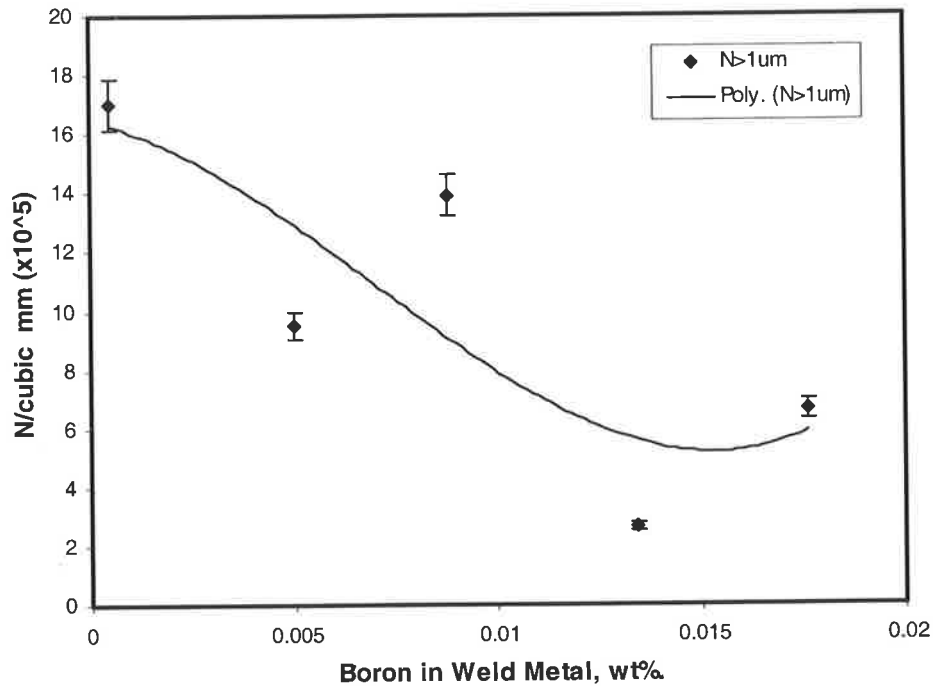


Figure 7.7: Number density of inclusions with diameter $> 1\mu\text{m}$ as a function of boron contents in the weld metal.

The total AF seems to vary from about 60% to 8% but taking into account that as solidified weld metal is about 60% of total weld metal, the variation in AF as a proportion of the total weld metal is 36% to 5%. Similarly variation in PF and FS as a proportion to the total weld metal will be less. The inclusions with diameter greater than $1\mu\text{m}$ ($N>1\mu\text{m}$) at low boron level will also be present in the 40% reheated region and could adversely affect the T100J temperature despite the high AF content in weld metal which has not been reaustenitised.

Influence of Boron on Weld Metal Properties

The main features of the observed low temperature impact behaviour may, to a reasonable extent in the case of boron, be explained on the basis of interaction between following factors:

1. the proportion of AF decreasing;
2. the proportion of FS increasing;
3. the proportion of PF decreasing (associated with prior austenite grain size increasing);
and,
4. the number density of large inclusions decreasing.

As AF tends to decrease and FS tends to increase continually with alloying addition, the PF decreases. Also the number density of large inclusions tends to decrease with alloying addition. Consequently, while low temperature impact properties may be expected to be continually degraded by lower AF and higher FS levels, this effect is offset by a reduction in PF and in particular the smaller number of the large inclusions ie inclusions with diameter greater than $1\mu\text{m}$ ($N > 1\mu\text{m}$) in weld metal, available to nucleate and propagate the cleavage fracture.

Chapter 8. Influence of Titanium and Boron on Weld Metal Properties

8.1 Introduction

The influence of boron on increasing acicular ferrite in weld metal microstructures is very small without sufficient titanium addition. The influence of titanium is also very small without sufficient levels of boron [130]. A large volume fraction of acicular ferrite (up to 95%) can be obtained by maintaining optimum boron and titanium contents. The decrease in low-temperature toughness with excess boron and titanium contents can be explained by the resulting increase in volume fraction of upper bainite [130].

Previous work has reported that balanced alloying with boron and titanium can almost eliminate formation of grain boundary ferrite [122-127]. The mechanism for the influence of boron is based on the fact that boron segregates extensively at the prior austenite grain boundaries, where it reduces the grain boundary energy [128]. It has been proposed that the

Influence of Titanium and Boron on Weld Metal Properties

reduction in grain boundary energy increases the energy barrier for nucleation of grain boundary ferrite by lowering the surface free energy ratio and therefore suppresses the formation of grain boundary ferrite and facilitating the nucleation of AF on oxide inclusions [2,129].

Titanium protects the boron from oxygen and nitrogen. Elemental boron hinders the formation of grain boundary ferrite resulting in increased undercooling of weld metal austenite which promotes the nucleation of fine intergranular acicular ferrite. The specific inclusion concentration and size distribution, with proper protection of weld metal boron, are the primary factors to achieve high intragranular acicular ferrite contents [131].

The role of titanium is mainly to protect boron from nitrogen (and oxygen) by forming titanium nitride (TiN) in the liquid state prior to solidification. The optimum titanium content will clearly be a function of the weld metal concentrations of nitrogen and nitride formers (V, Nb and Al). Mori, et al. [174], proposed that oxide particles with a surface coating of TiO, or those particles that were completely TiO, would be the most potent site for the nucleation of acicular ferrite. This is due to the 3.0% lattice discrepancy between TiO and ferrite is the smallest of all the potential nucleating agents. Compounds that have high values of discrepancy, such as BN and Al₂O₃, will not be as likely nucleation sites for the acicular ferrite.

Ohkita et al. [173], suggested the following mechanistic description of notch toughness improvement in the titanium-boron containing weld metal:

Influence of Titanium and Boron on Weld Metal Properties

1. During solidification, highly segregated boron reacts preferentially with nitrogen to form BN. The titanium protects the boron from oxygen.
2. During cooling in the austenite range, titanium protects the remaining boron from nitrogen by forming TiN. Free boron segregates to the austenite grain boundaries. The formation of nitrogen compounds with boron and titanium by the above reactions reduces the amount of nitrogen in solution.
3. On further cooling of the austenite to the ferrite transformation range, active boron, present at the austenite grain boundaries, reduces the grain boundary energy and retards the nucleation of proeutectoid ferrite.
4. Oxide inclusions that contain titanium promote the nucleation of acicular ferrite within austenite grains.

The purpose of this chapter is to characterise in greater detail the combined effects of boron and titanium on the microstructure and mechanical properties of multi-layer gas-shielded metal-cored arc weld metals.

8.2 Results

8.2.1 Weld Metal Composition

The chemical compositions of the all-weld-metal deposits studied are given in table 8.1 for the titanium-boron series. For 0.0005wt% boron, as the titanium level increased the oxygen level reduced from 0.0530wt% to 0.0380wt%, while the nitrogen level varied between 0.0054wt% and 0.0037wt%. For 0.0100wt% boron, as the titanium level increased the oxygen level varied between 0.046wt% to 0.039wt%, while the nitrogen level varied between 0.0036wt% and 0.0027wt%. These levels of oxygen and nitrogen are considered normal for this type of weld metal and process.

Influence of Titanium and Boron on Weld Metal Properties

Table 8.1: Weld metal compositions (wt %) with varying titanium and boron levels.

Si	Mn	C	S	P	Ni	Cr	Mo	Cu	V	Nb	Ti	Al	B	O	N
0.64	1.34	0.04	0.012	0.014	0.02	0.01	<0.01	0.01	0.0058	0.0005	0.0054	0.0133	< 0.0005	0.0530	0.0047
0.58	1.26	0.05	0.011	0.013	0.02	0.01	0.01	0.01	0.0058	<0.0005	0.0273	0.0142	< 0.0005	0.0420	0.0054
0.66	1.38	0.05	0.011	0.013	0.02	0.01	0.01	0.01	0.0066	<0.0005	0.0458	0.0111	< 0.0005	0.0380	0.0037
0.67	1.44	0.04	0.013	0.015	0.01	0.01	<0.01	0.01	0.0087	<0.0005	0.0054	0.0150	0.0095	0.0390	0.0027
0.68	1.47	0.05	0.013	0.015	0.01	0.01	<0.01	0.01	0.0096	<0.0005	0.0228	0.0150	0.0112	0.0430	0.0036
0.68	1.49	0.05	0.014	0.015	0.01	0.01	<0.01	0.01	0.0110	<0.0005	0.0430	0.0147	0.0110	0.0460	0.0036

8.2.2 Mechanical Properties

8.2.2.1 Tensile Properties

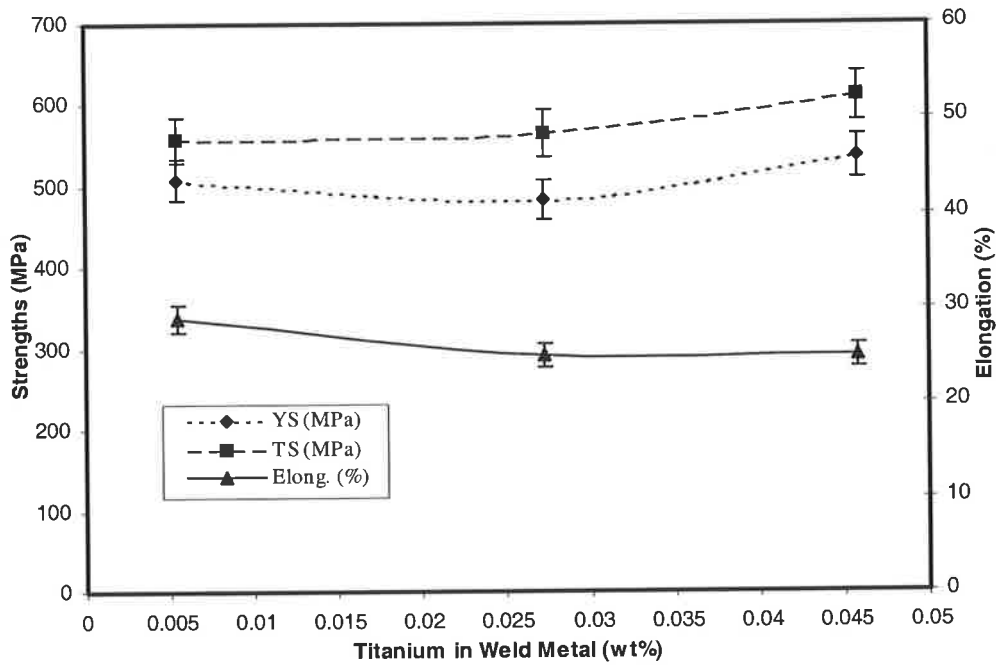
Results of the tensile test are presented in table 8.2 and figure 8.1 (a & b) for the titanium-boron series. The measured yield strengths varied between 482MPa and 556MPa, while tensile strengths varied between 557MPa and 610MPa and elongations were between 24% and 29%. For 0.0005wt% (figure 8.1 (a)) boron content, yield and tensile strength decreased as titanium increased to 0.0273wt% and then increased again at 0.0458wt%. This could be due to changes in manganese and silicon. While elongation decreased by about 14% as the titanium level increased in the weld metal. For 0.0100wt% boron (figure 8.1 (b)), as the titanium increases to 0.0228wt% both yield and tensile strength increased by about 5% to 12%, decreasing again at higher titanium levels. Elongation increased by about 8% as titanium increased. These changes in the titanium-boron series, over the range tested, are reasonably small for this type of process.

Influence of Titanium and Boron on Weld Metal Properties

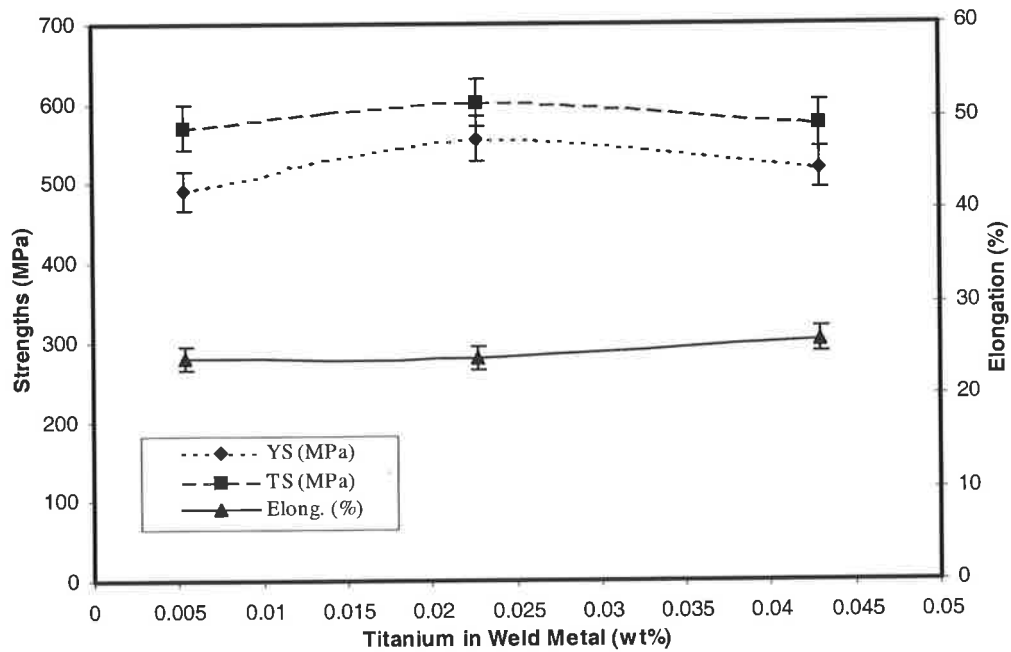
Table 8.2: Weld metal tensile properties with varying titanium and boron levels.

Boron %	Titanium %	Yield Strength (MPa)	Tensile Strength (MPa)	Elongation (%)
<0.0005	0.0054	507	557	29
<0.0005	0.0273	482	565	25
<0.0005	0.0458	535	610	25
0.0095	0.0054	491	571	24
0.0112	0.0228	556	602	24
0.0110	0.0430	519	575	26

Influence of Titanium and Boron on Weld Metal Properties



(a)



(b)

Figure 8.1: Variation in yield, tensile strength and percent elongation as a function of titanium for (a) 0.0005wt% boron (b) 0.0100wt% boron in the weld metal.

8.2.2.2 CVN Impact Results

The variations of mean CVN energy with test temperature for the various titanium-boron series weld metals are plotted in figure 8.2 (a) and (b) respectively. Figure 8.2 (a) shows CVN energies at 0.0005wt% boron versus titanium content. Mean CVN energies across the temperature range appear highest at 0.0054wt% titanium level. For 0.0100wt% boron, with an increase in titanium, figure 8.2 (b) the mean CVN energies across the temperature range are highest at 0.0228wt% titanium level.

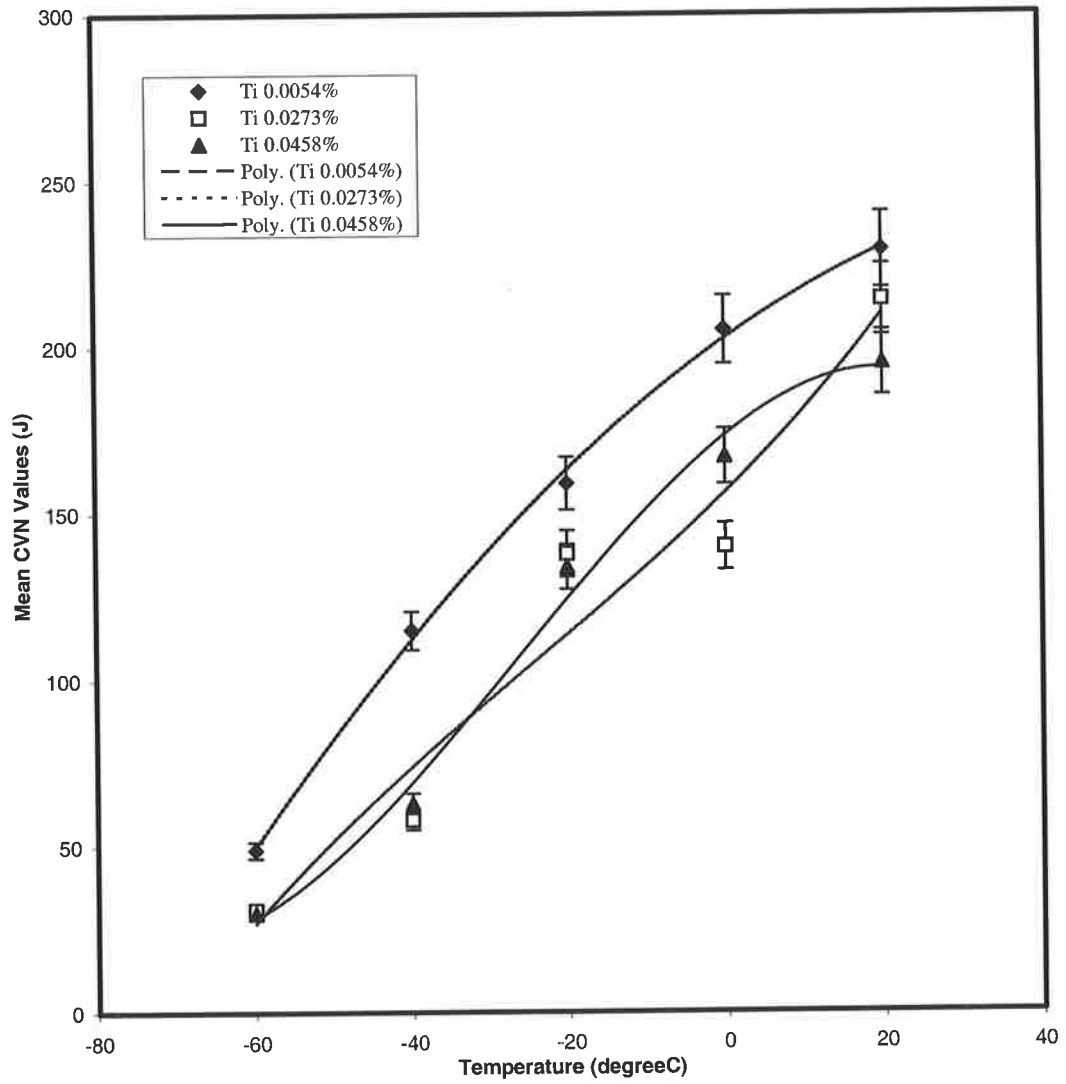
For each case the upper-shelf energy (at +20°C), the lower-shelf energy (at -60°C) and the temperature corresponding to a CVN energy of 100J (T100J) were found. These values are plotted in figure 8.3 (a) and (b) against weld titanium contents respectively.

Figure 8.3 (a) with 0.0005wt% boron shows that as titanium increases the upper-shelf and lower-shelf values tend to decrease. The T100J values, show minimum value of about -45°C at titanium contents of approximately 0.0054wt%, any further addition deteriorates T100J values.

The variations with 0.0100wt% boron with different titanium levels, as plotted in figure 8.3 (b) shows that the highest upper and lower-shelf values occur at the 0.0228wt% and 0.0430wt% titanium. Similarly the lowest T100J value of -62.5°C and -60.0°C occurs at the 0.0228wt% and 0.0430wt% titanium. The low temperature properties are best at high boron

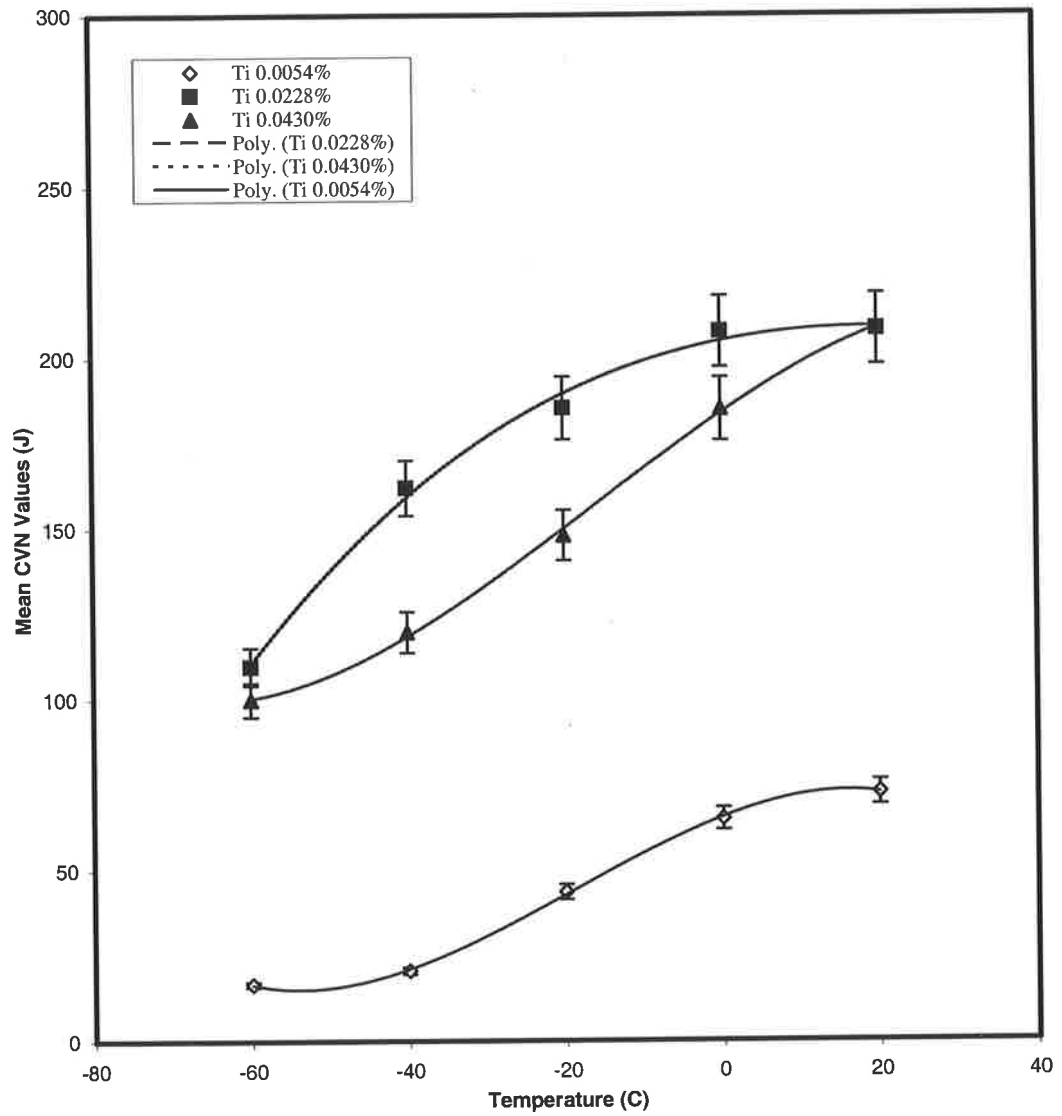
Influence of Titanium and Boron on Weld Metal Properties

and high titanium levels, but the best overall impact properties occur at 0.0100wt% boron and 0.0228wt% titanium.



(a) 0.0005wt% boron

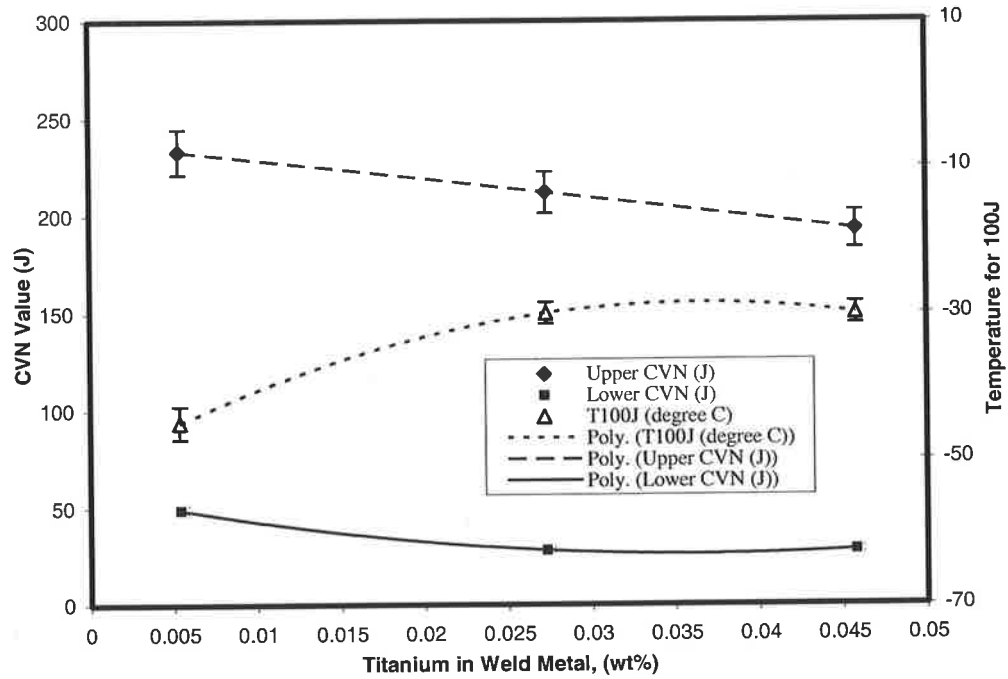
Influence of Titanium and Boron on Weld Metal Properties



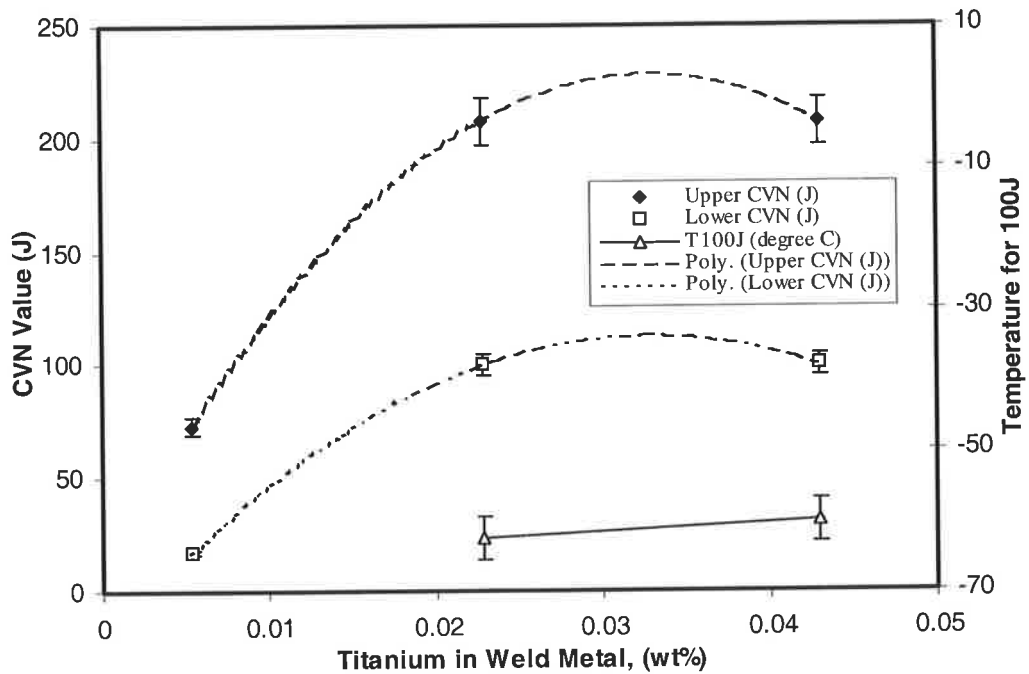
(b) 0.0100wt% boron

Figure 8.2: Mean CVN impact energy as a function of temperature at different titanium and boron levels in the weld metal.

Influence of Titanium and Boron on Weld Metal Properties



(a)



(b)

Figure 8.3: The upper CVN (J), lower CVN (J) and T100J ($^{\circ}$ C) values as a function of titanium contents for (a) 0.0005wt% boron and (b) 0.0100wt% boron in the weld metal.

8.2.3 Weld Metal Microstructure

Area measurements from cross-sections of welds indicated that the region of the weld from which mechanical test specimens (particularly CVN specimens) were extracted contained approximately 60% as-deposited and 40% reheated weld metal. Area fractions of acicular ferrite (AF), ferrite with second phase (FS) and primary ferrite (PF) were determined in as-deposited regions of the top layer from each weld.

Plots of the area fraction of AF, FS and PF with weld metal titanium at 0.0005wt% and 0.0100wt% boron levels are shown in figure 8.4 (a) and (b) respectively. In figure 8.4 (a) it can be seen that variation in titanium at 0.0005wt% boron. Here the area of AF tends to decrease in the range from 62.4% to 48% with an increase in the titanium level. A corresponding increase in FS is seen, as the changes in PF are relatively low. The extent of changes in the as-deposited microstructure with titanium levels at 0.0005wt% boron are relatively low in the range tested. A representative micrograph is shown in figure 8.5 (a) which show a weld containing 0.0458wt% titanium. It is interesting to note the areas of primary ferrite (PF).

Figure 8.4 (b) shows the variation in titanium at 0.0100wt% boron. Here the area of AF tends to increase sharply with 0.0228wt% titanium to 77.4% and then decreases slightly as titanium increases further to 0.0430wt%. As shown in figure 8.4 (b), FS also decreases as titanium increases to 0.0228wt% from 29% to 11%, with a further increase in titanium, FS increases to

Influence of Titanium and Boron on Weld Metal Properties

15% of as-deposited weld metal. PF shows a continuous and significant decrease as titanium increases from 33% to below 9% of as deposited weld metal.

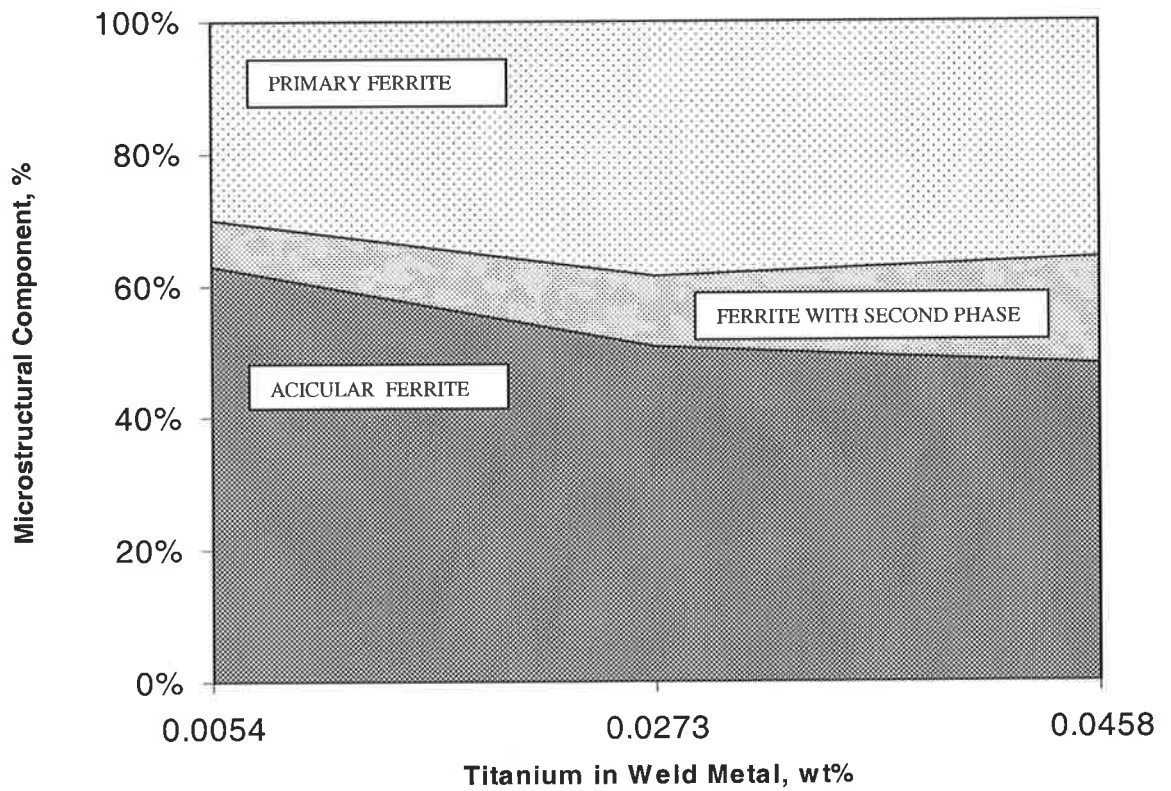
In addition to these measurements of area of the ferrite morphologies, measurements were also made of the prior austenite grain size, the grain size of the equiaxed reheated zone and of the mean lath width of acicular ferrite (see tables 8.3). For 0.0005wt% boron, as the titanium content increases, the prior austenite grain size and the grain size in the reheated zone were largely independent of titanium, except perhaps at the 0.0273wt% titanium level where it tended to increase slightly. The acicular ferrite lath width decreased with increasing titanium levels.

With higher boron levels, as the titanium content increases changes are significant; the prior austenite grain size, acicular ferrite lath width and grain size of the reheated zone decreased with an increase in titanium, with a maximum reduction at the middle titanium level of 0.0228wt%. Another important observation is that the overall grain size of the reheated zone for 0.0100wt% boron at all titanium levels decreased significantly by about 20%. The extents of changes in the re-heated weld microstructure with titanium levels are illustrated in figure 8.5 (b & c) which shows a weld containing 0.0273wt% titanium with 0.0005wt% boron and 0.0228wt% titanium with 0.0100wt% boron, respectively.

The extent of changes in the as-deposited microstructure with titanium levels at 0.0100wt% boron are illustrated in figure 8.5 (d, e & f), which shows welds containing 0.0054wt%,

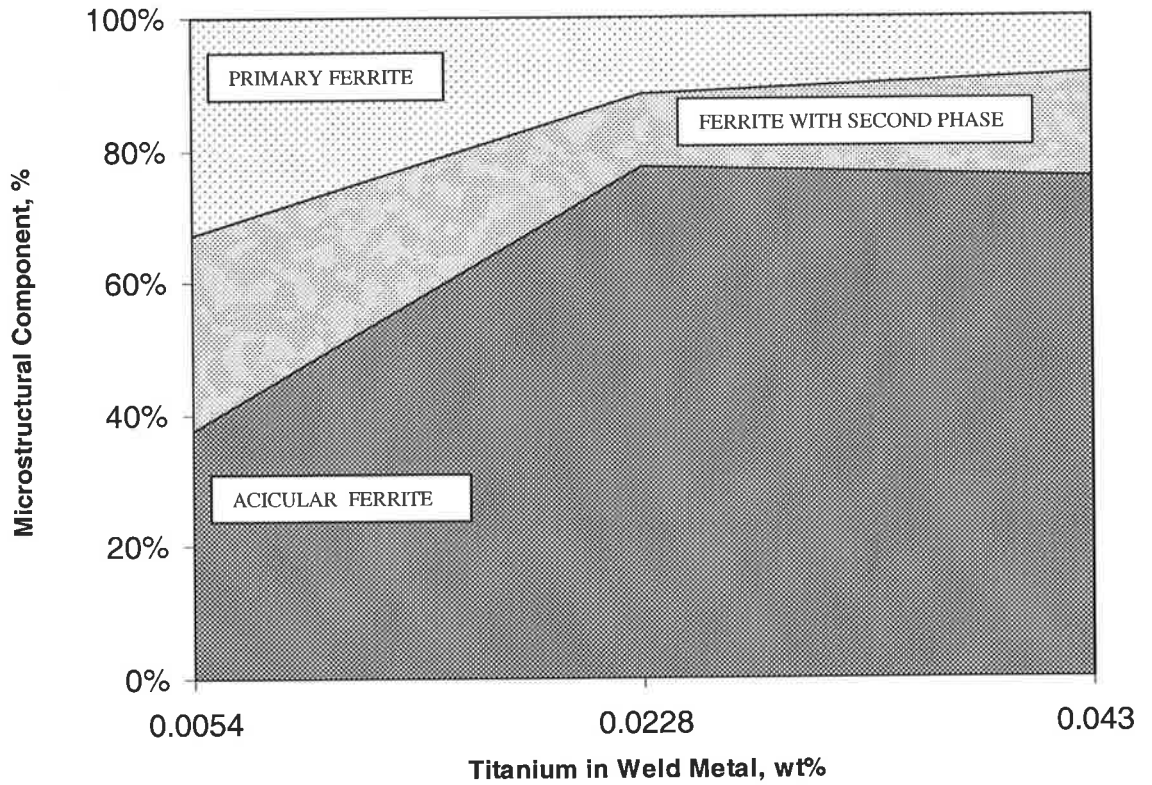
Influence of Titanium and Boron on Weld Metal Properties

0.0228wt% and 0.0430% titanium. It is interesting to note the areas of primary ferrite (PF) and changes in the size of acicular ferrite lath width.



(a) 0.0005wt% boron in weld metal

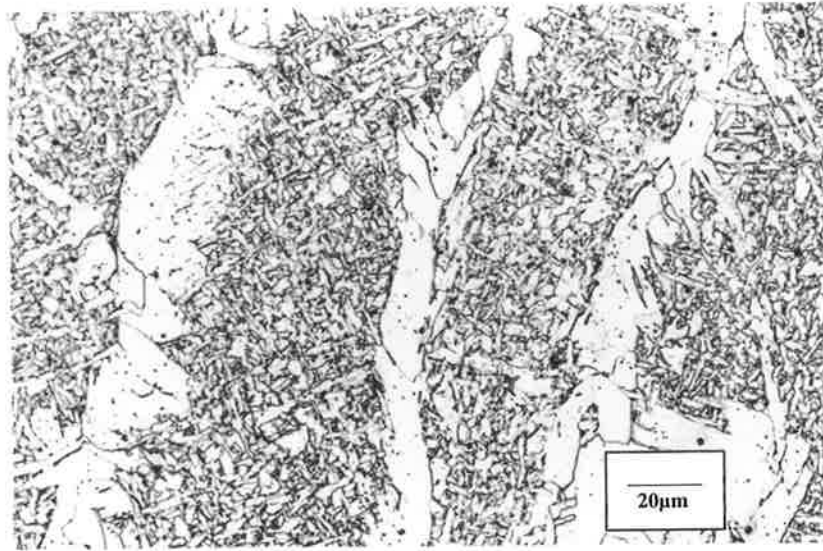
Influence of Titanium and Boron on Weld Metal Properties



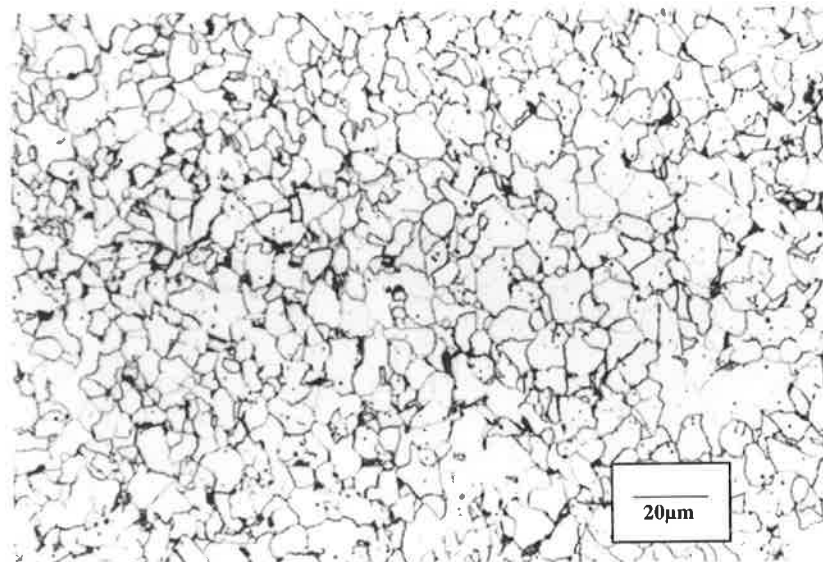
(b) 0.0100wt% boron in weld metal

Figure 8.4: Variation in the proportions of ferrite morphologies in as-deposited weld metal as a function of titanium contents at two boron levels.

Influence of Titanium and Boron on Weld Metal Properties

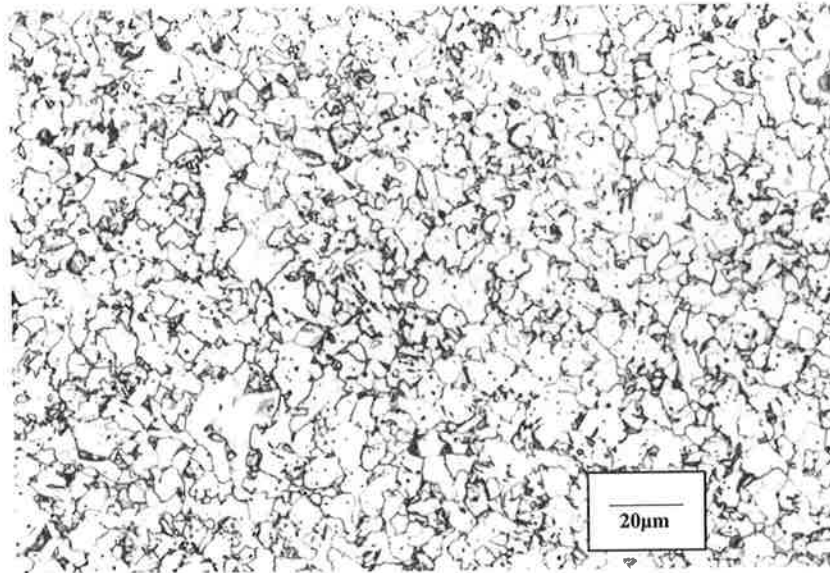


(a) as-deposited weld metal, 0.0005wt% boron and 0.0458wt% titanium

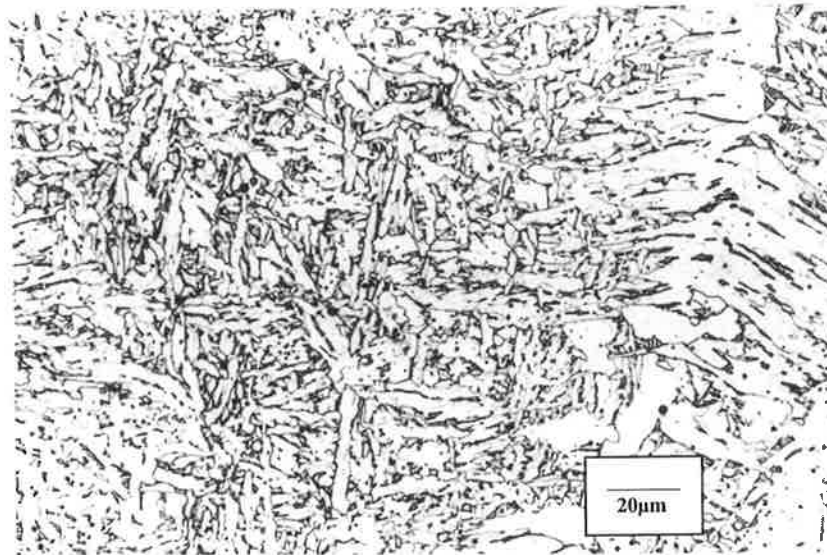


(b) re-heated weld metal, 0.0005wt% boron and 0.0273wt% titanium

Influence of Titanium and Boron on Weld Metal Properties

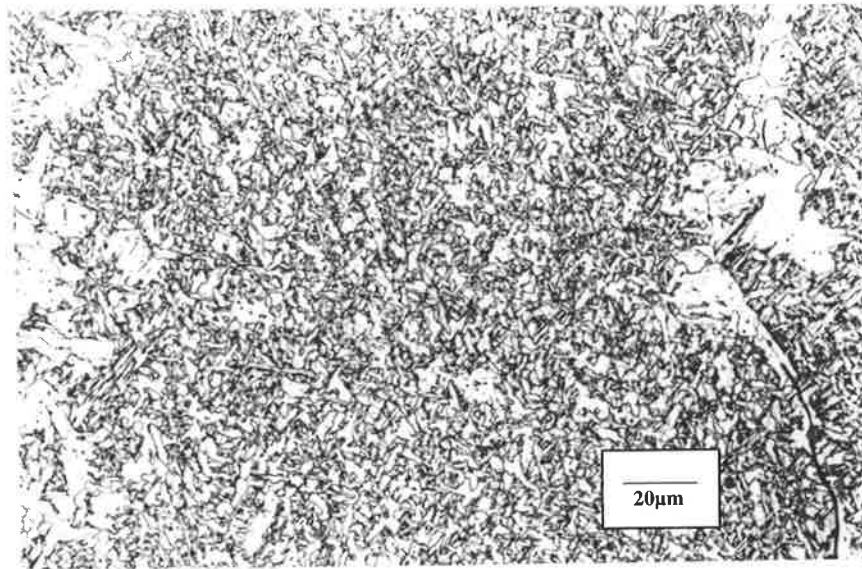


(c) re-heated weld metal, 0.0112wt% boron and 0.0228wt% titanium

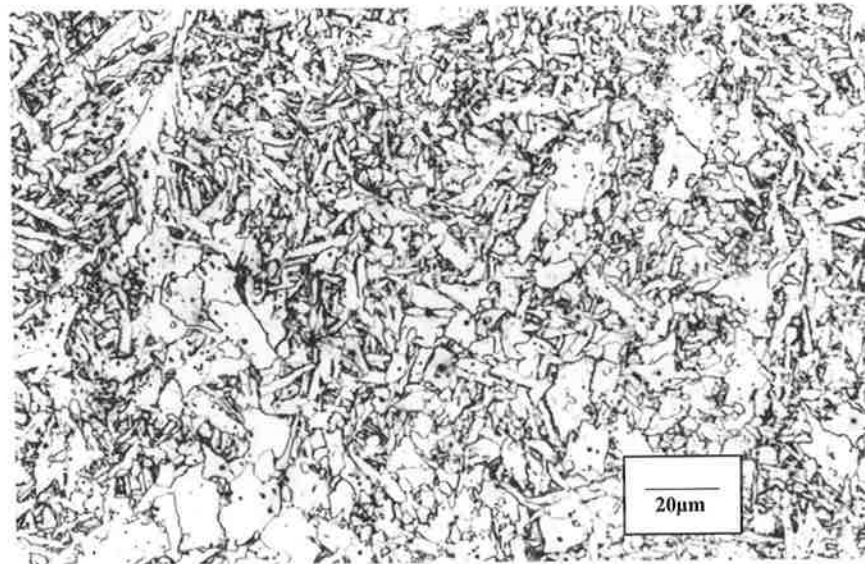


(d) as-deposited weld metal, 0.0095wt% boron and 0.0054wt% titanium

Influence of Titanium and Boron on Weld Metal Properties



(e) as-deposited weld metal, 0.0112wt% boron and 0.0228wt% titanium



(f) as-deposited weld metal, 0.0110wt% boron and 0.0430wt% titanium

Figure 8.5: Photomicrographs of as-deposited and re-heated weld metal for various titanium and boron levels.

Influence of Titanium and Boron on Weld Metal Properties

Table 8.3: Acicular ferrite lath width and reheated grain sizes for titanium and boron series.

Boron %	Titanium %	Columnar Austenite Grain Width (μm)	Acicular Ferrite Lath Width (μm)	Grain Size of Reheated Zone (μm)
<0.0005	0.0054	135	2.86	5.13
<0.0005	0.0273	150	2.44	5.56
<0.0005	0.0458	130	2.44	5.13
0.0095	0.0054	174	2.94	4.65
0.0112	0.0228	125	1.85	4.17
0.0110	0.0430	134	2.50	4.44

8.2.4 Non-metallic Inclusions

Influence of Titanium and Boron on Weld Metal Properties

Table 8.4 and figure 8.6 (a) & (b) show the details of the non-metallic inclusions, including number per unit volume, mean three dimensional (3D) diameter and percentage of diameter equal to or larger than $1\mu\text{m}$ for each weld, as measured using the SEM with an automated image analyser. For 0.0005wt% boron, as the titanium content increased both the mean 3D inclusion diameter and percentage of inclusions with a diameter greater than $1\mu\text{m}$ decreased, whilst the number density of inclusions measured tends to increase with weld-metal titanium, with a maximum at 0.0273wt% titanium.

The inclusion data for 0.0100wt% boron with an increase in titanium, indicates that the mean 3D inclusion diameter decreases with an increase in titanium whilst the number density of the inclusions appears to increase with an increase in weld-metal titanium level. The percentage of inclusions with a diameter greater than $1\mu\text{m}$ tends to decrease significantly as titanium increases to 0.0228wt% but increases again with a further increase in titanium even though this increase is quite small.

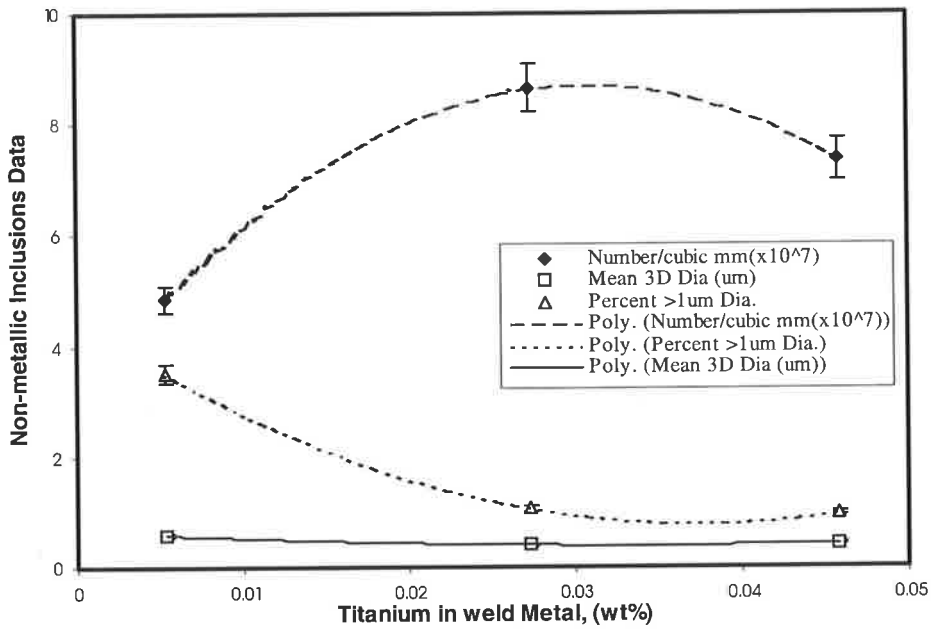
Mean compositions of non-metallic inclusion obtained using energy dispersive X-ray analysis in an SEM, are also listed in table 8.4. These values indicate that for both boron levels, as the titanium level increases, inclusions composition increases in TiO_2 at the expense principally of SiO_2 . MnO also decreases with an increase in titanium, while Al_2O_3 remains relatively unchanged. Note that boron present in the inclusions does not appear in the energy dispersive analysis.

Influence of Titanium and Boron on Weld Metal Properties

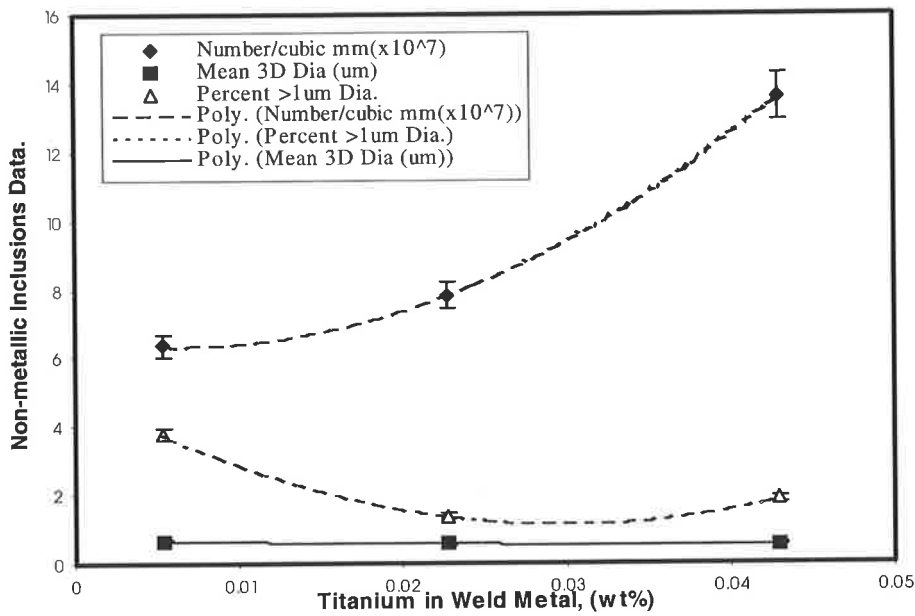
Table 8.4: Non-metallic inclusions with varying titanium and boron levels.

Weld Boron (%)	Weld Titanium (%)	Number/ Cubic mm ($\times 10^7$)	Mean 3D Dia (μm)	Percent > $1\mu\text{m}$ Dia	Composition of Inclusions (wt%)			
					SiO ₂	MnO	Al ₂ O ₃	TiO ₂
<0.0005	0.0054	4.86	0.58	3.5	34.5	46.7	14.1	3.82
<0.0005	0.0273	8.63	0.40	1.06	14.93	47.79	7.18	29.91
<0.0005	0.0458	7.36	0.42	0.96	11.77	29.42	10.53	48.28
0.0095	0.0054	6.35	0.66	3.76	19.15	65.39	10.13	5.34
0.0112	0.0228	7.81	0.57	1.38	12.17	48.71	16.59	22.54
0.0110	0.0430	13.6	0.55	1.87	9.18	44.61	10.67	35.54

Influence of Titanium and Boron on Weld Metal Properties



(a) 0.0005wt% boron in weld metal



(b) 0.0100wt% boron in weld metal

Figure 8.6: Variation of non-metallic inclusions number/mm³, mean 3D diameter and percent>1μm diameter with titanium level at two boron levels.

8.3 Discussion

8.3.1 Weld Metal Tensile Properties

The tensile test data for the titanium and boron series shows that both yield and tensile strength showed some variation, which reflects changes in weld metal microstructural component and refinement in acicular ferrite lath width and grain size of the reheated zone. However these changes, for the range of titanium and boron tested, are reasonably small. This is in agreement with data from other arc welding processes such as MMAW and SAW [123,168].

8.3.2 Weld Metal Impact Properties

Micro alloying influences impact properties of weld metal by varying the microstructure (area fraction of various phases) of the as-deposited and reheated weld metal region, non-metallic inclusions, strength levels and grain size.

The effect of boron on steel transformation kinetics is significant and has been the subject of research for many years. A number of mechanisms for notch toughness of steels have been proposed to explain the behaviour of boron [169]. Most work have assumed that boron influences notch toughness by increasing the energy barrier against ferrite nucleation at austenite grain boundaries, without influencing the thermodynamic properties of the austenite

Influence of Titanium and Boron on Weld Metal Properties

and ferrite phases, i.e. reduce the A_{F3} temperature of the steel. The notch toughness effect of boron is sensitive to variations in the applied steel deoxidation and alloying. If steel contains small amounts of dissolved oxygen and nitrogen, these elements may combine with boron to reduce the free, diffusible boron content [170].

Results confirm that the influence of boron on increasing acicular ferrite in weld metal microstructures was very small without sufficient titanium addition. The influence of titanium was also very small without sufficient levels of boron. A large volume fraction of acicular ferrite can be obtained by maintaining optimum boron and titanium contents. This compares well with work by several authors who reported that boron segregates extensively to the prior austenite grain boundaries and reduces the grain boundary energy, which increase the energy barrier to nucleation by lowering the surface free energy ratio and therefore suppress the formation of grain boundary ferrite, facilitating nucleation on oxide inclusions [2,122-129].

The present results show, in the range tested, that the fraction of AF present generally decreases with the addition of titanium for 0.0005wt% boron. A corresponding increase in FS and PF is seen. As the boron level increases to 0.0100wt%, an increase in titanium results in a significant increase in AF at the expense of FS and PF. The extent of this change in as-deposited microstructure with titanium-boron level is consistent with earlier studies, which mainly conducted using other welding processes [130,168].

In the as-deposited regions of welds, measurements were made of the prior austenite grain size, the grain size of the equiaxed reheated zone and of the mean lath width of acicular ferrite

Influence of Titanium and Boron on Weld Metal Properties

(see table 8.3). The acicular ferrite lath width and the grain size in the reheated zone were largely independent of titanium at the lower boron level. At higher boron levels for all titanium levels, the grain size in the reheated zone showed refinement particularly with 0.0228wt% titanium. AF on the other hand showed significant refinement with only 0.0228wt% titanium and 0.0100wt% boron. The prior austenite grain size shows some scatter with changes in boron and titanium, and does not show any clear trend within the range tested.

Another important thing for this series of titanium and boron compositions, figure 8.7 shows a summary plot of the variation in AF as a function of weld metal T100J (°C) temperature values. Here a direct relationship is seen between low temperature impact properties and AF. A higher percentage of AF gives a lower 100J temperature. Another important feature to note is that as-deposited weld metal only represents 60% of weld metal, therefore other factors must be considered. Figure 8.8 shows summary plot of the variation in grain size in the reheated zone (μm) as a function of weld metal T100J(°C) temperature values. It is clear from the graph that refinement in grain size of the reheated zone also contributes towards obtaining better low temperature impact properties.

Influence of Titanium and Boron on Weld Metal Properties

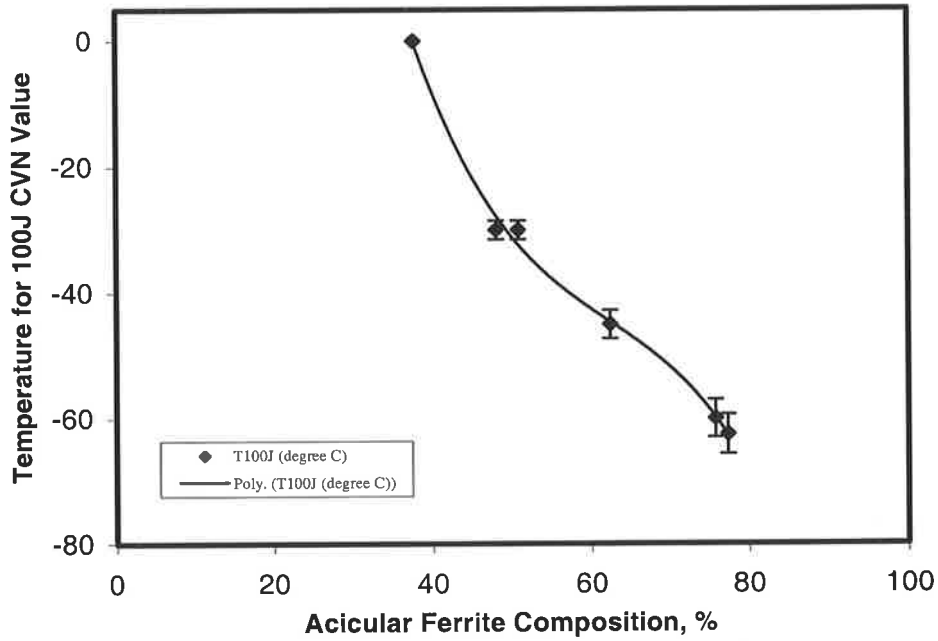


Figure 8.7: Summary plot of the variation in weld metal T100J ($^{\circ}\text{C}$) temperature values as a function of percentage of acicular ferrite.

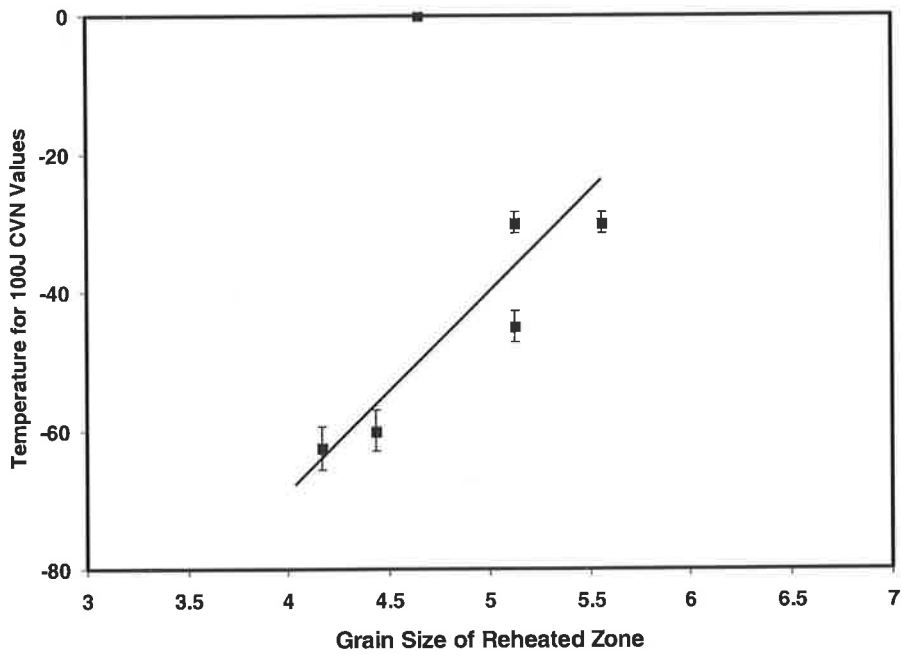


Figure 8.8: Summary plot of the variation in weld metal T100J ($^{\circ}\text{C}$) temperature values as a function of grain size of reheated zone (μm).

Influence of Titanium and Boron on Weld Metal Properties

Figure 8.3 shows that the upper-shelf values tend to decrease with titanium level whilst the lower-shelf values increase slightly for lower boron levels. The T100J values show a minimum at -45°C at 0.0005wt% boron and 0.0054wt% titanium, any further increase in titanium adversely affects T100J values. For higher boron, as titanium increases both the upper-shelf values and lower-shelf energy values increase significantly, and T100J temperature values improve substantially going down to -62.5°C .

With boron and titanium additions the nucleation and growth of grain boundary ferrite is hindered, and the weld metal intra-granular inclusions become the primary ferrite nucleation sites. Ohkita et al.[173] measured the inclusion size distributions for weld metal containing oxygen from 100ppm to 300ppm. They showed that the most frequent inclusion size is in the range 0.3-0.7 microns, and that the average size of non-metallic inclusions increases as the oxygen content of titanium and boron containing weld metal increases. This observation suggests that there is a specific range of weld metal oxygen content or inclusion size distribution, which is most favourable for acicular ferrite nucleation. Liu and Olsen [140] studied submerged arc welds containing 250-350ppm oxygen. Their results showed that the welds which had an inclusion size distribution in the range 0.2-0.4 microns had the largest volume fraction of acicular ferrite. Results in this study show an inclusion size distribution in the range 0.4-0.5 microns yields the highest volume fraction of AF. This compares favourably with Ohkita et al but is a little higher than the range found by Liu and Olsen. This variation may be due to the higher oxygen content associated with this GMAW process, which is in the range of 400-500ppm. It is also acknowledged that larger inclusions, of $1\mu\text{m}$ or greater

Influence of Titanium and Boron on Weld Metal Properties

diameter, have been shown to be initiation sites for cleavage fracture [148,152,156], which is the main mode of impact fracture at low temperatures.

Figure 8.6 shows the variation in percentage of inclusions with a diameter greater than $1\mu\text{m}$ ($N>1\mu\text{m}$) with an increase in titanium level. This shows that the percentage $>1\mu\text{m}$ tends to decrease with alloy level to reach relatively low values at titanium levels greater than about 0.0228wt%. Whilst the number density of inclusions generally increases, the mean 3D diameter of inclusions is independent of an increase in titanium levels.

The main features of the observed low temperature impact behaviour may, to a reasonable extent in the case of titanium and boron, be explained on the basis of interactions between following factors:

In the as deposited weld metal:

- (a) the proportion of AF increasing,
- (b) the proportion of FS and PF decreasing;

and in the reheated weld metal:

refinement in grain size of the reheated zone.

AF tends to increase and FS and PF tend to decrease continually with alloy addition, and the percentage of large inclusions also tends to decrease with alloy addition. Also refinement in grain size in the reheated zone combines to give the best low temperature impact properties.

Chapter 9. Summary and Conclusions

9.1 Introduction

The aim of the research presented in this thesis was to investigate the influence of alloying additions on weld metal mechanical properties from gas-shielded metal-cored wires for joining structural grade steel. It was further aimed at understanding the reasons for these effects of alloying on mechanical properties through assessment of the details of weld microstructures including details of as-welded and reheated regions as well as non-metallic inclusions.

A review of the literature showed that little research has been carried out in the field of GMAW, most of the work having been done for MMAW and SAW processes. Detailed knowledge of the influence of alloying and microalloying elements on the weld microstructure and mechanical properties from the gas shielded processes lags well behind, and the purpose of the current study is to address this lack of information.

To achieve this aim, batches of specially formulated metal-cored wires were manufactured in which alloy additions were varied over predetermined ranges. The alloying elements

Summary and Conclusions

investigated were: manganese, silicon, titanium, aluminium and boron. Test plates were welded from each of these wires, (using multi-pass welds) under a controlled set of welding conditions so that weld metal tensile and low temperature impact properties could be assessed. This fundamental study of metal-cored welding consumables for gas-shielded welding is required for designing microalloyed consumables with optimum low temperature impact properties.

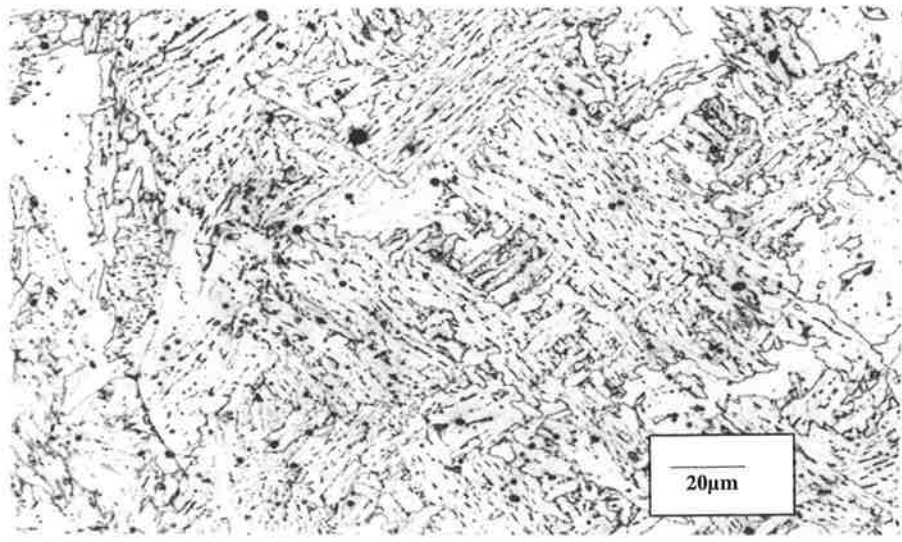
A desired improvement in properties may require only a few tenths of one percent of an alloying element. Sometimes improved properties are gained by stringent control and/or reduction of an element that may have been tolerated as a residual element in other welding processes. This is a relatively new approach in alloying technology that can be credited with improving the quality of welding consumables. In the present study all of the alloy compositions studied belong to one class of steel ie low carbon low alloy steel. All compositions are similar with only slight changes in residual alloying elements. These are varied less than few hundred parts per million (ppm). For these minor variations the microstructural changes observed are significant (figure 9.1 (a)(b)&(c)). The figures clearly show a transition in the microstructure of as-deposited weld metal. Figure 9.1(a) shows structure dominated by primary ferrite, while figure 9.1(b) is dominated by ferrite with second phase. Figure 9.1(c) shows more desirable microstructure of acicular ferrite.

These major changes produced by relatively small variations in alloying addition should be carefully and systematically studied to accomplish a desired improvement in properties that will result in a superior consumable with optimised properties.

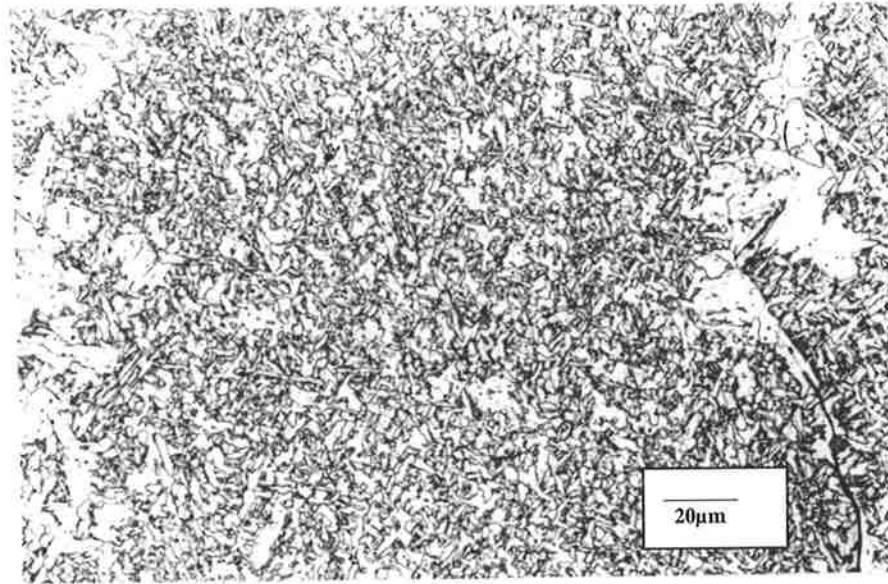
Summary and Conclusions



(a) 0.0570wt% aluminum in weld metal.



(b) 0.0176wt% boron in weld metal.



(c) 0.0112wt% boron and 0.0228wt% titanium in weld metal.

Figure 9.1: Photomicrographs of as-deposited weld metal with (a) 0.0570wt% aluminum, (b) 0.0176wt% boron, (c) 0.0112wt% boron and 0.0228wt% titanium in weld metal.

9.2 Influence of Manganese and Silicon on Weld Metal Properties

Both yield strength and tensile strength increase in a fairly regular manner, the most likely explanation for this behaviour of the result is decrease in effective grain size and solid solution strengthening over both the as-deposited and reheated regions, with increase in manganese and silicon. This essentially linear increase has been observed previously for other arc welding processes such as MMAW [7,9].

The best low temperature impact properties were obtained with manganese contents between 1.3 and 1.6wt%, provided the silicon content was maintained below 0.7wt%. The

Summary and Conclusions

main features of the observed low temperature impact behaviour in the case of manganese and silicon can be explained on the basis of the interaction between following factors;

1. Increase in both yield strength and tensile strength.
2. A decrease in the proportion of PF.
3. An increase in the proportion of AF.
4. Decrease in AF lath size.
5. Decrease in re-heated grain size.
6. Increase in the number density of large inclusion.

The decrease in proportion of PF is associated with an increase in the proportion of AF as the manganese and silicon is increased in weld metal. A continuous refinement of AF lath size and re-heated grain size also occurs with increase in alloy content. Low temperature impact properties may be expected to continually improve over the range of alloys tested.

The inclusions with diameter greater than $1\mu\text{m}$ ($N > 1\mu\text{m}$) at all manganese and silicon levels were also present in the 40% reheated region and adversely affect T100J temperature. Another factor that influences weld metal impact properties is the increase in weld metal strength. Increase in strength has a deleterious effect on impact properties.

Consequently, while low temperature impact properties may be expected to be continually improved by lower PF, higher AF levels and refinement of AF lath size and re-heated grain size, these effects are offset by increases in yield strength and tensile strength and the increased number of large inclusions in the weld metal, available to nucleate and propagate the cleavage fracture.

Summary and Conclusions

These observations suggest that low manganese contents did not result in sufficient AF and grain refinement to significantly increase impact properties while high manganese and silicon resulted in high values of both $N > 1\mu\text{m}$ and weld strength, thus degrading the impact properties. Best impact properties were obtained with weld metal manganese contents between 1.3 and 1.6wt%, provided the silicon level was less than 0.7wt% as shown in figure 4.5. These impact properties are better than those obtained from other welding processes as Charpy-V-Notch values of 100J were achieved at temperatures lower than -40°C . This could be due to the close control of the composition in the production of the experimental wires compared with commercially produced wires. The carbon contents are also generally lower (as are oxygen and nitrogen levels) compared to strength equivalent commercial flux-cored and metal-cored consumables.

9.2.1 Conclusions

1. The yield and tensile strengths of the welds depend primarily on the weld manganese and silicon levels with both yield and tensile strength values increasing approximately linearly with manganese and silicon value. In terms of microstructure, increase in manganese and silicon levels gives rise to an overall decrease in grain size in both as-deposited and reheated regions and this is most likely responsible for the strength increases.
2. The impact behaviour cannot be explained by any single microstructural feature, but while low temperature impact properties may be expected to continually improve by lower PF, higher AF levels and refinement of AF lath size and reheated grain size, this effect is offset by increases in both yield strength and tensile strength and the increased number of the large inclusions in the weld metal to nucleate and propagate the cleavage fracture.

Summary and Conclusions

3. The optimum weld metal low temperature impact properties occur in a zone when weld manganese is in the range 1.3 to 1.6wt% and weld silicon is in the range 0.3 to 0.6wt%.

9.3 Influence of Titanium and Aluminium on Weld Metal Properties

The optimum manganese and silicon values determined previously in this study were used. Further the influence of titanium and aluminium was studied. Both yield and tensile strength increased by about 50MPa as the weld titanium level was increased from 0.005wt% to 0.095wt%, but were approximately constant as the weld aluminum level was increased from 0.013wt% to 0.065wt%. The tensile properties are consistent with those reported for MMAW [157].

It was observed that there was little apparent difference in either the appearance of the reheated zones or in the measured grain sizes of the equiaxed portions of these zones between the trial welds. This is in agreement with other investigators. It can be concluded that the reheated regions play a minor part in determining weld impact properties [148,158].

AF is widely considered to be the most beneficial to impact properties because it consists of small non-aligned grains with high angle boundaries and therefore provides a difficult path for cleavage. It has been shown that maximum AF occurs at total aluminum and titanium of around 0.02wt% which is at a ratio of aluminum to titanium of approximately 2.4:1, This is consistent with earlier studies which were mostly concerned with other welding processes [157,159,160].

Summary and Conclusions

Number density of inclusions with diameter greater than $1\ \mu\text{m}$ ($N > 1\ \mu\text{m}$) tends to decrease with alloy level to reach relatively low values at titanium levels between about 0.04 and 0.09wt% and aluminum levels greater than about 0.04wt%. The inclusions with diameter greater than $1\ \mu\text{m}$ ($N > 1\ \mu\text{m}$) at low titanium and aluminum level will also be present in the 40% reheated region and could adversely affect T100J temperature despite the high AF content in weld metal which has not been reaustenitised. The total AF seems to vary from about 60% to 20% but taking into account that as solidified weld metal is about 60% of total weld metal, the variation in AF as a proportion of the total weld metal is 36% to 12%.

The main features of the observed low temperature impact behaviour may, to a reasonable extent, be explained on the basis of the interaction between two factors: the proportion of AF present and the number density of large inclusions. This is because, although AF tends to decrease continually with alloy addition, the number density of large inclusions also tends to decrease with alloy addition. Consequently, while low temperature impact properties may be expected to be continually degraded by lower AF levels, this effect is offset by the smaller number of the large inclusions available to nucleate the cleavage fracture.

9.3.1 Conclusions

1. Yield and tensile strength increased by about 50 MPa as weld metal titanium level was increased, but were independent of increases in aluminium level. These changes in strength are relatively small and do not appear to have any effect on impact properties.
2. For the range tested, results show that the proportion of AF decreases with additions of either titanium or aluminum. The maximum AF occurs at total

Summary and Conclusions

aluminum and titanium of around 0.02wt% with ratio of aluminum to titanium around 2.4:1.

3. The number density of large non-metallic inclusions decreased with increased additions of either titanium or aluminium.
4. Low temperature impact behaviour appears to largely depend on the combination of the proportion of AF and the number density of large inclusions. More AF or fewer large inclusions results in improved impact properties.
5. The optimum weld metal low temperature impact properties occur at the lowest weld aluminium level tested and at weld titanium levels of either 0.005wt% (the lowest tested) or 0.085wt%.

9.4 Effect of Stress Relief on Low and High Titanium containing Weld

Metals

The metallographic studies have confirmed that stress relieving has a pronounced effect on the microstructure, causing precipitation and spheroidisation of second phase particles. The phenomenon has been documented by Cochrane [161] for plate steel, by Farrar et al [162] for submerged-arc weld metal, and by Evans [163] for MMAW.

Hardness levels were reduced by stress relieving throughout the bulk of the all-weld-metal deposits studied. This agrees with the results obtained by Evans [163]. Bush and Kelly [164] also found that hardness and tensile strength decreased during tempering and this behaviour is also found during tempering of martensite in the weld metal (Leslie) [165].

The main consequence of stress relieving is to affect the shift in the transition range, which is dependent on the levels of carbon and manganese [163]. For both low and high

Summary and Conclusions

titanium levels with carbon 0.05wt% and manganese 1.35wt%, the mean notch toughness at all temperatures tested showed an increase after heat treatment. For low titanium an increase of about 50J over the whole temperature range was found, while for the higher titanium levels this increase was 20 to 50J. This positive response to heat treatment is clearly a desirable feature and the idealised composition remains optimised.

9.4.1 Conclusions

1. For both the low and high titanium-containing weld metals, stress relief heat treatment gave an improvement in CVN impact values of 20 to 50J over the whole temperature range.
2. Measurements of grain size and the percentage area of AF, FS and PF gave very similar results for both low and high titanium levels. Improvement in toughness is due to softening of the ferrite and tempering of any martensite in the M/A constituent.

9.5 Influence of Boron on Weld Metal Properties

The boron series shows that both yield and tensile strength were largely independent of boron content over the range tested. While elongation tended to decrease by about 30%. This is in agreement with results using other arc welding processes such as MMAW and SAW [123,168].

Boron influences toughness by increasing the energy barrier against ferrite nucleation at austenite grain boundaries. It is not thought to influence the thermodynamic properties of the austenite and ferrite phases, ie reduce the A_{e3} -temperature of the steel. The toughness effect of boron is sensitive to variations in steel deoxidation and alloying practice. If the

Summary and Conclusions

steel contains small amounts of dissolved oxygen and nitrogen, these elements may combine with boron to reduce the free, diffusible boron content [170].

The acicular ferrite lath width and the grain size in the reheated zone were largely independent of boron except at the lowest boron level. The prior austenite grain size increased significantly with boron level but the proportion of AF present decreased with the addition of boron. A corresponding increase in FS is also seen. This suggests that other factors are important as the boron level increases.

The T100J values show minimum values of about -45°C and -41°C at boron contents of approximately 0.0005wt% and 0.0134wt%. For all other boron levels T100J values tend to be insensitive to boron content and suggests that factors other than the area of the ferrite morphologies are becoming important.

The total AF seems to vary from about 60% to 8% but taking into account that as solidified weld metal is about 60% of total weld metal, the variation in AF as a proportion of the total weld metal is 36% to 5%. Similarly variation in PF and FS as a proportion to the total weld metal will be less. The inclusions with diameter greater than $1\mu\text{m}$ ($N > 1\mu\text{m}$) at low boron levels will also be present in the 40% reheated region and could adversely affect the T100J temperature despite the high AF content in weld metal, which has not been reaustenitised.

The main features of the observed low temperature impact behaviour may, to a reasonable extent in the case of boron, be explained on the basis of interaction between the following factors. With increasing boron levels;

1. The proportion of AF decreases.
2. The proportion of FS increases.

Summary and Conclusions

3. The proportion of PF decreases (associated with the prior austenite grain size increasing).
4. The number density of large inclusions decreases.

As AF tends to decrease and FS tends to increase continually with alloying addition, the PF decreases. Also the number density of large inclusions tends to decrease with alloying addition. Consequently, while low temperature impact properties may be expected to be continually degraded by lower AF and higher FS levels, this effect is offset by a reduction in PF and in particular the smaller number of the large inclusions, i.e. inclusions with diameter greater than $1\mu\text{m}$ ($N > 1\mu\text{m}$) in weld metal, available to nucleate and propagate the cleavage fracture.

9.5.1 Conclusions

1. Yield and tensile strengths were virtually independent of the weld boron level over the range tested.
2. The proportion of AF decreased markedly with increased boron addition, this was accompanied by an increase in FS, and a decrease in the proportion of large non-metallic inclusions.
3. Low temperature impact properties of the weld metal were best with no added boron or with boron levels of around 0.013wt%. However the variation in low temperature impact over the range of boron values tested was small.

9.6 Influence of Titanium and Boron on Weld Metal Properties

Small changes are seen in both yield and tensile strength, which reflect changes in the proportions of the weld metal microstructural components and refinement of the acicular

Summary and Conclusions

ferrite lath width and grain size of the reheated zone. This is in agreement with data from other arc welding processes such as MMAW and SAW [123,168].

Results confirm that the influence of boron on increasing acicular ferrite in weld metal microstructures was very small without sufficient titanium addition. The influence of titanium was also very small without sufficient levels of boron. A large volume fraction of acicular ferrite can only be obtained by maintaining optimum boron and titanium contents. This conclusion is suggested by several authors who have reported that boron suppresses the formation of grain boundary ferrite, facilitating nucleation of AF on oxide inclusions [2,122-129].

The acicular ferrite lath width and the grain size in the reheated zone were largely independent of titanium at the lower boron level. However at higher boron levels for all titanium levels, the grain size in the reheated zone showed refinement particularly with 0.0228wt% titanium. AF on the other hand showed very significant refinement with only 0.0228wt% titanium and 0.010wt% boron.

Also of importance is the direct relationship between low temperature impact properties and AF. A higher percentage of AF gives a lower 100J temperature. Another feature to note is the grain refinement in the reheated zone which can be directly related to the weld metal T100J(°C) temperature values.

The T100J values show minima of about -45°C at 0.0005wt% boron and 0.0054wt% titanium, any further increase in titanium degrades T100J values. For higher boron, as titanium is increased both the upper-shelf values and the lower-shelf values increase significantly, and the T100J temperature values improve substantially to -62.5°C. The

Summary and Conclusions

percentage of inclusions $>1\mu\text{m}$ tend to decrease with increasing alloy level to reach relatively low values for titanium levels greater than about 0.0228wt%. Whilst the number density of inclusions generally increased, the mean 3D diameter of inclusions is independent of an increase in titanium levels.

The main features of the observed low temperature impact behaviour may, to a reasonable extent in the case of titanium and boron, be explained on the basis of the interactions between the following factors when the titanium level is increased at different boron levels. In the as deposited weld metal:

- (a) the proportion of AF increases,
- (b) the proportion of FS and PF decreases,
- (c) in the reheated weld metal refinement in the grain size,
- (d) the percentage of large inclusions tends to decrease.

9.6.1 Conclusions

1. Yield and tensile strengths of weld metal were nominally independent of weld titanium-boron level over the range tested.
2. Low temperature impact properties of the weld metal were best with 0.0100wt% boron level and 0.0228wt% and 0.0430wt% titanium levels.
3. There is a direct relationship between low temperature impact properties and the proportions of AF. A higher percentage of AF gives a lower 100J temperature.
4. The refinement in grain size of the reheated zone contributes towards obtaining better low temperature impact properties.

9.7 Combined Influence of Alloying Elements on Weld Metal Properties

Microalloying influences impact properties of weld metal by varying the microstructure (area fraction of various phases) of the as-deposited and reheated weld metal region, the size distribution of non-metallic inclusions, grain size and strength levels.

A reference or controlled weld metal alloy was obtained by optimising the manganese and silicon contents then maintaining them constant whilst varying aluminium, titanium and boron. Finally the combined effect of boron and titanium was studied to obtain an optimised composition. This is shown in table 9.1 and its properties in table 9.2. The factors that influence the low temperature properties of low carbon low alloy steel welds are the proportions of AF, FS, PF, the AF lath size, the prior austenite grain size, the grain size of the reheated zone and the number density of inclusions with a diameter >1µm, as shown in figure 9.2 to figure 9.8. Even though in many cases there is a direct relationship with low temperature properties, it is important to understand their interrelationship to optimise the alloy composition. The effect of individual alloying elements has been discussed earlier.

Table 9.1: Optimised weld metal composition (wt%) with best low temperature properties.

Si	Mn	C	S	P	Ni	Cr	Mo	Cu	V	Nb	Ti	Al	B	O	N
Overall Best Properties (1)															
0.68	1.47	0.05	0.013	0.015	0.01	0.01	<0.01	0.01	<0.01	<0.01	0.0228	0.0150	0.0112	0.0430	0.0036
Second Best Properties (2)															
0.68	1.49	0.05	0.014	0.015	0.01	0.01	<0.01	0.01	<0.01	<0.01	0.0430	0.0147	0.0110	0.0460	0.0036
Third Best Properties (3)															
0.64	1.34	0.04	0.012	0.014	0.02	0.01	<0.01	0.01	<0.01	0.0005	0.0054	0.0133	<0.0005	0.0530	0.0047

Summary and Conclusions

Table 9.2: Weld metal properties with optimised composition (wt%) to produce the best low temperature properties.

Composition	Yield Strength (MPa)	Tensile Strength (MPa)	Elongation (%)	Impact (Charpy V Notch) Temperature for 100J Absorbed Energy °C
1	556	602	24	-62.5
2	519	575	26	-60
3	507	557	29	-45
Typical Requirement (AWS)	400 (minimum)	480 (minimum)	22 (minimum)	27J@-29°C (minimum)

Figure 9.2 shows the variation in acicular ferrite as a function of weld metal T100J temperature values. It shows that a higher proportion of AF gives the best low temperature properties. The scatter in the values of AF is due to other factors, which play an important role and should be considered. Figure 9.3 is a summary plot of the variation in FS as a function of weld metal T100J temperature values. Again, lower proportions of FS and PF are associated with the best low temperature properties (figure 9.4).

Summary and Conclusions

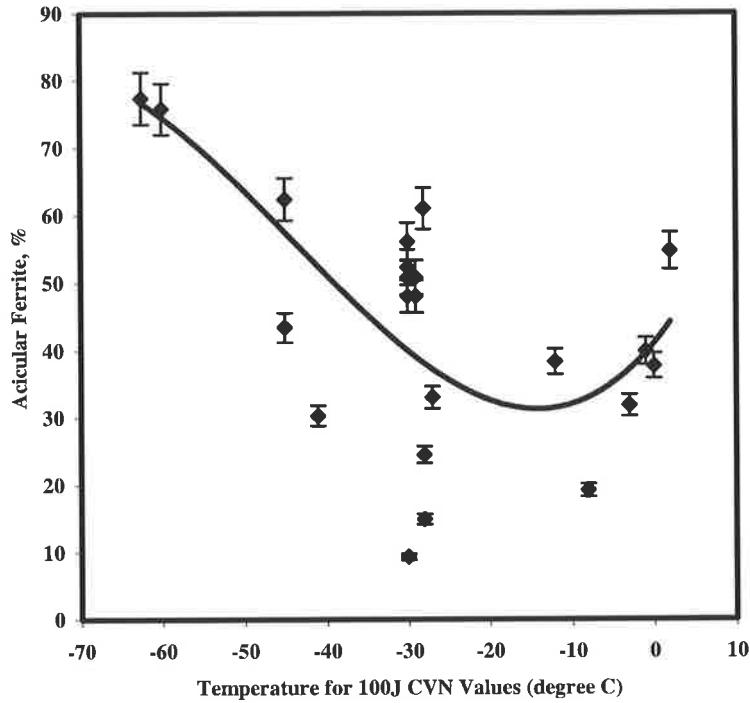


Figure 9.2: Summary plot of the variation in acicular ferrite as a function of weld metal T100J temperature values (°C).

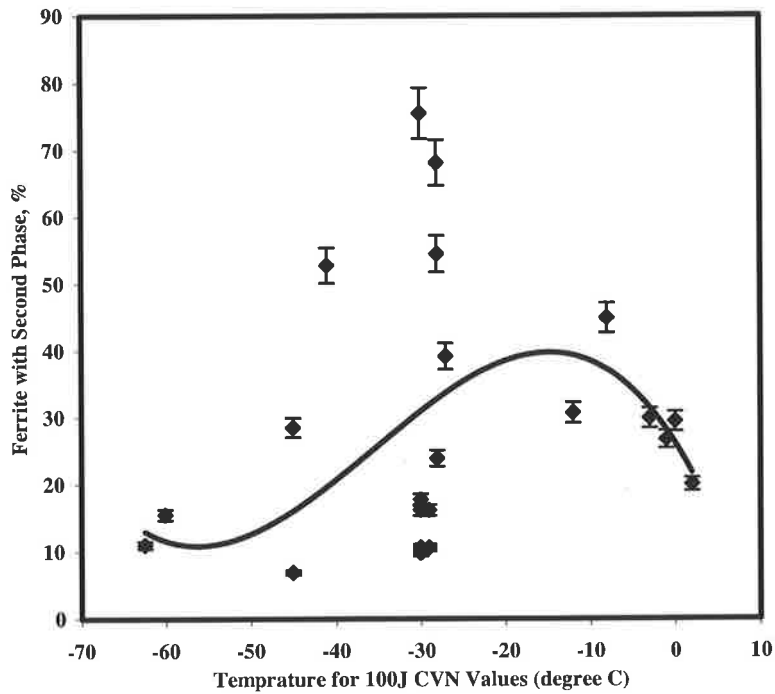


Figure 9.3: Summary plot of the variation in ferrite with second phase as a function of weld metal T100J temperature values (°C).

Summary and Conclusions

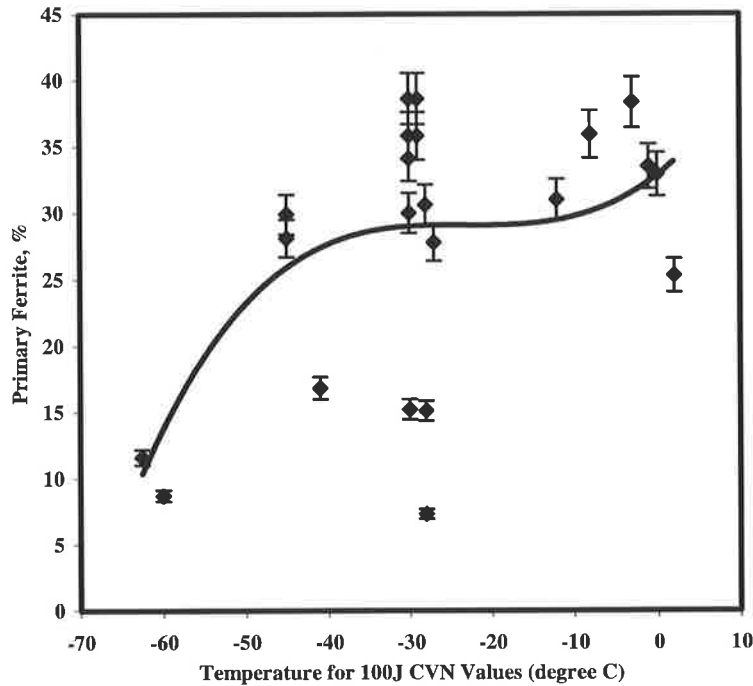


Figure 9.4: Summary plot of the variation in primary ferrite phase as a function of weld metal T100J temperature values ($^{\circ}\text{C}$).

Figure 9.5 to figure 9.7 show summary plots of the variation in acicular ferrite lath size (μm), prior austenite grain size (μm) and grain size of reheated zone (μm) as a function of weld metal T100J temperature values ($^{\circ}\text{C}$). As seen in figure 9.6 variation in prior austenite grain size does not show any direct relationship with the low temperature impact properties within the range tested. Variation in prior austenite grain size is seen with boron additions only, for all other alloying elements the prior austenite grain size remained unchanged.

Acicular ferrite lath size (μm) within the composition range tested varied little and remains independent of small changes in alloying elements. On the other hand refinement in grain size of reheated zone (μm) improves low temperature properties. Figure 9.8 shows lower percentage of inclusions with diameter $>1\mu\text{m}$ results in improved low temperature properties for the alloy range tested.

Summary and Conclusions

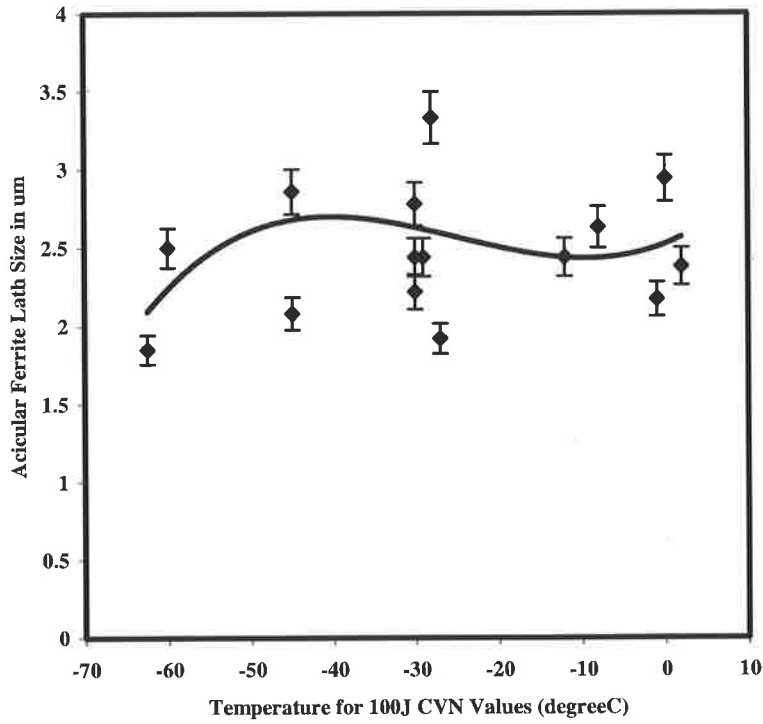


Figure 9.5: Summary plot of the variation in acicular ferrite lath size (μm) as a function of weld metal T100J temperature values ($^{\circ}\text{C}$).

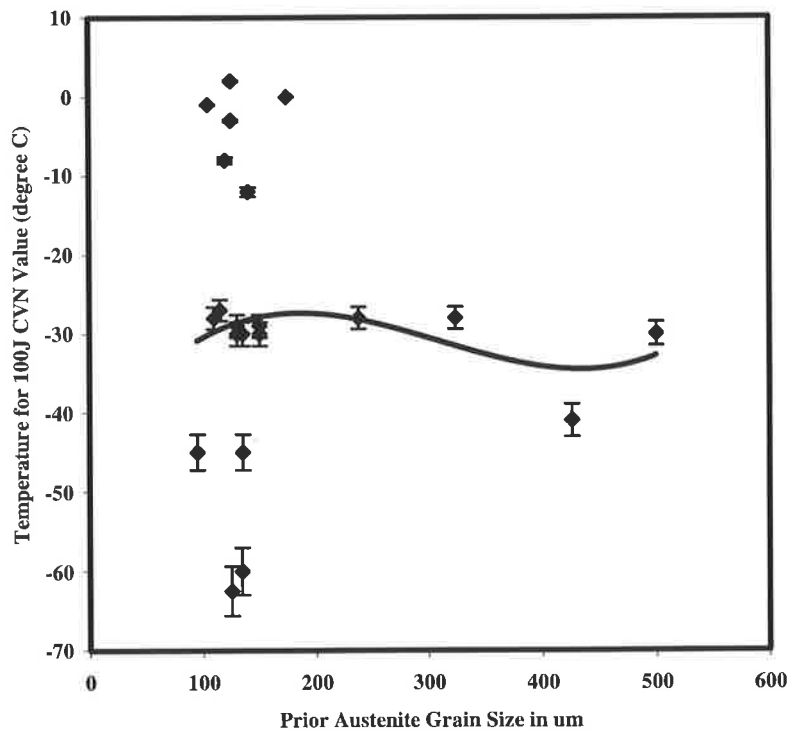


Figure 9.6: Summary plot of the variation in prior austenite grain size (μm) as a function of weld metal T100J temperature values ($^{\circ}\text{C}$).

Summary and Conclusions

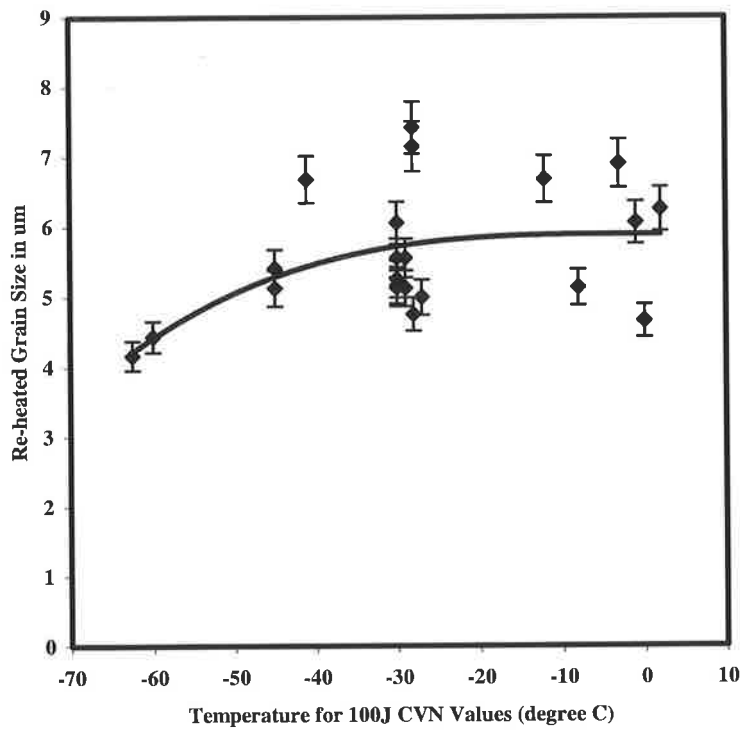


Figure 9.7: Summary plot of the variation in grain size of reheated zone (μm) as a function of weld metal T100J temperature values ($^{\circ}\text{C}$).

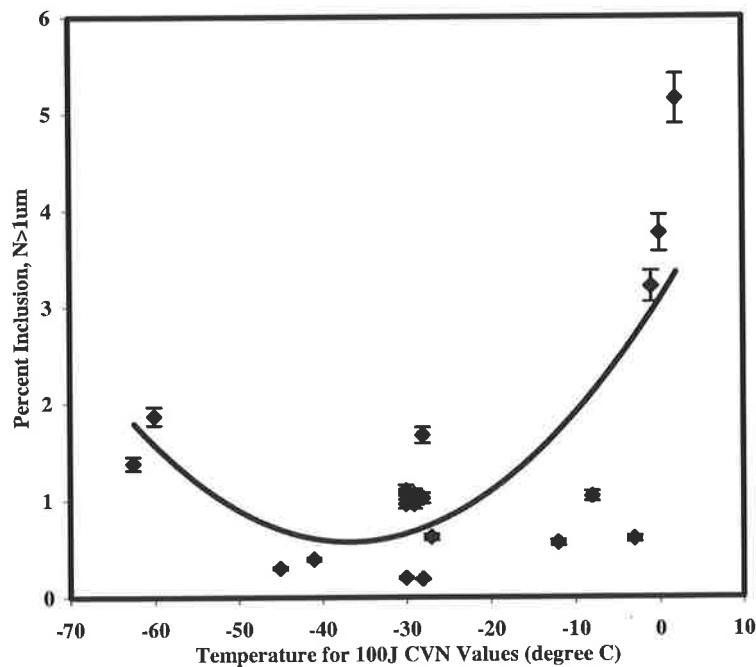


Figure 9.8: Summary plot of the variation of percent inclusions with diameter $> 1 \mu\text{m}$ as a function of weld metal T100J temperature values ($^{\circ}\text{C}$).

Summary and Conclusions

For low carbon low alloy steel welds changes in low temperature impact properties due to minor additions of manganese, silicon, aluminium, titanium and boron are quite significant. The optimum composition listed in table 9.1 and the corresponding weld metal properties in table 9.2, were obtained by adjusting microalloying elements to produce very high proportion of acicular ferrite and reduction in ferrite with second phase and primary ferrite. In addition refinement of the reheated grain size and a reduction in inclusions with diameter $>1\mu\text{m}$ also occurred.

9.8 Recommendations for Future Work

An extensive programme of experimental work has been carried out to investigate the influence of alloying additions on weld metal mechanical properties from gas-shielded metal-cored wires for joining structural steel. However, further work is required to understand effect of other variables. The following summarises these suggested extensions.

- Effect of aluminium and titanium were studied individually, however it would be of interest to study the effect of aluminium on different levels of titanium. This will produce a 3-dimensional behaviour chart for various elements in the weld metal.
- Another important variable is the gas mixture. The effect of varying the gas mixture should be studied on the optimised composition, i.e. varying gas mixtures will produce different levels of oxygen and nitrogen which may influence the inclusions in the weld metal and therefore its microstructure.
- Inclusion modelling to verify existing models which are based on data available for SAW and MMAW processes. Some preliminary calculations have shown a shift in these equations for the GMAW process.

References

- [1] Schumann, G.O. and French, I.E., 'The Control of Weld Metal Microstructure from Gas-Shielded Arc Welding Processes in Structural Steels', CSIRO MST Report No MTA383 Oct. 1996.
- [2] Schumann, O., Powell, G., and French, I., WTIA Australian Welding Research CRC No 1 Nov.1994.
- [3] French, I., Schumann, O. and Gordon T. Proceedings of the 42 National Welding Conference (WTIA), Melbourne, Vol 2, Paper 40, 1994.
- [4] Schumann, O. and French, I., WTIA Australian Welding Research CRC No 7, May1995.
- [5] Schumann, O. French, I., Accepted for 4th International Conference on Trends in Welding Research (ASM), June 1995.

References

- [6] Schumann, O. French, I., Accepted for Materials in Welding and Joining Conference (IMMA), Aug 1995.
- [7] Evans G.M., The Welding Journal, 59(3), 67s, 1980.
- [8] Evans G. M., The Welding Journal, 62(11), 313s, 1983.
- [9] Evans G.M., Metal Construction, 18(7), 438R, 1986.
- [10] Evans G.M., The Welding Journal, 70(1), 32s, 1991.
- [11] Evans G.M., Oerlikon-Scheissmitt, 49. No125, 22, 1991.
- [12] Esab – Welding and Cutting Technology for a rapidly developing industry, Welding Review International, Feb 1995.
- [13] Gas-Metal Arc Welding ASM Handbook Vol 6. (1993).
- [14] Pargeter, R.J. and Dolby, R.E., IIW Doc. IXJ-29 (1980).
- [15] Grong, O., Siewert, T.A., Martins, G.P. and Olson, D.L., Metal Transactions, 17A, (10)1797 (1986).
- [16] Nature and Behaviour of Fluxes Used for Welding. ASM Handbook Vol 6. (1993).

References

- [17] Frost, R.H., Olson, D.L. and Liu, S., Pyrochemical Evaluation of Weld Metal Inclusion Evolution, Proc. 3rd Int. Conf. Trends in Welding, ASM International, June 1992.

- [18] Making, Shaping and Treating of Steel, United States Steel Corporation, 1984.

- [19] Watanabe, I. and Kojima, T., Journal of the Japanese Welding Society, 49 (11), 772 (1980).

- [20] Ito, Y., Nakanishi, M., and Komizo, Y., Metal Construction, 14,9,427 (1982).

- [21] Grong, O. and Christensen, N., Scandinavian Journal of Metals, 4, 155 (1983).

- [22] Halmoy, E., "Wire melting rate, droplet temperature and effective anode melting potential", International Conference Arc Physics and Weld Pool Behaviour, London, May 1979, 49 Publ. The Welding Inst.(1979).

- [23] Heile, R. F., and Hill, D. C., The Welding Journal, 54,201s (1975).

- [24] Dunn, P.S., Natalie, C.A. and Olson, D.L., Proceedings of the ASM Welding Congress, Toronto, Ontario (ASM, Metals Park, OH) paper 8513-004, 1985.

- [25] Savage, G.L., Metal Construction, 15(8), 448, 1983.

- [26] Lathabai, S. and Stout, R.D., The Welding Journal, 64(11), 303s, 1985.

References

- [27] Es-souni, M., Beaven, P.A. and Evans, G.M., Microstructure and AEM Studies of Self-Shielded Flux Cored Arc Weldments, *Welding Journal*, Feb, 1992.
- [28] Huseen, L.A. and Hawkins, D.N. *Microstructural Science*, Vol.11, 1983.
- [29] Mejias, H.D., Perez, T.E. and De-Vedia, L., *Advances in Welding Science and Technology*, ASM Int., 1986.
- [30] *Fundamentals of Weld Solidification* ASM Handbook Vol 6. (1993).
- [31] Tiller, W.A., Jackson, K.A., Rutter, J.W., and Chalmers, B., *Acta Metall.*, Vol 1, 1953, p428-437.
- [32] Burton, J.A., Prim, R.C., and Slichter, J., *J. Chem. Phys.*, Vol 21, 1953, p1987-1991.
- [33] Tiller, W.A., and Rutter, J.W., *Can. J. Phys.*, Vol 34, 1956, p 96-121.
- [34] Savage, W.F., Nippes, E.F., and Miller, T.W., *Weld. J.*, Vol 55, 1976, p 165S-173S.
- [35] Matsuda, F., Hashimoto, T., and Senda, T., *Trans. Natl. Res. Inst. Met. (Jap)*, Vol 11, 1969, p43.
- [36] Brooks J.A., and Mahin, K.W., "Solidification and Structure of Welds", *Welding*

References

- Theory and Practice edited by Dolby, D.L., Dixon, R., and Liby, A.L., Elsevier Science Publishers B.V., North Holland (1990).
- [37] Bower, T.W., Brody, H.D., and Flemings, C.M., Trans. AIME, 236, 624 (1966).
- [38] Flemings, C.M., Poirier, D.R., Barone R.V., and Brody, H.D., Journal of the Iron and Steel Institute, Steel Institute, 208,37(1970).
- [39] Rohatgi, P.K., and Adams, C.M., Jr, Transactions AIME, 239, 1729(1967).
- [40] Rohatgi, P.K., and Adams, C.M., Jr, Transactions AIME, 239, 1737(1967).
- [41] Suzuki, A., Suzuki, T., Nagaoka, Y., and Tawata, Y., Nippon Kinzoku Gakkaishi, 32, 1301 (1968), (also Brucher, translation 7804, 1969).
- [42] Lanzafame, J.N., and Kattamis, T.Z., The Welding Journal, 52, 226s (1973).
- [43] Brown, P.E., and Adams, C.M. Jr., The Welding Journal, 39,520 (1960).
- [44] Jarman, R.A., and Jordan, M.F., Journal of the Institute of Metals, 98, 55 (1970).
- [45] Savage, W.F., Lundin, C.D., and Aronson, A.H., Weld. J., Vol 44, 1965, p420S-425S.
- [46] Davies,G.J., and Garland,J.G., International Metals Review, 20, 83 (1975).

References

- [47] Miller, T.W., M.S. Thesis, Rensselaer Polytechnique Inst., Troy, N.Y. (1967).
- [48] Bell, J.R., MS Thesis, Rensselaer Polytechnique Institute (1966).
- [49] Fukui, F., and Namba, K., Transactions of the Japanese Welding Society, 4, 49 (1983).
- [50] Garland, J.G., Metals Construction, 6, 121 (1974).
- [51] Cole, W., and Colvin, P., Metal Construction, 3, 131 (1971).
- [52] Widgery, D., The Welding Institute Members Report M/76/73 (1973).
- [53] Makas, A.M., and Rossoshinskii, A.A., Automatic Welding, 9 (16), 65 (1956).
- [54] Cheever, D.L., and Howden, D.G., The Welding Journal, 48 (4), 197s(1969).
- [55] D'Annessa, A.T., The Welding Journal, 45 (12), 569s (1966).
- [56] Dadian, M., in: Conf. Proc. on Advances in Welding Science and Technology, Gatlinburg, T.N., ASM, Metals Park, OH (6), 101 (1986).
- [57] Kotecki, D.J., Cheever, D.L., and Howden, D.J., Welding Journal, 51 (8), 386s (1972).

References

- [58] Ishizaki, K., *Journal of the Japanese Welding Society*, 32 (11), 38 (1963).
- [59] Garland, J.G., and Davies, G.J., *Metals Construction and British Welding Journal*, 61, 171 (1970).
- [60] Smith, V.G., Tiller, W.A., and Rutter, J.W., *Canadian Journal of Physics*, 33 (12), 723 (1955).
- [61] Brooks, J.A., and Mahin, K.W., "Solidification and Structure of Welds", *Welding Theory and Practice* edited by Dolby, D.L., Dixon, R. and Liby, A.L., Elsevier Science Publishers B.V., North Holland (1990).
- [62] Davies, G.J. and Garland, J.G., *International Metals Review*, 20, 83 (1975).
- [63] Matsuda, F., et al, *Transactions of the Japanese Welding Society*, 11, 43 (1969).
- [64] Koto, M., et al, *Transactions of the Japanese Welding Society*, 3, 69 (1972).
- [65] Savage, W.F., "Solidification, Segregation and Weld Defects, in Weldments", *Physical Metallurgy and Failure Phenomena*, 5th Bolton Landing Conference, eds R.J. Chistoffel, Nippes E.F. and Solomon, H.D., August 1978.
- [66] Lancaster, J.F., *Metallurgy of Welding*, 5th Ed., Chapman and Hall, New York, London 1993.

References

- [67] Tiller, W.A., et al, Acta Met., 1, 428 (1953).

- [68] Savage, W.F., The Welding Journal, 18 (5/6), (1989).

- [69] Easterling, K.E., Materials Science and Engineering, 65,191 (1984).

- [70] Savage, W.F., et al, The Welding Journal, 47, 420s (1968).

- [71] Guide to the light microscope examination of ferritic steel weld metals, Welding in the World, 29(7/8), 160 (1991).

- [72] Cochrane, R.C., Int. Inst. Welding Doc. IX-1248-82, 1982.

- [73] Savage, W.F. and Aronson, A.H., Weld. J. 45, 85, 1966.

- [74] Calvo, F.A., Bently, K.P. and Baker, R.G., Studies of the Welding Metallurgy of Steels, BWRA, Aabington, Cambridge, 71, 1975.

- [75] Widgery, D.J. and Saunders, G.G., Weld. Inst. Res. Bull. 16, 277, 1975.

- [76] Rodrigues, P. and Rogerson, J.H., Low Carbon Structural Steels for the Eighties, Inst. Metall., London, p. IIIB33, 1977.

- [77] Dube, C.A., PhD thesis, Carnegie Inst. of Technology, 1948.

References

- [78] Abson, D.J. and Dolby, R.E., Ins. Inst. Welding, Doc. IXJ-29-80, 1980.
- [79] Abson, D.J. and Dolby, R.E., Weld. Inst. Res. Rep. 19/1978, Welding Institute, Abington, Cambridge, 1978.
- [80] Grong, O., and Kluken, A.O., Microstructure and Properties of Steel Weld Metals, Ferrous Alloy Weldments, Ed. Olsen, D.L., and North, T.H., Trans. Tech. Publications Ltd, USA (1992). IIW Doc. 115/IIW 999-88.
- [81] Ricks, R.A., Barrite, G.S. and Howell, P.R., Proceedings of the International Conference on Solid-Solid Phase Trans., Pittsburgh,PA, Met.Soc. of AIME, 463, August 1981.
- [82] Ricks, R.A., Howell, P.R. and Barrite, G.S., Journal Material Science, 17,732, 1982.
- [83] Barrite, G.S., Ricks, R.A. and Howell, P.R., Strength of Metals and Alloys, (ICSMA 6), Pergamon Press, 121, 1982.
- [84] Kayali, E.S., Corbett, J.M. and Kerr, H.W., Journal Material Science, Lett, 2, 123, 1983.
- [85] Keville, B.R., and Cochrane, R.C., in Proceedings of the 30th Annual Convention of Australian Welding Institute, 263, November 1982.

References

- [86] Abson, D.J., Dolby, R.E. and Hart, P.M.H., The Role of Nonmetallic Inclusions in Ferrite Nucleation in carbon Steel Weld Metal, Intl. Conf. Proc. on Trends in Steel and Consumables for Welding, paper 25, 1978.
- [87] Garland, J.G. and Krikwood, R.R., Proceedings of Symposium, Welding of line pipe steel, St. Louis, Welding Research Council, 176, 1977.
- [88] Dolby, R.E., Welding Institute Report, 14/1976/M, 1976.
- [89] Farrar, R.A., and Harrison, P.L., Journal of Material Science, 22, 3812, 1987.
- [90] Linnert, G.E., Welding Metallurgy 4th Eddition, Vol. 1, 1994.
- [91] Den Ouden, G., Verhagen, J.G., and Ticholaar C.W., The Welding Journal, 54, 82s (1975).
- [92] Farrar, R.A., Zhang, Z., Bannister, S.R., Journal of Material Science, 28, 1385 (1993).
- [93] Taylor, D.S., and Evans, G.M., Metal Construction, 15, 438 (1983).
- [94] Harrison, P.L., PhD Thesis: Continuous cooling transformation kinetics and microstructure of mild and low alloy steel weld metals, University of Southampton, UK (1983).

References

- [95] Yoshino, Y., and Stout, R.D., *The Welding Journal*, 58, 59s (1979).
- [96] Garland, J.C., and Kirkwood, P.R., *Metal Construction*, 7,320 (1975).
- [97] Novaes Gomes, S.I., PhD Thesis, University of Sao Paulo (Sao Carlos Eng. School) Brazil (1985).
- [98] Easterling, K.E., *Introduction into the Physical Metallurgy of Welding*, Butterworths, London 1983.
- [99] Dolby, R.E., in *Steels for line pipe and pipeline fittings*, The Metal Society, London, 302 (1983).
- [100] Levine, E., and Hill, D.C., *Metal Construction*, 9, 346 (1977).
- [101] Bernard, G., Faure, F., and Maitrepierre, P., in the *Proceedings of the International Conference "Welding of HSLA 80 structural steels"*, Rome, Am. Society for Metals, 187, Nov. 1976.
- [102] Abson, D.J. and Pargeter, R.J., *Factors Influencing As-Deposited Strength, Microstructure, and Toughness of Manual Metal Arc Welds Suitable for C-Mn Steel Fabrications*, *Int. Metals Reviews* Vol.31, No.4, 1986.
- [103] Widgery, D.J., *Weld. J.*, 1976, 55, (3), 57s-68s.

References

- [104] Tuliani, S.S., in Int. Conf., Welding Research Related to Power Plant, University of Southampton, 1972, paper 17, 232-246.
- [105] Bosward, I.G. and John, R., Trends in Steels and Consumables for Welding, 135-150, 1979, Abington, The Welding Institute.
- [106] Widgery, D.J., Weld. Res. Int., 1975, 5, (2), 1-39.
- [107] Svensson, L., Control of Microstructures and Properties in Steel Arc Welds 1994.
- [108] Harrison, P.L. and Hart, P.H.M., Influences of Steel Composition and Welding Procedure on the HAZ Toughness of Thick Section Structural Steels. in Proc. 8th Int. Conf. Offshore Mechanics and Arctic Engineering, The Hague, The Netherlands, March 1989.
- [109] Sagen, S.S., and Campbell, H.C., Factors which affect Low-alloy Weld Metal Notch Toughness, Welding Research Council bulletin no.59, April,1960.
- [110] Masubuchi, K., Monroe, R.E., and Martin, D.C., Interpretive report on Weld-Metal Toughness. Welding Research Council bulletin no.111, January,1966.
- [111] Dorsch, K.E., Factors Affecting Weld Metal Properties in Carbon and Low Alloy Pressure Vessel Steels, Welding Research Council bulletin no.231, October,1977.

References

- [112] Harrison, P.L., and Farrar, R.A., *Metal Construction*, 19, 392R (1987).
- [113] Harrison, P.L., PhD Thesis, University of Southampton (1983).
- [114] Court, S.A., PhD Thesis, University of Leeds (1985).
- [115] Evans, G.M., *Welding in the World*, 31, (1), 12 (1993).
- [116] Abson, D.J., *Welding in the World*, 27, 3/4, 76 (1989).
- [117] Evans, G.M., *Oerlikon Schweissmitt.*, 49, No 127 (1991).
- [118] Kluken, A.O., *Modelling of the Reaction Sequence During Deoxidation and Solidification of Steel Weld Metals*, PhD thesis, Trondheim University of Technology, Norway, 1990.
- [119] Terashima, H. and Hart, P.H.M., *Effect of Aluminum on C-Mn Steel Submerged-Arc Weld Metal Properties*, *Weld. J.*, 63(June), 173-s, 1984.
- [120] Abson, D.J., *The TWI Welding Journal*, 1(1), 99 (1992).
- [121] Powell, G.L.F., CSIRO Adelaide, Australia, MTA 211, May 1992.
- [122] Tsuboi, J., and Terashima, H., *Welding in the World*, 21, 304 (1983).

References

- [123] Mori N., Homma H., Wakabayashi M., and Okita S., Characteristics of Mechanical Properties of Ti-B Bearing Weld Metals, IIW DOC IX-1229-82, May 1982.
- [124] Watanabe, I., and Kohma, T., in the Proceedings of the International Conference, "Effect of residual, impurity and microalloying elements on weldability and weld properties" The Welding Institute of London Page 51, Nov. (1983).
- [125] Kohno, R., Takami, T., Mori, N., and Nagano, K., The Welding Journal, 62, 373s (1983).
- [126] Davis, M.L.E., Pargeter, R.J., and Baily, N., Metal Construction, 15 338 (1983).
- [127] Watanabe, I., Suzuki, M., and Kojima, T., '80, in the Proceedings of the International Conference "Welding research in the 1980's" Welding Research Institute, Osaka, Paper B-8, October 1980.
- [128] Hondros, E.D., and Seah, M.P., in Physical Metallurgy, 3rd edn. (ed.R.W. Chan and P. Haasen), Amsterdam, North Holland Physics Publishing, Part I, 855 (1983).
- [129] Widgery, D.J., Welding Research International, 4, 54 (1974).
- [130] Oh, D.W., Olson, D.L. and Frost, R.H., The Influence of Boron and Titanium on Low-Carbon Steel Weld Metal, AWS Welding Journal 151-s, April 1990.
- [131] Oh, D.W., Olson, D.L. and Frost, R.H., The Influence of Zirconium and Boron on

References

Low-Carbon Steel Weld Metal Microstructure, Transactions of the ASME Vol.116,
February 1994.

[132] Kotecki, D.J., Foreword, *ibid*,i.

[133] Menon, R.,and Kotecki, D.J., Nitrogen in Stainless Steel Weld Metal, *ibid*,pp142-
161.

[134] Van Nassau, L. and van der Mee, V., Nitrogen in Manual Metal Arc Weld Metal,
ibid, pp85-97.

[135] Morigaki, O., Tanigaki, T., Kuwabara, M., Fujibayashi, K. and Otawa, M.,
Development of a Covered Electrode for Steel Structures in Low Temperature
Service. IIW/IIS Doc.II pp746-75.

[136] Cochrane, R.C. and Krickwood, P.R., The Effect of Oxygen on Weld
Microstructure, Intl. Conf. Proc. on Trends in Steel and Consumables for Welding,
paper 35, 1978.

[137] Harrison, P.L. and Farrar, R.A., Influence of Oxygen-Rich Inclusions on the
Gamma to Alpha Phase Transformation in High Strength Low Alloy Steel Weld
Metals, Journal of Materials Science, Vol.16,pp2218,1981.

[138] Ferrante, M.and Farrar, R.A., The Role of Oxygen Rich Inclusions in Determining
the Microstructure of Weld Metal Deposit, Journal of Materials Science, Vol. 17,

References

pp3293, 1982.

- [139] Kobayashi, T. and Sakai, Y., The Effects of Shielding Gas Composition on the Characteristics of Carbon Steel Weld Metal, Japan Welding Engineering Society Report, IIW DOC XII-E-32-28 and IIW DOC XII-B-26-82, 1982.
- [140] Liu, S. and Olson, D.L., The Role of Inclusions in Controlling HSLA Steel Weld Microstructures, Welding Journal, Vol.65, No.6, pp139s, 1986.
- [141] Eager, T., Weld. J., 57(march), 76s, 1978.
- [142] Francis, R.E., Jones, J.E. and Olson, D.L., Effect of Shielding Gas Oxygen Activity on Weld Metal Microstructure of GMA Welded Microalloyed HSLA Steel, Welding Research Supplement, AWS Welding Journal, 408s Nov. 1990.
- [143] Australian Standard 3678 'Structural steel - hot rolled plates, floor plates and slabs' 1990.
- [144] Kluken, A.O., Grong, O. and Hjelen, J., Materials Science and Technology, 4, 649, 1988.
- [145] Huisman, M.D., Svetsaren 51, 1996.
- [146] Tyagi, V.K., French, I.E. and Bee, J.V., Australian Welding Research, CRC No 20, 1996.

References

- [147] Fleck, N.A., Grong, O., Edwards, G.R. and Matlock, D.K. *The Welding Journal*, 65, 113s, 1986.
- [148] Tweed, J.H. and Knott, J.F., "Effect of Reheating on Microstructure and Toughness of C-Mn Weld Metal", *Metals Science*, Vol. 17, pp 45-54, 1983.
- [149] Abson, D.J., *The Welding Institute Report 68/1978/M*, July 1978.
- [150] Their, H. and Killing, R., *Schweissen und Schneiden*, 43, 541, 1991.
- [151] Barbaro, F.J., Kraukis, P. and Easterling, K.E., *Materials Science and Technology*, Vol. 5, pp1057-1068, Nov. 1989.
- [152] Tweed, J.H., and Knott, J.F., *Acta Metall.*, 35(7), 1401, 1987.
- [153] Grong, O. and Matlock, D.K., *Int. Metals Reviews*, 31, No. 1, 27-48, 1986.
- [154] Hart, P., *Metal Construction*, 18(10), 610, 1986.
- [155] Knott, J.F., *Trans. ISIJ*, 21, 1981.
- [156] Schumann, G.O. and French, I.E., *Scripta Materialia*, Vol. 36, No. 12, pp. 1443-1450, 1997.

References

- [157] Evans, G. M. and Bailey, N., "Metallurgy of Basic Weld Metal" Abington Publishing Ltd., 1997.
- [158] Gedeon, S.A., Rudd, S.J. and Braid, J.E.M., International Conference on Pipeline Reliability, Vol 2, Paper VI-12, 1992.
- [159] Fox, A.G., and Brother, D.G., Scripta Metallurgica et Materialia, Vol.32, No.7, pp. 1061-1066, 1995.
- [160] Powell, G.L.F., and Herfurth, G., Metallurgical and Materials Transactions pp2775-2784, Volume 29A, Nov 1998.
- [161] Cochrane, R.C., The effect of second-phase particles on the mechanical properties of steel, The Iron and Steel Institute, London, pp 101-106, 1971.
- [162] Farrar, R.A., Taylor, L.G. and Harrison, E.M., Effect of stress relieving on fracture properties of submerged arc welds of C-Mn steels, Metals Technology, pp 380-389, Oct. 1979.
- [163] Evans, G.M., The effect of stress-relieving on the microstructure and properties of C-Mn all-weld metal deposits, OERLIKON-Schweissmitt. No. 103, pp 15-27, 41 (1983).
- [164] Bush, M.E. and Kelly, P.M., Acta Metall. Pp 1363-1371, 19, 1971.

References

- [165] Leslie, W.C., Physical Metallurgy of Steels, McGraw-Hill Kogakusha, Tokyo, Japan, 1982.
- [166] Banerji, S.K., and Morral, J.E., Conference Proceedings. Boron in Steel TMS-AIME, Warrendale, PA, USA, 1-215, 1980.
- [167] Ohmori and Yamanaka. Proc. Int. Symp. on Boron in Steel, Milwaukee, Wis. Pp. 44-60, 1979.
- [168] Evans, G.M., Microstructure and Properties of Ferritic Steel Welds Containing Titanium and Boron, Welding Research Supplement, Welding Journal, pp 251-260, August, 1996.
- [169] Morral, J.E., and Cameron, T.B., Proc. Int. Symp. on Boron in Steel, Milwaukee, Wis. Pp. 19-32, 1979.
- [170] Bhadeshia, H.K.D.H., and Svensson, L.E., In Mathematical Modelling of Weld Phenomena, The Institute of Materials, London, 1993.
- [171] Yamanaka, K., and Ohmori, Y., Transactions ISIJ 17, pp 92-101, 1977.
- [172] Fleck, N., The effect of filler wire and flux compositions on the microstructural and properties of microalloyed steel weld metals, M.S. Thesis, No, T-2942, Colorado School of Mines, Golden, Colorado, 1984.

References

- [173] Ohkita, S., Homma, H., Tsushima, S., and Mori, N., The effect of oxide inclusions on the microstructure of Ti-B containing weld metal, IIW Doc. II-1070-86, American Council, AWS, Miami, FL. 1986.
- [174] Mori, N., Homma, H., Ohkita, S., and Wakabayashi, M., Mechanisms of notch toughness improvement in Ti-B bearing weld metals, IIW Doc. IX-1196-81k, American Council, American Welding Society, Miami, Fla. 1981.

Publications Originating from this Thesis Work

A. Refereed Publications

- [1] Tyagi V.K., French I.E. and Bee J.V., 'Influence of Titanium and Aluminium on the Properties of Multi-pass Weld Metal from Gas-shielded, Metal-cored Wires', Welding Research Supplement, Australasian Welding Journal, Vol. 44, 1999.
- [2] Tyagi V.K., French I.E. and Bee J.V., 'Influence of Mn and Si on the Properties of Multi-pass Weld Metal from Gas-shielded, Metal-cored Wires', Welding Research Supplement, Australasian Welding Journal, Vol. 43, 1998.
- [3] Tyagi V.K., French I.E. and Bee J.V., Literature Review on 'Understanding the influence of alloy additions on microstructural and mechanical properties of weld metal from gas-shielded processes', Australasian Welding Research Publications, WTIA, CRC No. 20, 1996.

B. Non-refereed Publications & Conference Papers

- [1] Tyagi V.K., French I.E. and Brown I., 'Influence of Titanium and Boron on the properties of multi-pass weld metal from gas-shielded, metal-cored wires', WTIA 49th Annual Conference, Adelaide, South Australia, 8-10 Oct., 2001.

C. Technical Reports

- [1] Tyagi V.K., Bee J.V. and French I.E., 'Understanding the influence of alloy additions on microstructural and mechanical properties of weld metal from gas-shielded processes', CMST-A-98-37, October 1998.
- [2] Tyagi V.K., French I.E. and Bee J.V., 'Influence of Mn and Si on the Properties of Multi-pass Weld Metal from Gas-shielded, Metal-cored Wires', Report No., MTA 441, June 1997.

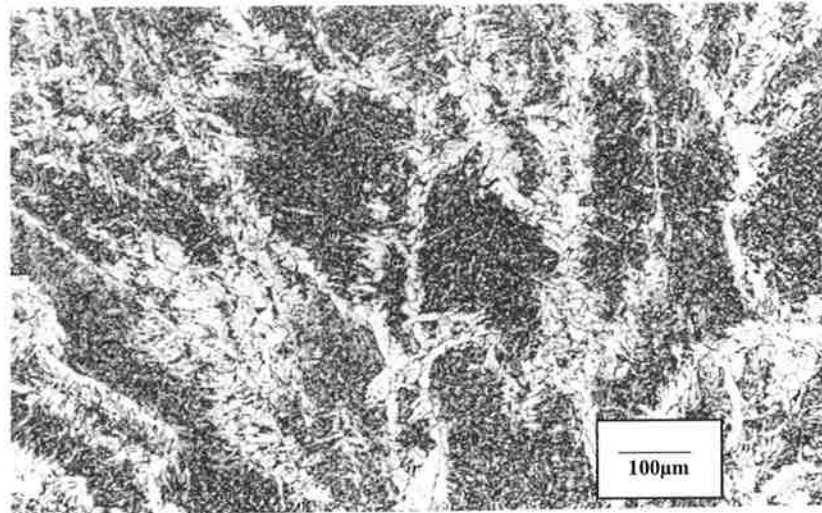
Appendix A

Manganese and Silicon Series

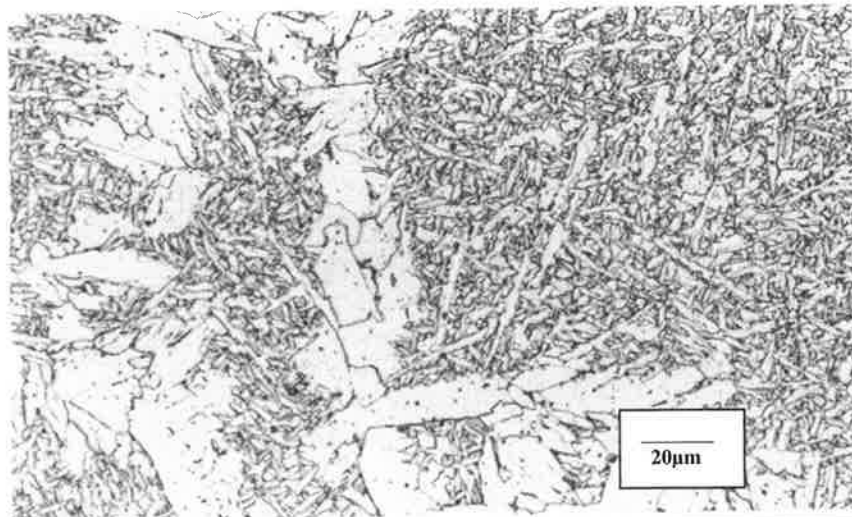
Composition

Si	Mn	C	S	P	Ni	Cr	Mo	Cu	V	Nb	Ti	Al	B	O	N
0.34	0.98	0.05	0.009	0.018	0.02	0.01	<0.01	0.01	0.0100	<0.01	0.0040	0.0120	<0.0005	0.0570	0.0160

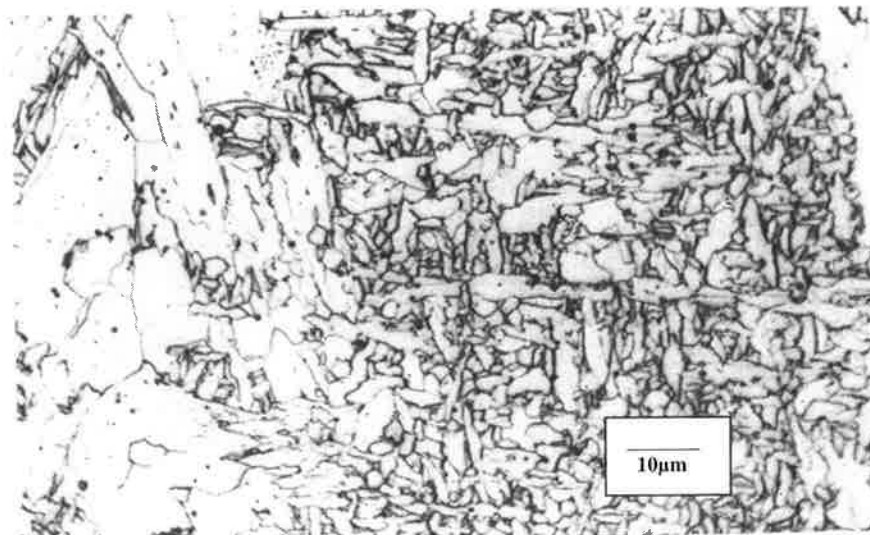
Microstructure photomicrograph



As-Welded x100

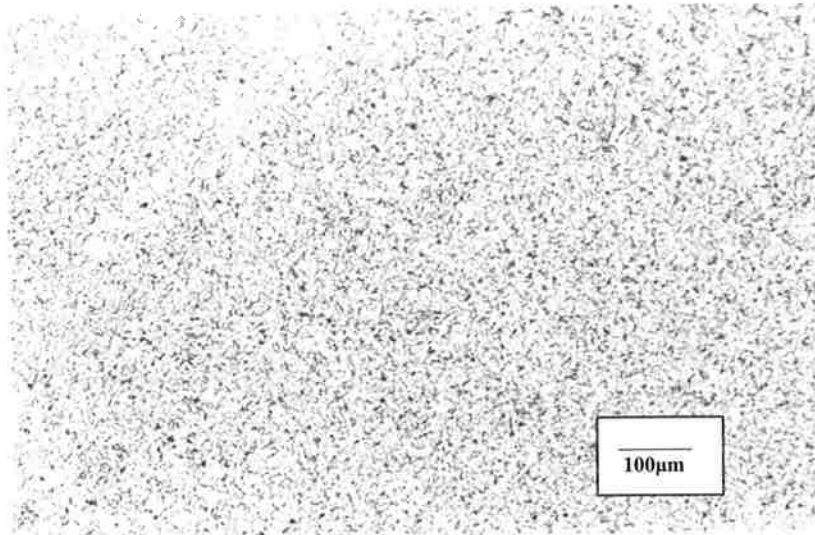


As-Welded x500

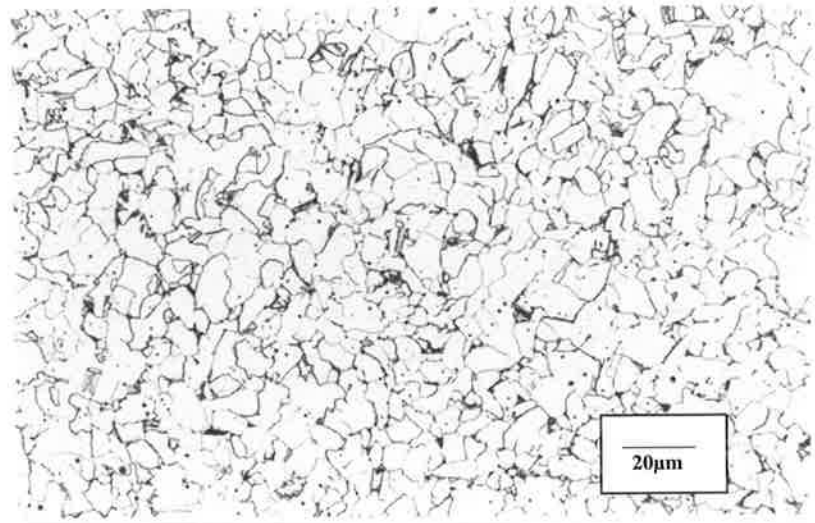


As-Welded x1000

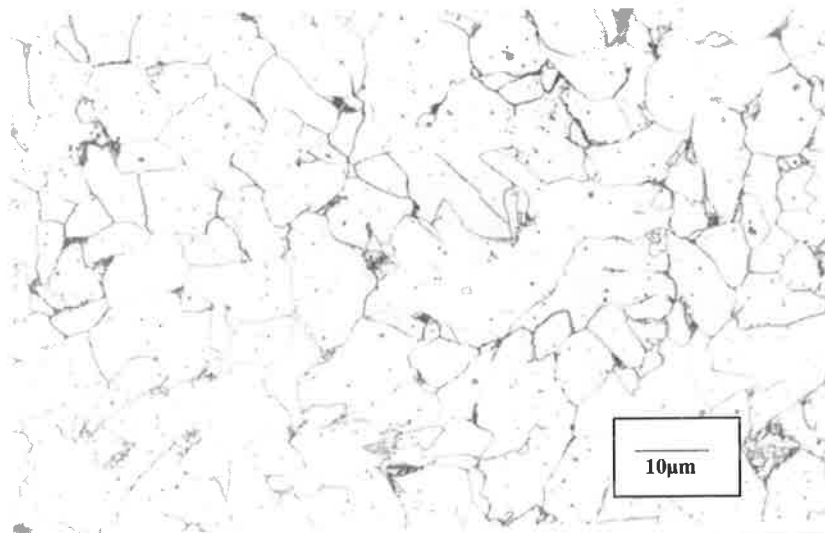
Appendix A



Re-Heated x100



Re-Heated x500



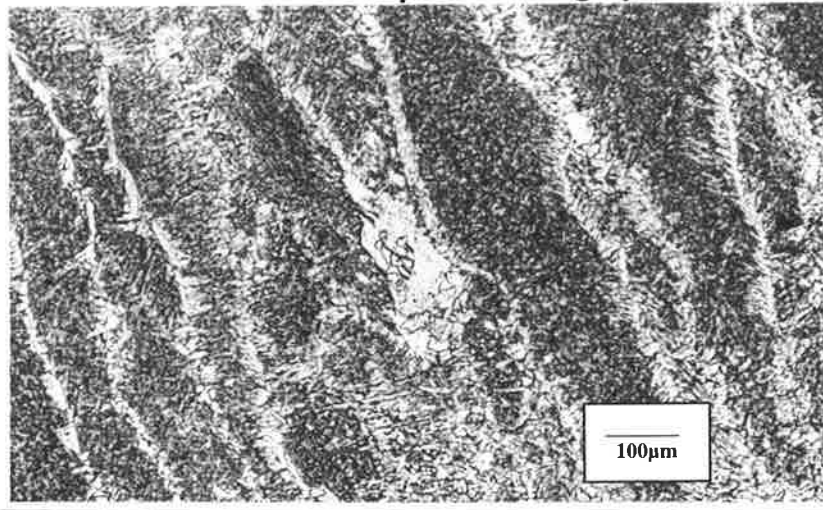
Re-Heated x1000

Manganese and Silicon Series

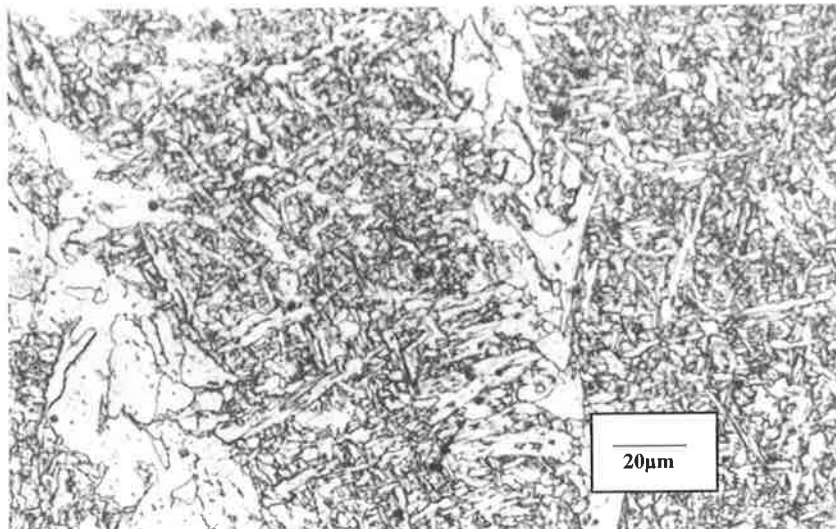
Composition

Si	Mn	C	S	P	Ni	Cr	Mo	Cu	V	Nb	Ti	Al	B	O	N
0.34	1.4	0.05	0.009	0.017	0.02	0.01	0.01	0.01	0.0100	<0.01	0.0051	0.0139	<0.0005	0.0430	0.0041

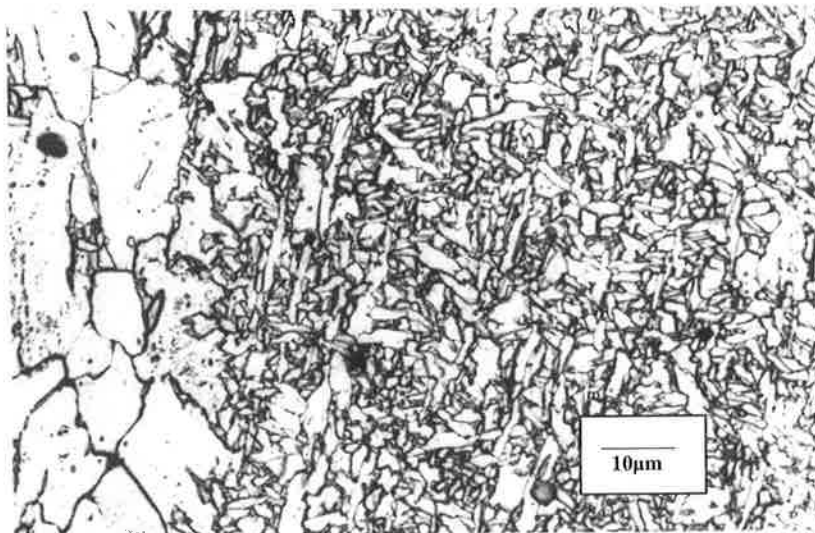
Microstructure photomicrograph



As-Welded x100

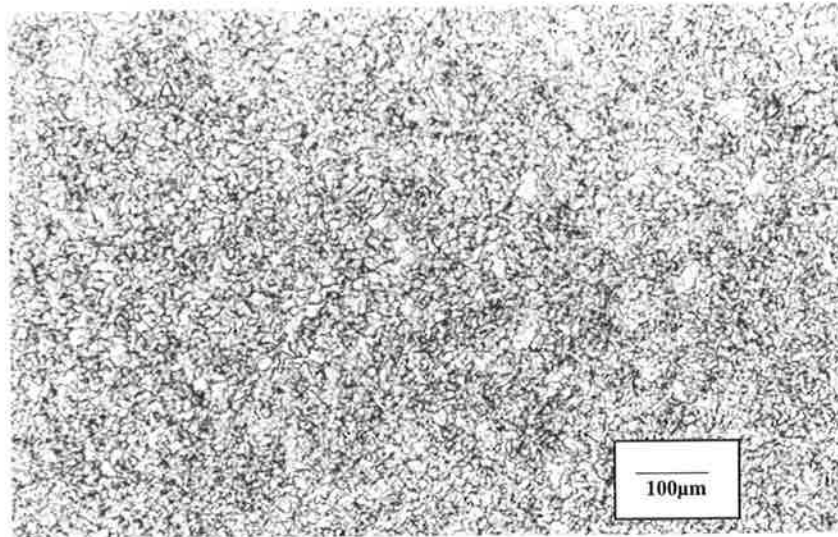


As-Welded x500

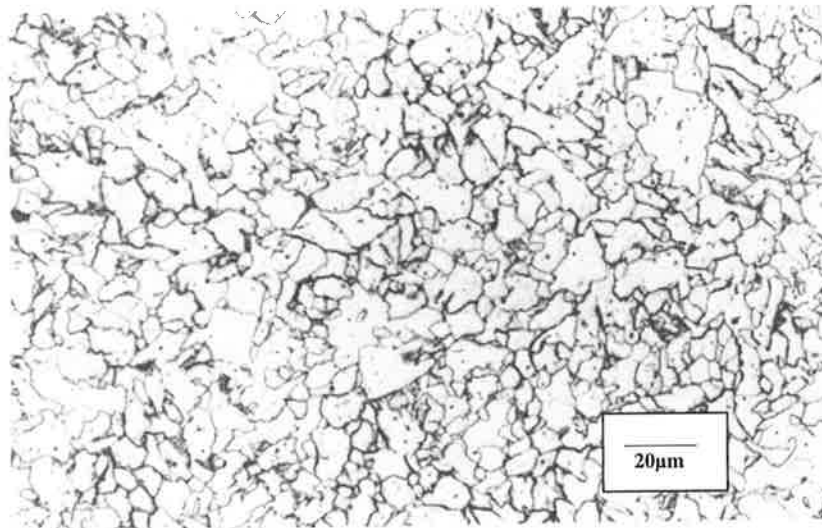


As-Welded x1000

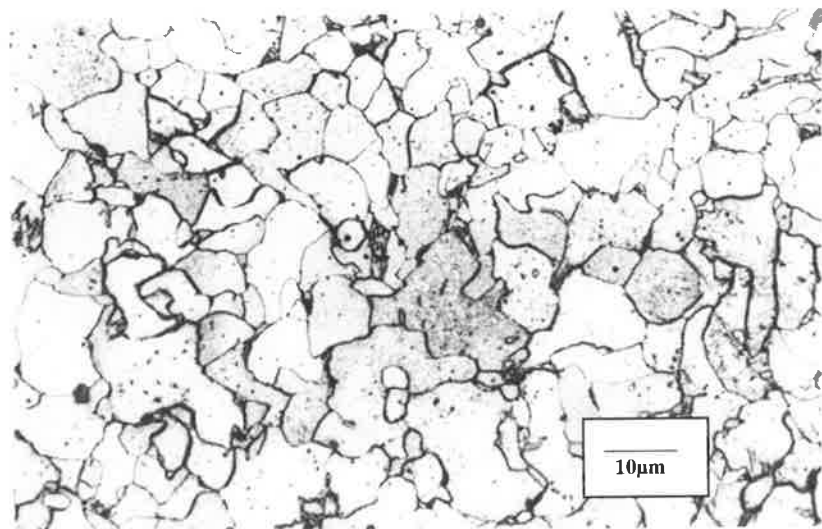
Appendix A



Re-Heated x100



Re-Heated x500



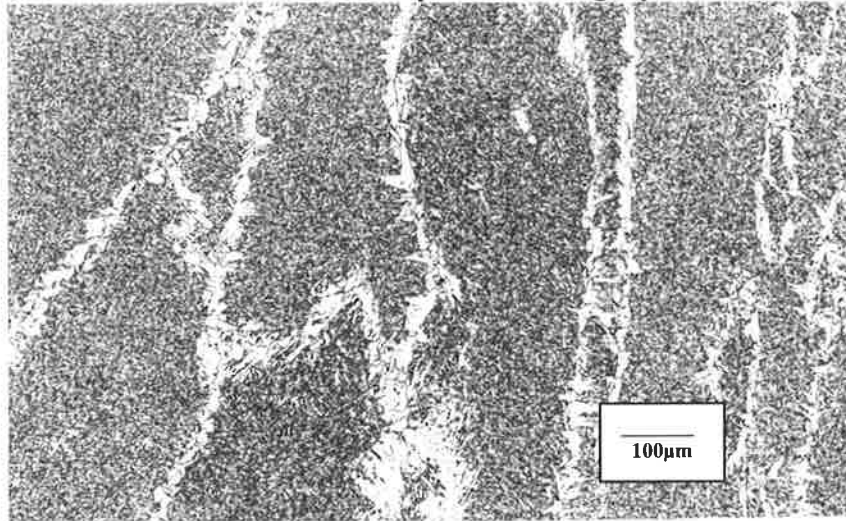
Re-Heated x1000

Manganese and Silicon Series

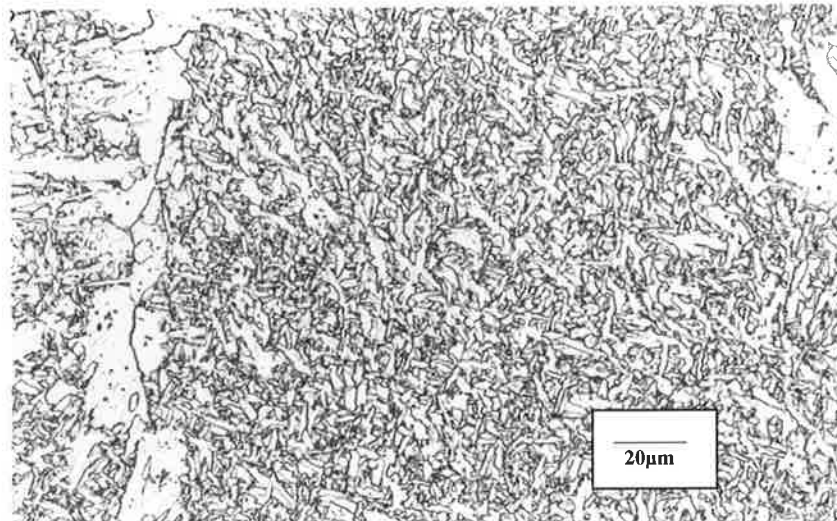
Composition

Si	<u>Mn</u>	<u>C</u>	<u>S</u>	<u>P</u>	<u>Ni</u>	<u>Cr</u>	<u>Mo</u>	<u>Cu</u>	<u>V</u>	<u>Nb</u>	<u>Ti</u>	<u>Al</u>	<u>B</u>	<u>O</u>	<u>N</u>
0.39	1.50	0.04	0.012	0.014	0.03	0.01	0.01	0.01	0.0067	0.001	0.0050	0.0123	<0.0005	0.0550	0.0063

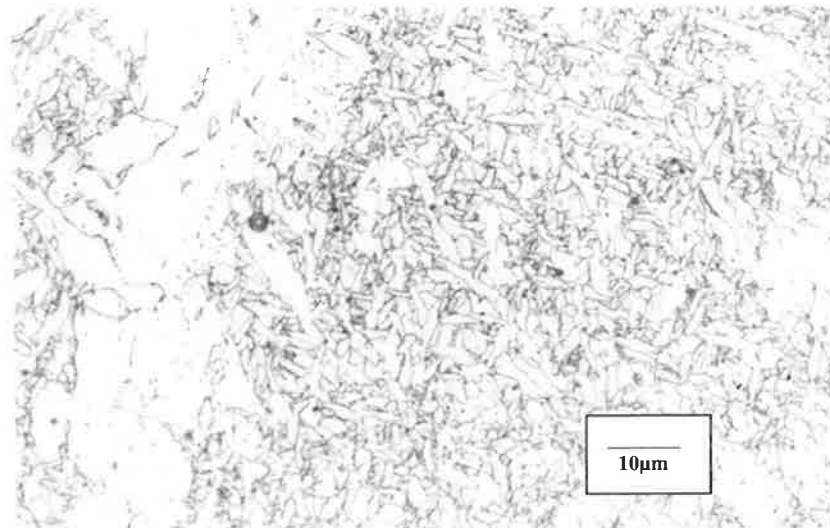
Microstructure photomicrograph



As-Welded x100

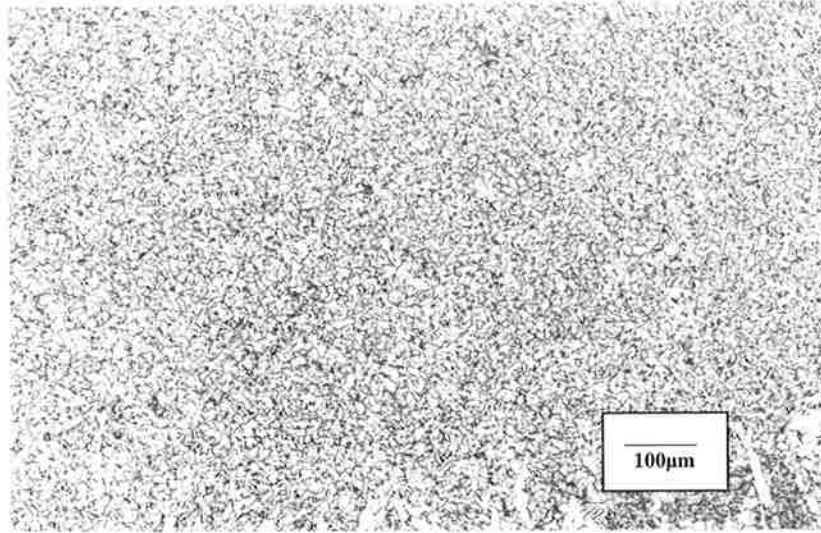


As-Welded x500

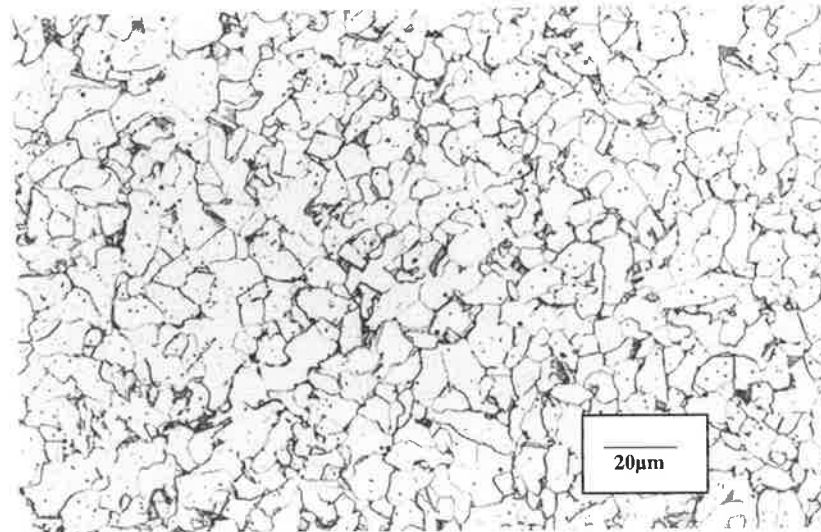


As-Welded x1000

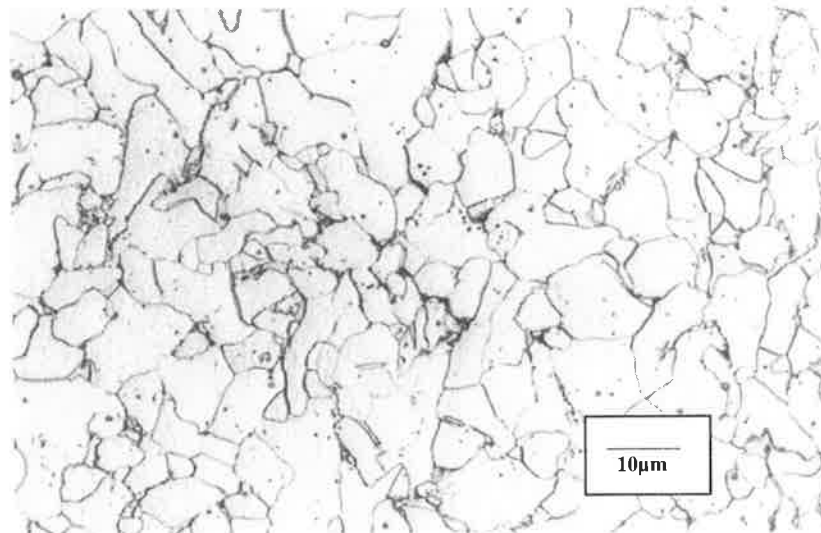
Appendix A



Re-Heated x100



Re-Heated x500



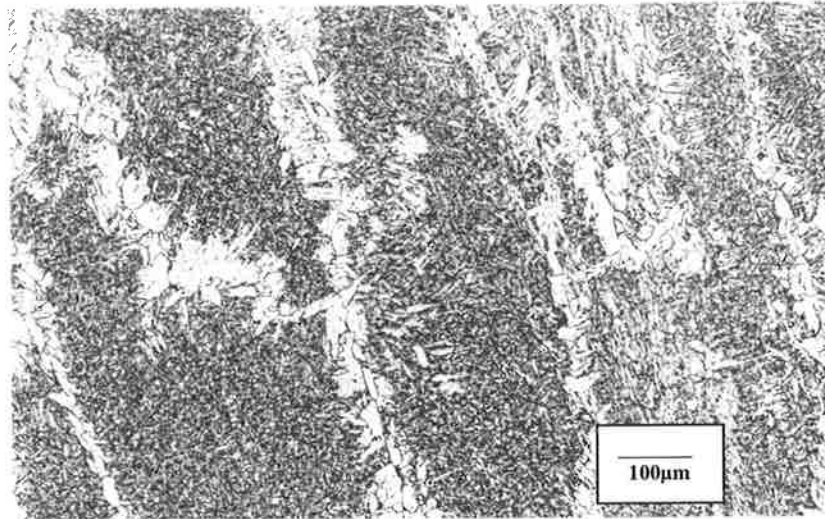
Re-Heated x1000

Manganese and Silicon Series

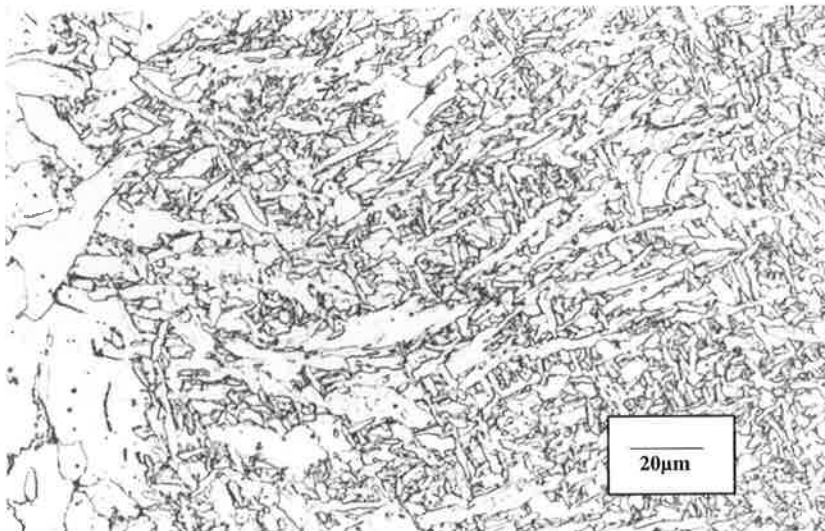
Composition

Si	<u>Mn</u>	<u>C</u>	<u>S</u>	<u>P</u>	<u>Ni</u>	<u>Cr</u>	<u>Mo</u>	<u>Cu</u>	<u>V</u>	<u>Nb</u>	<u>Ti</u>	<u>Al</u>	<u>B</u>	<u>O</u>	<u>N</u>
0.57	1.0	0.04	0.007	0.016	0.02	0.01	<0.01	0.01	0.0063	0.0001	0.0045	0.0134	<0.0005	0.0470	0.0057

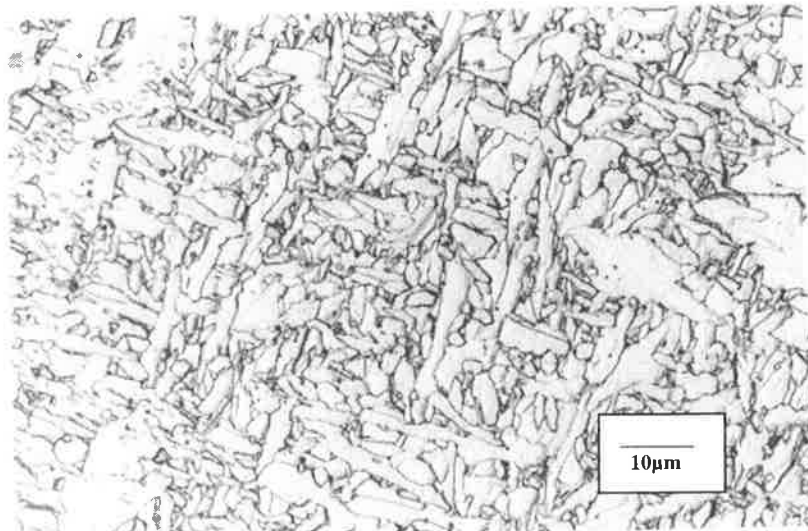
Microstructure photomicrograph



As-Welded x100

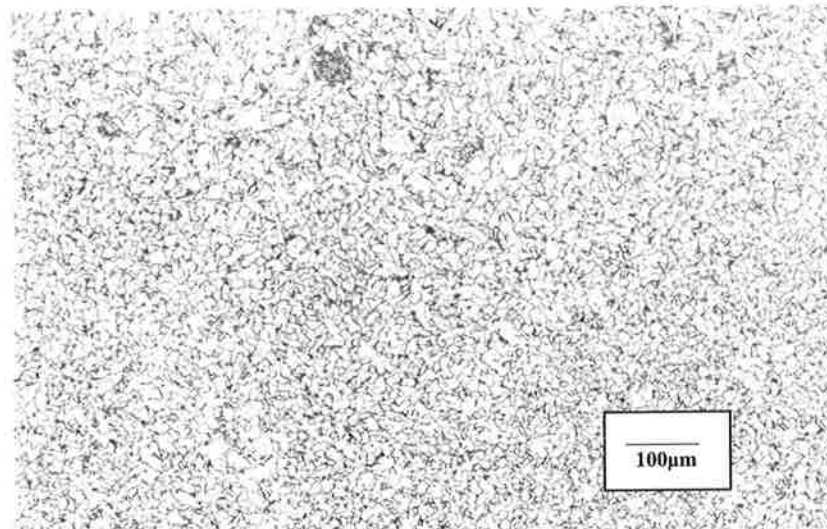


As-Welded x500

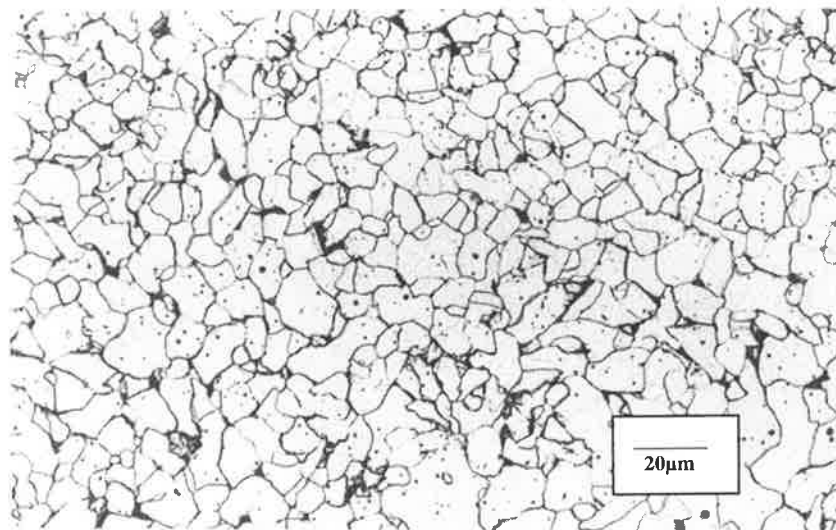


As-Welded x1000

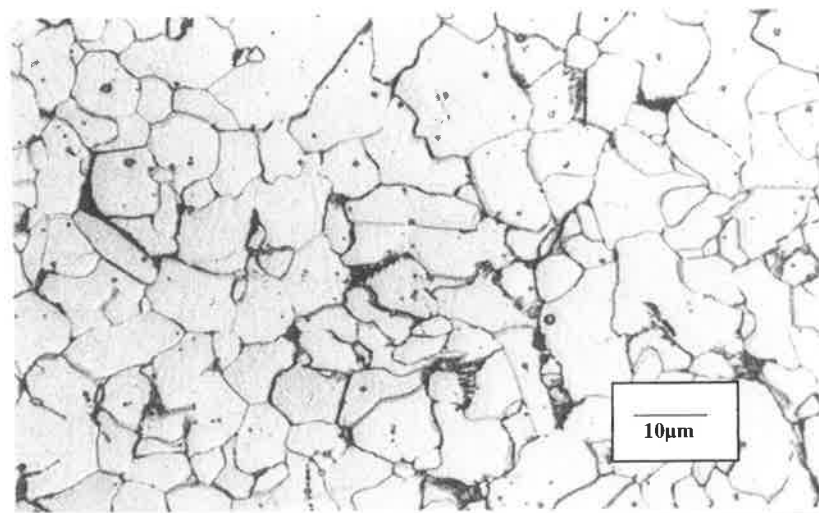
Appendix A



Re-Heated x100



Re-Heated x500

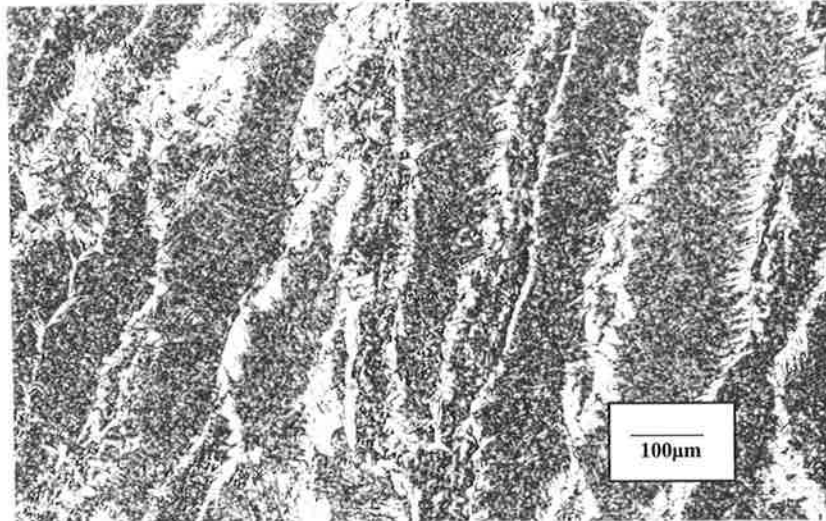


Re-Heated x1000

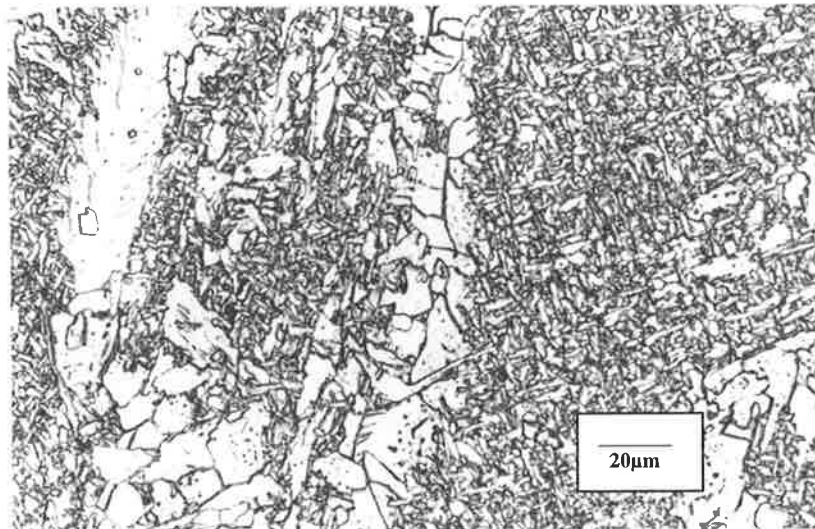
Manganese and Silicon Series**Composition**

Si	Mn	C	S	P	Ni	Cr	Mo	Cu	V	Nb	Ti	Al	B	O	N
0.67	1.27	0.04	0.007	0.016	0.02	0.01	0.01	0.01	0.0100	<0.01	0.005	0.0140	<0.0005	0.0420	0.0106

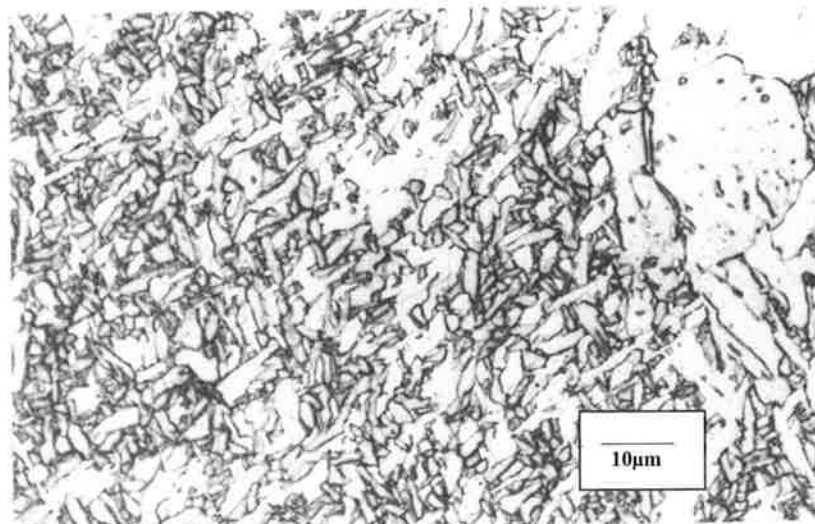
Microstructure photomicrograph



As-Welded x100

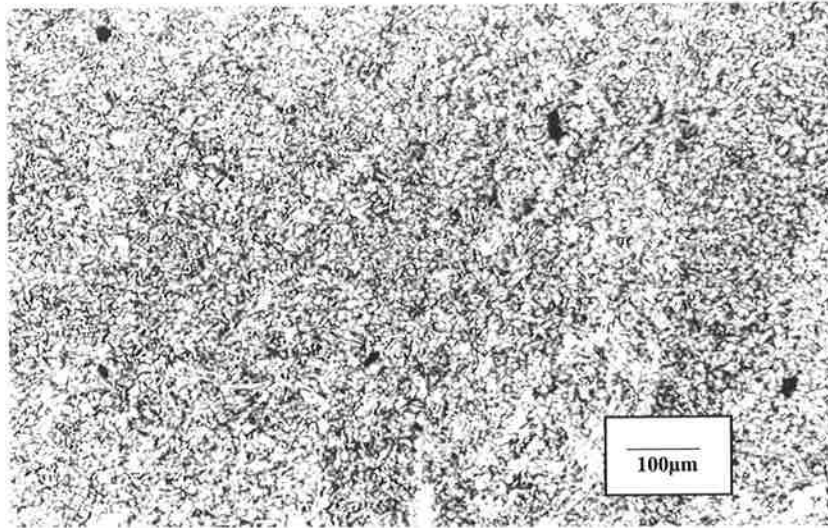


As-Welded x500

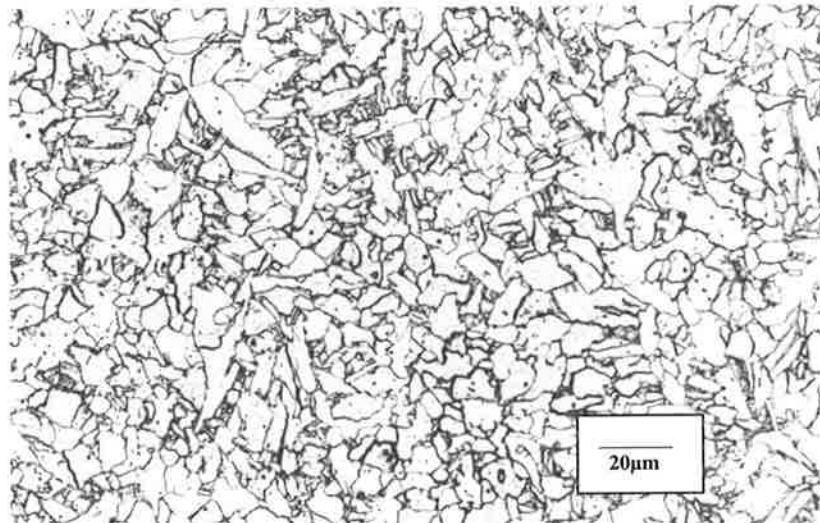


As-Welded x1000

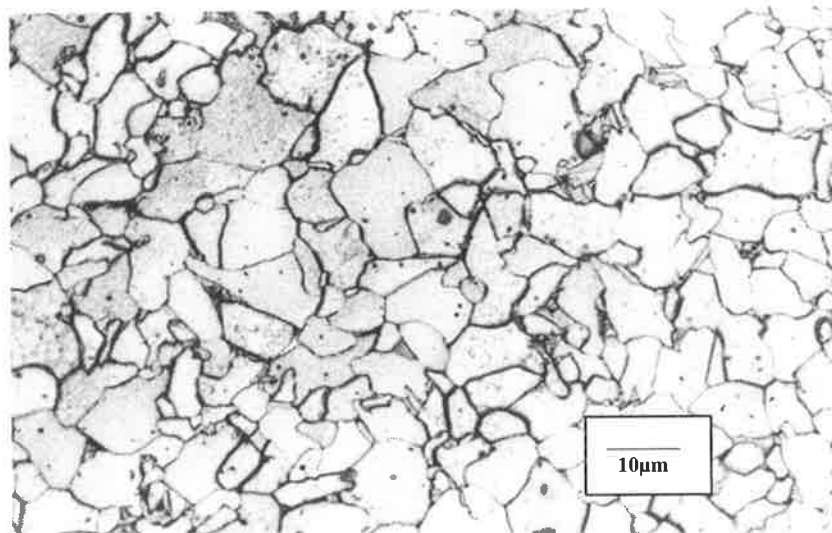
Appendix A



Re-Heated x100



Re-Heated x500

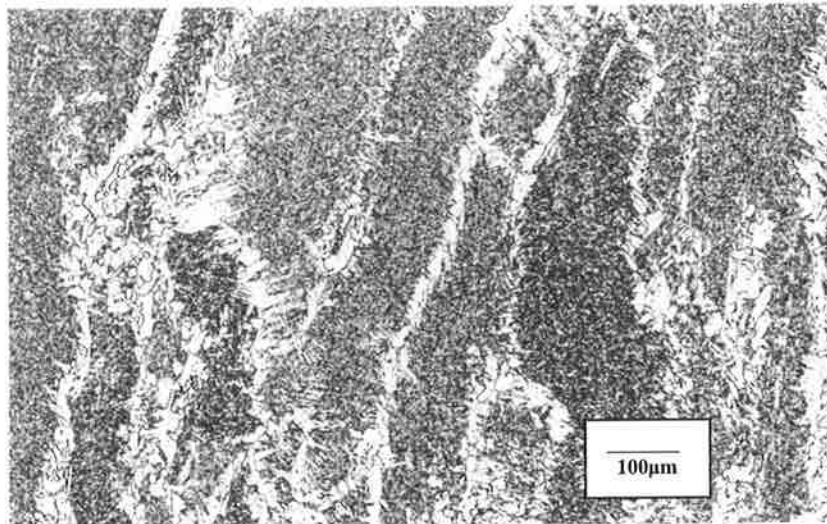


Re-Heated x1000

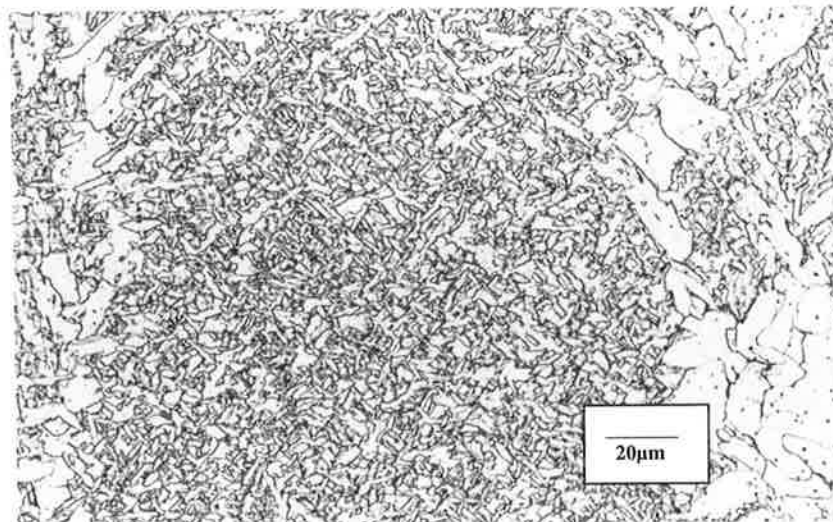
Manganese and Silicon Series**Composition**

Si	Mn	C	S	P	Ni	Cr	Mo	Cu	V	Nb	Ti	Al	B	O	N
0.64	1.34	0.04	0.012	0.014	0.02	0.01	<0.01	0.01	0.0058	0.0005	0.0054	0.0133	<0.0005	0.0530	0.0047

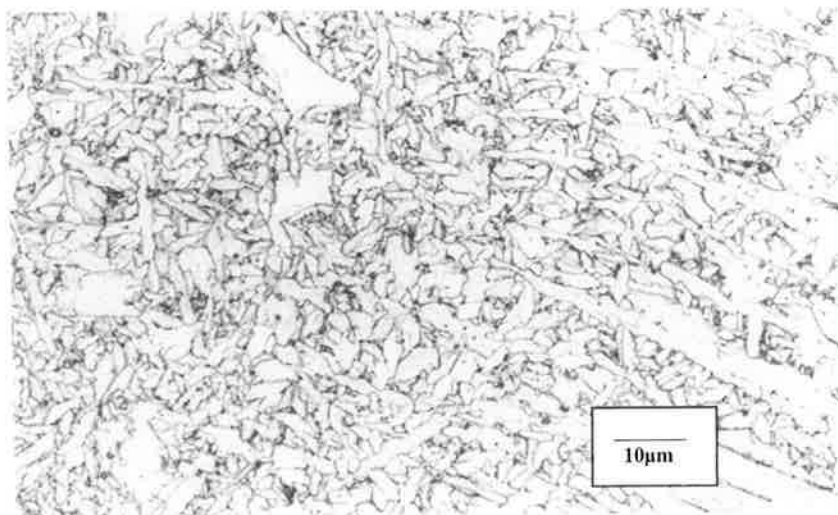
Microstructure photomicrograph



As-Welded x100

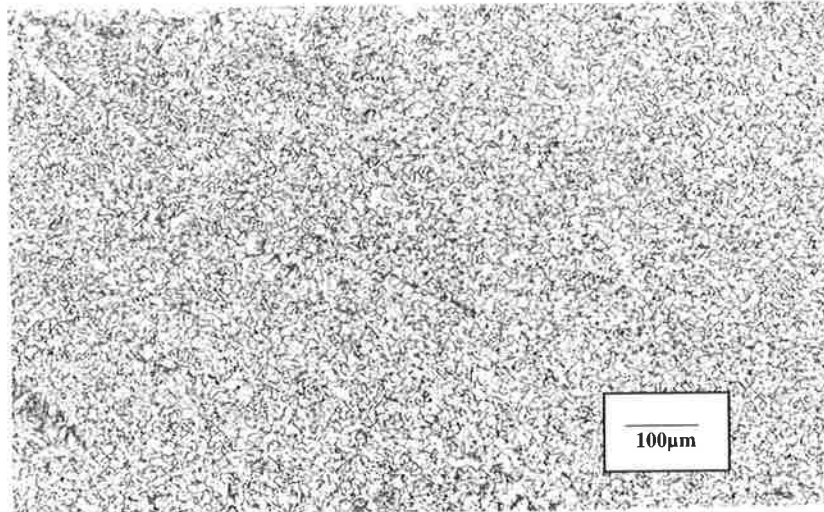


As-Welded x500

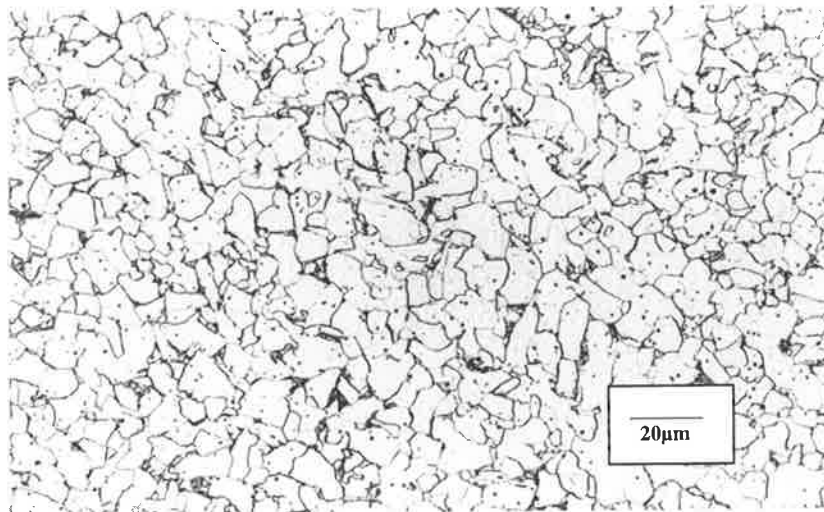


As-Welded x1000

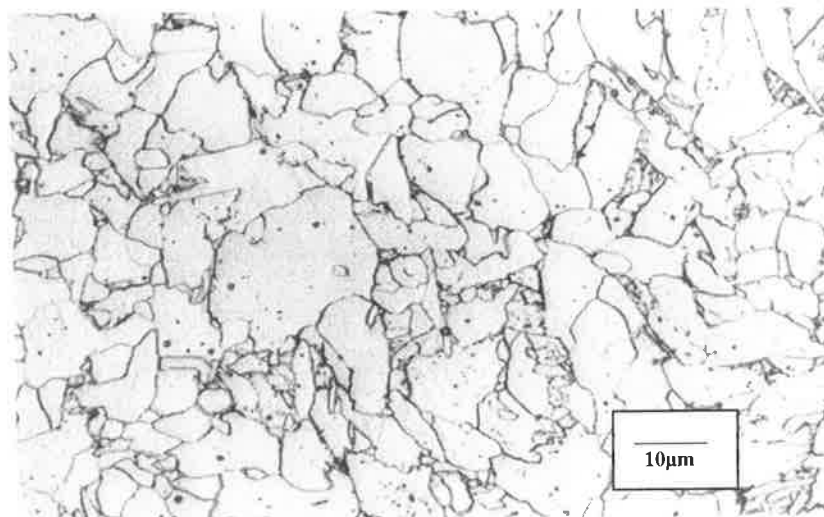
Appendix A



Re-Heated x100



Re-Heated x500



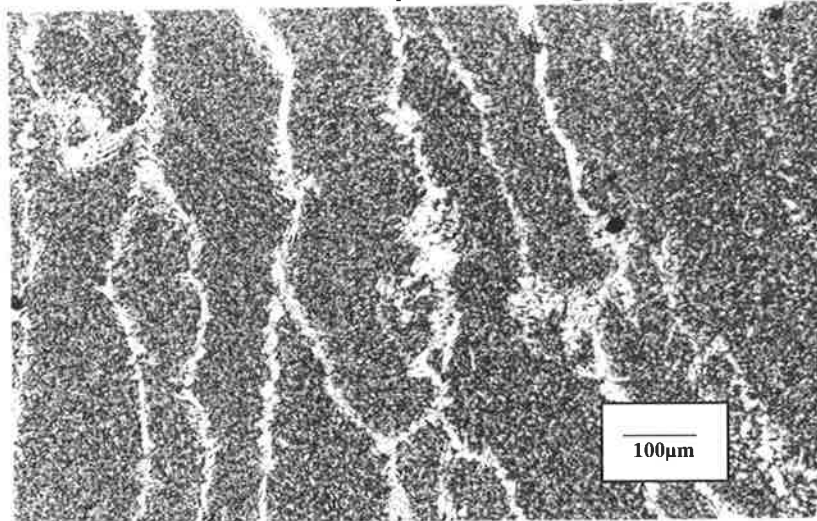
Re-Heated x1000

Manganese and Silicon Series

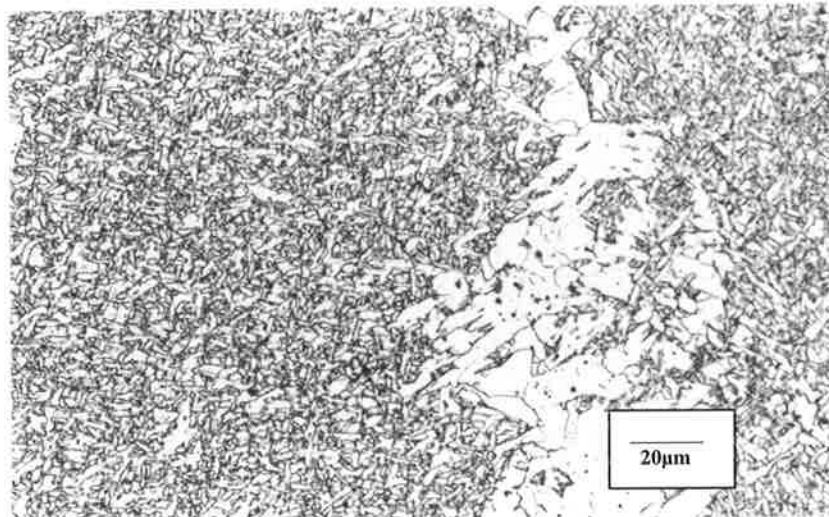
Composition

Si	Mn	C	S	P	Ni	Cr	Mo	Cu	V	Nb	Ti	Al	B	O	N
0.57	1.64	0.04	0.007	0.016	0.02	0.01	0.01	0.01	0.0100	<0.01	0.0060	0.0148	<0.0005	0.0480	0.0098

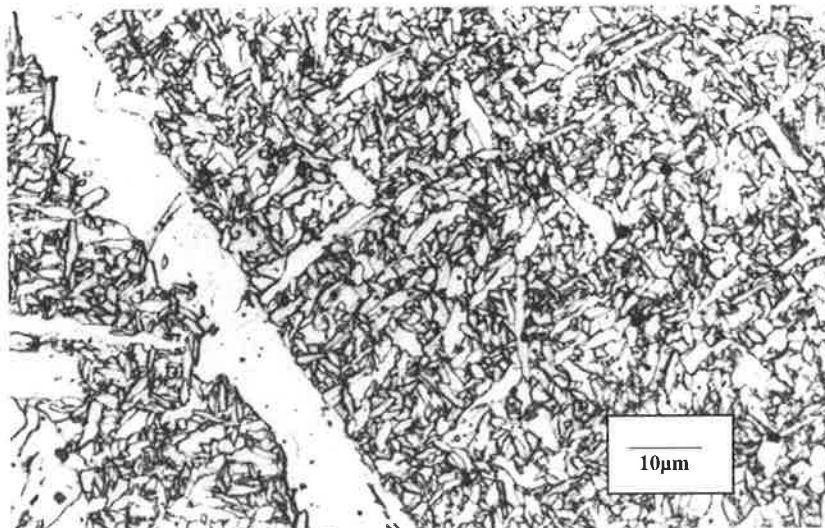
Microstructure photomicrograph



As-Welded x100

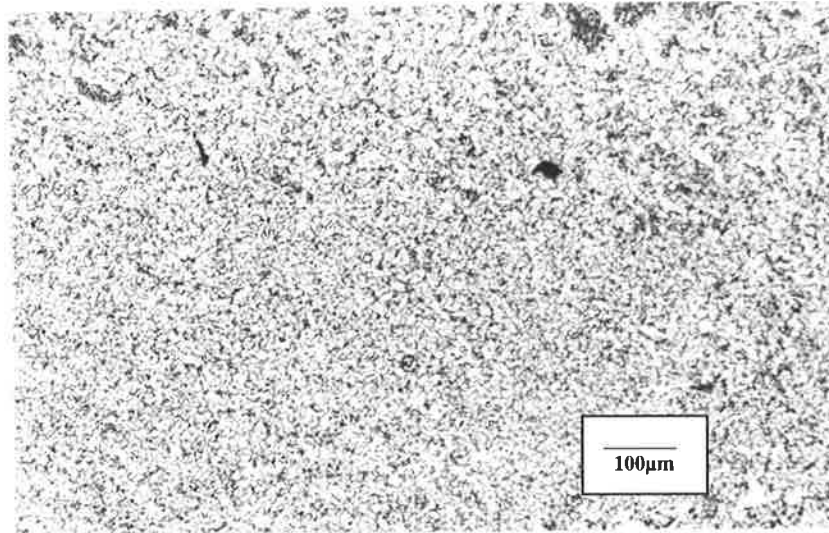


As-Welded x500

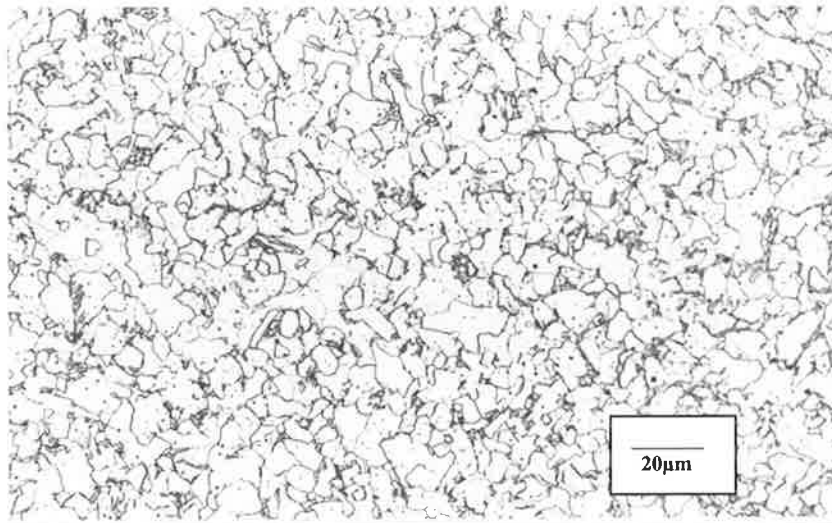


As-Welded x1000

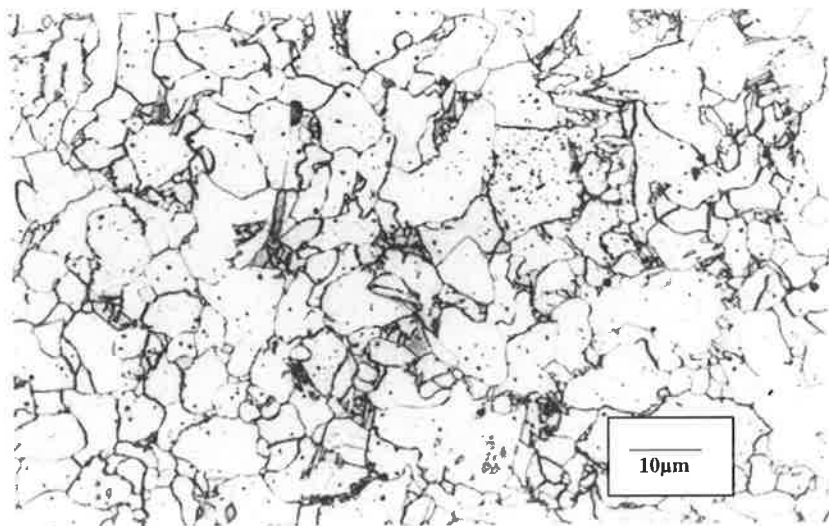
Appendix A



Re-Heated x100



Re-Heated x500



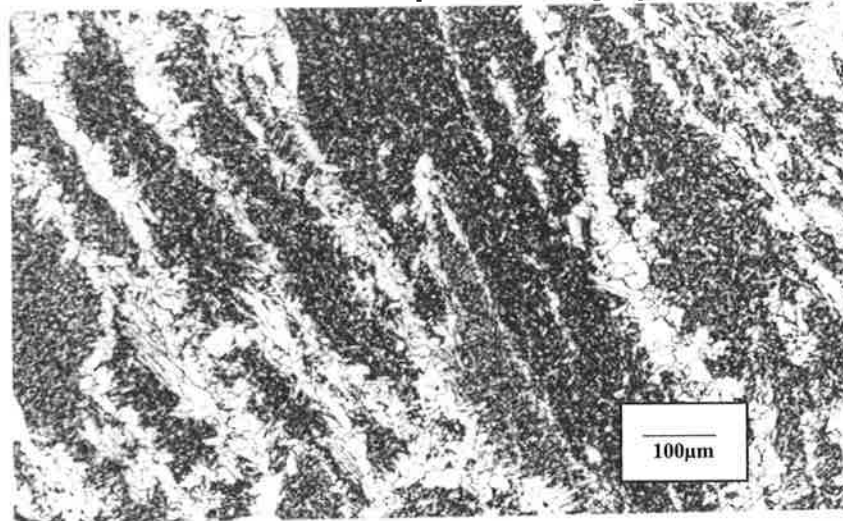
Re-Heated x1000

Manganese and Silicon Series

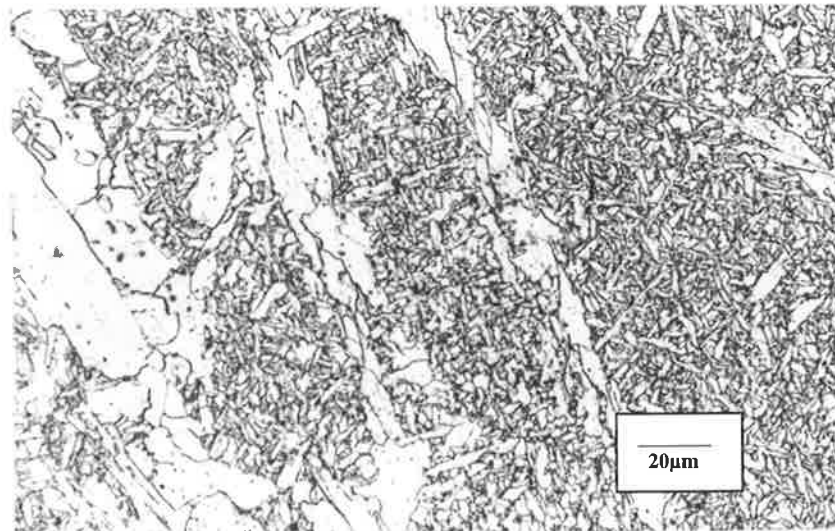
Composition

Si	Mn	C	S	P	Ni	Cr	Mo	Cu	V	Nb	Ti	Al	B	O	N
0.8	1.21	0.05	0.009	0.017	0.02	0.01	0.01	0.01	0.0100	<0.01	0.0059	0.0158	<0.0005	0.0440	0.0080

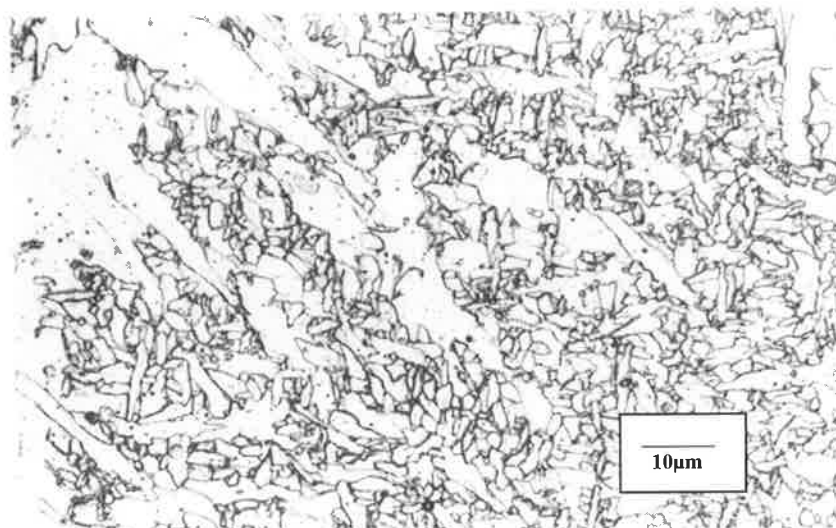
Microstructure photomicrograph



As-Welded x100

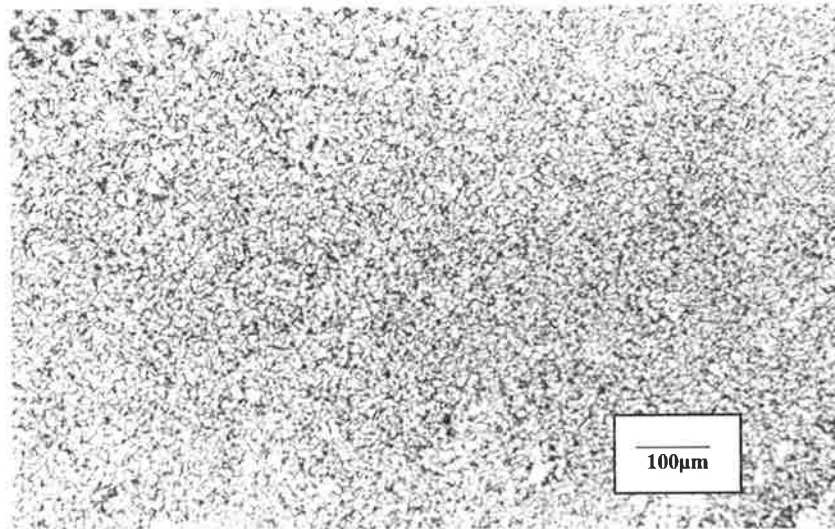


As-Welded x500

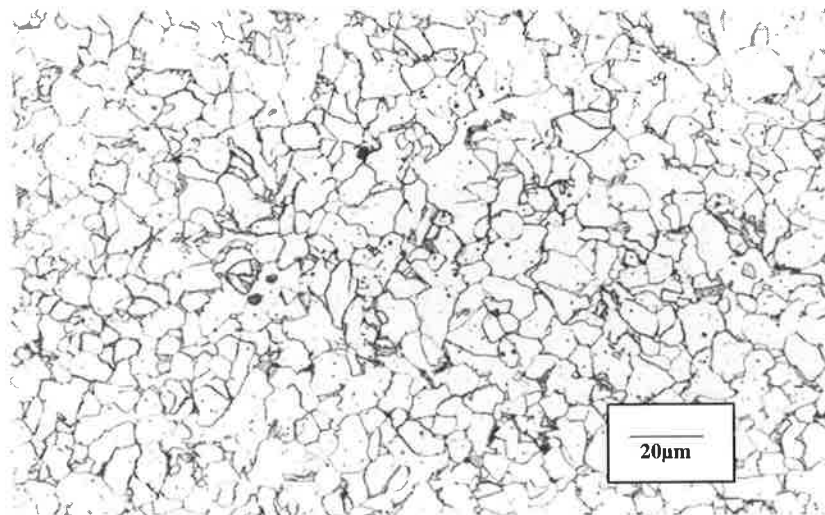


As-Welded x1000

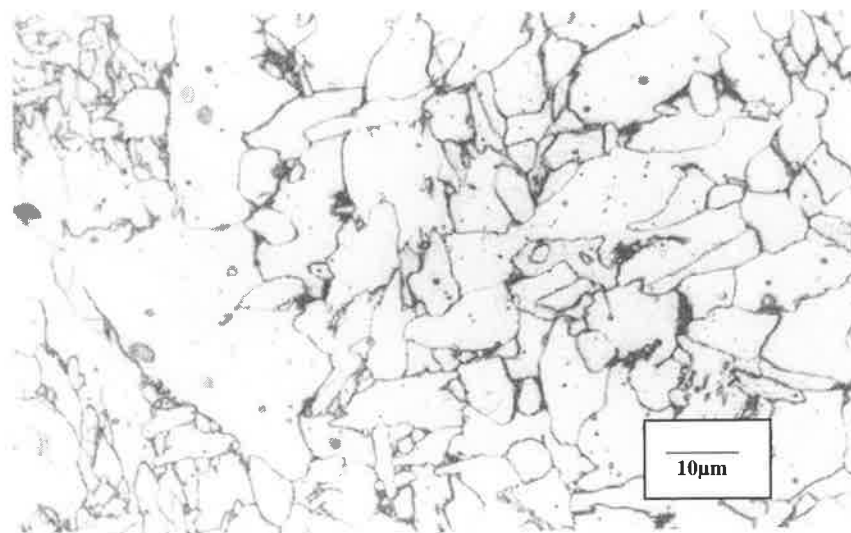
Appendix A



Re-Heated x100



Re-Heated x500

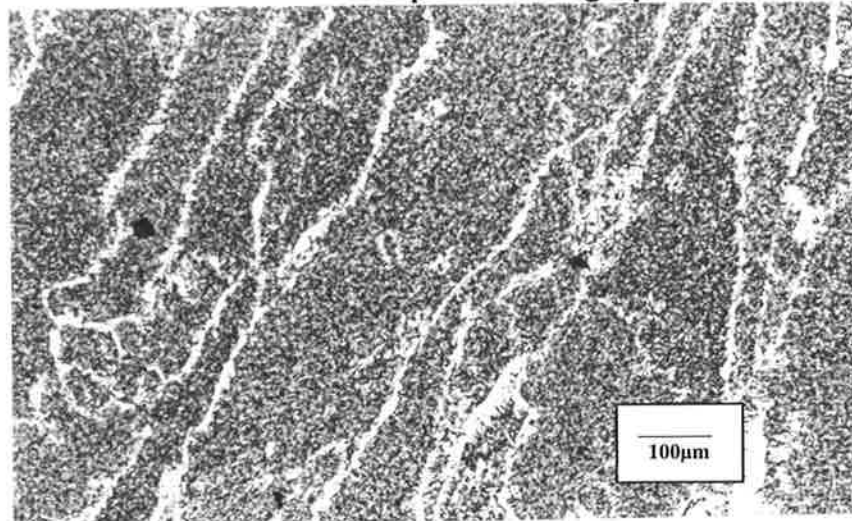


Re-Heated x1000

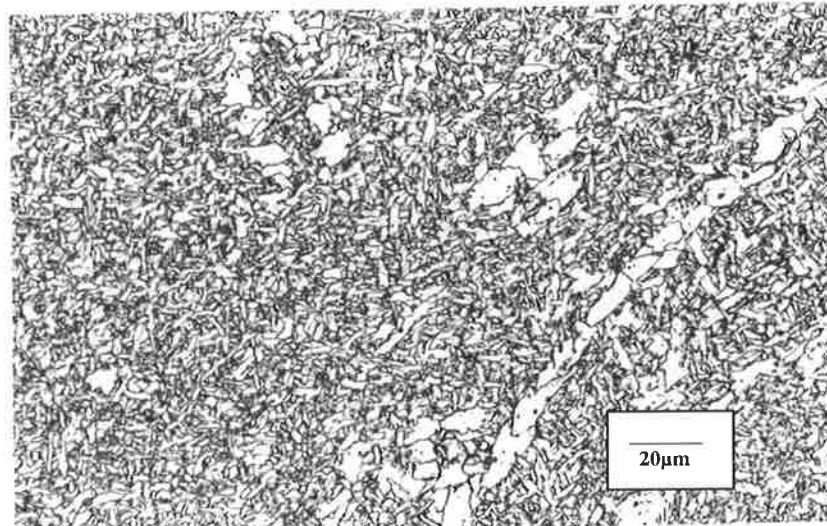
Manganese and Silicon Series**Composition**

Si	Mn	C	S	P	Ni	Cr	Mo	Cu	V	Nb	Ti	Al	B	O	N
0.84	1.66	0.05	0.014	0.017	0.02	0.01	0.01	0.01	0.0080	0.005	0.0060	0.0130	<0.0005	0.0480	0.0116

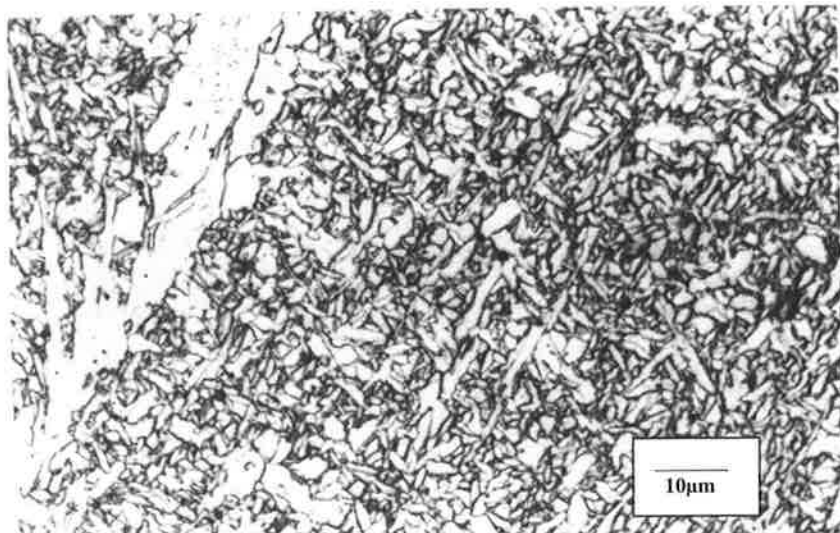
Microstructure photomicrograph



As-Welded x100

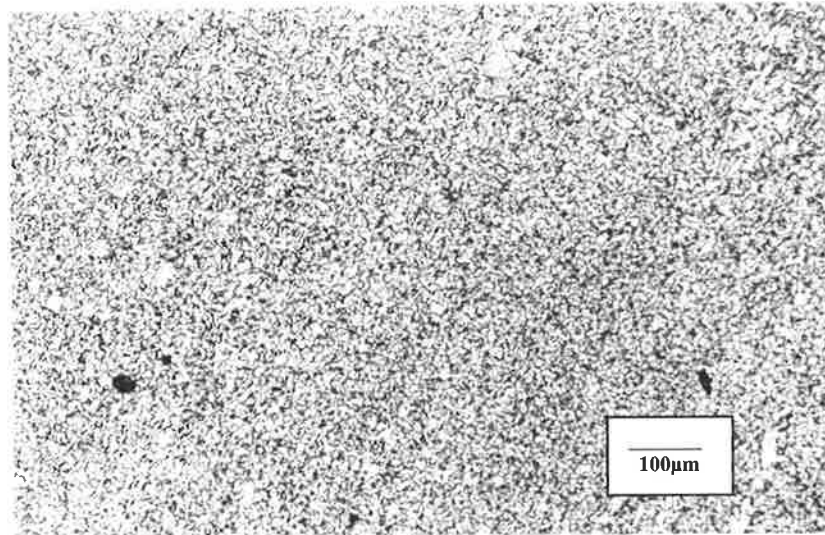


As-Welded x500

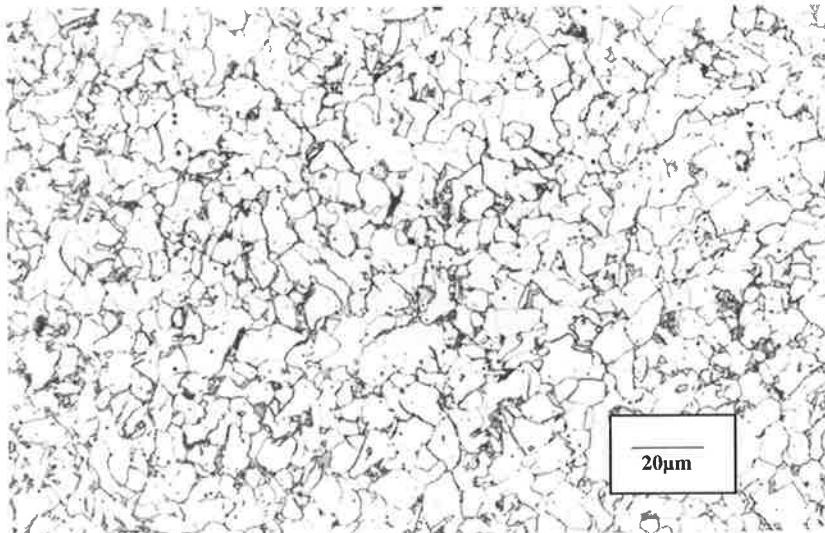


As-Welded x1000

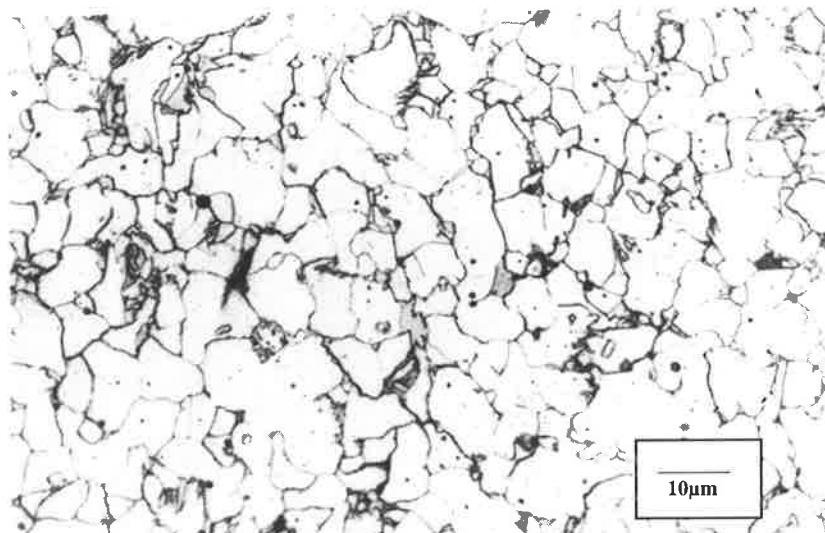
Appendix A



Re-Heated x100



Re-Heated x500



Re-Heated x1000

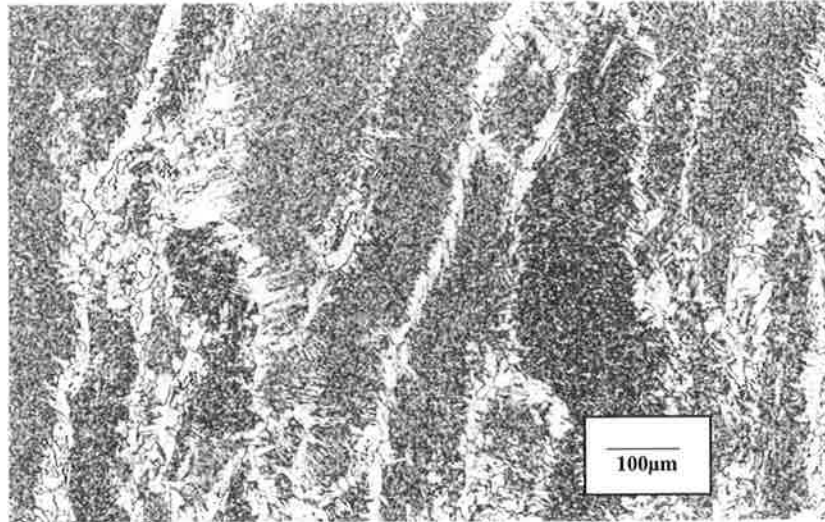
Appendix B Titanium Series

Titanium Series

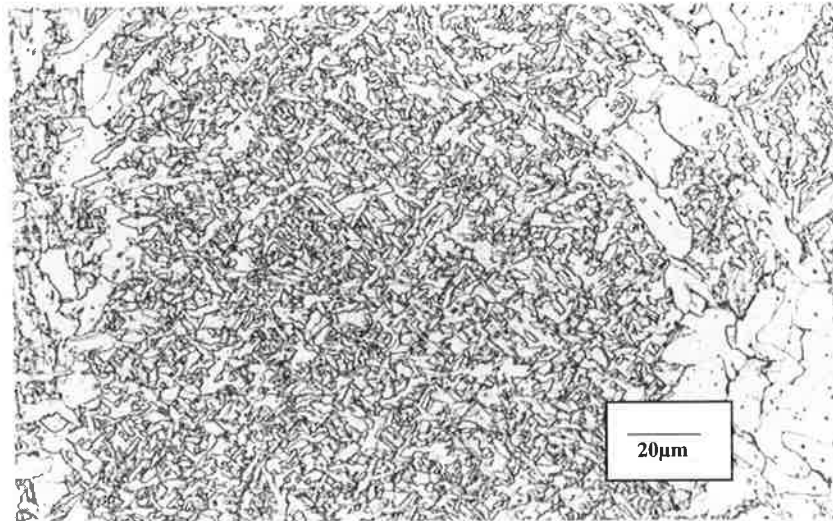
Composition

<u>Si</u>	<u>Mn</u>	<u>C</u>	<u>S</u>	<u>P</u>	<u>Ni</u>	<u>Cr</u>	<u>Mo</u>	<u>Cu</u>	<u>V</u>	<u>Nb</u>	<u>Ti</u>	<u>Al</u>	<u>B</u>	<u>O</u>	<u>N</u>
0.64	1.34	0.04	0.012	0.014	0.02	0.01	<0.01	0.01	0.0058	0.0005	0.0054	0.0133	<0.0005	0.0530	0.0047

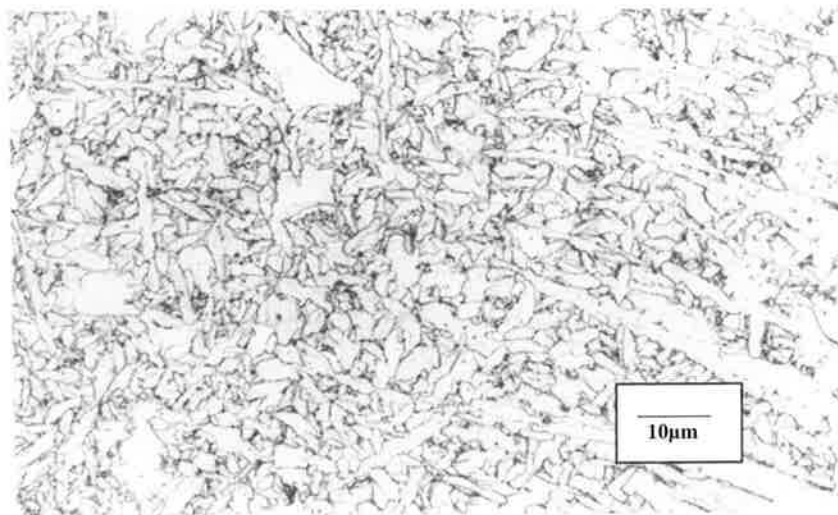
Microstructure photomicrograph



As-Welded x100

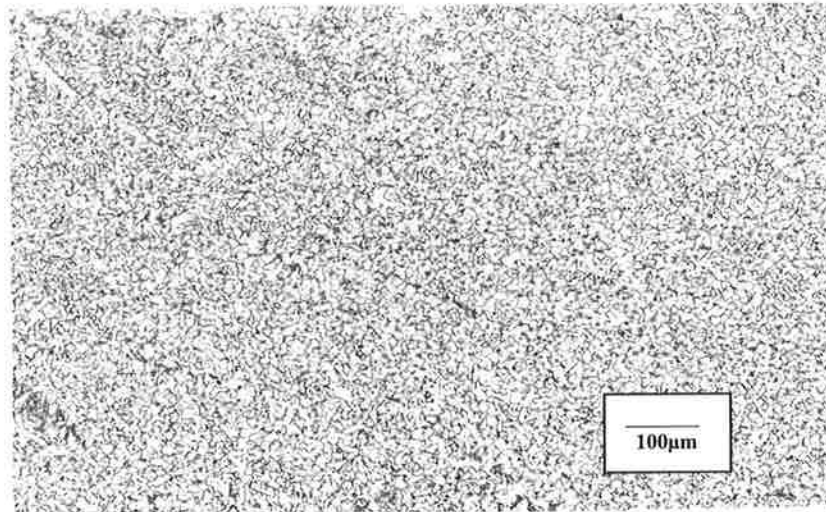


As-Welded x500

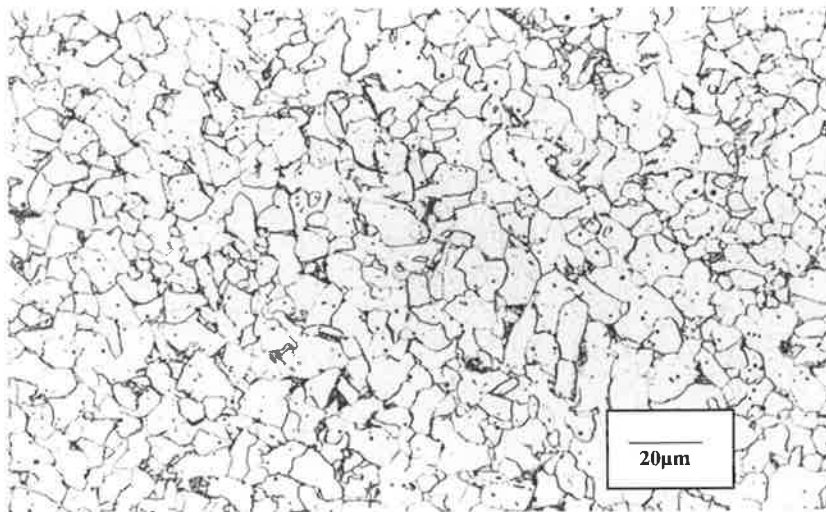


As-Welded x1000

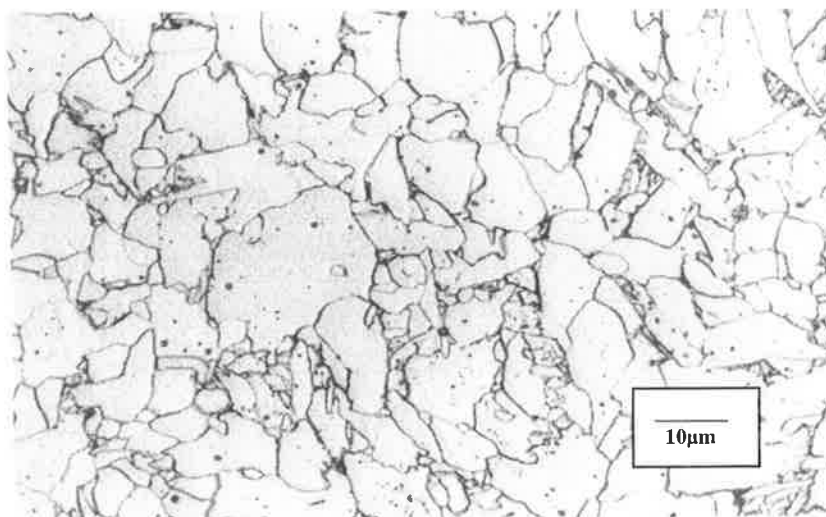
Appendix B



Re-Heated x100



Re-Heated x500

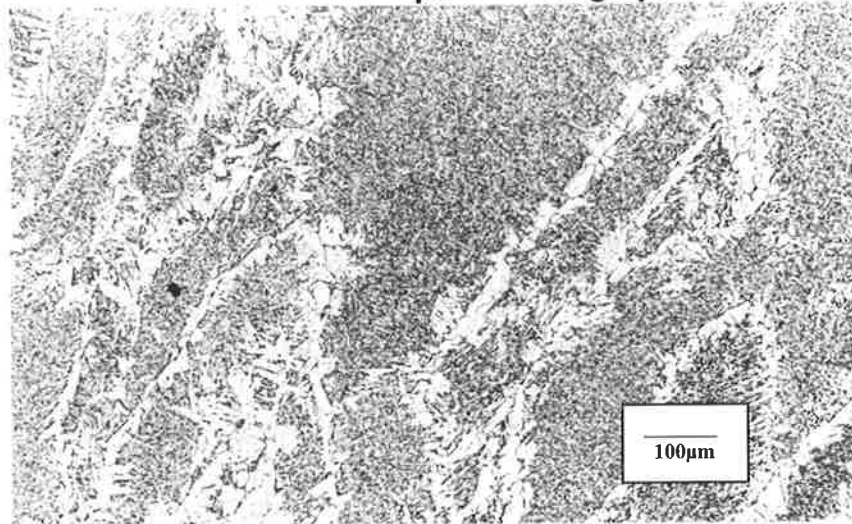


Re-Heated x1000

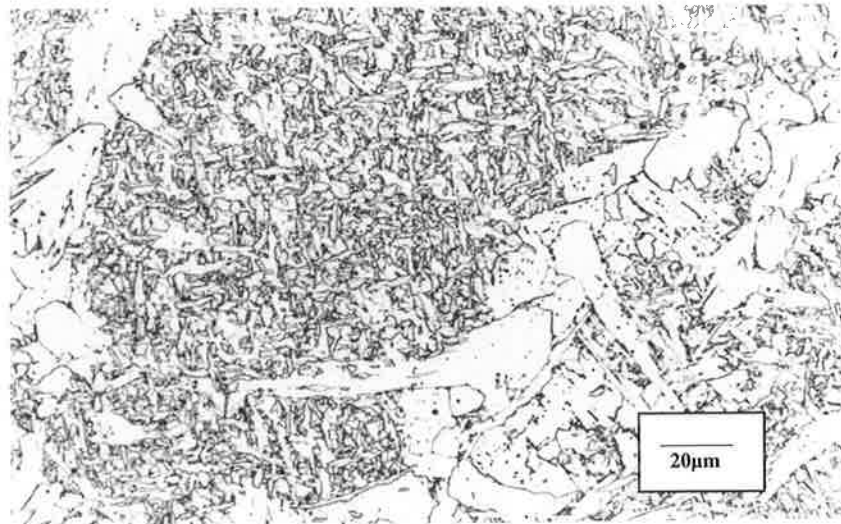
Titanium Series**Composition**

Si	Mn	C	S	P	Ni	Cr	Mo	Cu	V	Nb	Ti	Al	B	O	N
0.55	1.30	0.05	0.008	0.015	0.02	0.01	0.01	0.010	0.0059	<0.0005	0.0124	0.0132	<0.0005	0.0450	0.0040

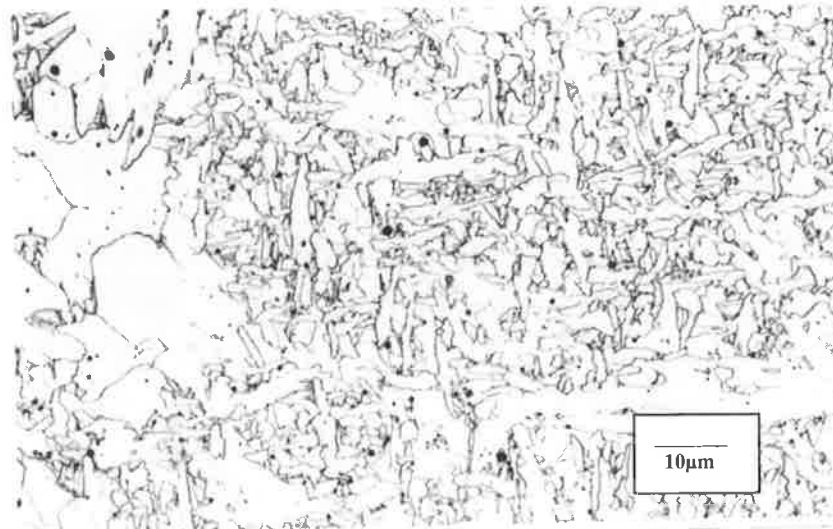
Microstructure photomicrograph



As-Welded x100

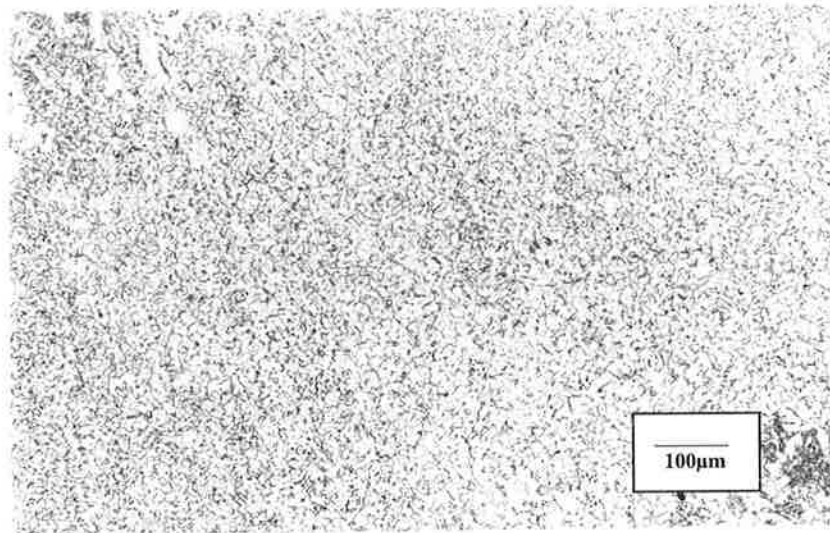


As-Welded x500

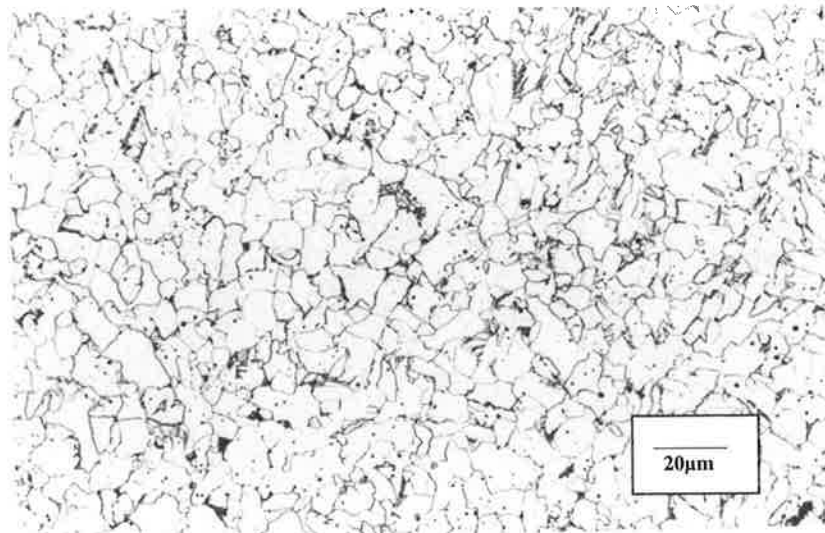


As-Welded x1000

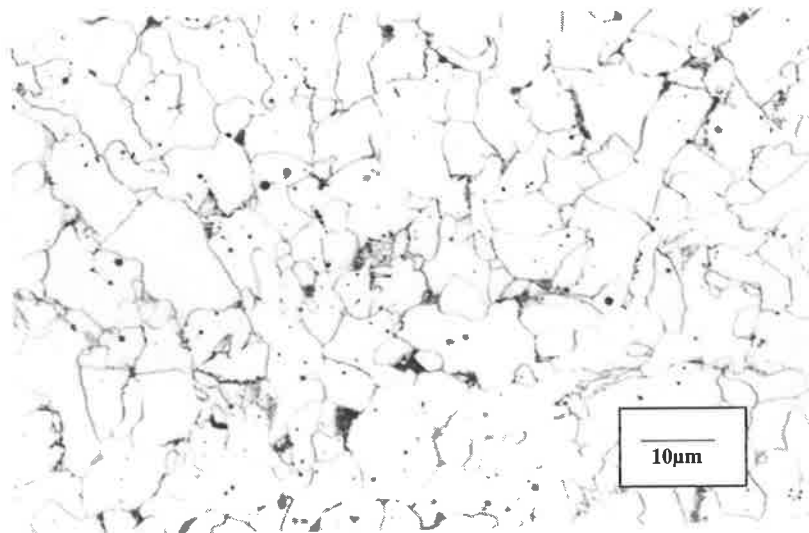
Appendix B



Re-Heated x100



Re-Heated x500



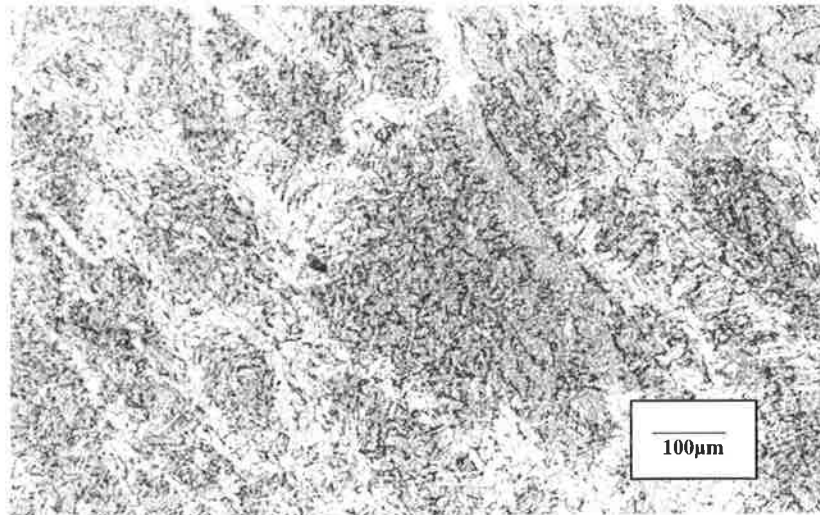
Re-Heated x1000

Titanium Series

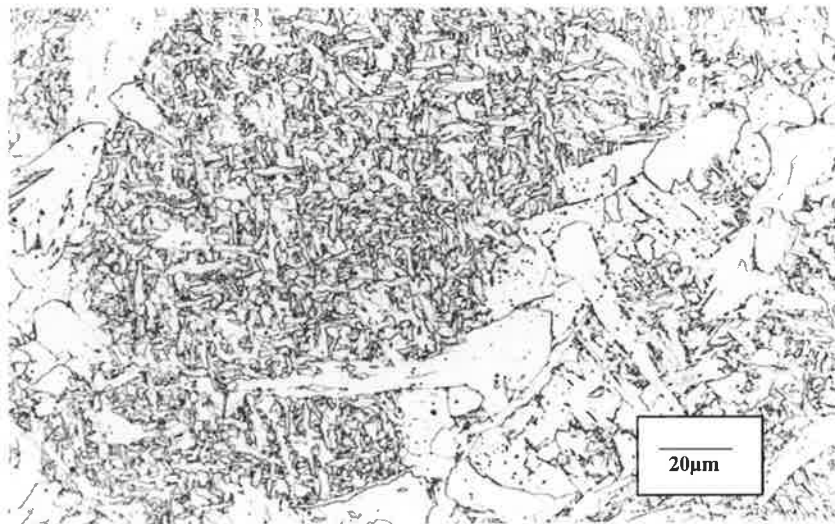
Composition

Si	Mn	C	S	P	Ni	Cr	Mo	Cu	Y	Nb	Ti	Al	B	O	N
0.58	1.26	0.05	0.011	0.013	0.02	0.01	0.01	0.01	0.0058	<0.0005	0.0273	0.0142	<0.0005	0.0420	0.0054

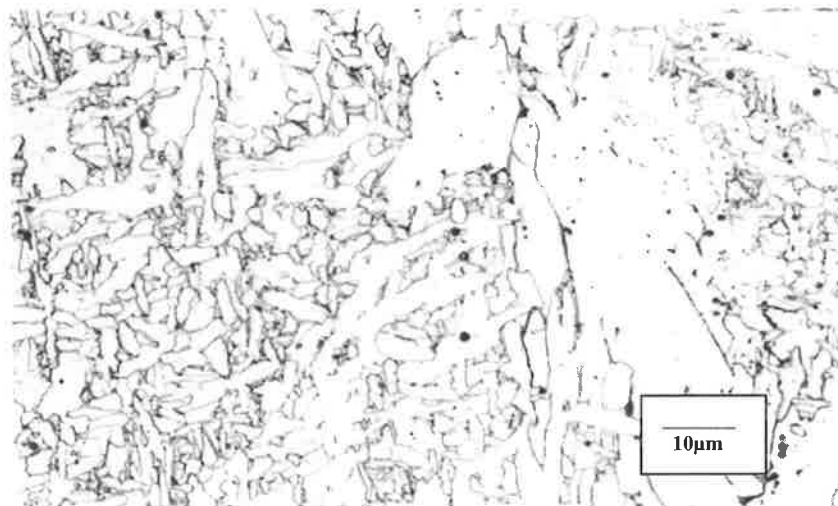
Microstructure photomicrograph



As-Welded x100

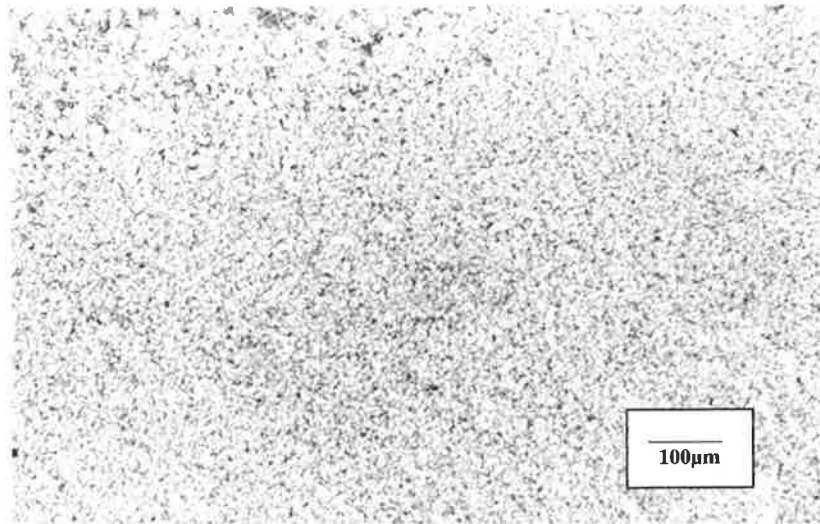


As-Welded x500

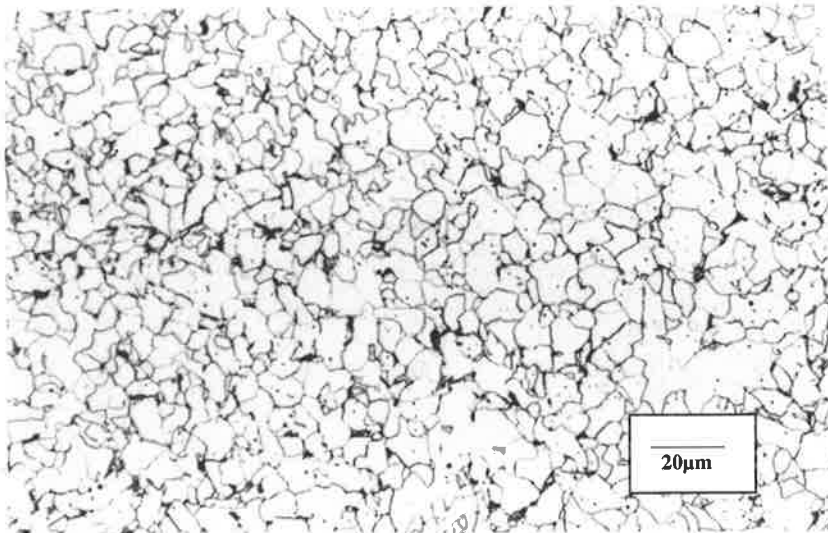


As-Welded x1000

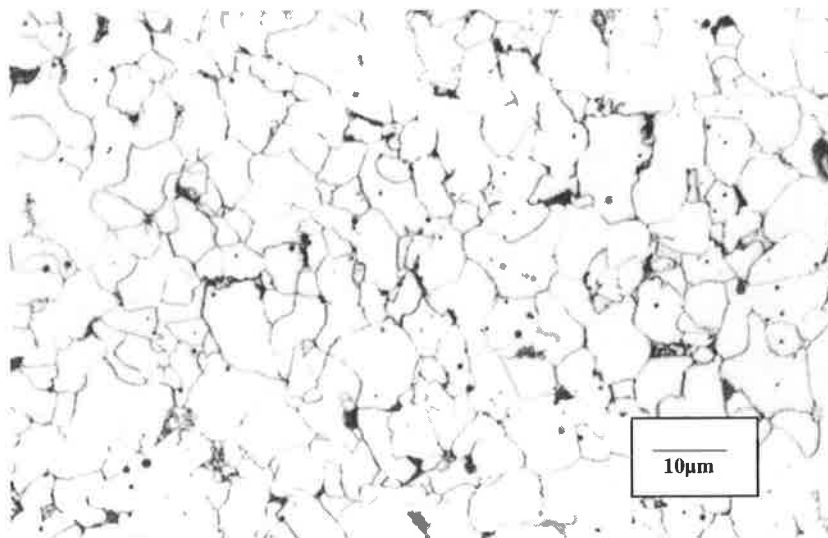
Appendix B



Re-Heated x100



Re-Heated x500

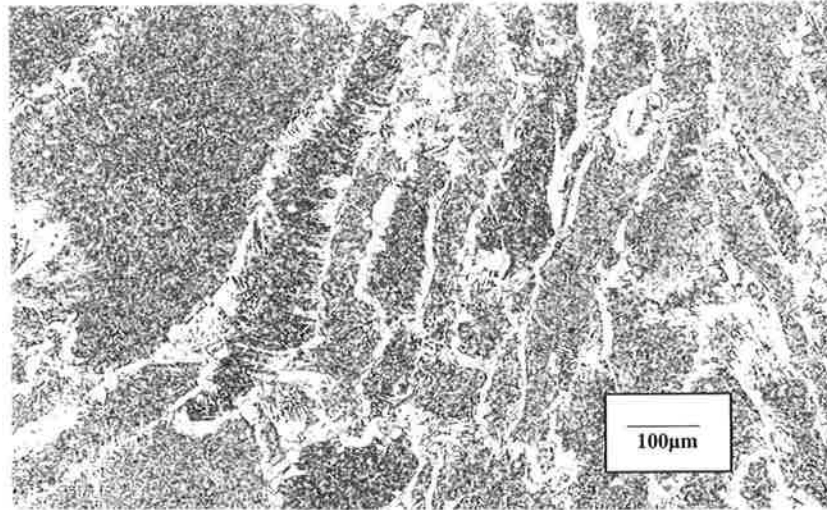


Re-Heated x1000

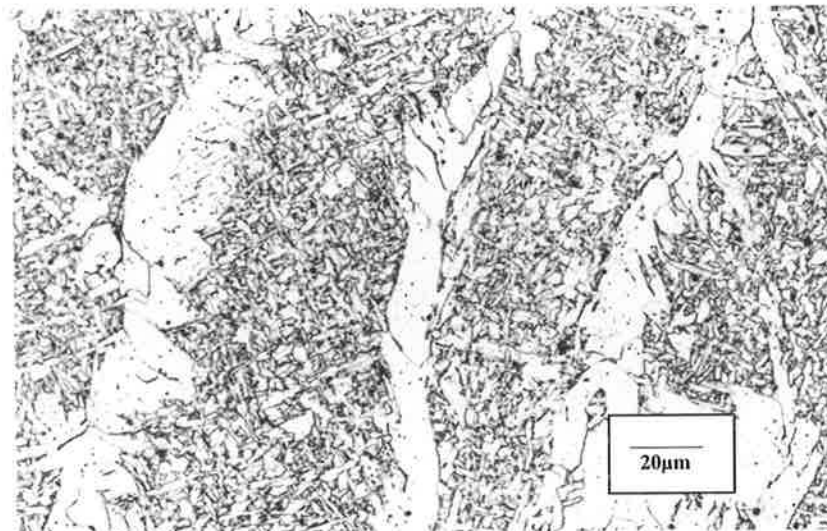
Titanium Series**Composition**

Si	Mn	C	S	P	Ni	Cr	Mo	Cu	V	Nb	Ti	Al	B	O	N
0.66	1.38	0.05	0.011	0.013	0.02	0.01	0.01	0.01	0.0066	<0.0005	0.0458	0.0111	<0.0005	0.0380	0.0037

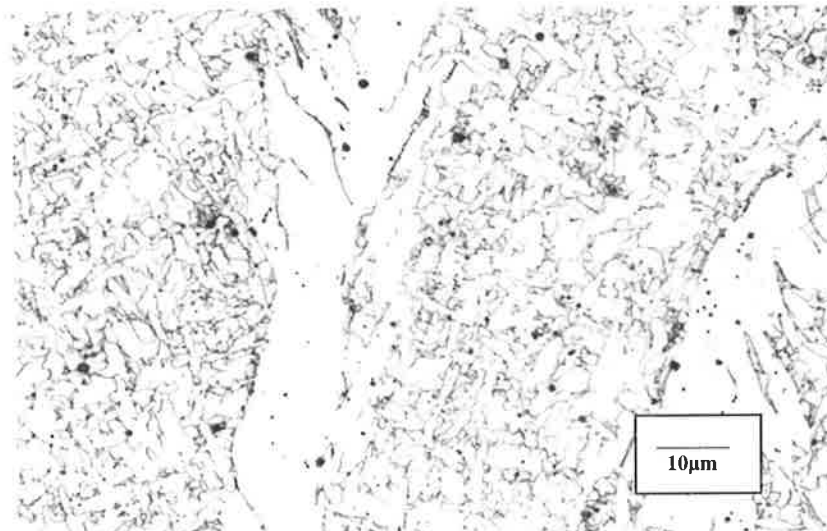
Microstructure photomicrograph



As-Welded x100

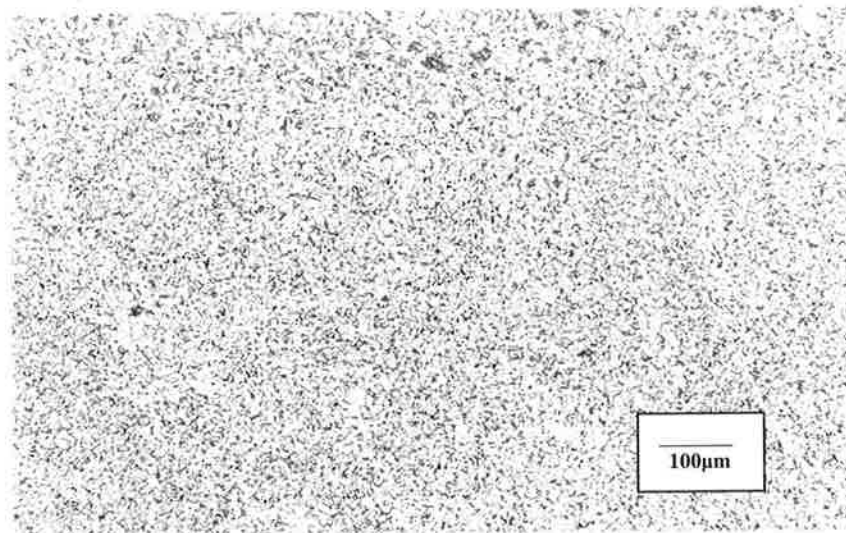


As-Welded x500

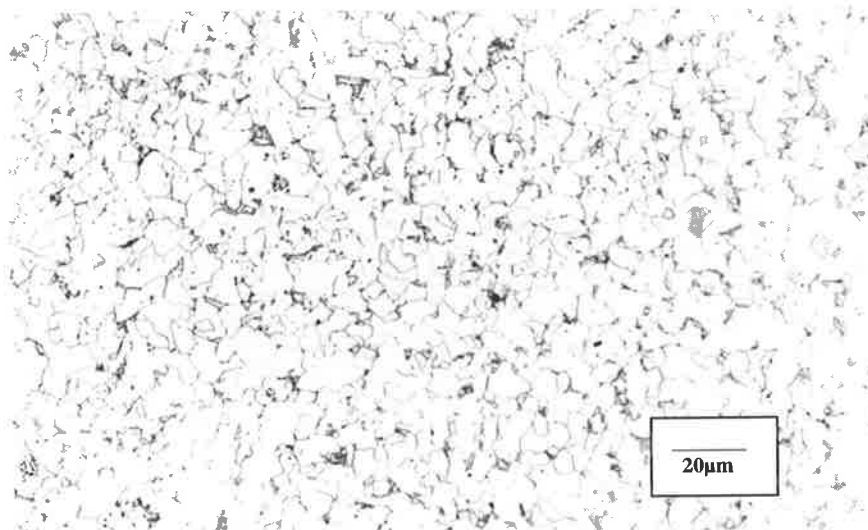


As-Welded x1000

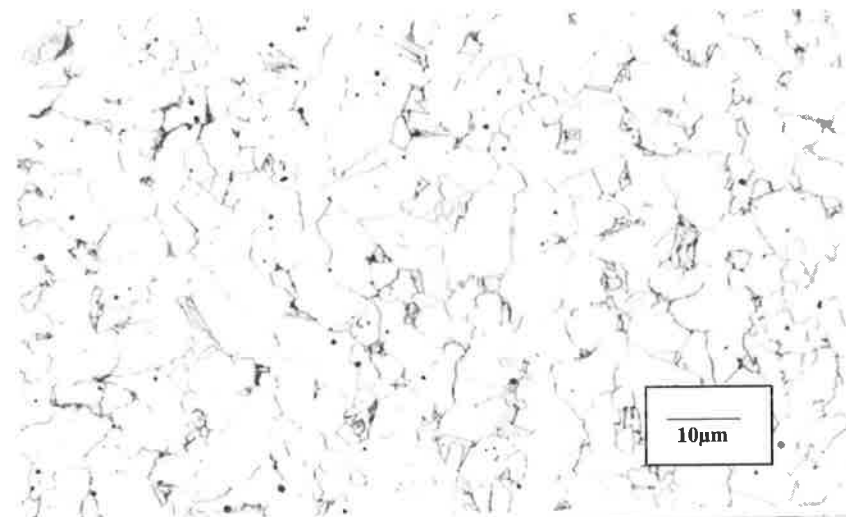
Appendix B



Re-Heated x100



Re-Heated x500



Re-Heated x1000

Appendix B

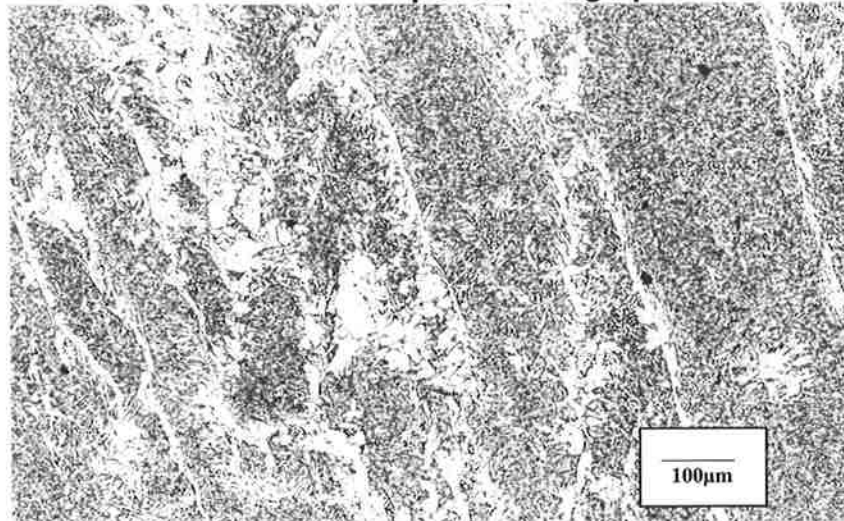
Titanium Series

Composition

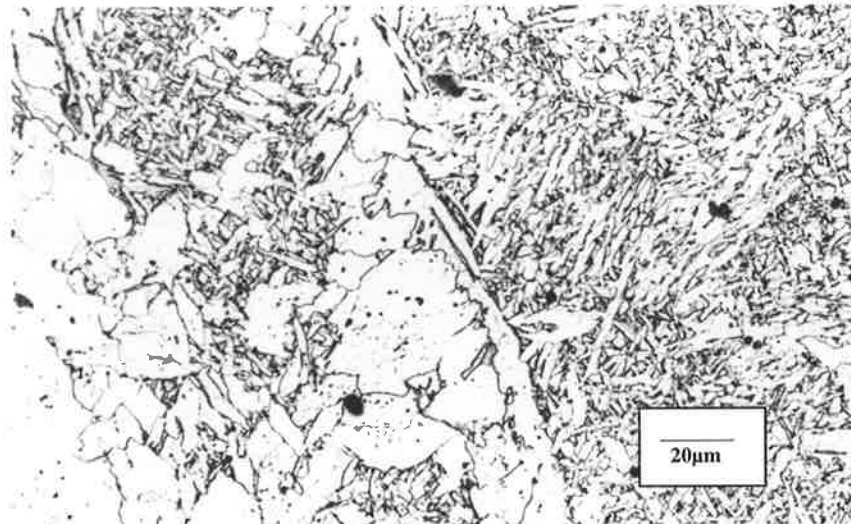
Si	Mn	C	S	P	Ni	Cr	Mo	Cu	V	Nb	Ti	Al	B	O	N
0.56	1.24	0.05	0.010	0.012	0.02	0.01	<0.01	0.02	0.01	<0.01	0.0588	0.0161	<0.0005	0.0380	0.0070

Appendix B

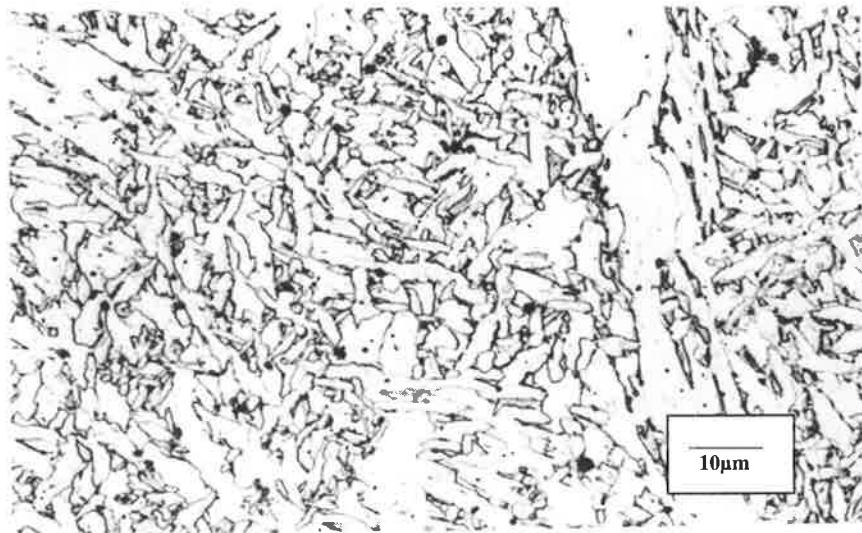
Microstructure photomicrograph



As-Welded x100

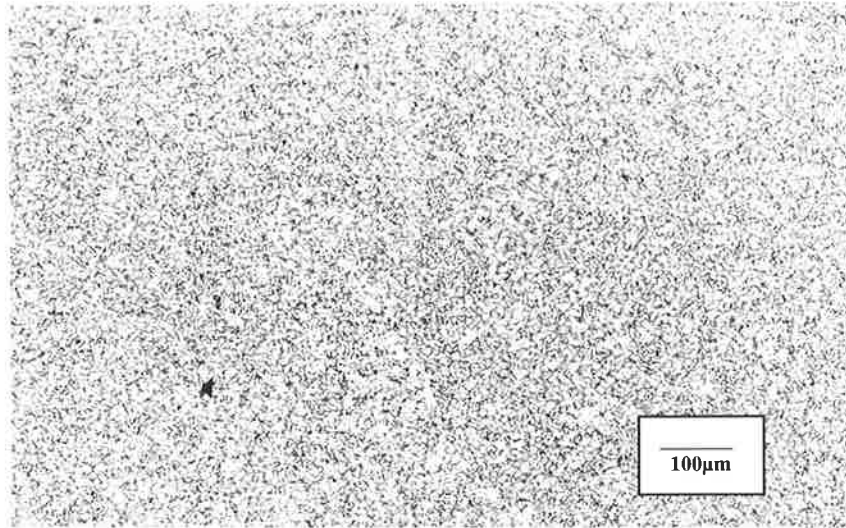


As-Welded x500

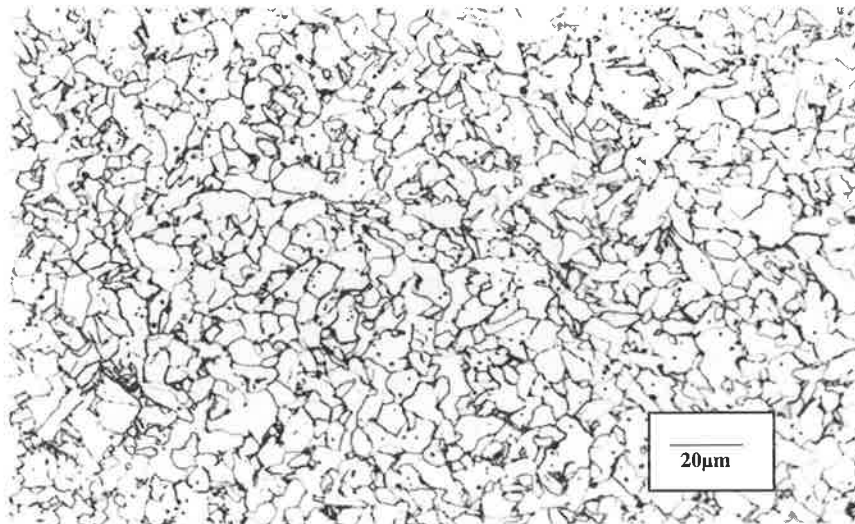


As-Welded x1000

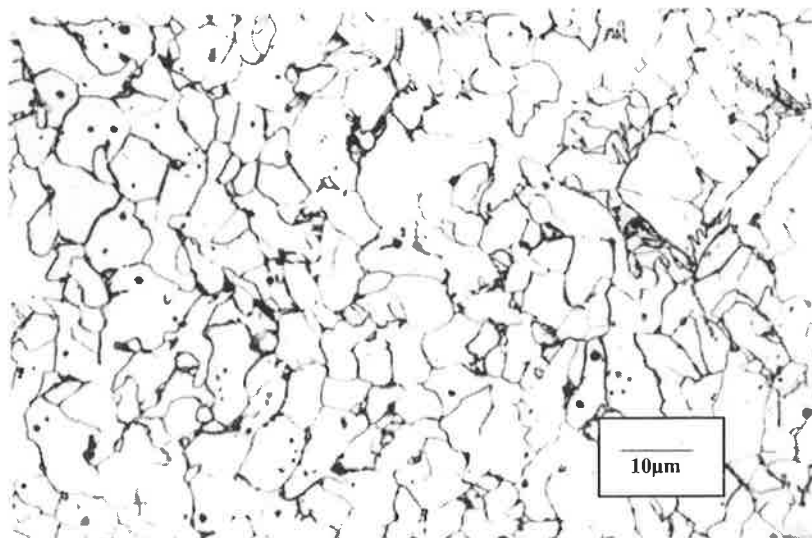
Appendix B



Re-Heated x100



Re-Heated x500



Re-Heated x1000

Appendix B

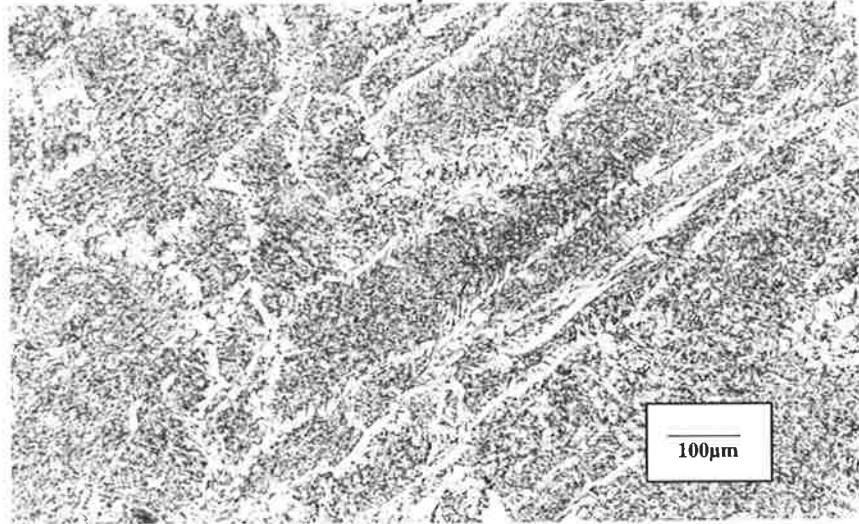
Titanium Series

Composition

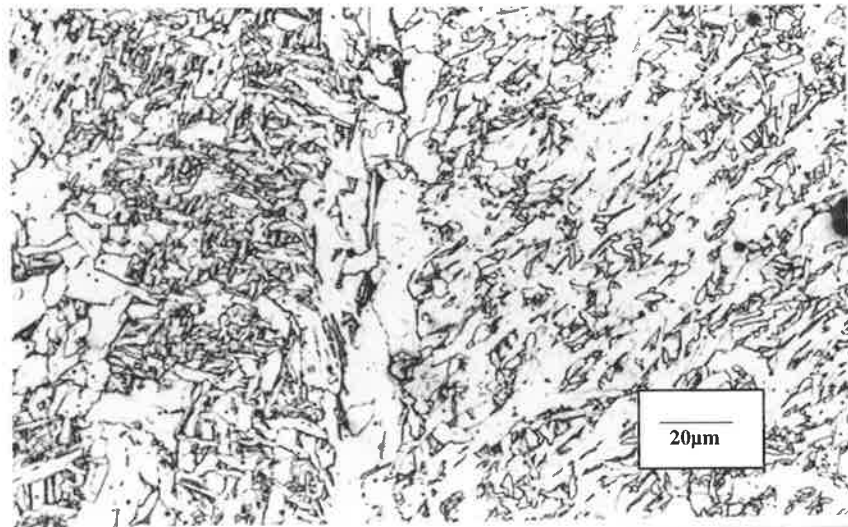
Si	Mn	C	S	P	Ni	Cr	Mo	Cu	V	Nb	Ti	Al	B	O	N
0.60	1.32	0.05	0.013	0.014	0.02	0.01	0.01	0.01	0.01	<0.01	0.0852	0.0147	<0.0005	0.0400	0.0038

Appendix B

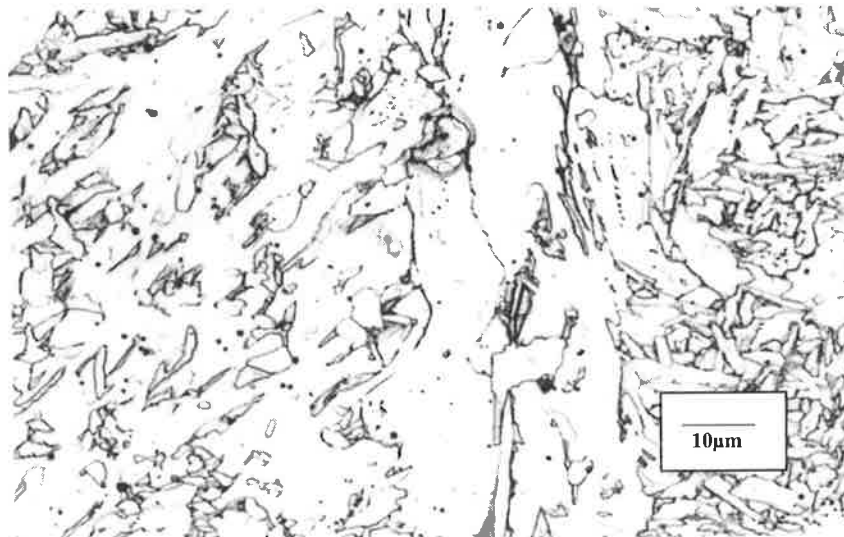
Microstructure photomicrograph



As-Welded x100

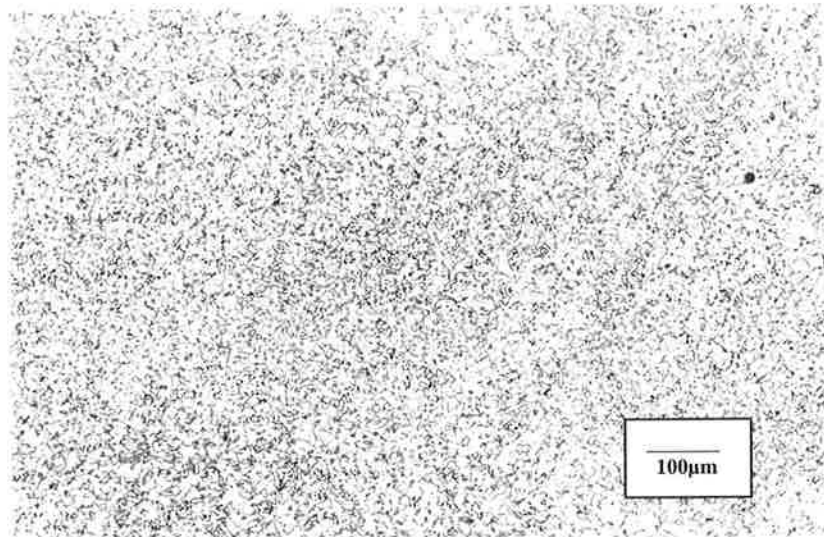


As-Welded x500

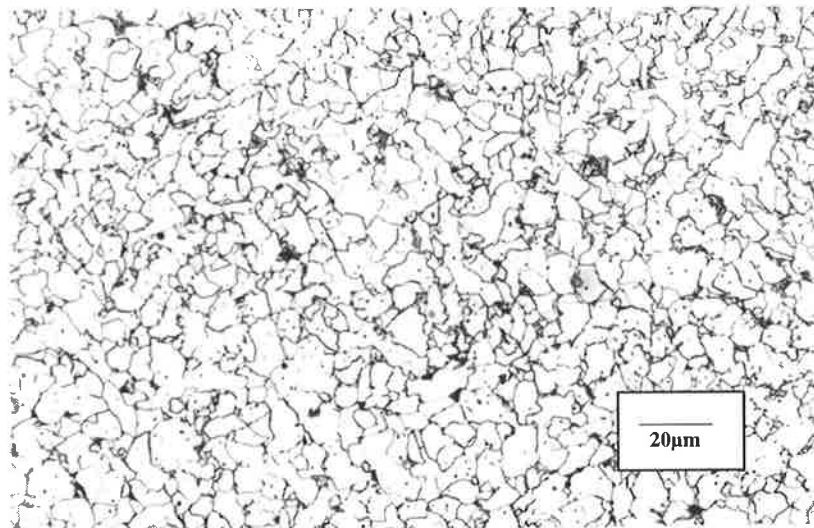


As-Welded x1000

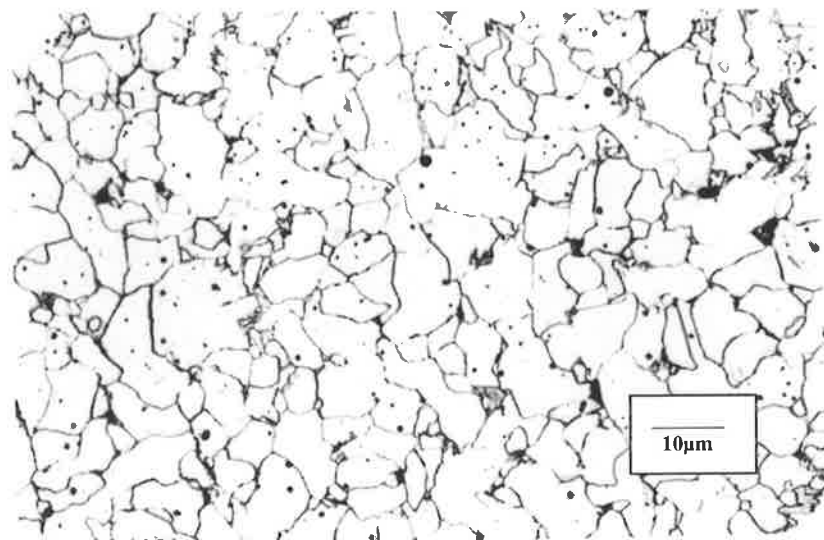
Appendix B



Re-Heated x100



Re-Heated x500



Re-Heated x1000

Appendix B

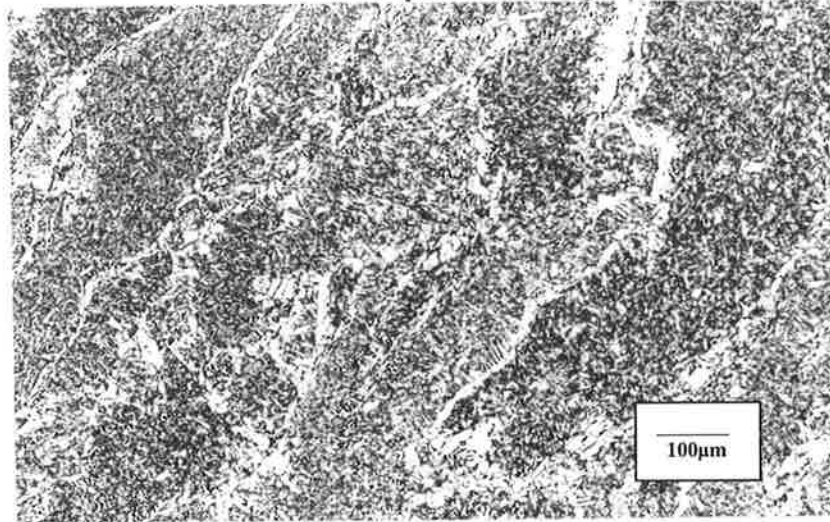
Titanium Series

Composition

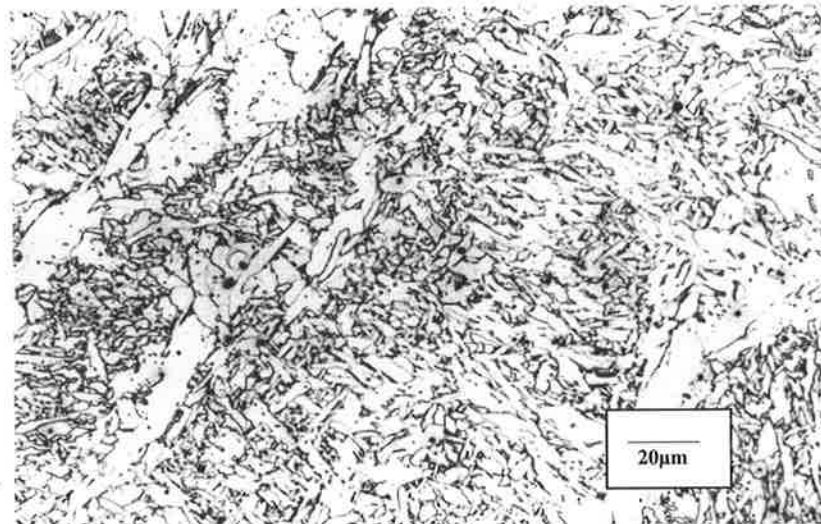
Si	Mn	C	S	P	Ni	Cr	Mo	Cu	V	Nb	Ti	Al	B	O	N
0.63	1.27	0.05	0.012	0.012	0.02	0.01	0.01	0.02	0.01	<0.01	0.0910	0.0164	<0.0005	0.0400	0.0080

Appendix B

Microstructure photomicrograph



As-Welded x100

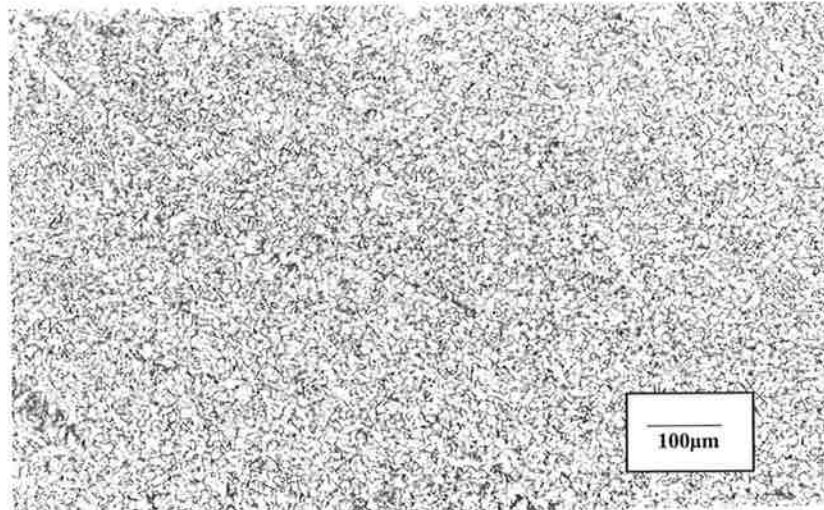


As-Welded x500

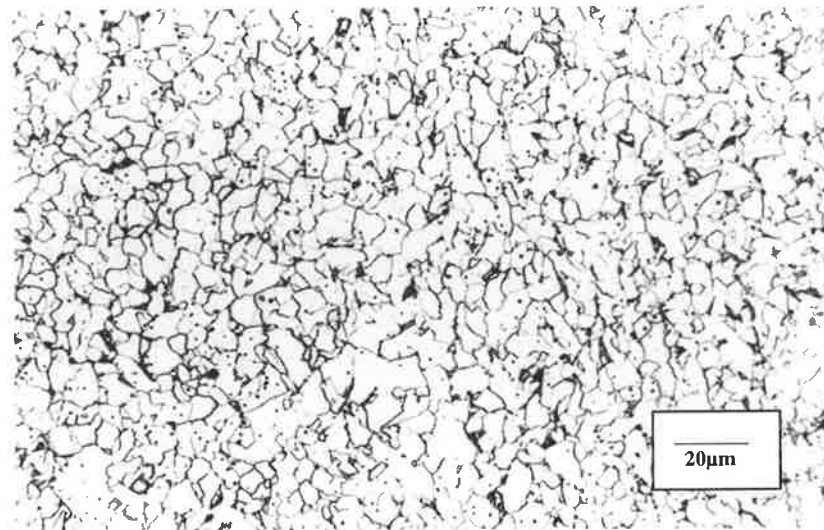


As-Welded x1000

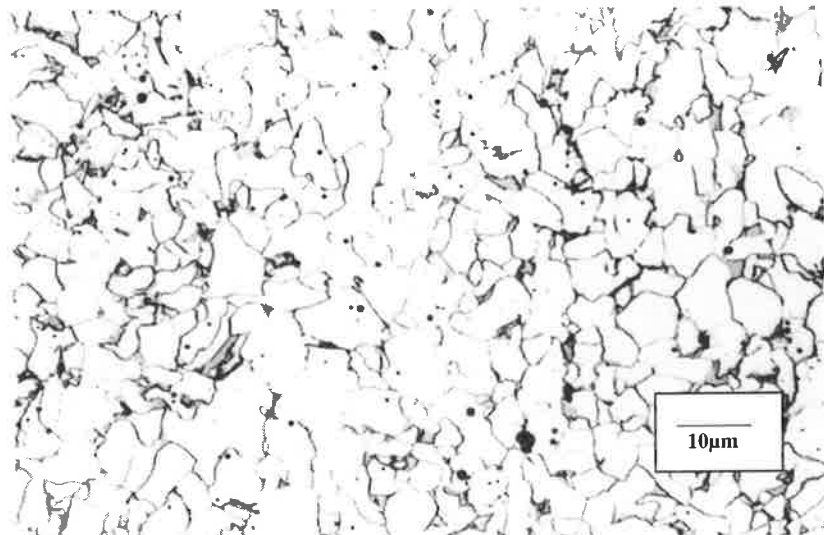
Appendix B



Re-Heated x100



Re-Heated x500



Re-Heated x1000

Appendix B

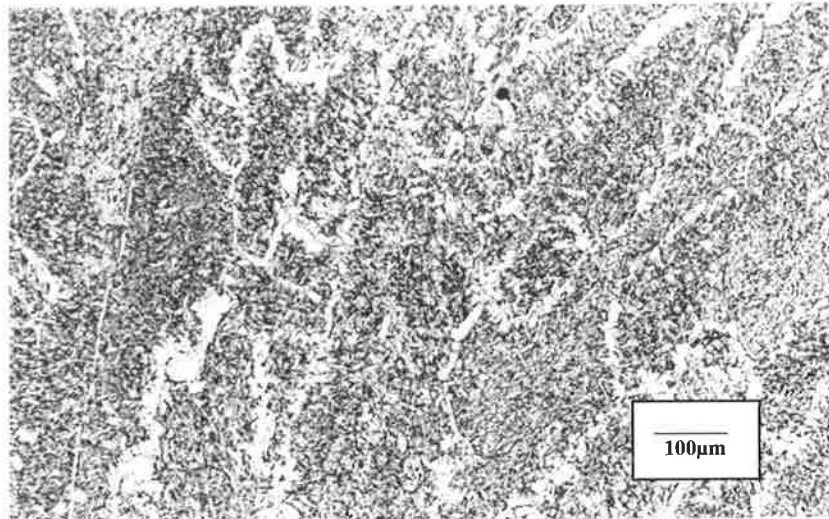
Titanium Series

Composition

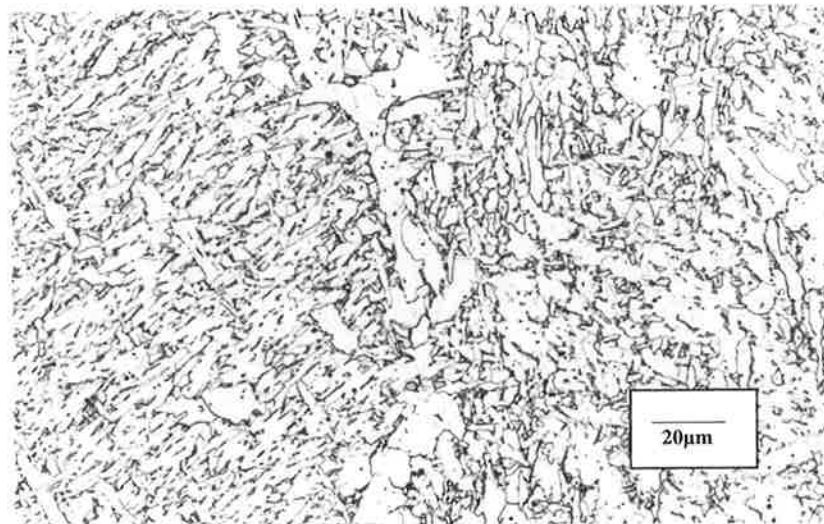
Si	Mn	C	S	P	Ni	Cr	Mo	Cu	V	Nb	Ti	Al	B	O	N
0.63	1.27	0.06	0.011	0.012	0.02	0.01	<0.01	0.02	0.01	<0.01	0.0940	0.0132	<0.0005	0.0430	0.0130

Appendix B

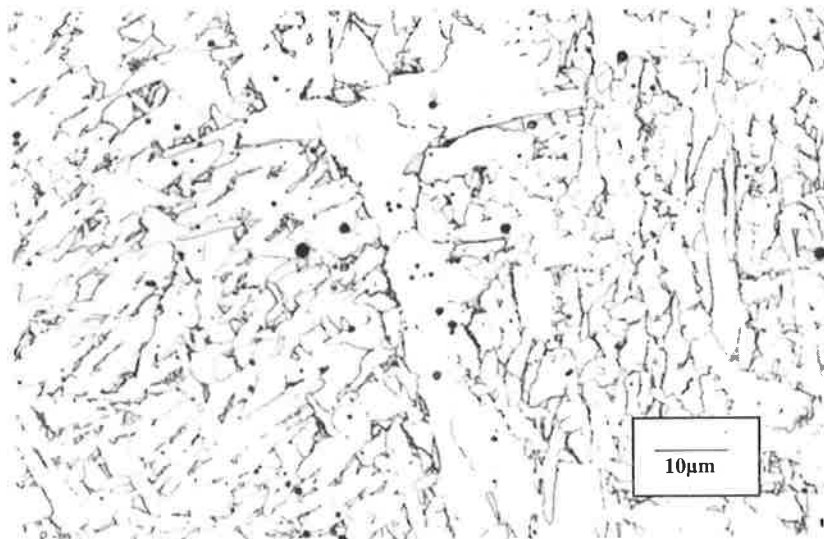
Microstructure photomicrograph



As-Welded x100

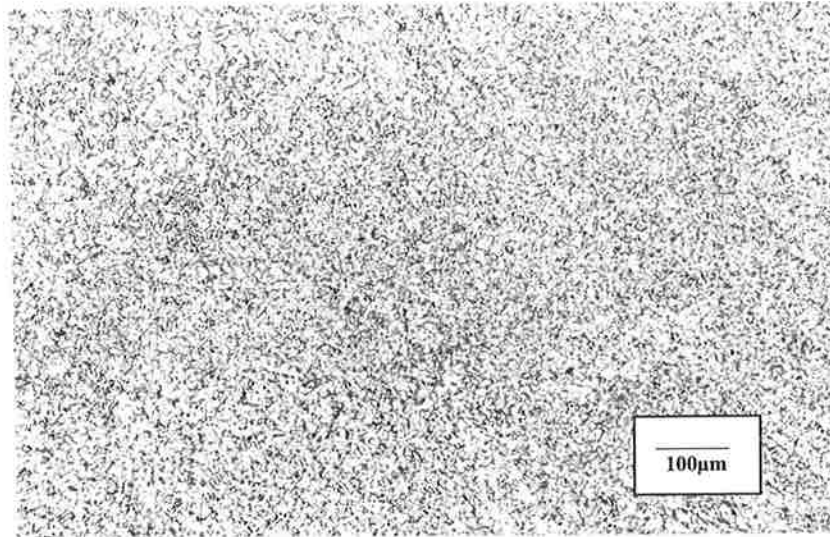


As-Welded x500

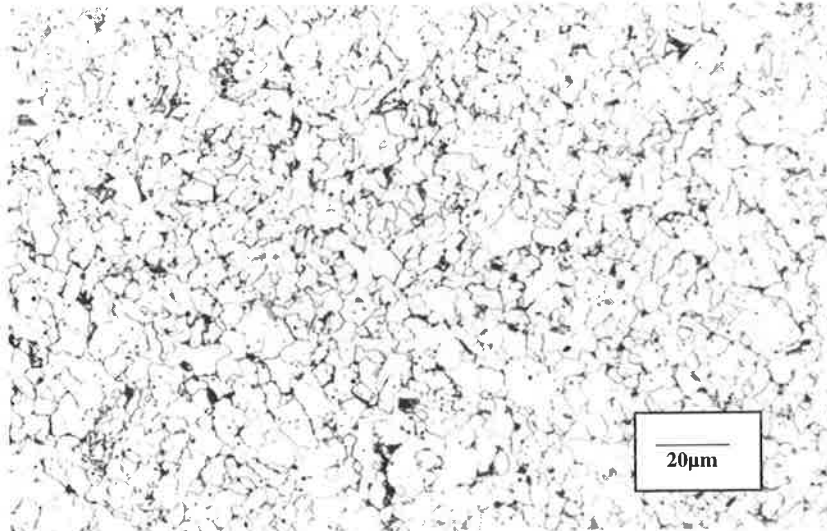


As-Welded x1000

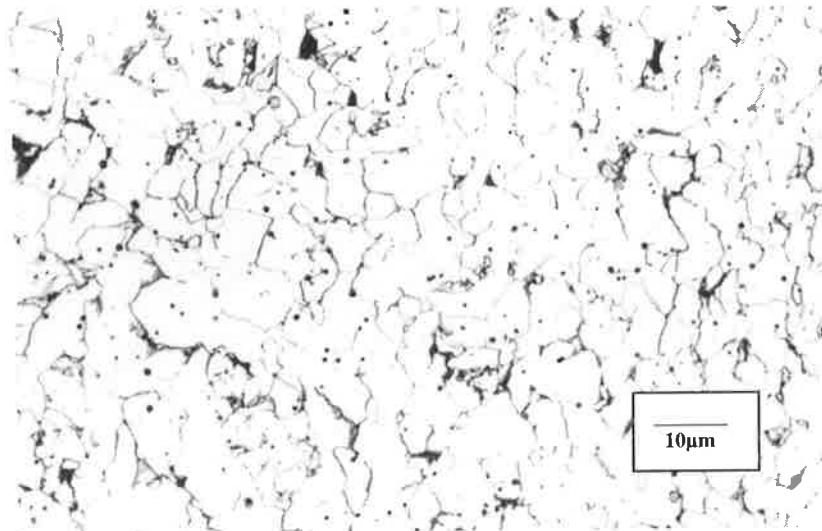
Appendix B



Re-Heated x100



Re-Heated x500



Re-Heated x1000

Appendix C Aluminium Series

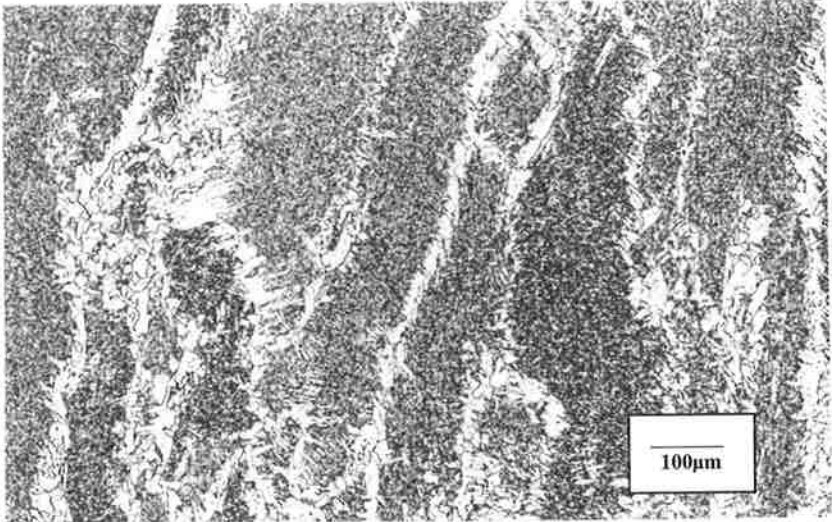
Aluminium Series

Composition

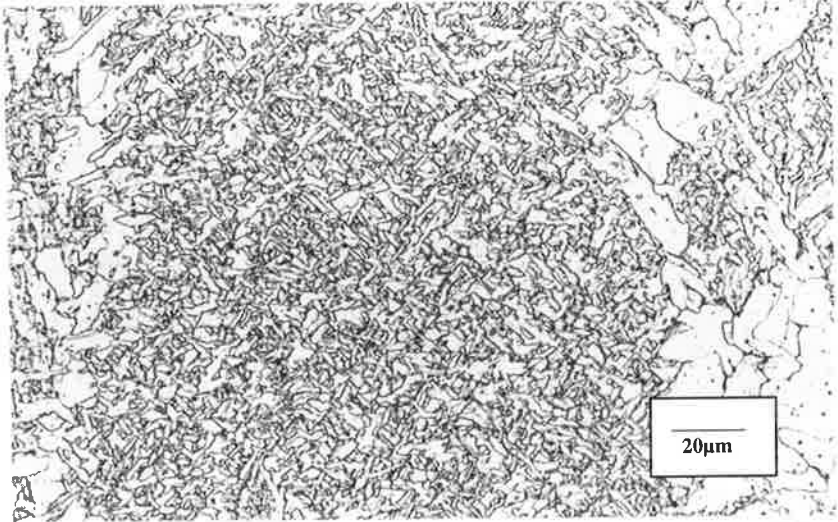
Si	Mn	C	S	P	Ni	Cr	Mo	Cu	V	Nb	Ti	Al	B	O	N
0.64	1.34	0.04	0.012	0.014	0.02	0.01	<0.01	0.01	0.0058	0.0005	0.0054	0.0133	<0.0005	0.0530	0.0047

Appendix C

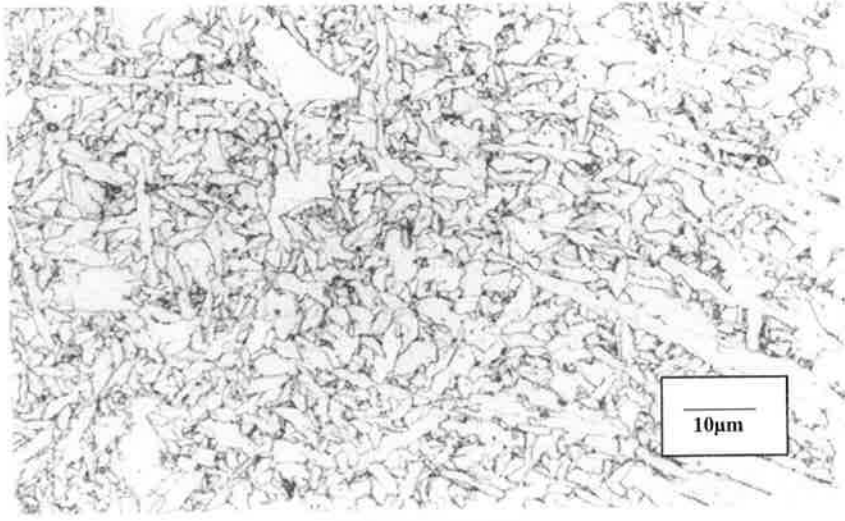
Microstructure photomicrograph



As-Welded x100

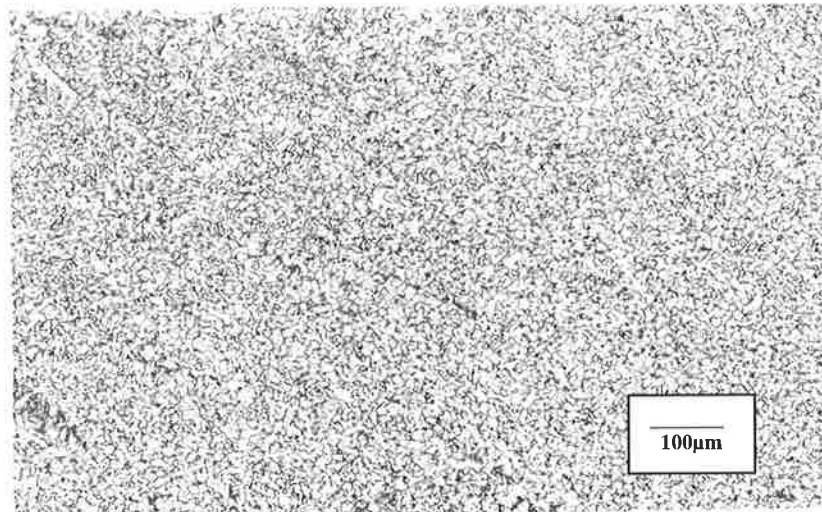


As-Welded x500

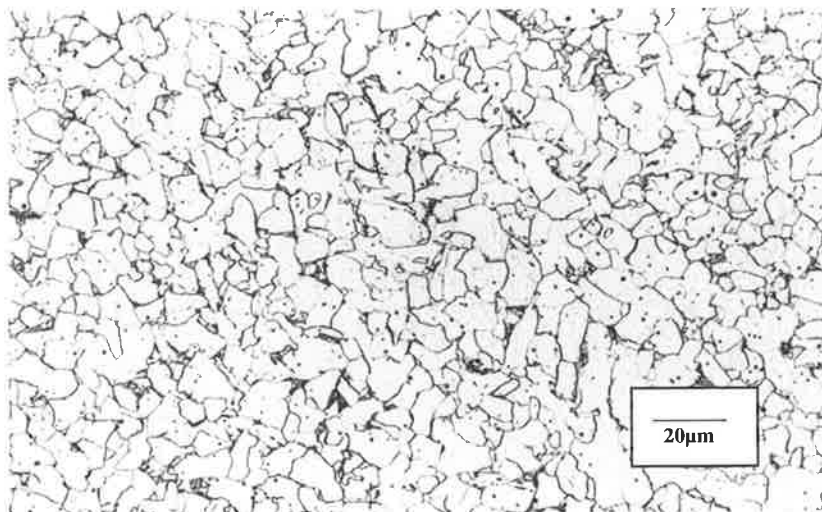


As-Welded x1000

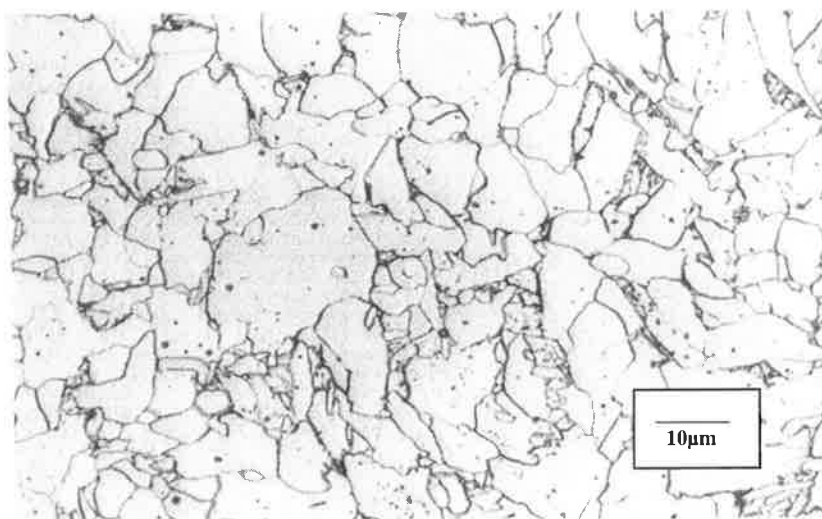
Appendix C



Re-Heated x100



Re-Heated x500



Re-Heated x1000

Appendix C

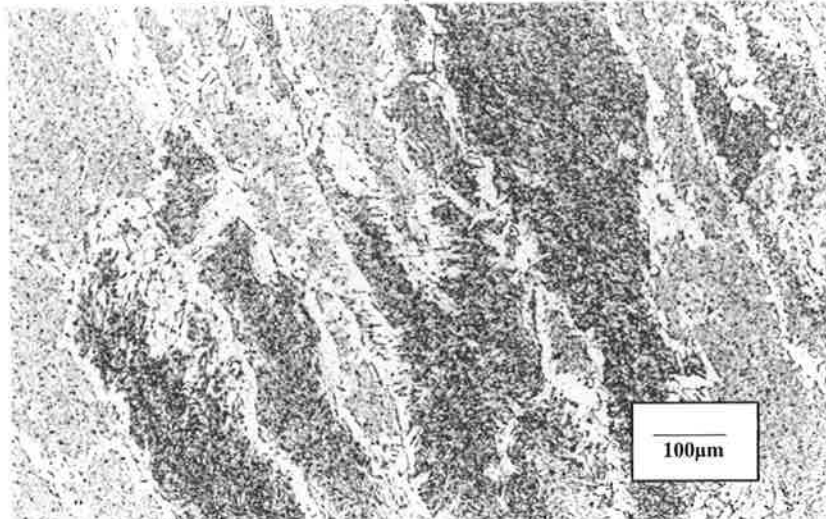
Aluminium Series

Composition

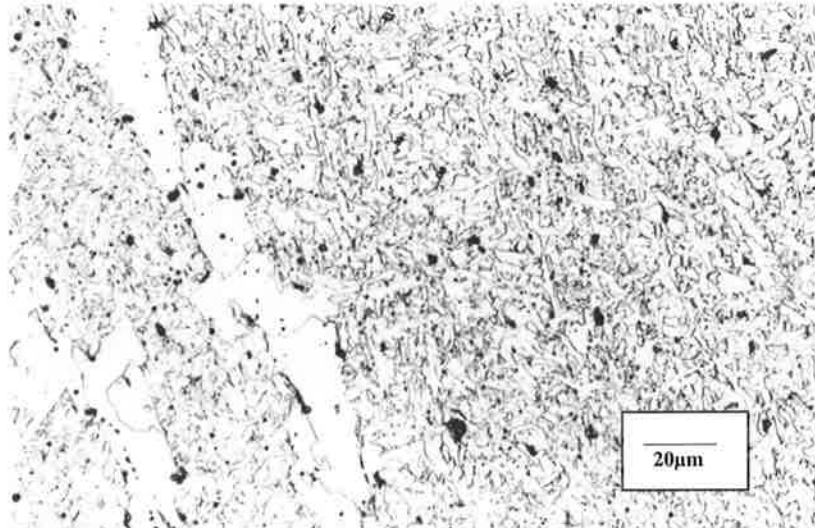
Si	Mn	C	S	P	Ni	Cr	Mo	Cu	V	Nb	Ti	Al	B	O	N
0.61	1.32	0.06	0.024	0.015	0.05	0.03	0.02	0.01	0.0055	<0.01	0.0060	0.0190	<0.0005	0.0580	0.0048

Appendix C

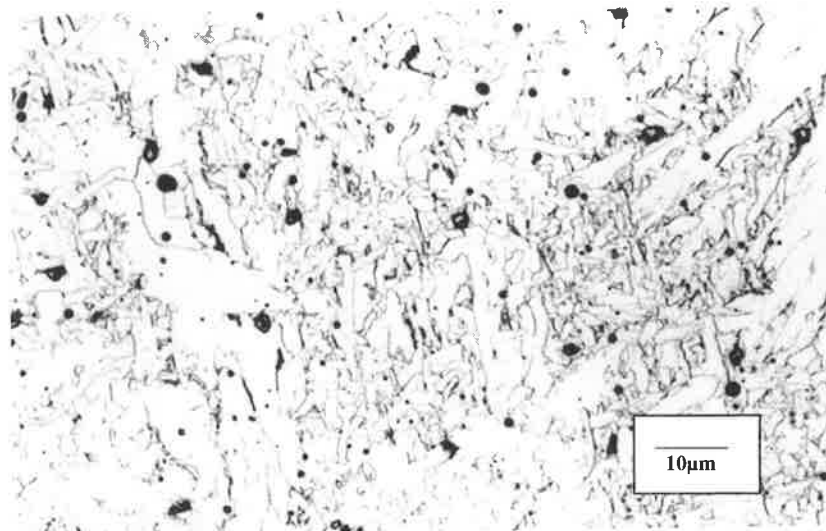
Microstructure photomicrograph



As-Welded x100

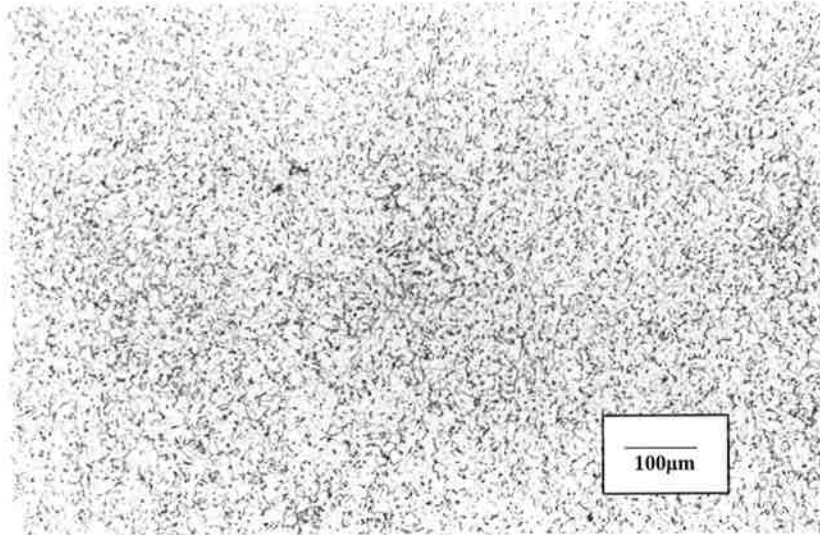


As-Welded x500

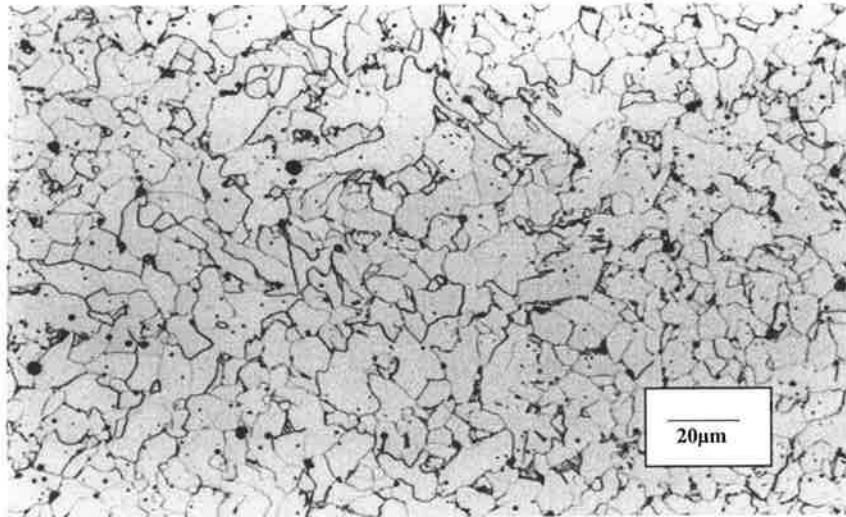


As-Welded x1000

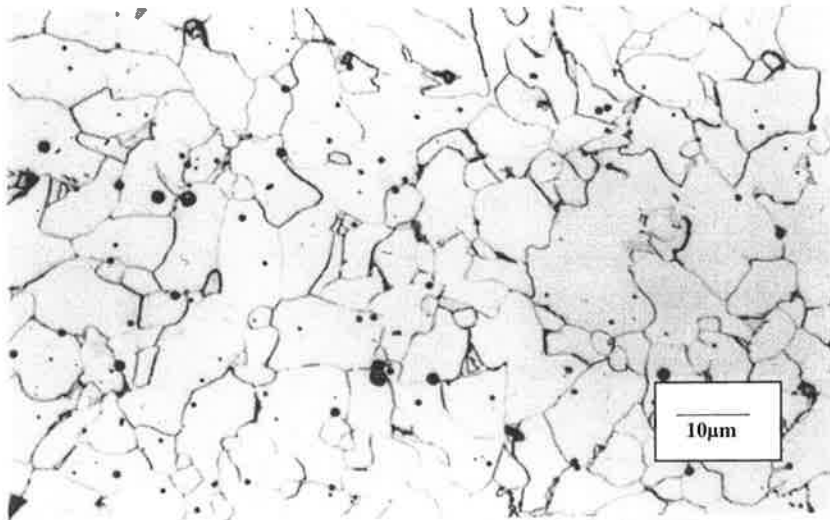
Appendix C



Re-Heated x100



Re-Heated x500



Re-Heated x1000

Appendix C

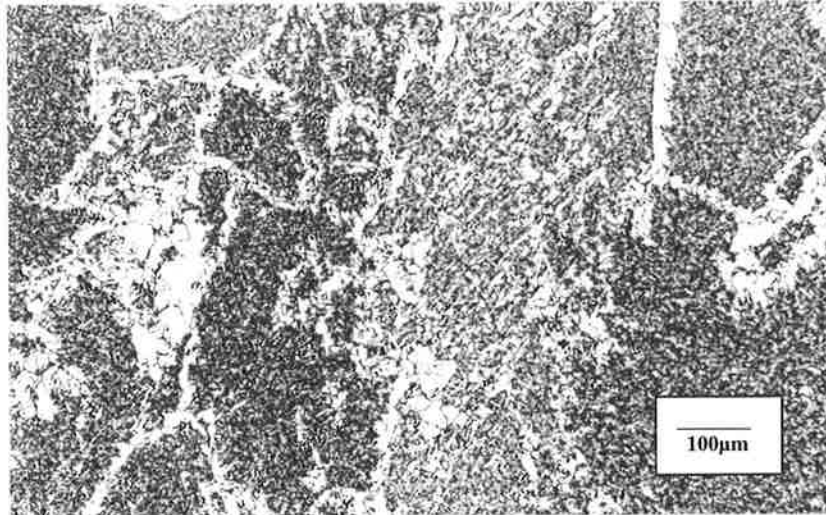
Aluminium Series

Composition

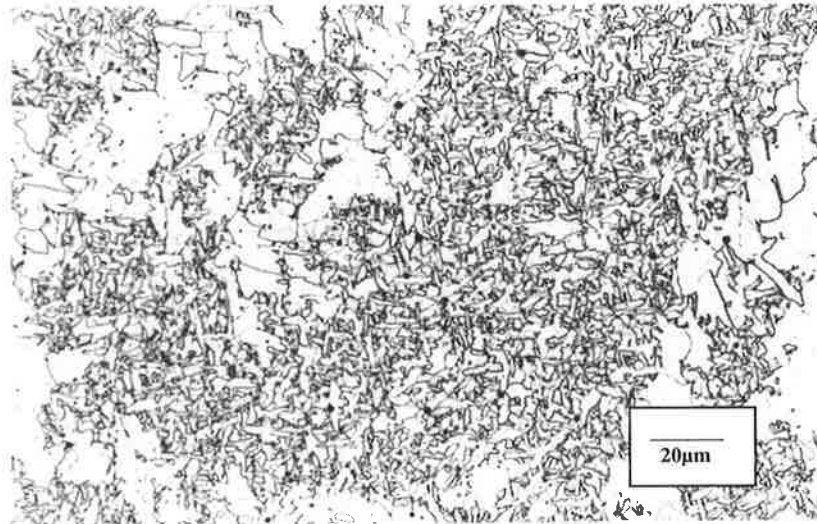
Si	<u>Mn</u>	<u>C</u>	<u>S</u>	<u>P</u>	<u>Ni</u>	<u>Cr</u>	<u>Mo</u>	<u>Cu</u>	<u>V</u>	<u>Nb</u>	<u>Ti</u>	<u>Al</u>	<u>B</u>	<u>O</u>	<u>N</u>
0.60	1.29	0.05	0.020	0.017	0.05	0.03	0.03	0.01	0.0057	<0.01	0.0049	0.0320	<0.0005	0.0650	0.0065

Appendix C

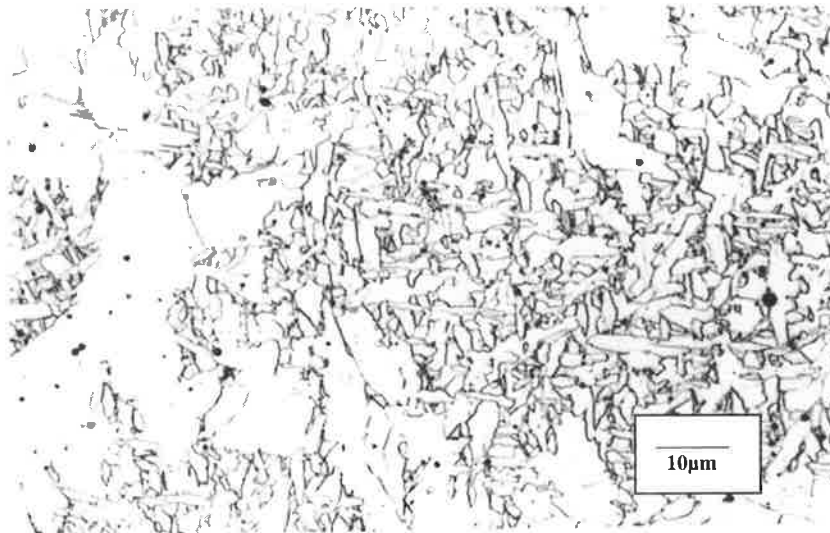
Microstructure photomicrograph



As-Welded x100

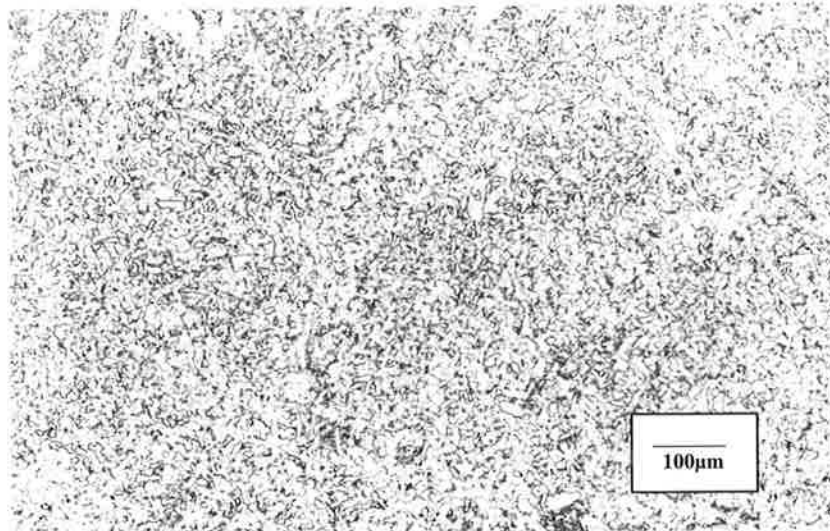


As-Welded x500

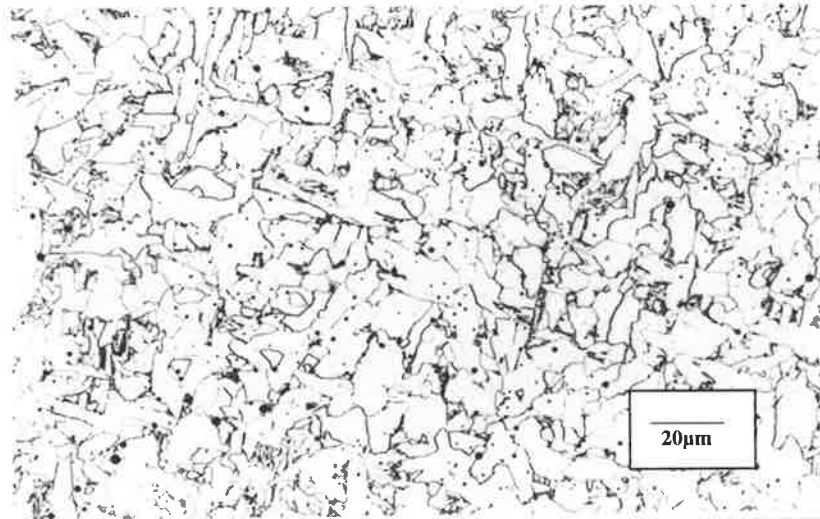


As-Welded x1000

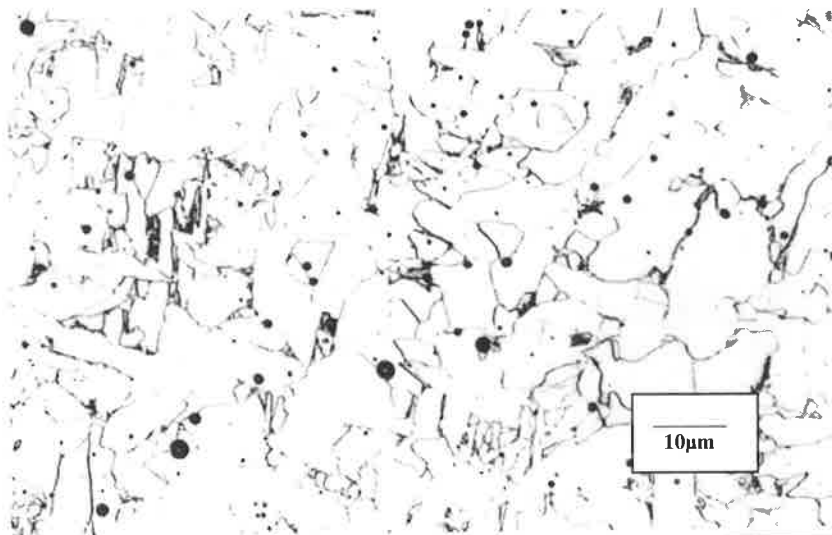
Appendix C



Re-Heated x100



Re-Heated x500



Re-Heated x1000

Appendix C

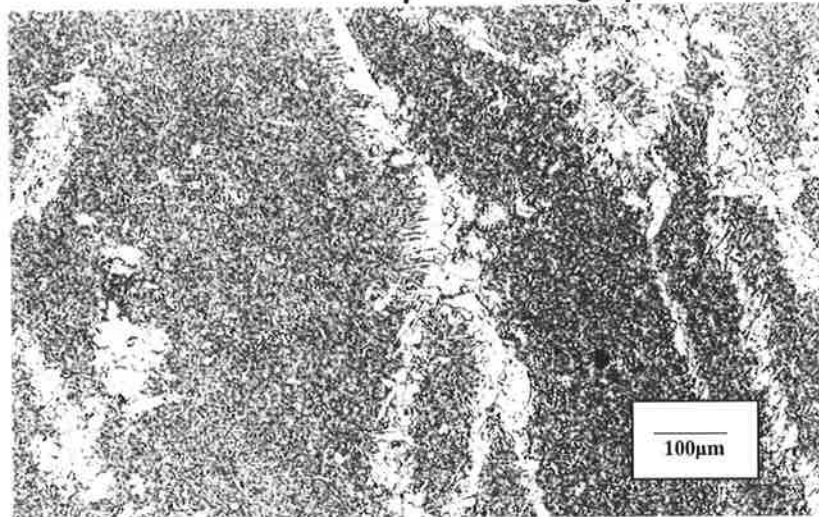
Aluminium Series

Composition

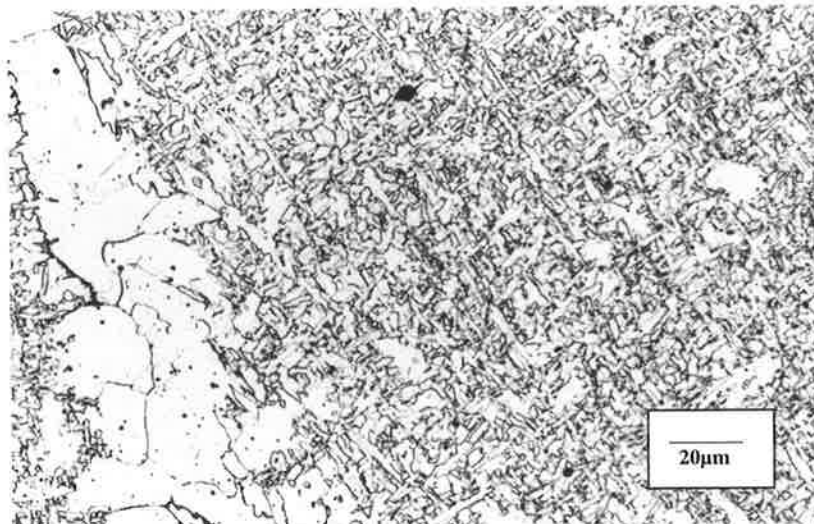
Si	Mn	C	S	P	Ni	Cr	Mo	Cu	V	Nb	Ti	Al	B	O	N
0.77	1.38	0.05	0.020	0.018	0.05	0.03	0.02	0.01	0.0067	<0.01	0.0058	0.0495	<0.0005	0.0530	0.0054

Appendix C

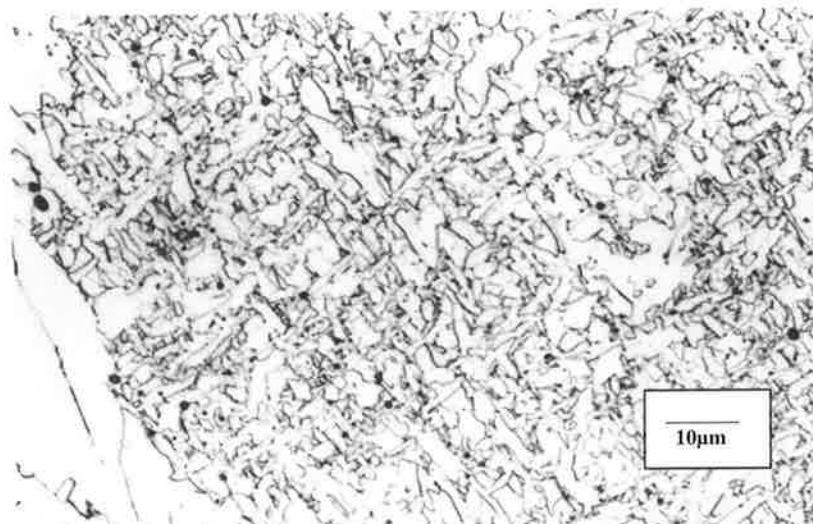
Microstructure photomicrograph



As-Welded x100

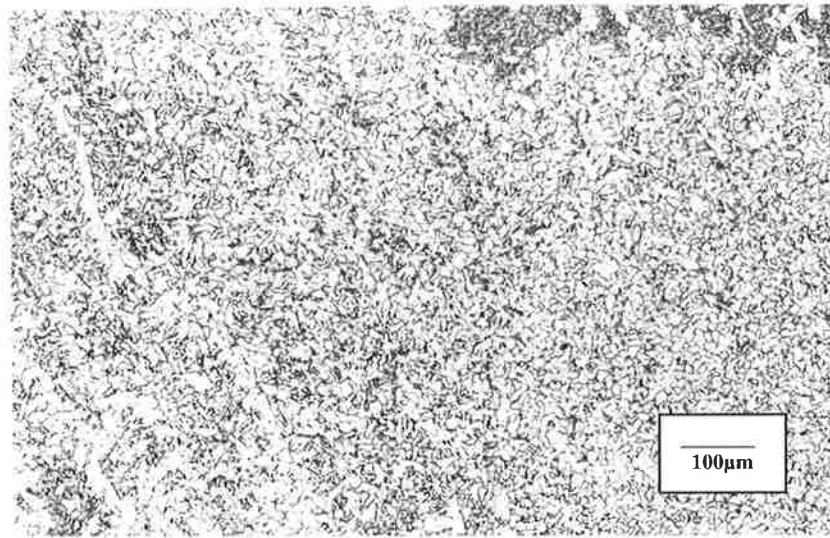


As-Welded x500

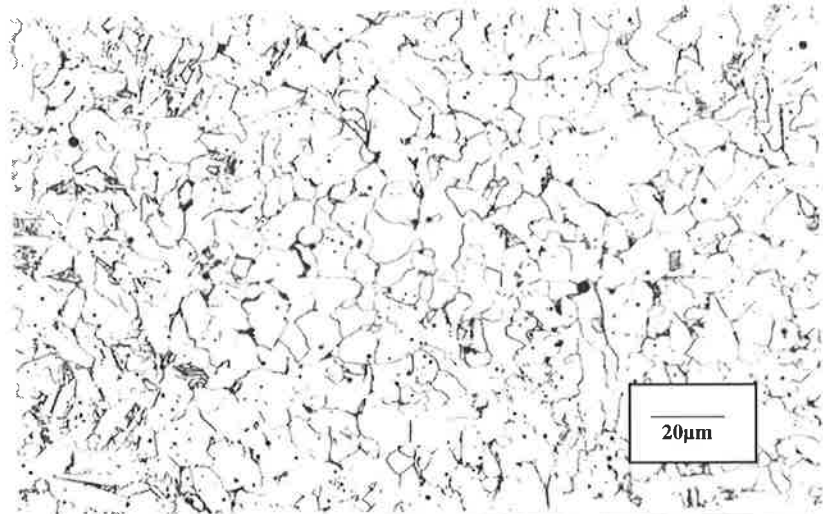


As-Welded x1000

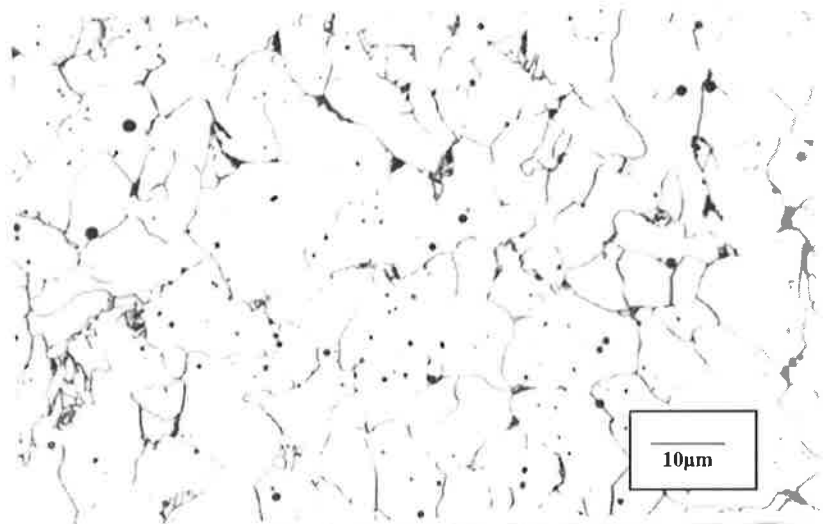
Appendix C



Re-Heated x100



Re-Heated x500



Re-Heated x1000

Appendix C

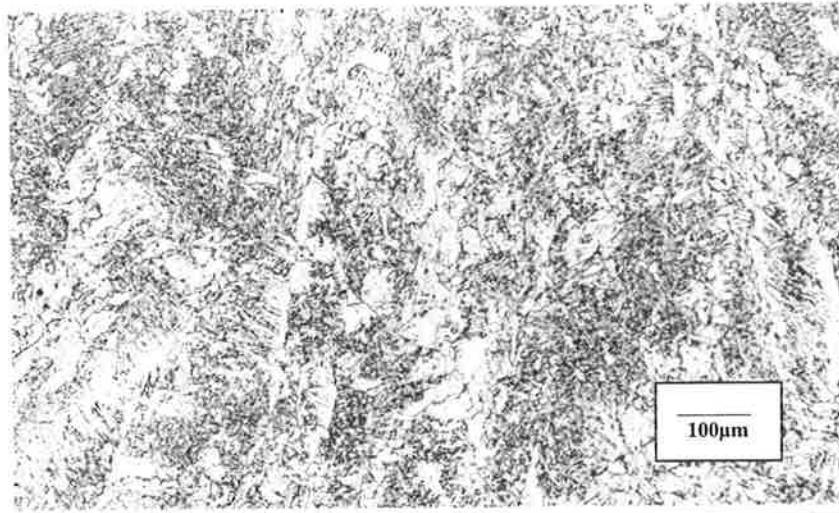
Aluminium Series

Composition

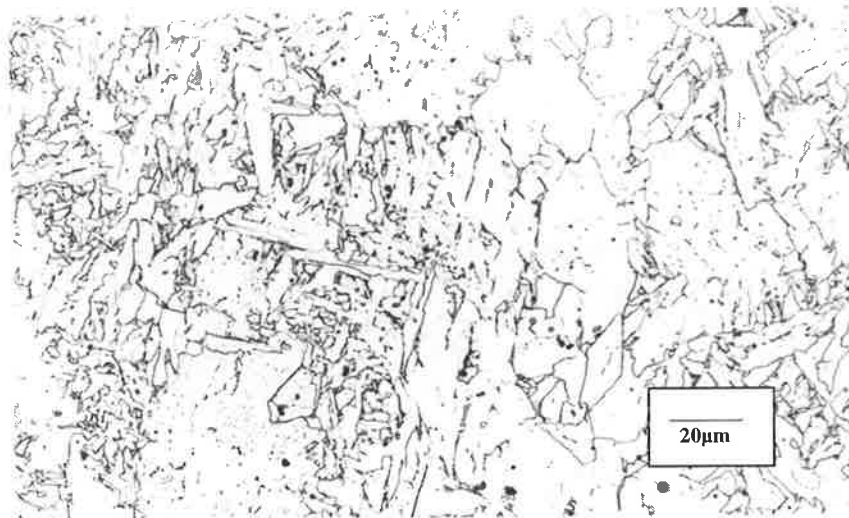
Si	<u>Mn</u>	<u>C</u>	<u>S</u>	<u>P</u>	<u>Ni</u>	<u>Cr</u>	<u>Mo</u>	<u>Cu</u>	<u>V</u>	<u>Nb</u>	<u>Ti</u>	<u>Al</u>	<u>B</u>	<u>O</u>	<u>N</u>
0.52	1.15	0.06	0.016	0.018	0.05	0.03	0.02	0.01	0.0053	<0.01	0.0050	0.0570	<0.0005	0.0580	0.0045

Appendix C

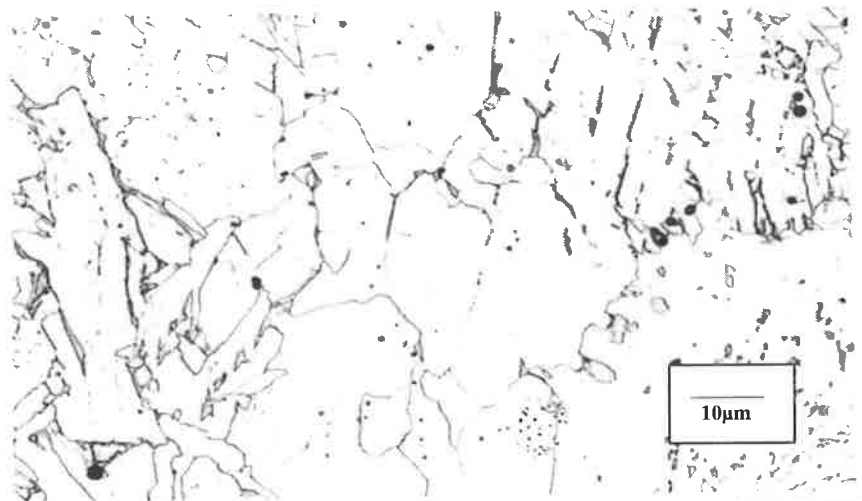
Microstructure photomicrograph



As-Welded x100

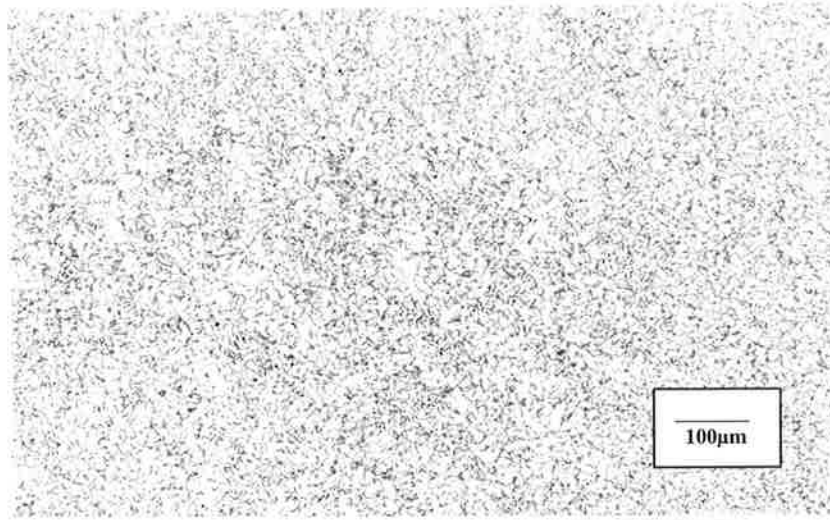


As-Welded x500

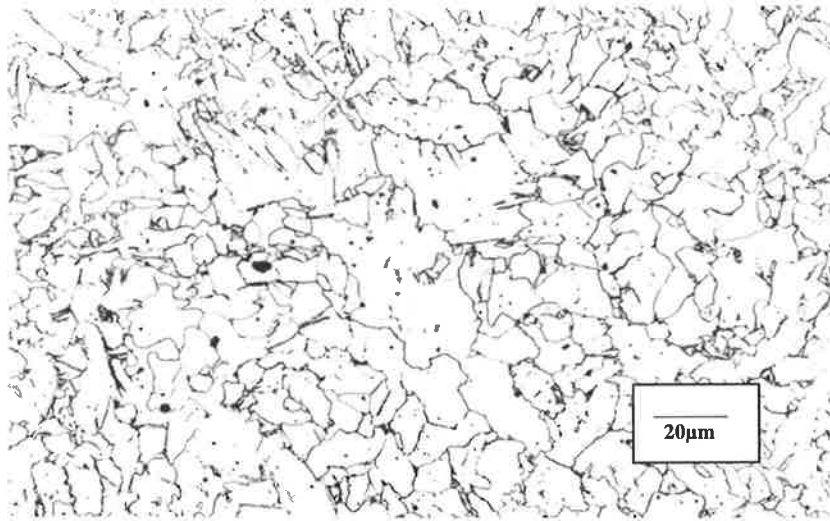


As-Welded x1000

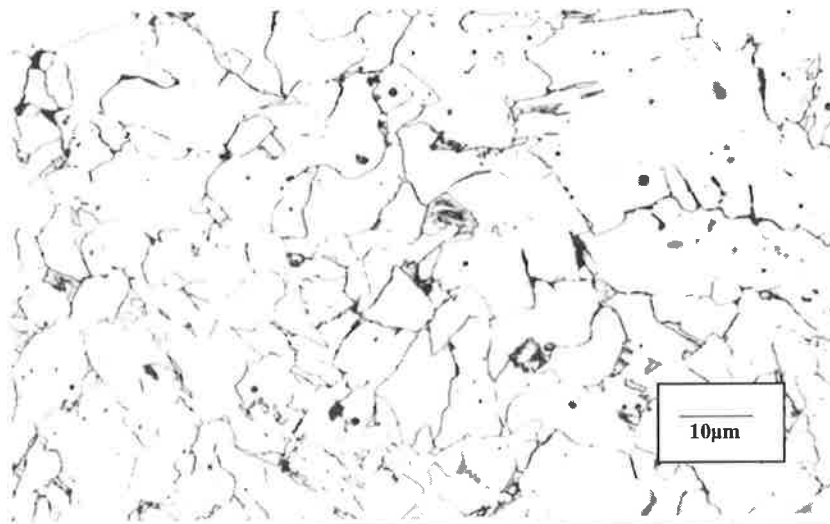
Appendix C



Re-Heated x100



Re-Heated x500



Re-Heated x1000

Appendix C

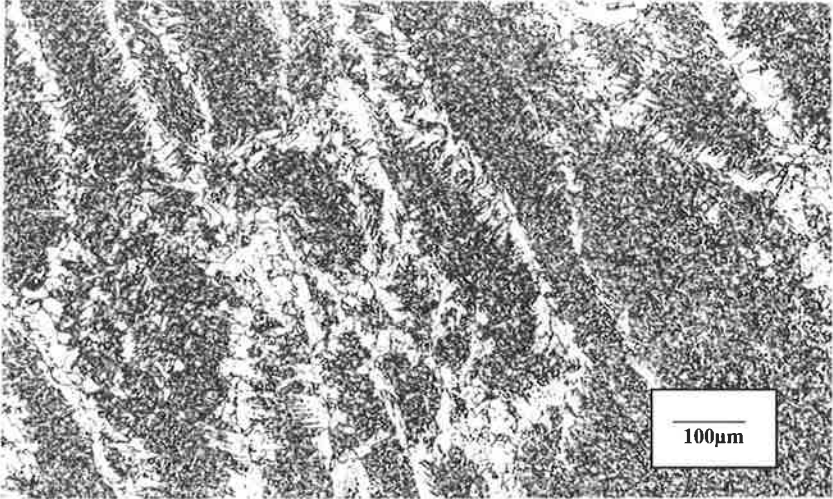
Aluminium Series

Composition

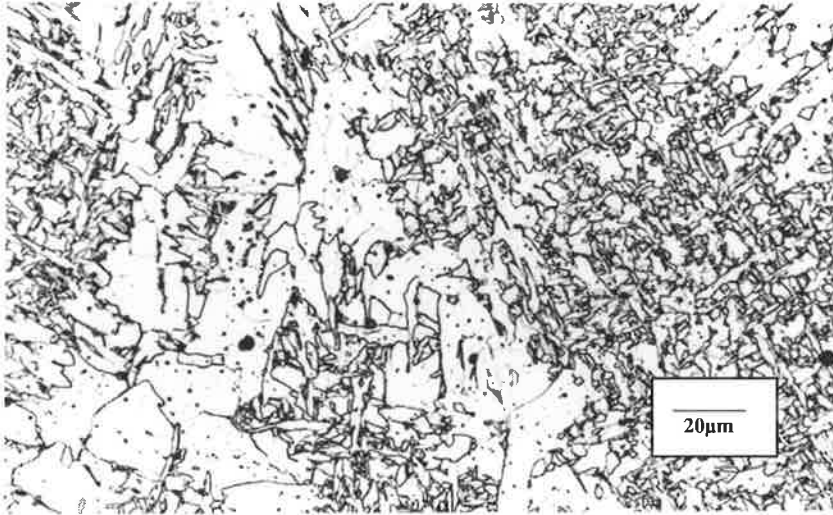
Si	Mn	C	S	P	Ni	Cr	Mo	Cu	V	Nb	Ti	Al	B	O	N
0.68	1.35	0.05	0.013	0.018	0.05	0.03	0.01	0.01	0.0065	<0.01	0.0058	0.0642	<0.0005	0.0580	0.0068

Appendix C

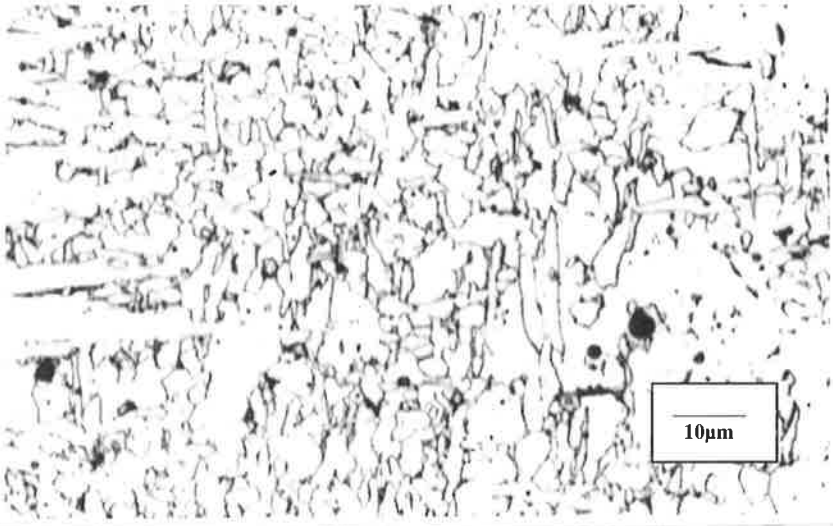
Microstructure photomicrograph



As-Welded x100

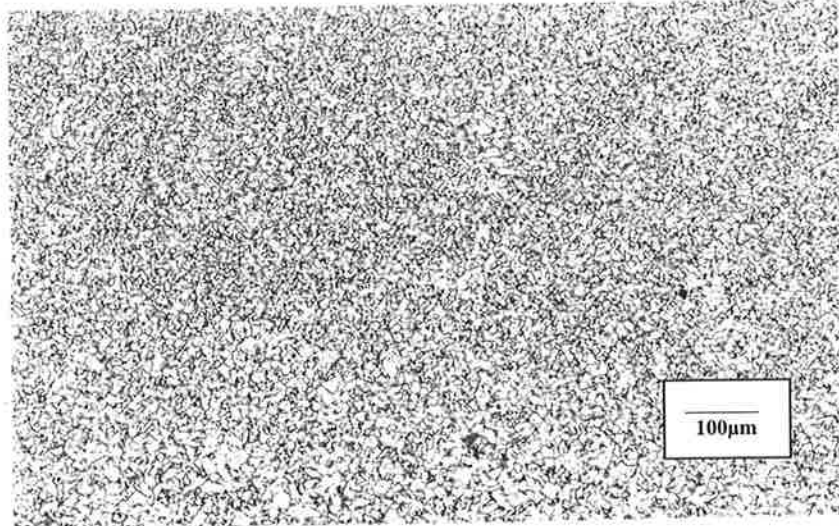


As-Welded x500

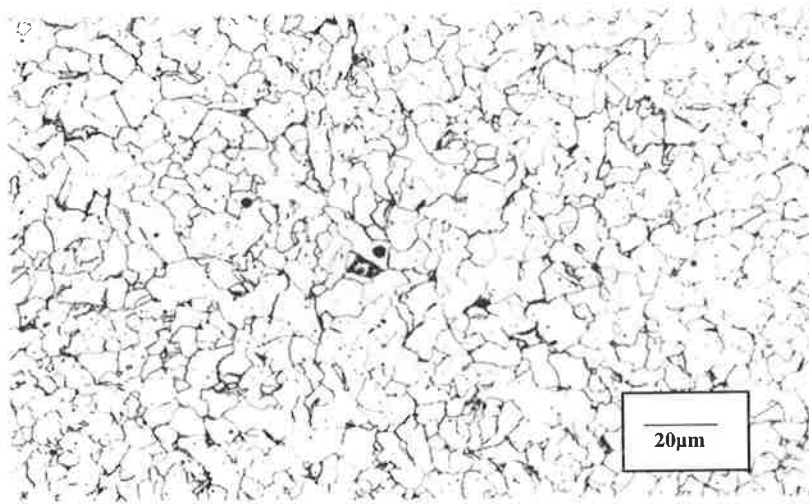


Appendix C

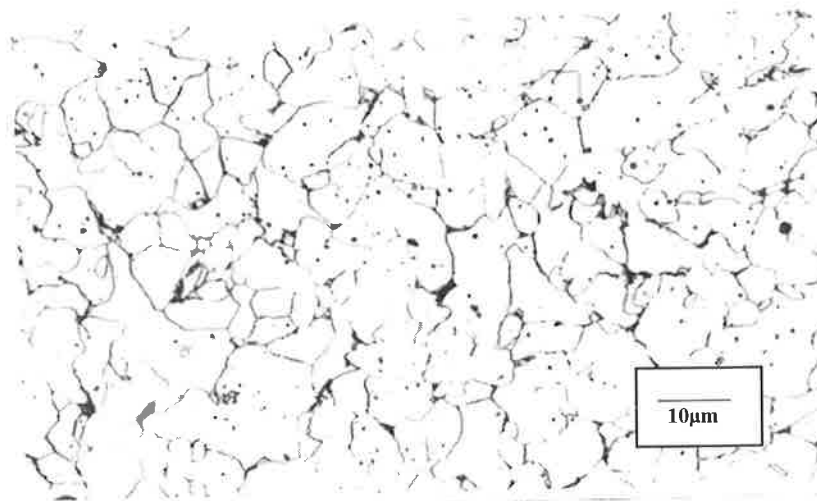
As-Welded x1000



Re-Heated x100



Re-Heated x500



Re-Heated x1000

Appendix D Boron Series

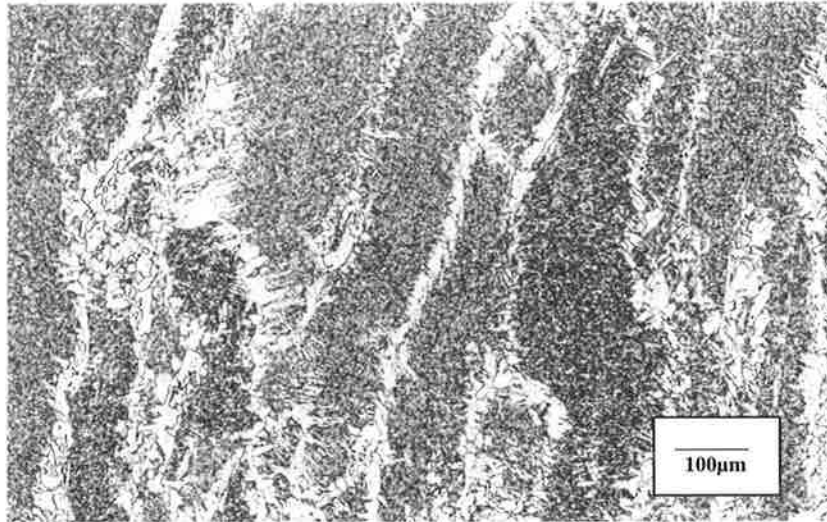
Boron Series

Composition

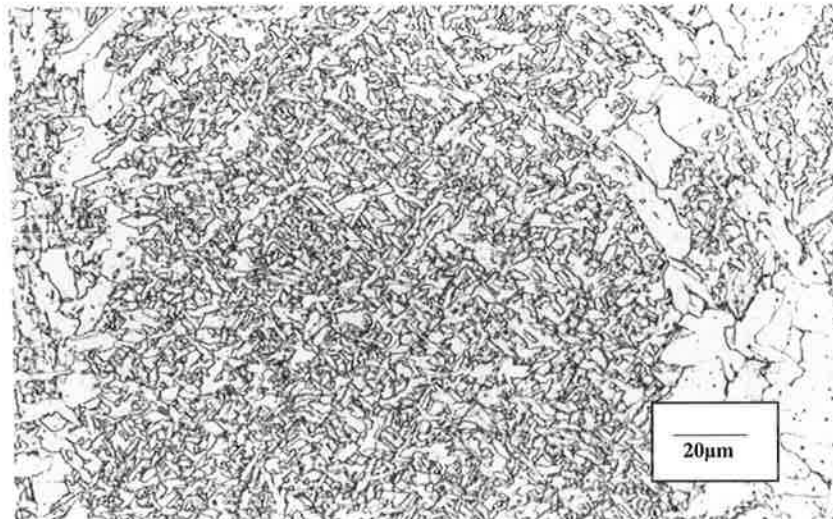
Si	<u>Mn</u>	<u>C</u>	<u>S</u>	<u>P</u>	<u>Ni</u>	<u>Cr</u>	<u>Mo</u>	<u>Cu</u>	<u>V</u>	<u>Nb</u>	<u>Ti</u>	<u>Al</u>	<u>B</u>	<u>O</u>	<u>N</u>
0.64	1.34	0.04	0.012	0.014	0.02	0.01	<0.01	0.01	0.0058	0.0005	0.0054	0.0133	<0.0005	0.0530	0.0047

Appendix D

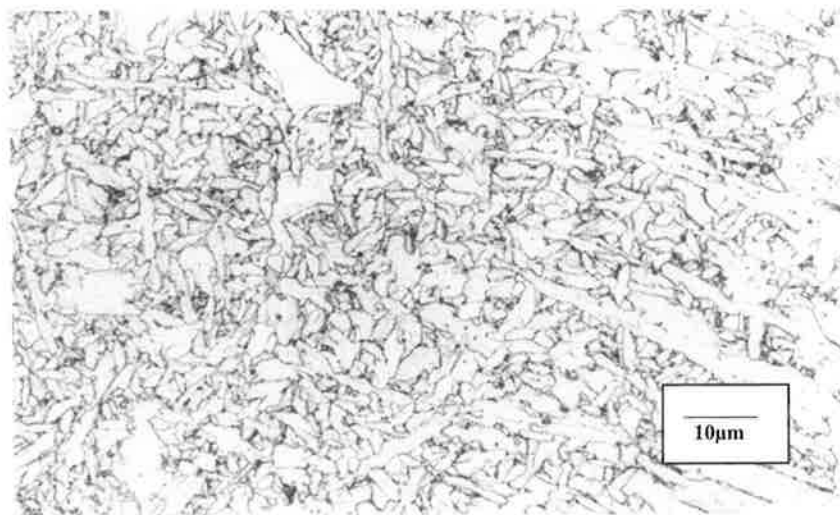
Microstructure photomicrograph



As-Welded x100

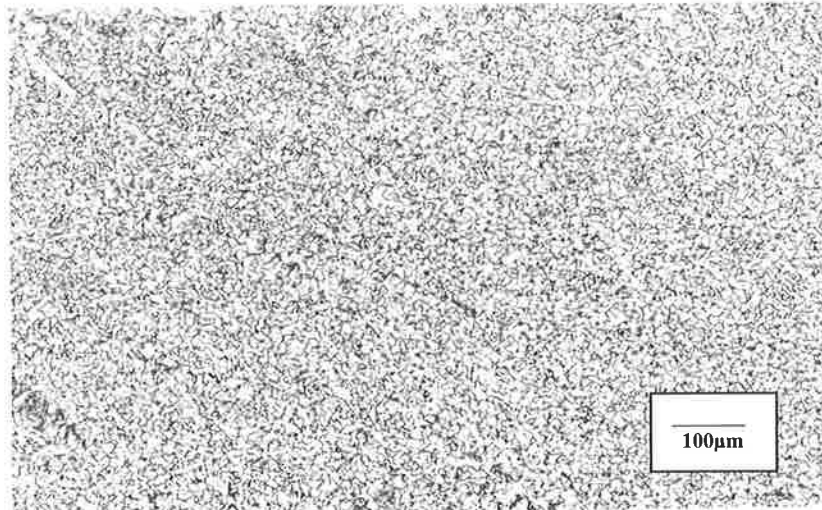


As-Welded x500

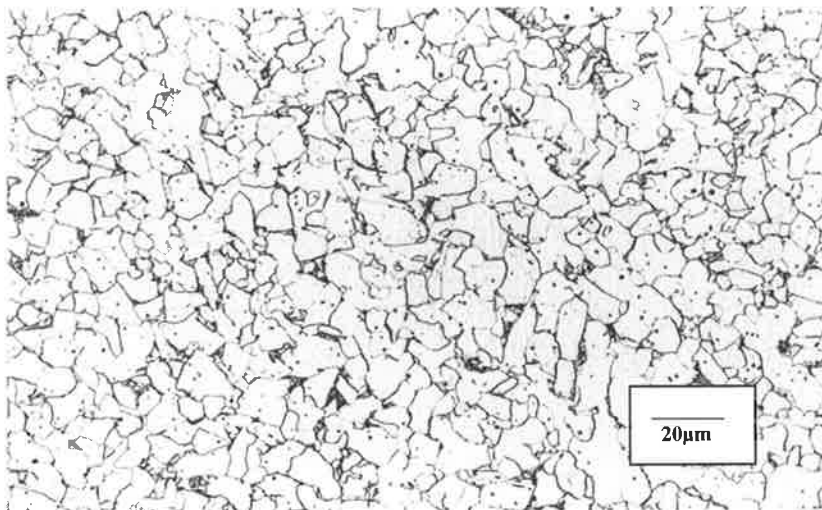


As-Welded x1000

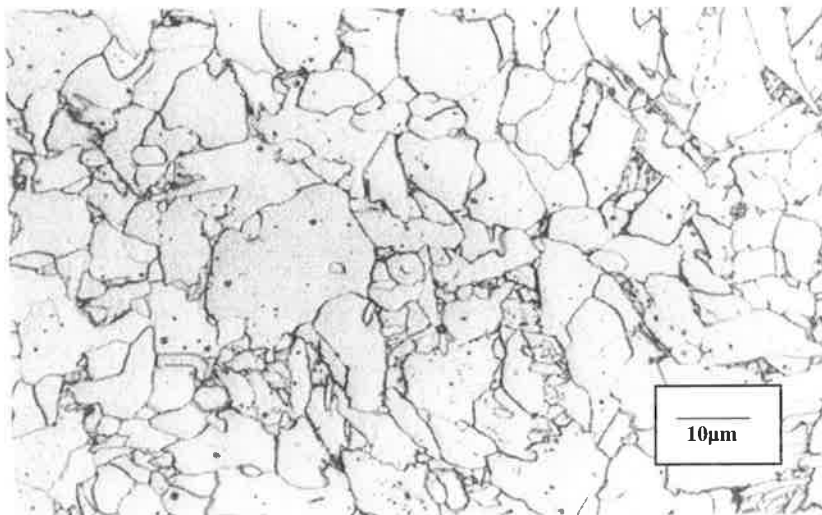
Appendix D



Re-Heated x100



Re-Heated x500



Re-Heated x1000

Appendix D

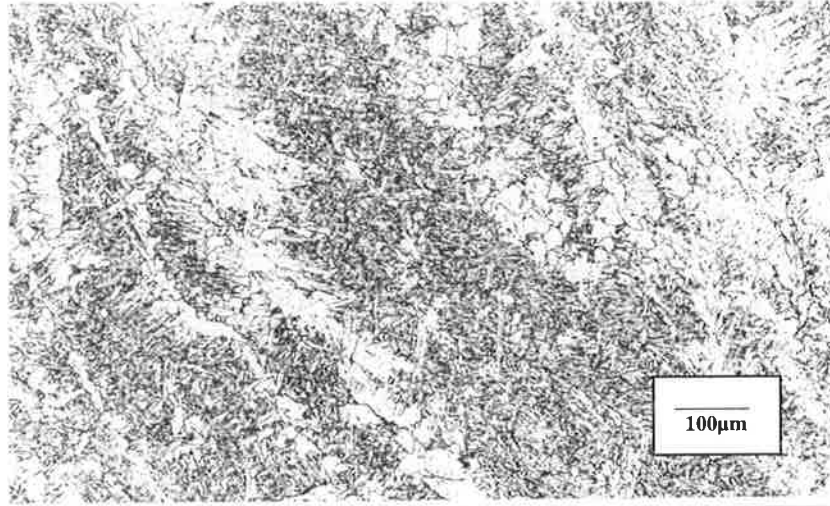
Boron Series

Composition

Si	<u>Mn</u>	<u>C</u>	<u>S</u>	<u>P</u>	<u>Ni</u>	<u>Cr</u>	<u>Mo</u>	<u>Cu</u>	<u>V</u>	<u>Nb</u>	<u>Ti</u>	<u>Al</u>	<u>B</u>	<u>O</u>	<u>N</u>
0.46	1.13	0.06	0.012	0.011	0.03	0.01	<0.01	0.21	<0.01	<0.01	0.0058	0.0149	0.0050	0.0530	0.0073

Appendix D

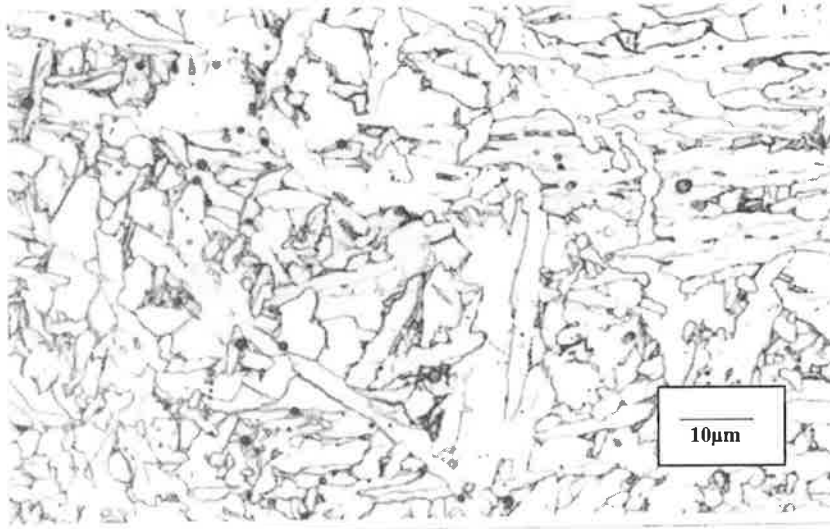
Microstructure photomicrograph



As-Welded x100

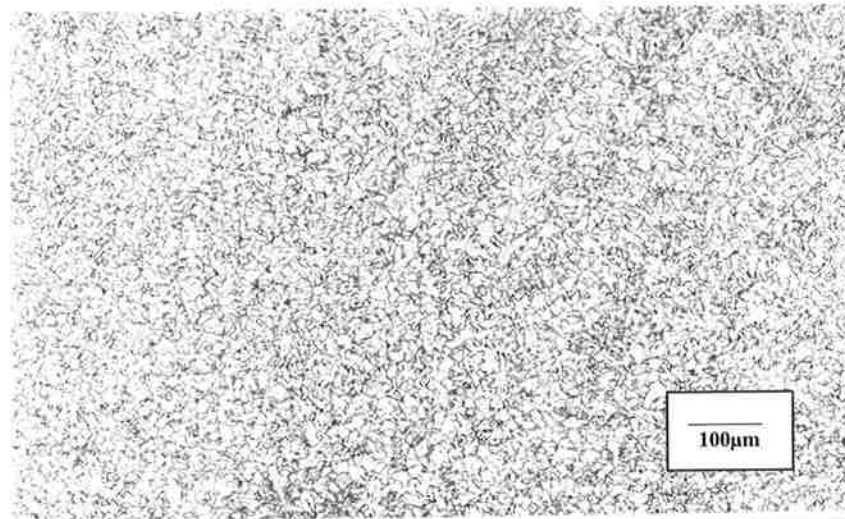


As-Welded x500

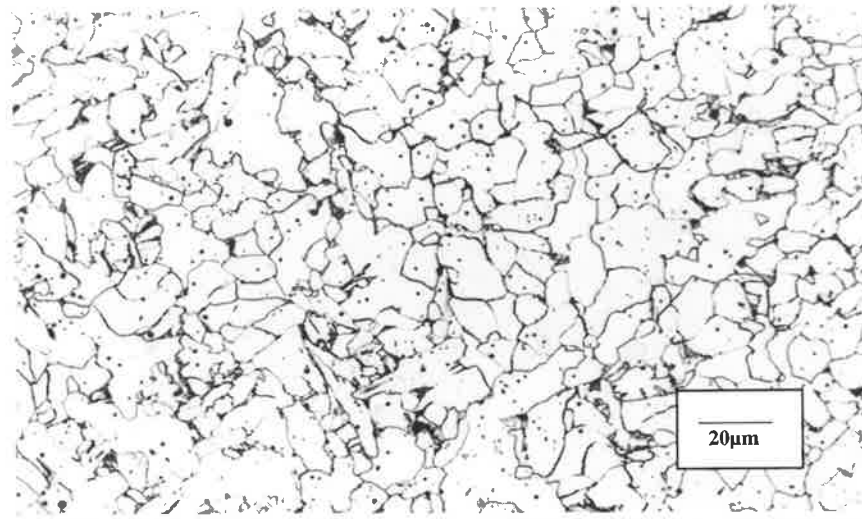


As-Welded x1000

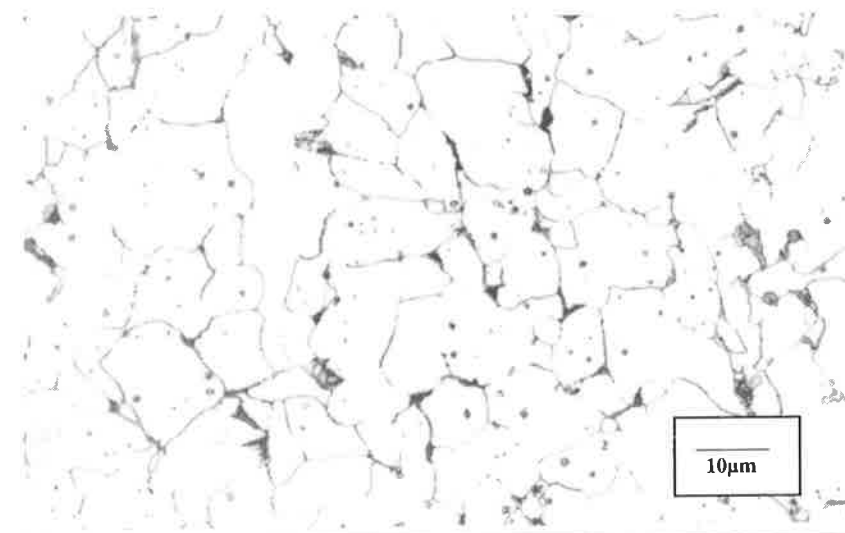
Appendix D



Re-Heated x100



Re-Heated x500



Re-Heated x1000

Appendix D

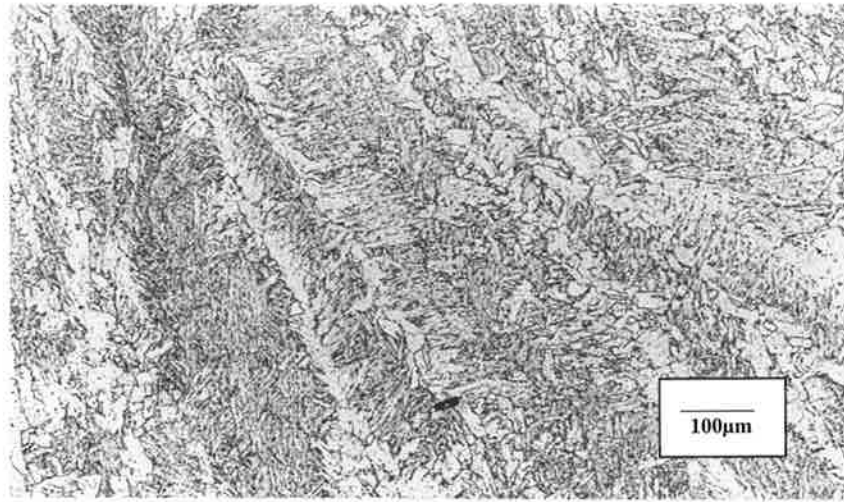
Boron Series

Composition

Si	Mn	C	S	P	Ni	Cr	Mo	Cu	V	Nb	Ti	Al	B	O	N
0.63	1.35	0.05	0.011	0.011	0.02	0.01	<0.01	<0.01	<0.01	<0.01	0.0057	0.0153	0.0088	0.0540	0.0067

Appendix D

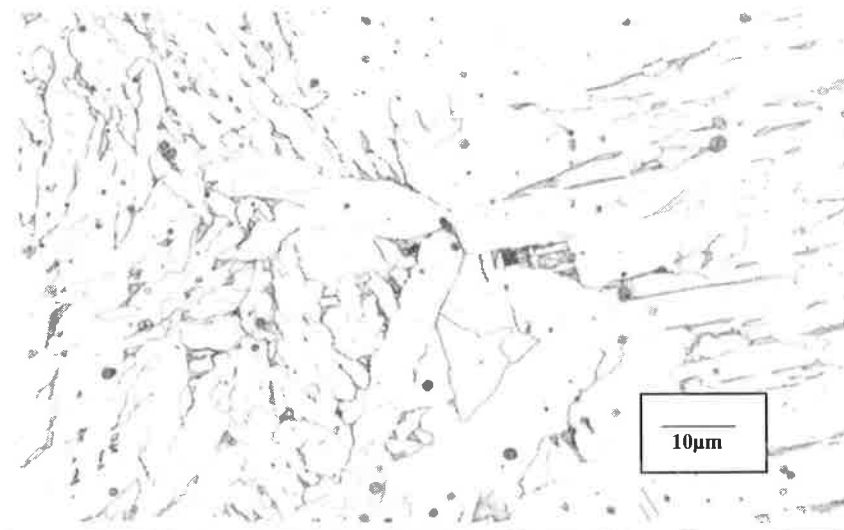
Microstructure photomicrograph



As-Welded x100

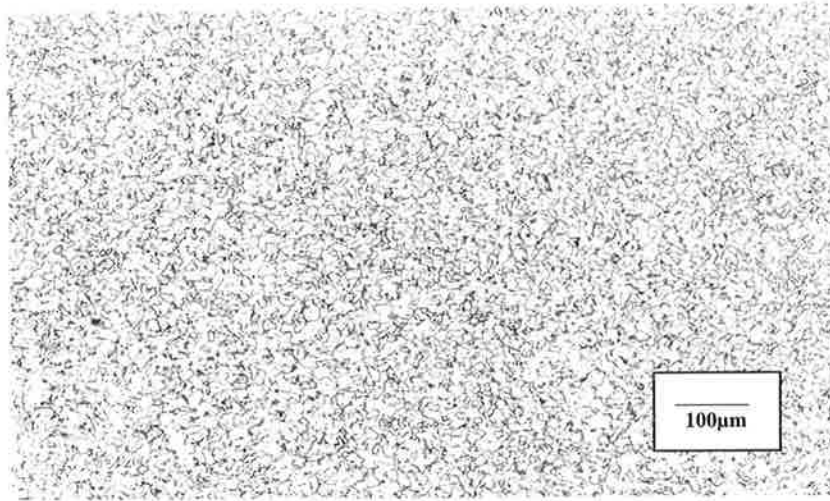


As-Welded x500

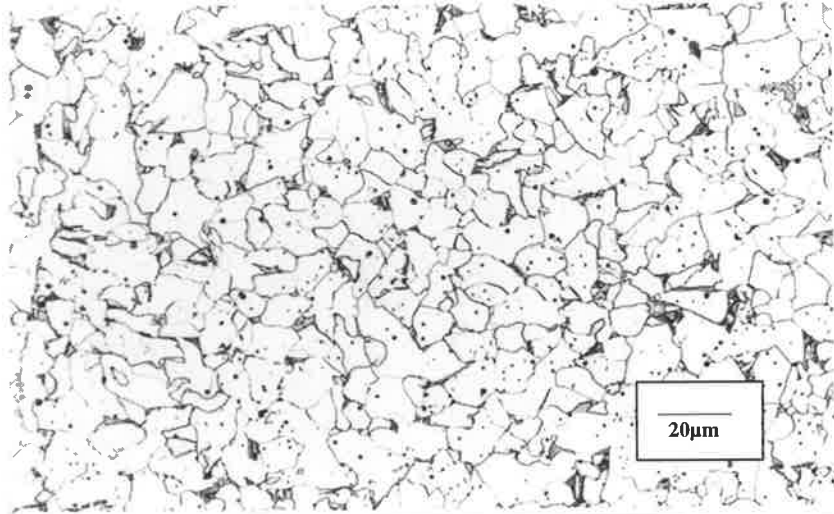


As-Welded x1000

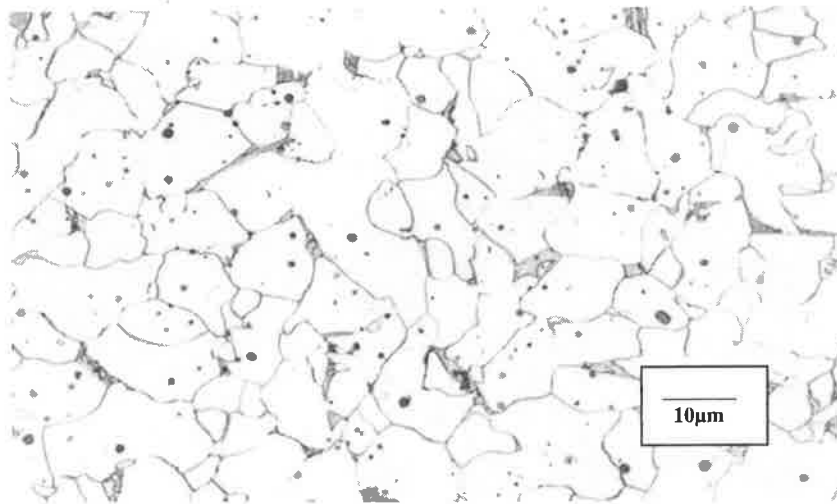
Appendix D



Re-Heated x100



Re-Heated x500



Re-Heated x1000

Appendix D

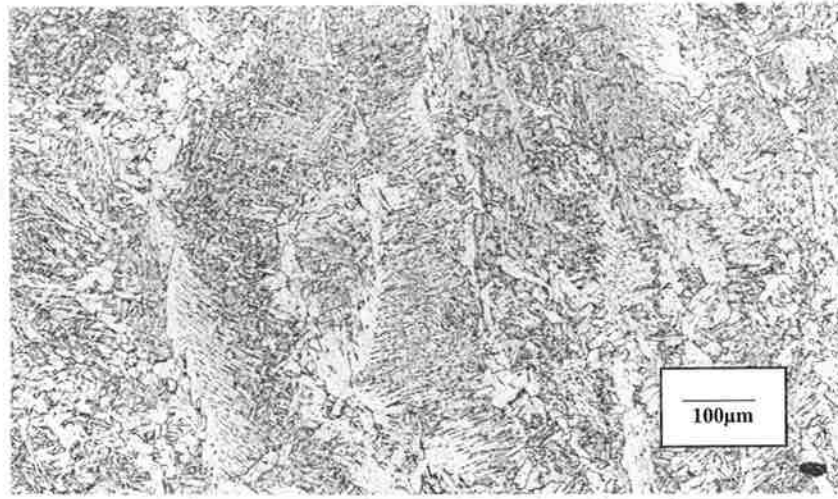
Boron Series

Composition

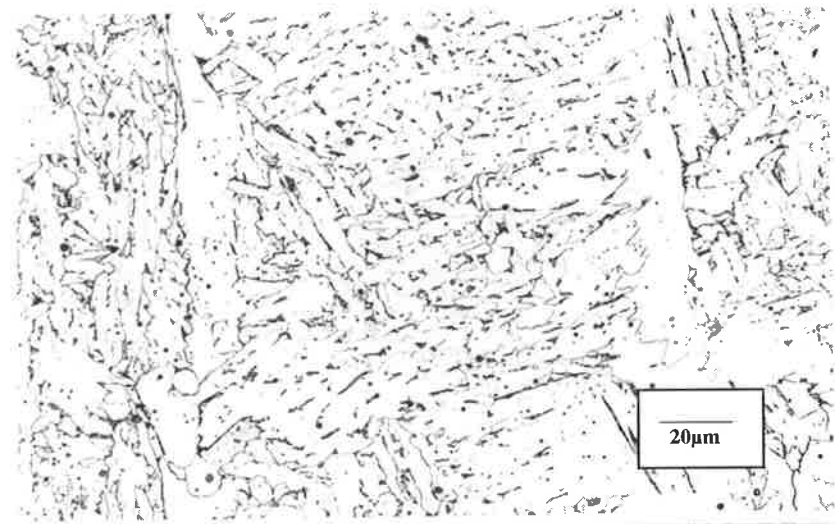
Si	Mn	C	S	P	Ni	Cr	Mo	Cu	V	Nb	Ti	Al	B	O	N
0.66	1.41	0.04	0.011	0.012	0.02	0.01	<0.01	<0.01	<0.01	<0.01	0.0057	0.0161	0.0134	0.0500	0.0063

Appendix D

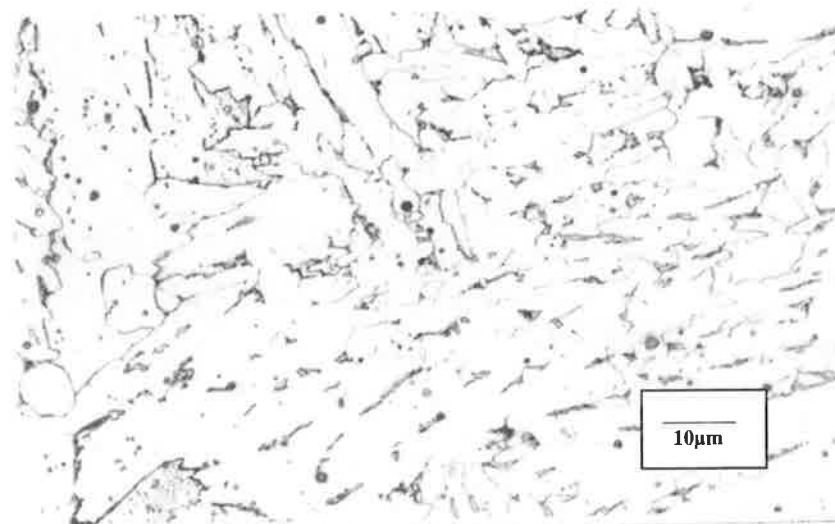
Microstructure photomicrograph



As-Welded x100

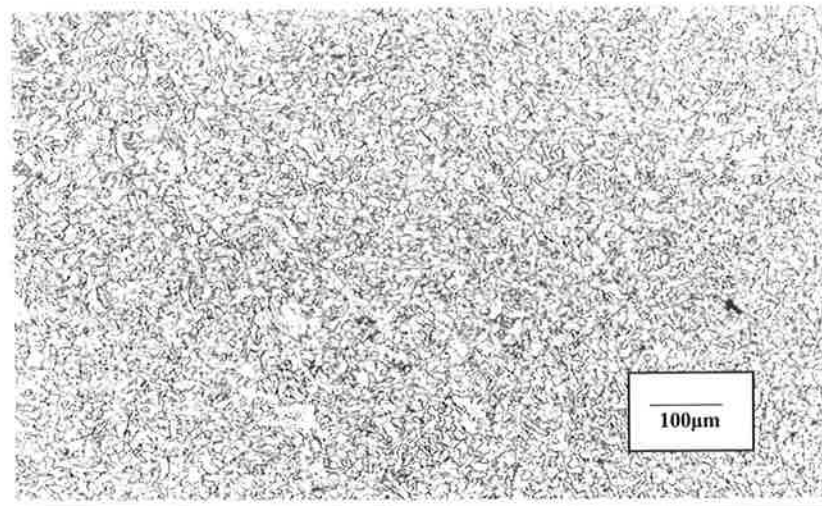


As-Welded x500

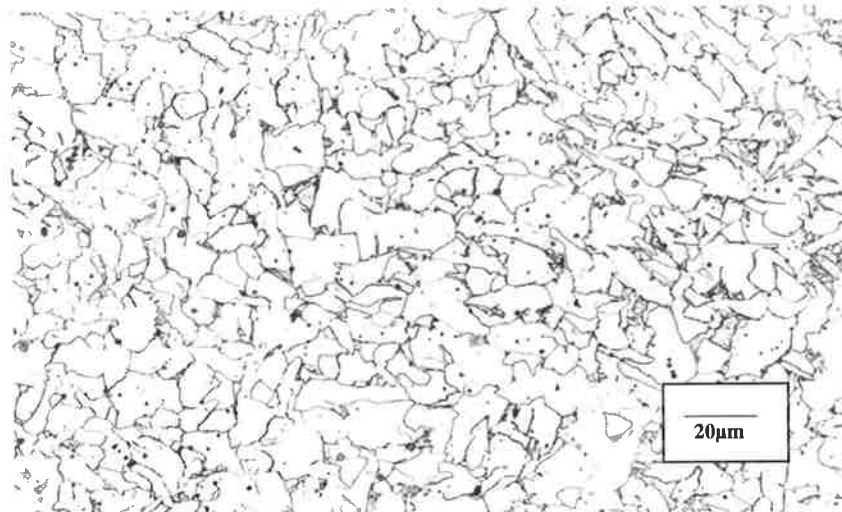


As-Welded x1000

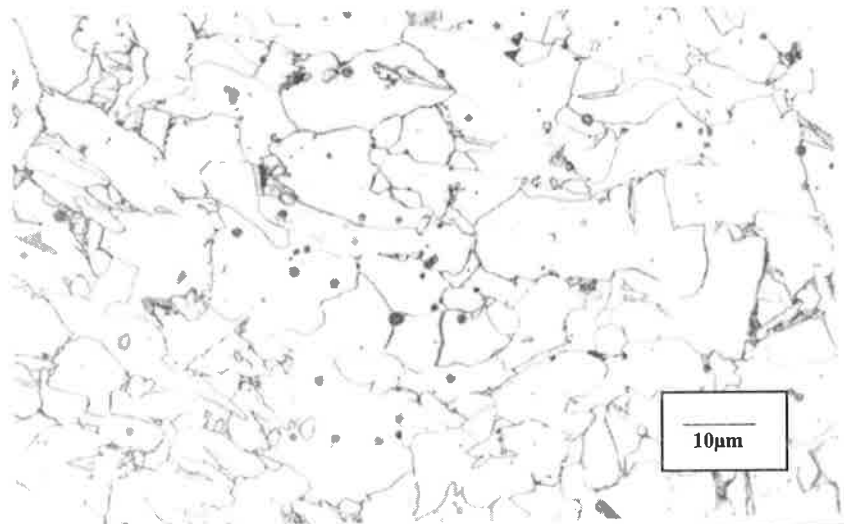
Appendix D



Re-Heated x100



Re-Heated x500



Re-Heated x1000

Appendix D

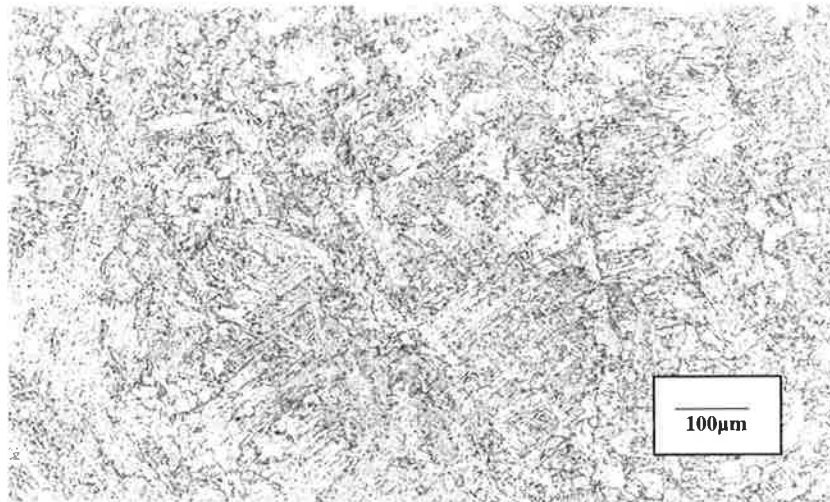
Boron Series

Composition

Si	Mn	C	S	P	Ni	Cr	Mo	Cu	V	Nb	Ti	Al	B	O	N
0.62	1.33	0.04	0.013	0.012	0.03	0.01	<0.01	0.02	<0.01	<0.01	0.0059	0.0150	0.0176	0.0500	0.0043

Appendix D

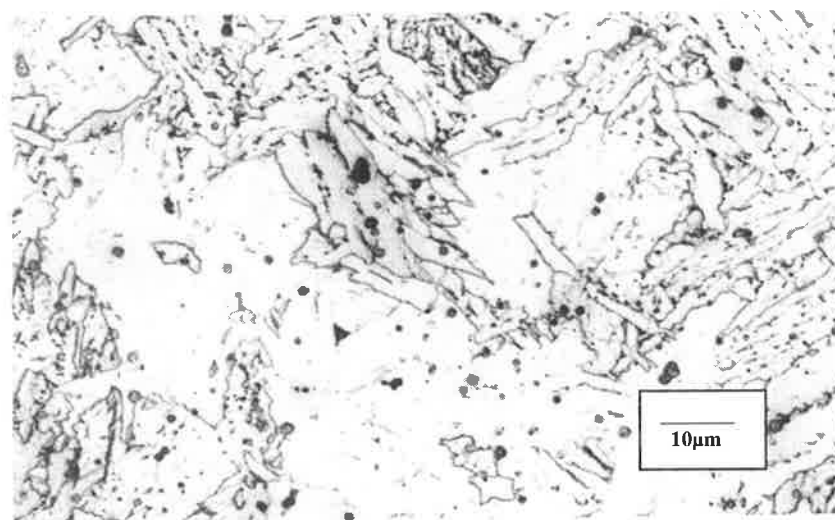
Microstructure photomicrograph



As-Welded x100

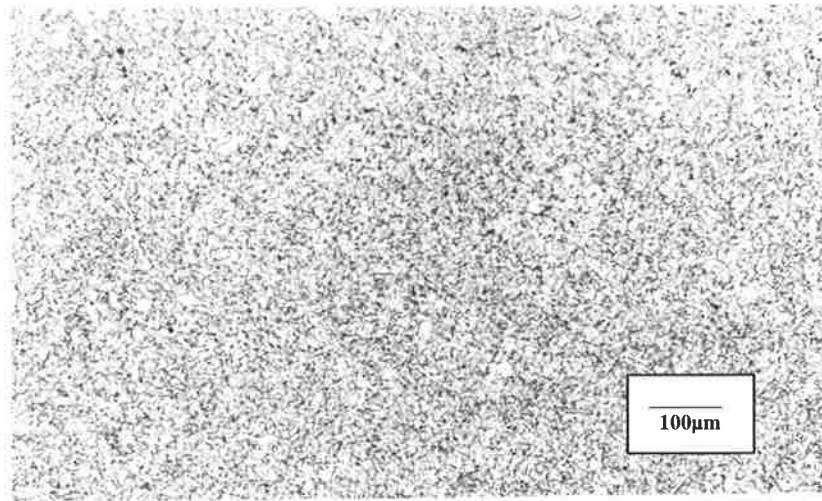


As-Welded x500

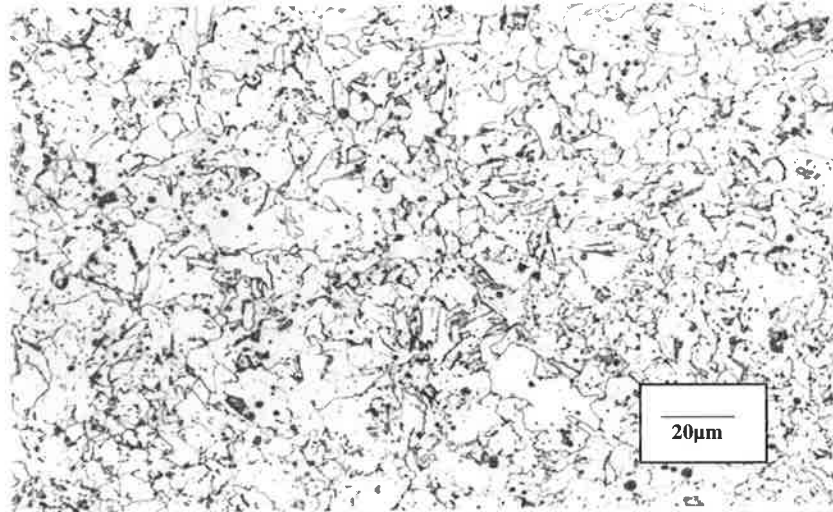


As-Welded x1000

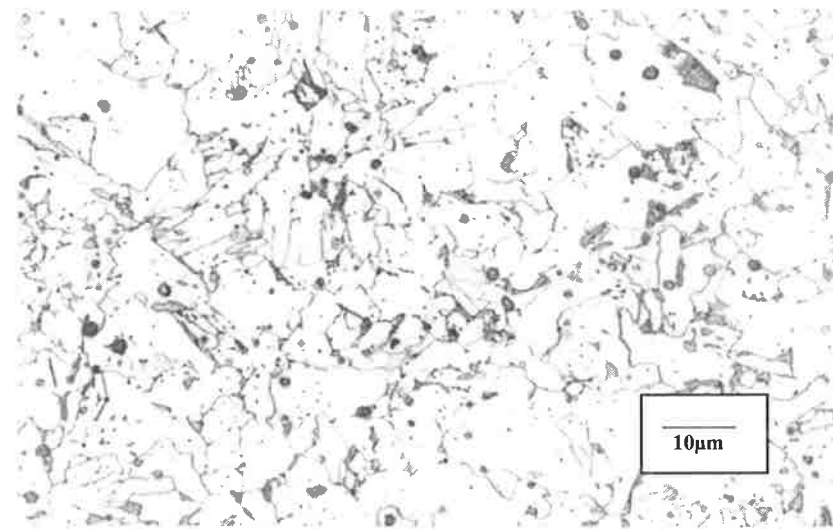
Appendix D



Re-Heated x100



Re-Heated x500



Re-Heated x1000

Appendix E Titanium and Boron Series

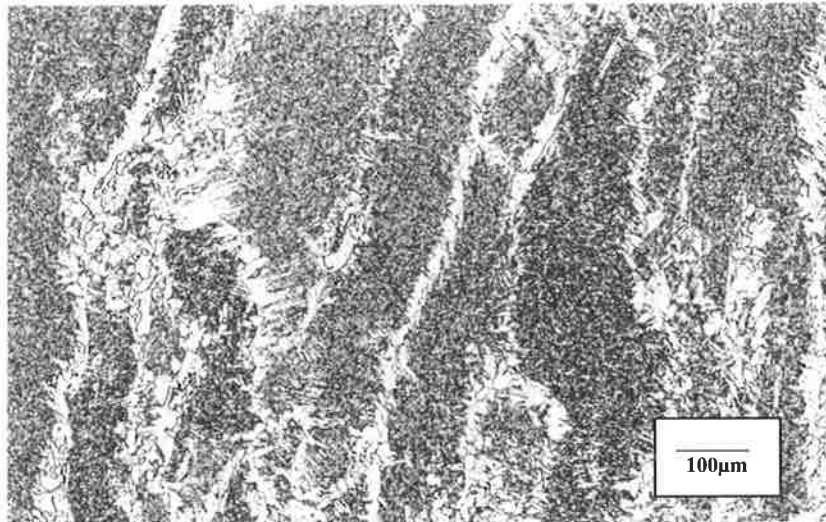
Titanium and Boron Series

Composition

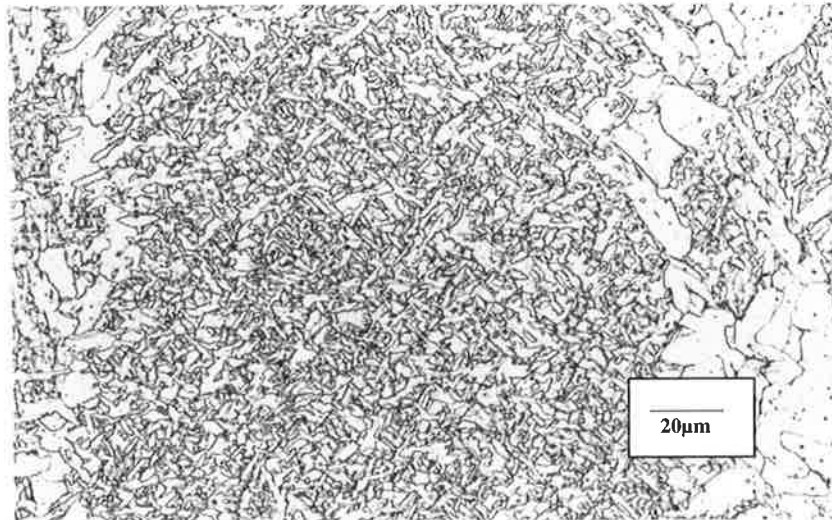
Si	Mn	C	S	P	Ni	Cr	Mo	Cu	V	Nb	Ti	Al	B	O	N
0.64	1.34	0.04	0.012	0.014	0.02	0.01	<0.01	0.01	0.0058	0.0005	0.0054	0.0133	<0.0005	0.0530	0.0047

Appendix E

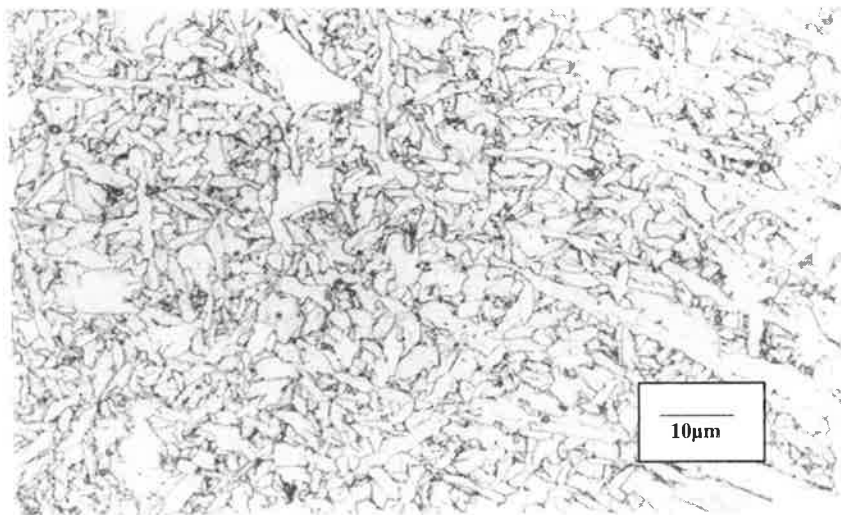
Microstructure photomicrograph



As-Welded x100

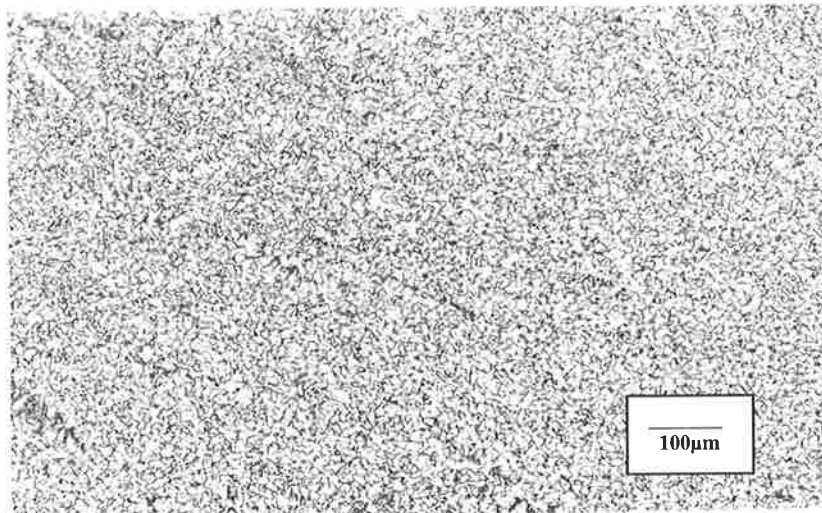


As-Welded x500

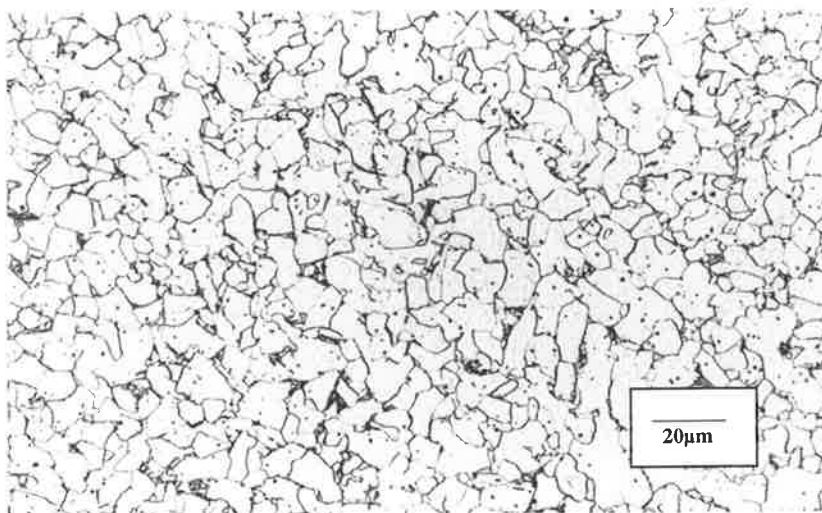


As-Welded x1000

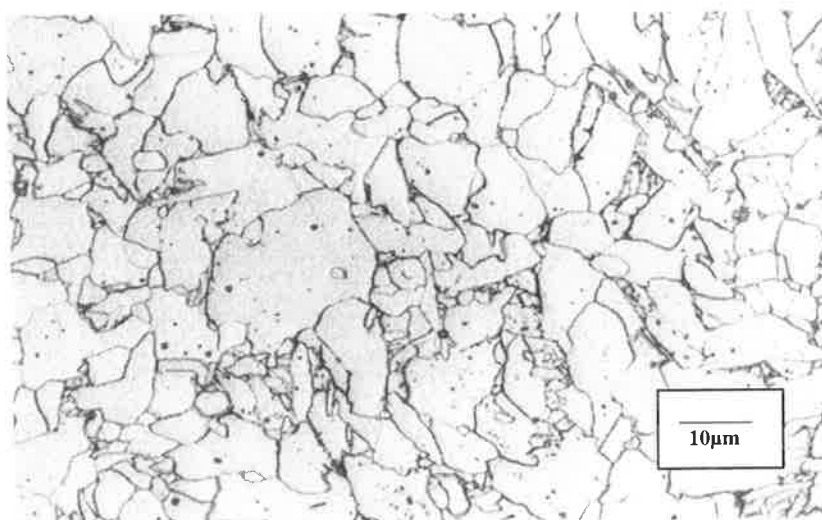
Appendix E



Re-Heated x100



Re-Heated x500



Re-Heated x1000

Appendix E

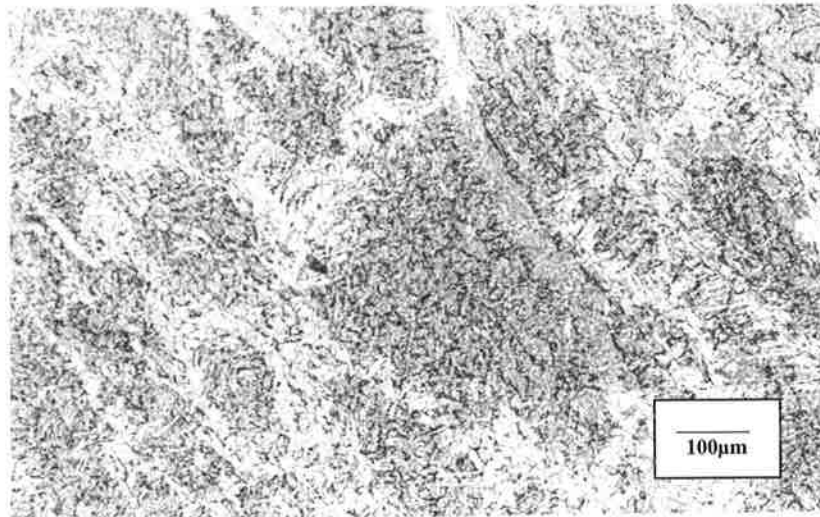
Titanium and Boron Series

Composition

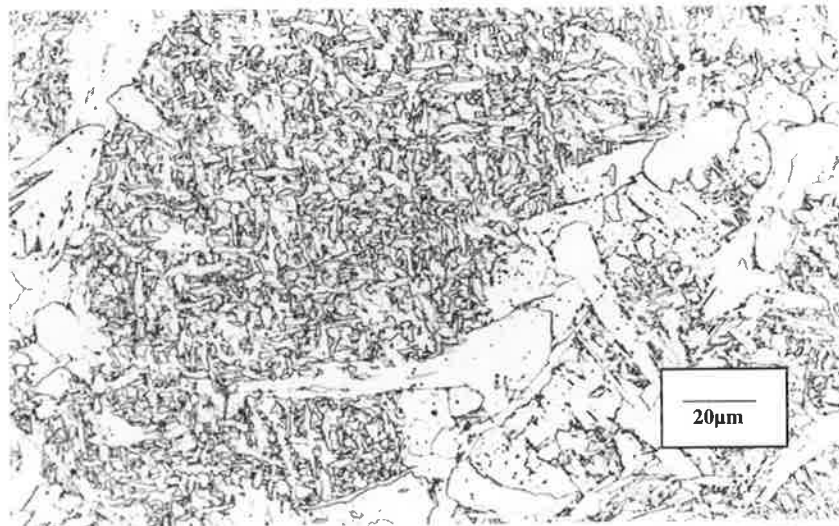
Si	Mn	C	S	P	Ni	Cr	Mo	Cu	V	Nb	Ti	Al	B	O	N
0.58	1.26	0.05	0.011	0.013	0.02	0.01	0.01	0.01	0.0058	<0.0005	0.0273	0.0142	<0.0005	0.0420	0.0054

Appendix E

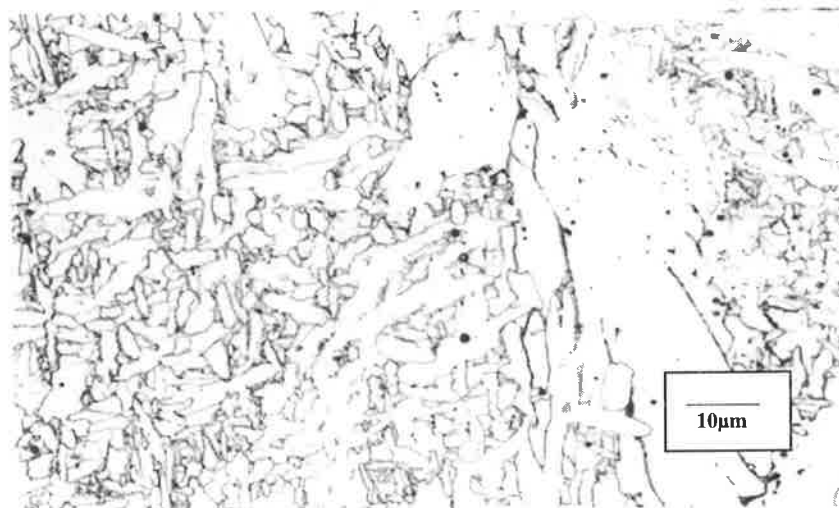
Microstructure photomicrograph



As-Welded x100

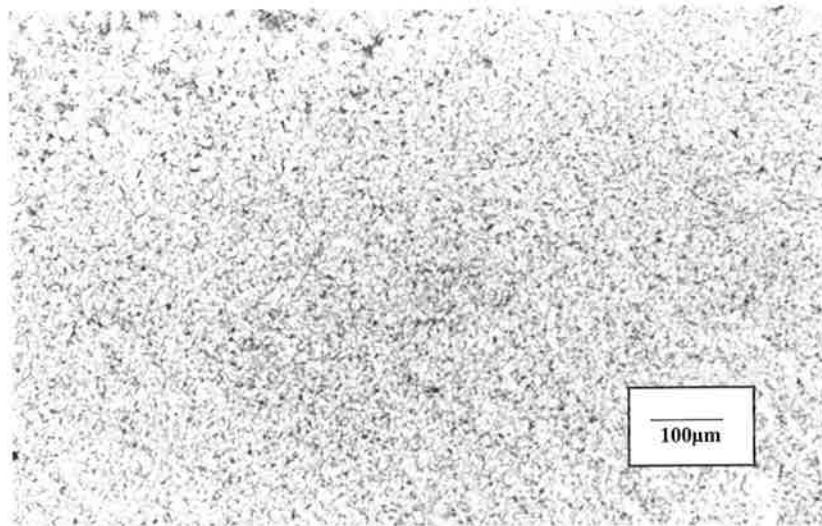


As-Welded x500

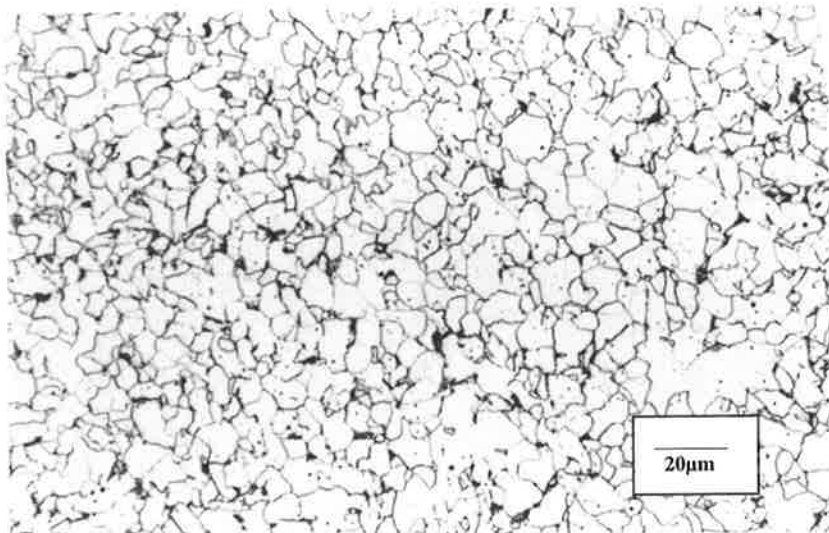


As-Welded x1000

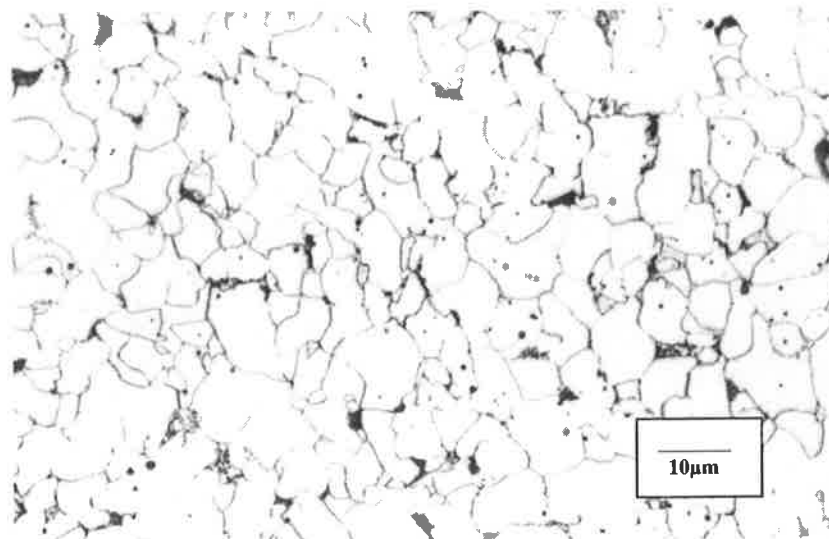
Appendix E



Re-Heated x100



Re-Heated x500



Re-Heated x1000

Appendix E

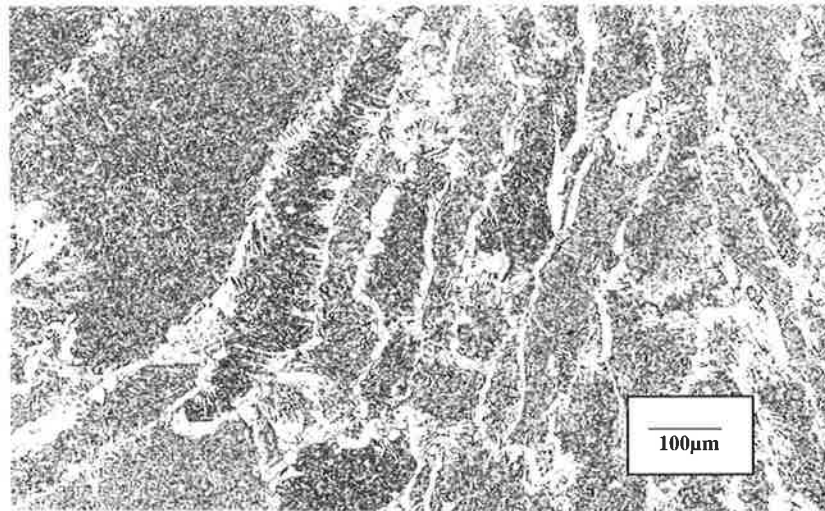
Titanium and Boron Series

Composition

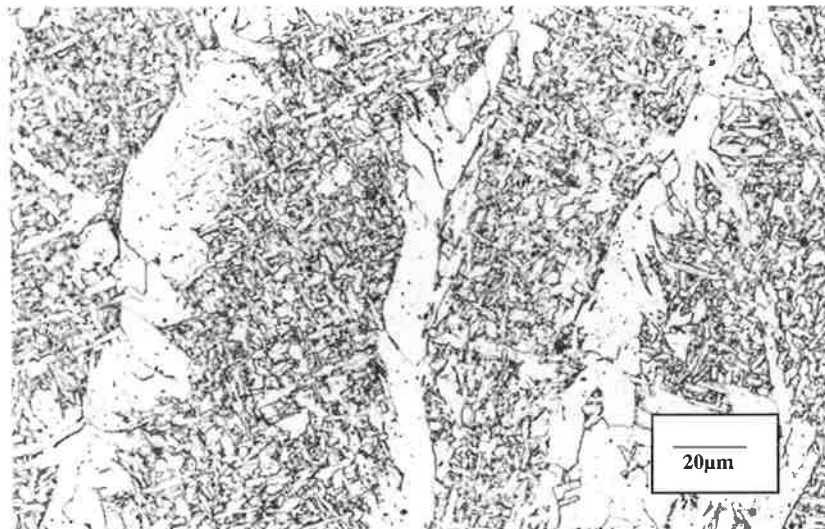
Si	Mn	C	S	P	Ni	Cr	Mo	Cu	V	Nb	Ti	Al	B	O	N
0.66	1.38	0.05	0.011	0.013	0.02	0.01	0.01	0.01	0.0066	<0.0005	0.0458	0.0111	<0.0005	0.0380	0.0037

Appendix E

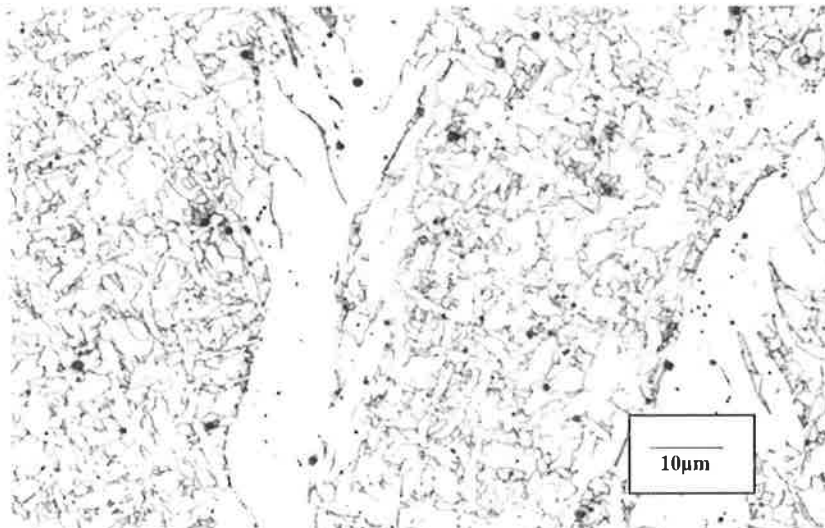
Microstructure photomicrograph



As-Welded x100

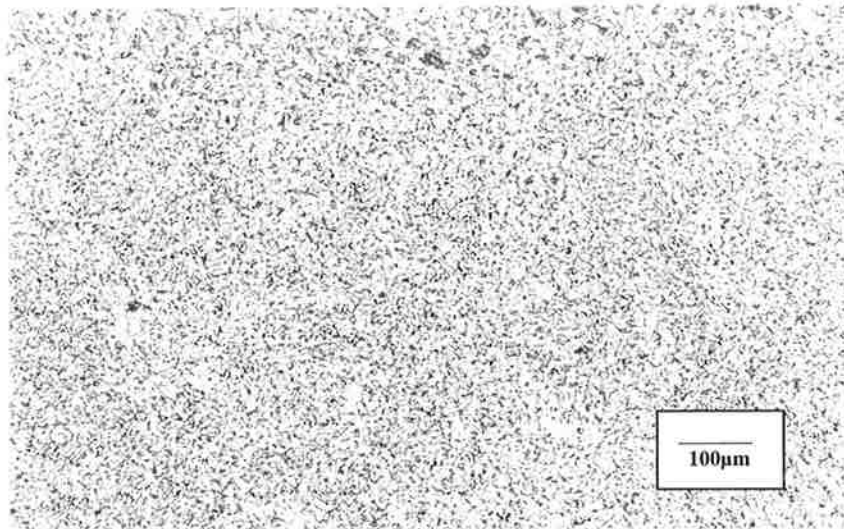


As-Welded x500

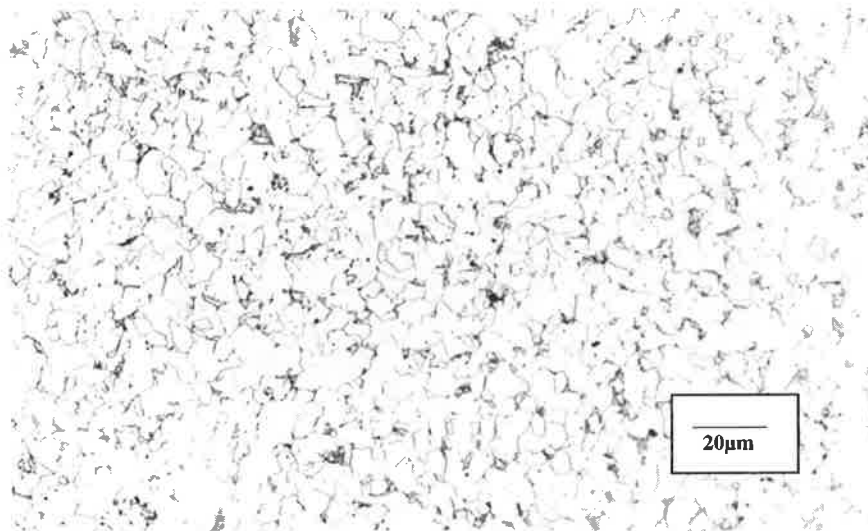


As-Welded x1000

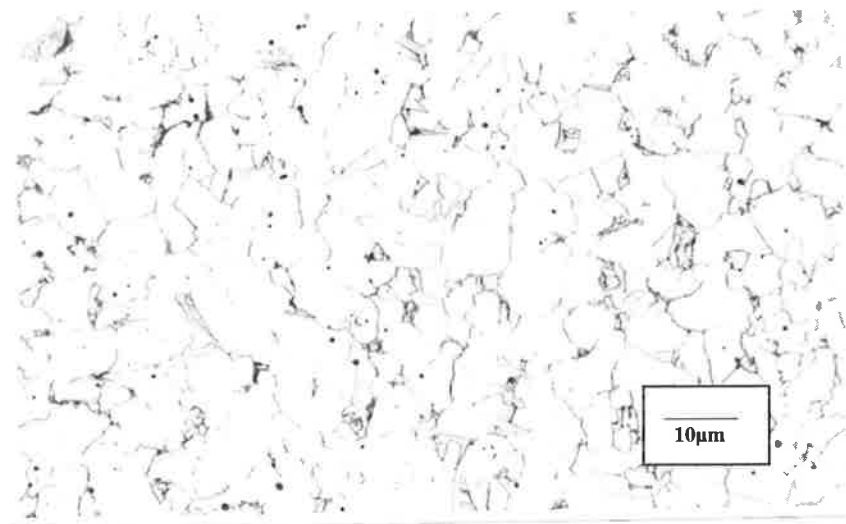
Appendix E



Re-Heated x100



Re-Heated x500



Re-Heated x1000

Appendix E

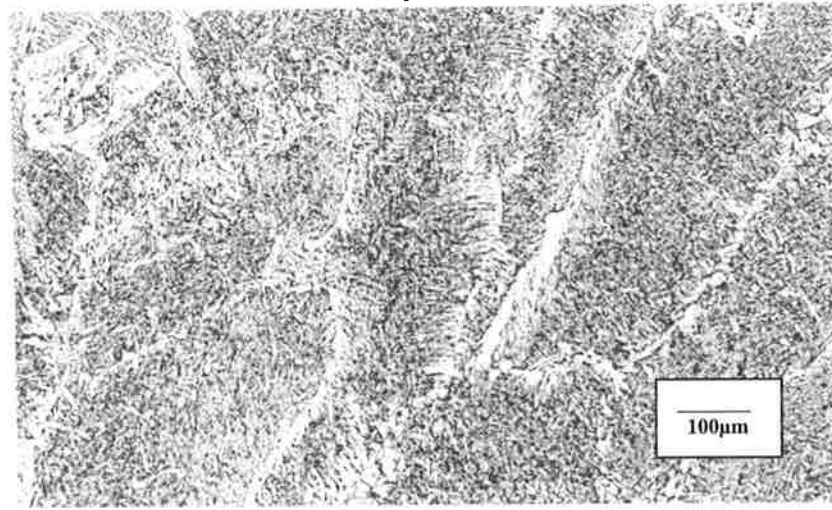
Titanium and Boron Series

Composition

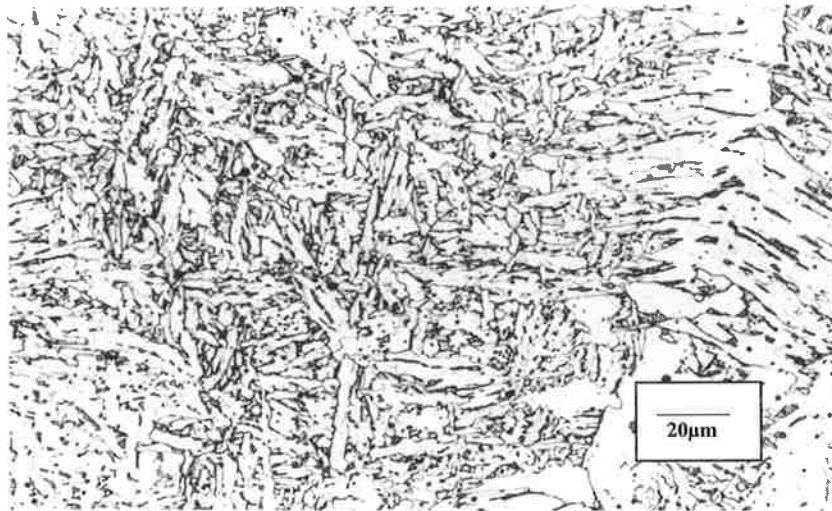
Si	Mn	C	S	P	Ni	Cr	Mo	Cu	V	Nb	Ti	Al	B	O	N
0.67	1.44	0.04	0.013	0.015	0.01	0.01	<0.01	0.01	0.0087	<0.0005	0.0054	0.0150	0.0095	0.0390	0.0027

Appendix E

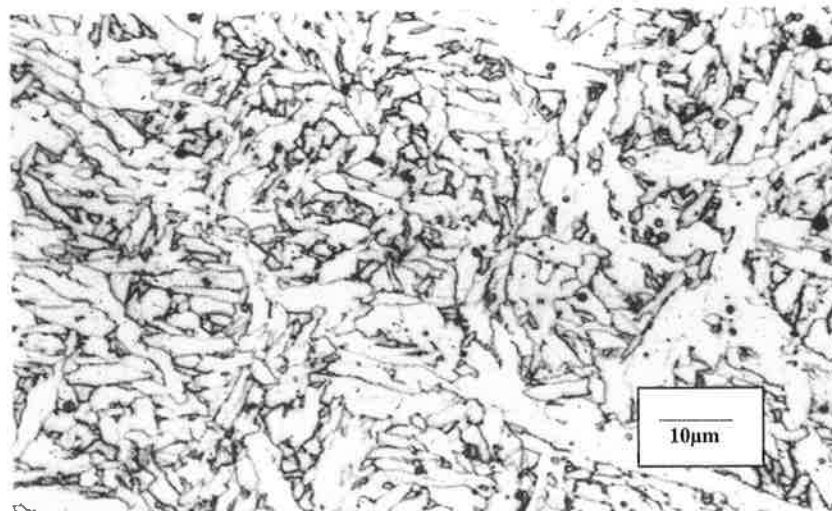
Microstructure photomicrograph



As-Welded x100

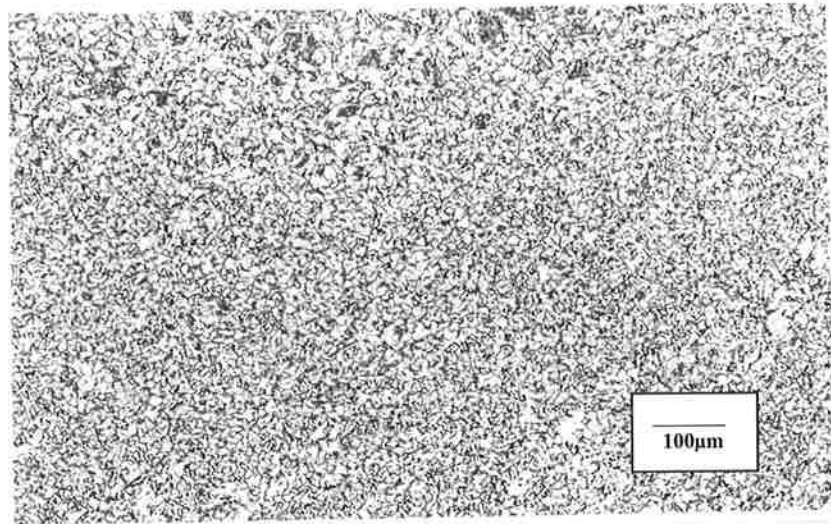


As-Welded x500

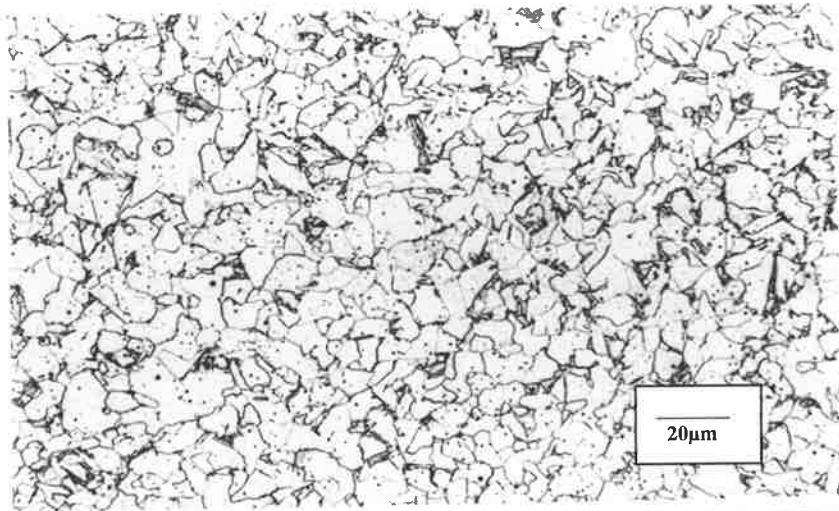


As-Welded x1000

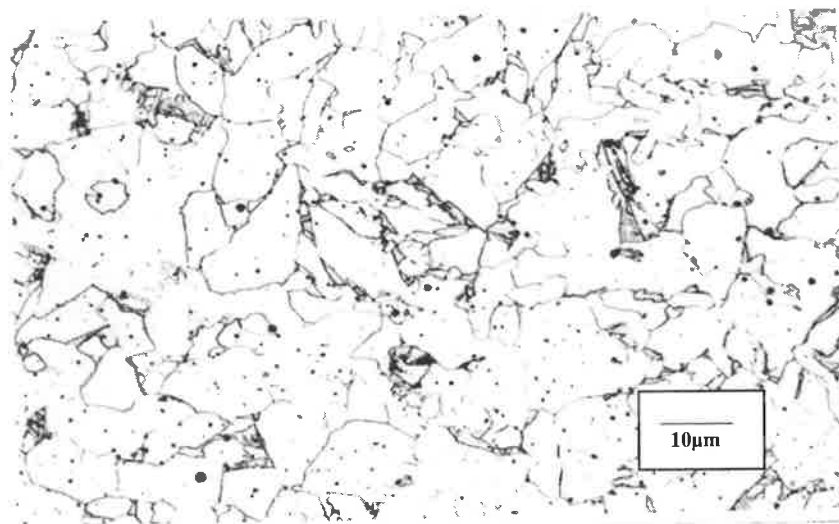
Appendix E



Re-Heated x100



Re-Heated x500



Re-Heated x1000

Appendix E

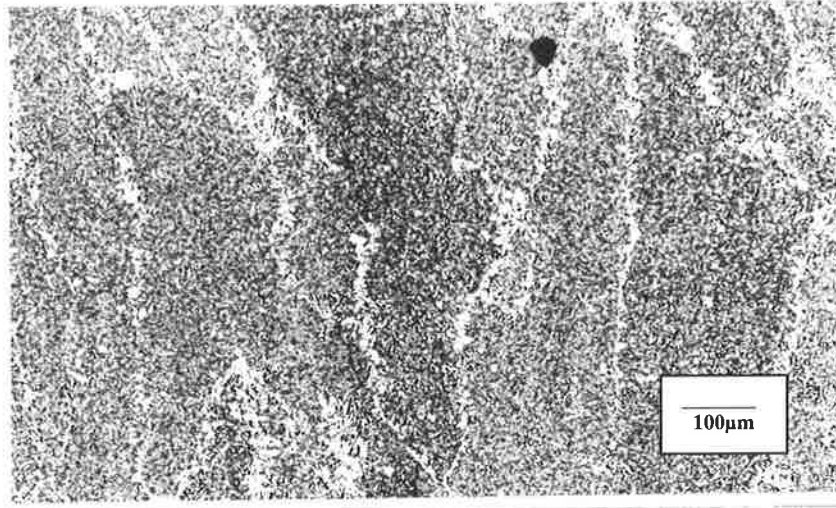
Titanium and Boron Series

Composition

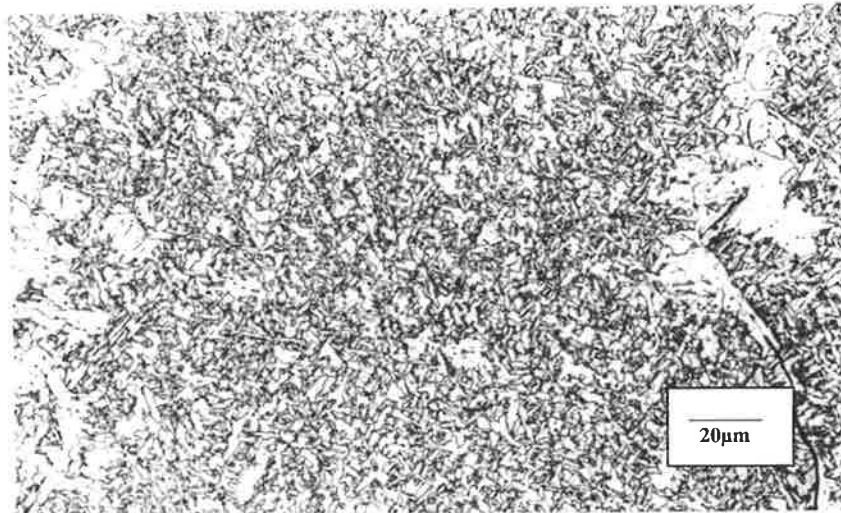
Si	Mn	C	S	P	Ni	Cr	Mo	Cu	V	Nb	Ti	Al	B	O	N
0.68	1.47	0.05	0.013	0.015	0.01	0.01	<0.01	0.01	0.0096	<0.0005	0.0228	0.0150	0.0112	0.0430	0.0036

Appendix E

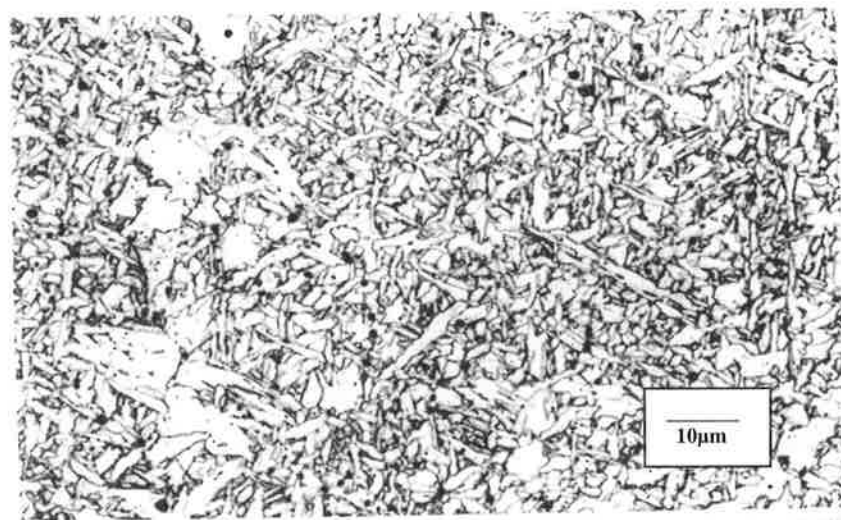
Microstructure photomicrograph



As-Welded x100

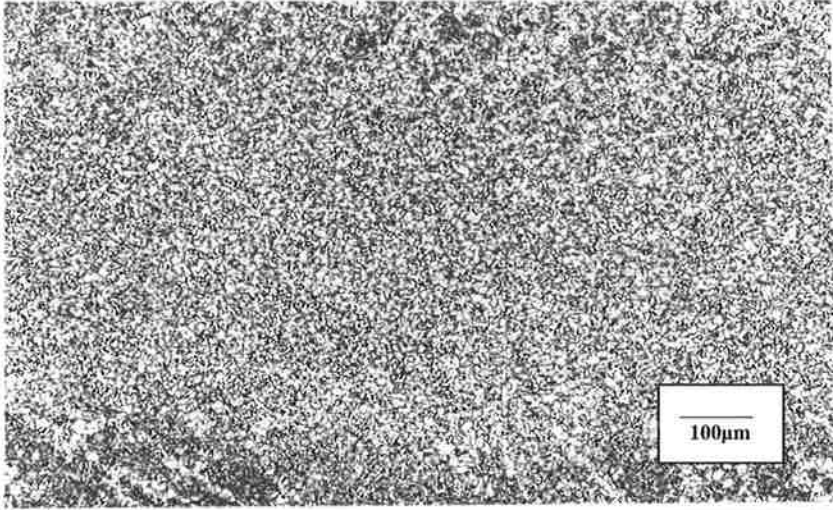


As-Welded x500

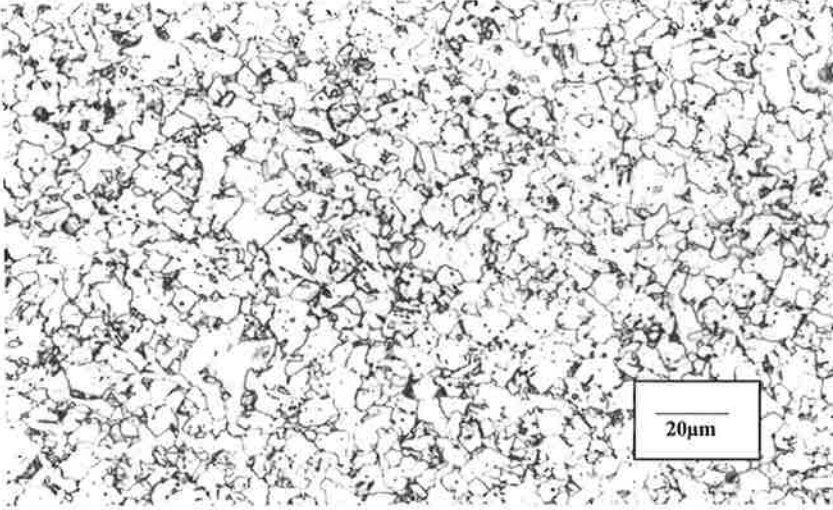


As-Welded x1000

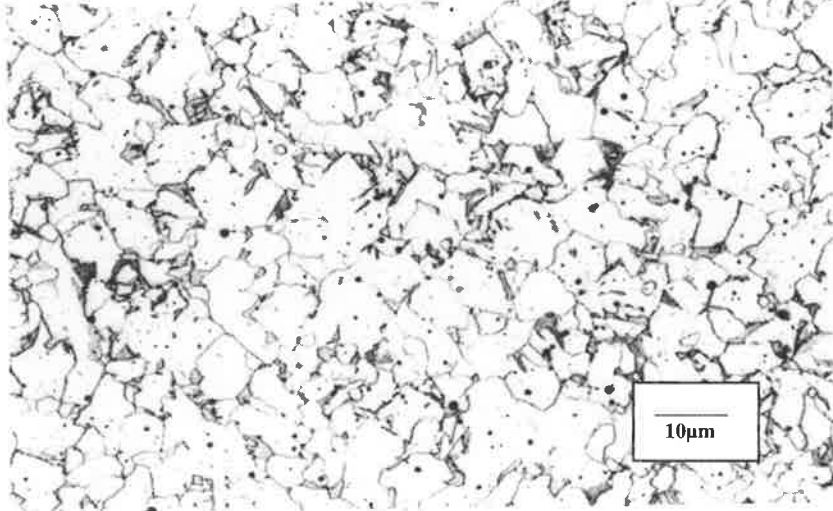
Appendix E



Re-Heated x100



Re-Heated x500



Re-Heated x1000

Appendix E

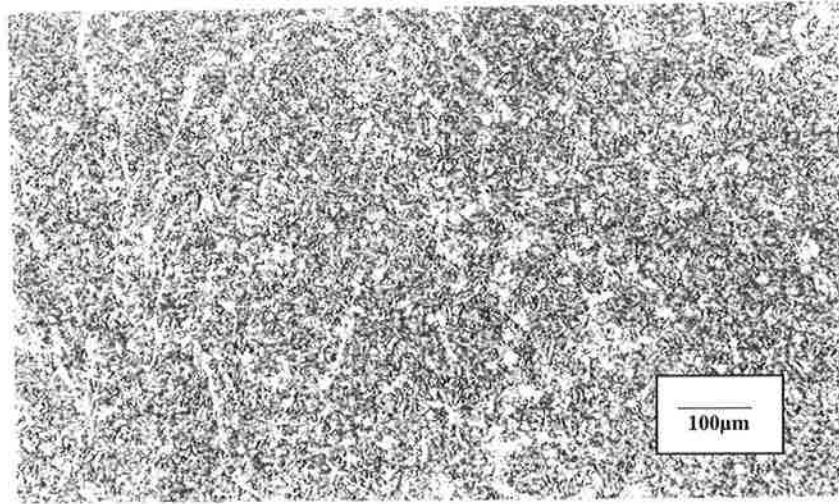
Titanium and Boron Series

Composition

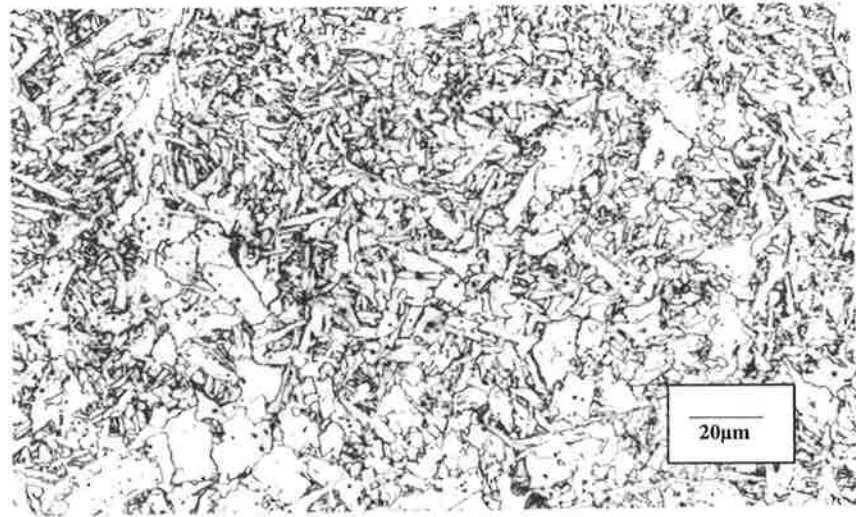
Si	Mn	C	S	P	Ni	Cr	Mo	Cu	Y	Nb	Ti	Al	B	O	N
0.68	1.49	0.05	0.014	0.015	0.01	0.01	<0.01	0.01	0.0110	<0.0005	0.0430	0.0147	0.0110	0.0460	0.0036

Appendix E

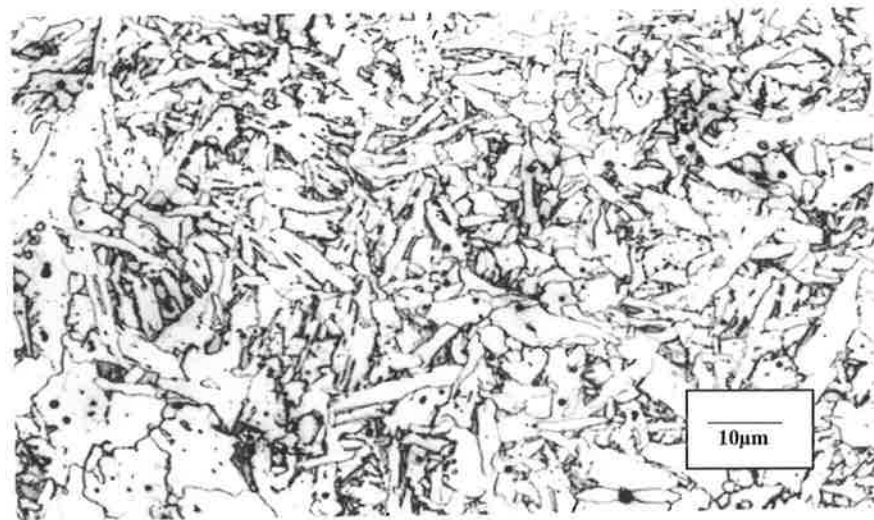
Microstructure photomicrograph



As-Welded x100

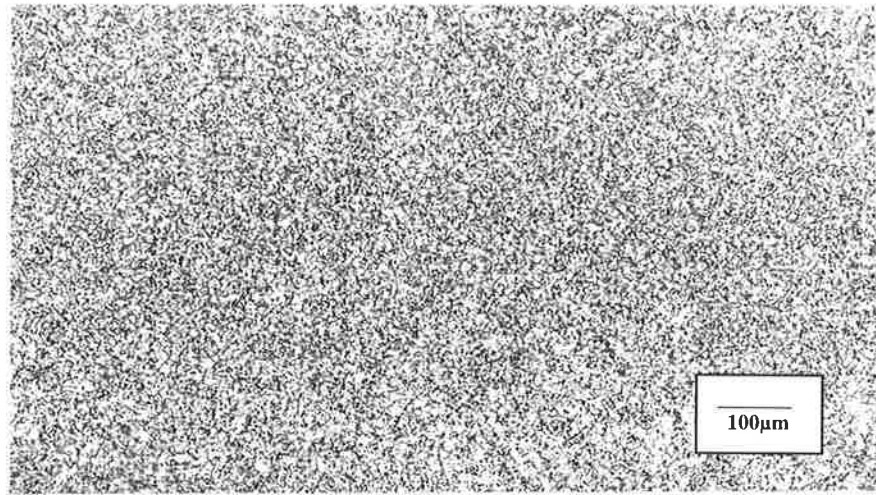


As-Welded x500

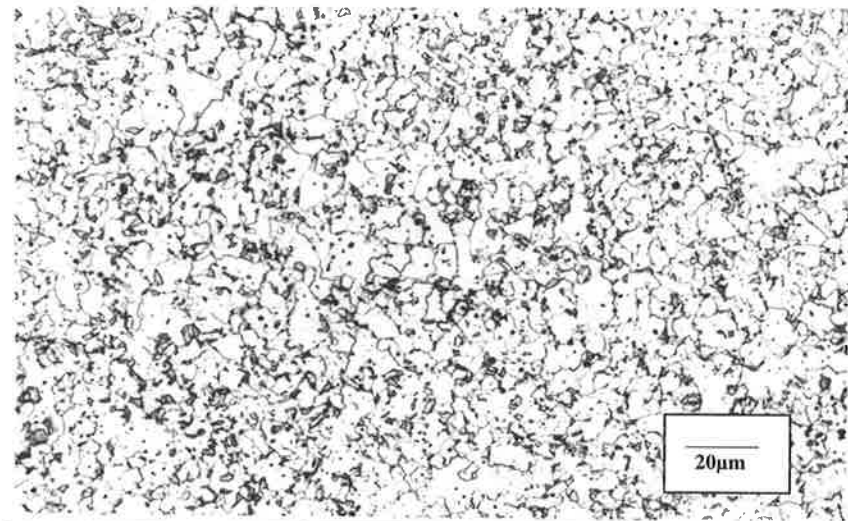


As-Welded x1000

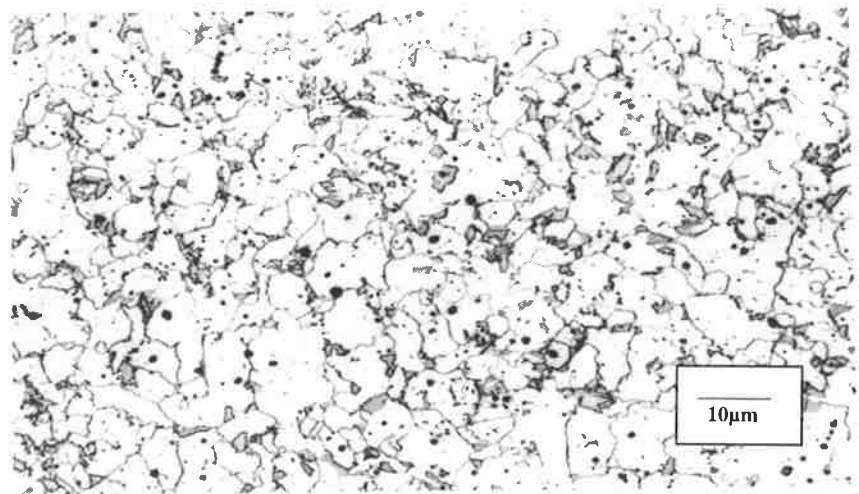
Appendix E



Re-Heated x100



Re-Heated x500



Re-Heated x1000

Appendix F

Example of Publications

Influence of Titanium and Boron on the Properties of Multi-pass Weld Metal from Gas-shielded, Metal-cored Wires

Tyagi V.K.⁽¹⁾, French I.E.⁽²⁾ and Brown I.⁽³⁾,

(1) CSIRO Manufacturing Science and Technology - a Core Partner
of the CRC-WS

(2) Former Member of CSIRO Manufacturing Science and Technology
- a Core Partner of the CRC-WS

(3) University of Adelaide, Australia - a Core Partner of the CRC-WS

Abstract

Boron and titanium additions and the microstructure and impact toughness of gas metal arc weld deposits made with metal-cored wires were investigated. It was found that a large volume fraction acicular ferrite (up to 95%) could be obtained by maintaining the optimum boron and titanium contents. Addition of titanium or boron alone has very little influence on acicular ferrite formation in the weld deposits. A direct relationship between the acicular ferrite content and the low temperature impact properties of the weld deposits was established.

Key words

Metal cored wires, gas shielding, multi-pass welds, weld metal titanium, weld metal boron, microstructure, properties.

1. Introduction

The influence of boron on increasing acicular ferrite in weld metal microstructures is very small without sufficient titanium addition. The influence of titanium is also very small without sufficient levels of boron [1]. A large volume fraction of acicular ferrite (up to 95%) can be obtained by maintaining optimum boron and titanium contents. The decrease in low-temperature toughness with excess boron and titanium contents can be explained by the resulting increase in volume fraction of upper bainite [1].

Previous work have reported that balanced alloying with boron and titanium can almost eliminate formation of grain boundary ferrite [2-7]. The mechanism for the influence of boron is based on the fact that boron segregates extensively at the prior austenite grain boundaries, where it reduces the grain boundary energy [8]. It has been proposed that the reduction in grain boundary energy increases the energy barrier for nucleation by lowering the surface free energy ratio and therefore suppress the formation of grain boundary ferrite facilitating the nucleation on oxide inclusions [9,10].

Titanium protect the boron from oxygen and nitrogen. Elemental boron hinders the formation of grain boundary ferrite resulting in increased undercooling of weld metal austenite which promotes the nucleation of fine intergranular acicular ferrite. The specific inclusion

Appendix F

concentration and size distribution, with proper protection of weld metal boron, are the primary factors to achieve high intragranular acicular ferrite contents [11].

The role of titanium is mainly to protect boron from nitrogen (and oxygen) by forming titanium nitride (TiN) in the liquid state prior to solidification. The optimum titanium content will clearly be a function of the weld metal concentrations of nitrogen and nitride formers (V, Nb and Al). Mori, et al. [12], proposed that oxide particles with a surface coating of TiO, or those particles that were completely TiO, would be the most potent site for the nucleation of acicular ferrite. The 3.0% lattice discrepancy between TiO and ferrite is the smallest of all the potential nucleating agents. Compounds that have high values of discrepancy, such as BN and Al₂O₃, will not be as likely nucleation sites for the acicular ferrite.

Ohkita et al. [13], suggested the following mechanistic description of notch toughness improvement in the titanium-boron containing weld metal:

1. During solidification, highly segregated boron reacts preferentially with nitrogen to form BN. The titanium protects the boron from oxygen.
2. During cooling in the austenite range, titanium protects the remaining boron from nitrogen by forming TiN. Free boron segregates to the austenite grain boundaries. The formation of nitrogen compounds with boron and titanium by the above reactions reduces the amount of nitrogen in solution.
3. On further cooling of the austenite to the ferrite transformation range, active boron, present at the austenite grain boundaries, reduces the grain boundary energy and retards the nucleation of proeutectoid ferrite.
4. Oxide inclusions that contain titanium promote the nucleation of acicular ferrite within austenite grains.

The purpose of this paper is to characterise in greater detail the combined effects of boron and titanium on the microstructure and mechanical properties of multi-layer gas-shielded metal cored arc weld metals.

2. Materials and Methods

2.1 Manufacture of Special Wires

For the present investigation, special metal cored wires were manufactured. The sheath material was cold rolled mild steel of approximate composition 0.05% C, 0.22% Mn, 0.01% Si and 0.015% Al. Core ingredients used included iron powder, silicon-manganese, ferro-silicon, electrolytic manganese, titanium metal and aluminium metal powders. All of these were commercial powders normally used for arc welding consumable manufacture. The wires were manufactured with a nominal core weight to total wire weight of 21% and were drawn to a final diameter of 1.6 mm.

The Mn and Si content of the wires was kept constant to yield weld metal containing nominally 0.60% Si and 1.34% Mn. Additions of Ti and B were aimed for obtaining three levels of titanium: 0.0054, 0.0230 and 0.0458%, and for each level of titanium two levels of boron, 0.0005 and 0.0100%, were used. In addition, the weld metal carbon content was kept constant at nominally 0.05%.

Appendix F

2.2 Welding Procedure

Welding was performed in the flat position (1G) on parent plate material of AS Grade 250 [14] under mechanised conditions. Direct current electrode positive was used with the welding current being 300A and 30V welding voltage. Energy input was nominally 1.5kJ/mm. The shielding gas used was Argon with 5% CO₂. Inter-pass temperature was standardised at 150 °C [see reference 15 for details].

2.3 Weld Composition

Chemical analyses of the all-weld-metal deposits were obtained using an optical emission spectrometer. The vanadium, niobium, titanium, aluminium and boron contents of the experimental welds were determined to four decimal places so that small variations could be detected. Oxygen and nitrogen contents in the weld metal were determined using a Leco TC136 analyser.

2.4 Mechanical Testing

The impact toughness of each weld metal was assessed by the Charpy-V-notch (CVN) test. Tests were carried out at -60, -40, -20, 0 and 20 °C respectively in order to obtain a transition curve for each weld. Three specimens were tested at each temperature and the mean absorbed energy calculated. An all-weld-metal tensile test was carried out. The tensile specimens were heat treated at 250 °C for 16 hours for hydrogen removal, prior to testing. The details of test specimens and procedures have been given previously [15].

2.5 Metallography

Transverse sections were prepared and detailed microstructural examination was carried out on top beads and on the adjacent reheated zones. The volume fraction of the different micro-constituents was obtained from point counts on more than 1000 points, following the IIW Guidelines [16]. The prior austenite grain sizes were determined by means of the mean linear intercept technique [17] for all welds as were the lath widths of the acicular ferrite.

2.6 Study of Inclusions

The size distribution of non-metallic inclusions on polished specimens of the as-deposited weld metal was examined, using a scanning electron microscope (SEM) based automatic image analyser. The methods used were in line with those detailed in [18]. In the present investigation, magnification of 10,000, accelerating voltage of 15kV, grid point spacing of 0.02 µm and working distance between 8 and 10 mm was used (see reference 15 for details).

3 Results

3.1 Weld Composition

The chemical compositions of the all-weld-metal deposits studied are given in Table 1 for the Ti-B series. For 0.0005% boron, as the titanium level increased the oxygen level reduced from 0.0530 to 0.0380%, while the nitrogen level varied between 0.0054 and 0.0037%. For 0.0100% boron, as the titanium level increased the oxygen level varied between 0.046 to

Appendix F

0.039%, while the nitrogen level varied between 0.0036 and 0.0027%. These levels of oxygen and nitrogen are considered normal for this type of weldmetal and process.

3.2 Mechanical Properties

3.2.1 Tensile Properties

Results of the tensile test are presented in Table 2 for the Ti-B series, the measured yield strengths varied between 482 and 556 MPa, while tensile strengths varied between 557 and 610 MPa and elongations were between 24 and 29%. For 0.0005% boron content, yield and tensile strength decreased as titanium increased to 0.0273% and then increased again at 0.0458%, this could be due to changes in Mn and Si, while elongation decreased by about 14% as the titanium level increased in the weld metal. While for 0.0100% boron, as titanium increases to 0.0228% both yield and tensile strength increased by about 5 to 12%, decreasing again at higher titanium levels. Elongation increased by about 8% as titanium increased. These changes in the Ti-B series, over the range tested, are reasonably small for this type of process.

3.2.2 CVN Impact Results

The variations of mean CVN energy with test temperature for the various Ti-B series weld metals are plotted in Figure 1 (a) and (b) respectively. Figure 1 (a) shows CVN energies at 0.0005% boron versus titanium content. Mean CVN energies across the temperature range appear highest at 0.0054% Ti level. For 0.0100% boron, with an increase in titanium, Figure 1 (b) the mean CVN energies across the temperature range are highest at 0.0228% Ti level.

For each case the upper-shelf energy (at +20 °C), the lower-shelf energy (at -60 °C) and the temperature corresponding to a CVN energy of 100J (T100J) were found. These values are plotted in Figure 2 (a) and (b) against weld Ti contents respectively.

Figure 2 (a) with 0.0005% boron shows that as titanium increases the upper-shelf and lower-shelf values tend to decrease. The T100J values, show minimum value of about -45 °C at Ti contents of approximately 0.0054%, any further addition deteriorates T100J values.

The variations with 0.0100% boron with different titanium levels, as plotted in Figure 2 (b) show that the highest upper and lower-shelf values occur at the 0.0228 and 0.0430% titanium. Similarly the lowest T100J value of -62.5 and -60.0 °C occurs at the 0.0228 and 0.0430% titanium. The low temperature properties are best at high boron and high titanium levels, but the best overall impact properties occurs at 0.0100% boron and 0.0228 titanium.

3.3 Weld Metal Microstructure

Area measurements from cross-sections of welds indicated that the region of the weld from which mechanical test specimens (particularly CVN specimens) were extracted contained approximately 60% as-deposited and 40% reheated weld metal [15]. Area fractions of acicular ferrite (AF), ferrite with second phase (FS) and primary ferrite (PF) were determined in as-deposited regions of the top layer from each weld.

Plots of the area fraction of AF, FS and PF with weld Ti at 0.0005% and 0.0100% boron levels are shown in Figure 3 (a) and (b) respectively. In Figure 3 (a) it can be seen that variation in titanium at 0.0005% boron. Here the area of AF tends to decrease in the range

Appendix F

from 62.4 to 48% with an increase in the Ti level. A corresponding increase in FS is seen, as the changes in PF are relatively low. The extent of changes in the as-deposited microstructure with Ti levels at 0.0005% boron are relatively low in the range tested. A representative micrograph is shown in Figure 4 (a) which shows a weld containing 0.0430% Ti. It is interesting to note the areas of primary ferrite (PF).

Figure 3 (b) shows the variation in titanium at 0.0100% boron. Here the area of AF tends to increase sharply with 0.0228% titanium to 74.4% and then decreases again as titanium increases further to 0.0430%. As shown in Figure 3 (b), FS also decreases as titanium increases to 0.0228% from 29% to 11%, with a further increase in titanium, FS increases significantly to 45% of as-deposited weld metal. PF shows a continuous decrease as titanium increases.

In addition to these measurements of area of the ferrite morphologies, measurements were also made of the prior austenite grain size, the grain size of the equiaxed reheated zone and of the mean lath width of acicular ferrite (see Tables 3). For 0.0005% boron, as the titanium content increases, the prior austenite grain size and the grain size in the reheated zone were largely independent of Ti, except perhaps at the 0.0273% Ti level where it tended to increase slightly. The acicular ferrite lath width decreased with increasing Ti levels.

With higher boron levels, as the titanium content increases changes are significant; the prior austenite grain size, acicular ferrite lath width and grain size of the reheated zone decreased with an increase in titanium, with a maximum reduction at the middle titanium level of 0.0228%. Another important observation is that the overall grain size of the reheated zone for 0.0100% boron at all titanium levels decreased significantly by about 20%. The extents of changes in the re-heated weld microstructure with Ti levels are illustrated in Figure 4 (b & c) which shows a weld containing 0.0228% Ti, with 0.0005 and 0.0100% boron, respectively.

The extent of changes in the as-deposited microstructure with Ti levels at 0.0100% boron are illustrated in Figure 4 (d, e & f), which shows welds containing 0.0054, 0.0228 and 0.0430% Ti. It is interesting to note the areas of primary ferrite (PF) and changes in the size of acicular ferrite lath width.

3.4 Non-metallic Inclusions

Table 4 and Figure 5 (a) & (b) show the details of the non-metallic inclusions, including number per unit volume, mean three dimensional (3D) diameter and percentage of diameter equal to or larger than 1 μ m for each weld, as measured using the SEM with an automated image analyser. For 0.0005% boron, as the titanium content increased both the mean 3D inclusion diameter and percentage of inclusions with a diameter greater than 1 μ m decreased, whilst the number density of inclusions measured tends to increase with weld-metal titanium, with a maximum at 0.0273% titanium.

The inclusion data for 0.0100% boron with an increase in titanium, indicates that the mean 3D inclusion diameter decreases with an increase in titanium whilst the number density of the inclusions appears to increase with an increase in weld-metal titanium level. The percentage of inclusions with a diameter greater than 1 μ m tends to decrease significantly as titanium increases to 0.0228% but increases again with a further increase in titanium.

Mean compositions of non-metallic inclusion obtained using energy dispersive X-ray analysis in an SEM, are also listed in Table 4. These values indicate that for both boron levels, as the

Appendix F

titanium level increases, inclusions composition increases in TiO_2 at the expense principally of SiO_2 . MnO also decreases with an increase in titanium, while Al_2O_3 remains relatively unchanged. Note that boron present in the inclusions does not appear in the energy dispersive analysis.

4 Discussion

4.1 Weld Metal Tensile Properties

The tensile test data for the titanium-boron series shows that both yield and tensile strength showed some variation, which reflect changes in weld metal microstructural component and refinement in acicular ferrite lath width and grain size of the reheated zone. However these changes, for the range of titanium and boron tested, are reasonably small. This is in agreement with data from other arc welding processes such as MMAW and SAW [3,19].

4.2 Weld Metal Impact Properties

Micro alloying influences impact properties of weld metal by varying microstructure (area fraction of various phases) of as-deposited and reheated weld metal region, non-metallic inclusions, strength levels and grain size.

The effect of boron on steel transformation kinetics is significant and has been the subject of research for many years. A number of mechanisms for notch toughness of steels have been proposed to explain the behaviour of boron [20]. Most work have assumed that boron influences notch toughness by increasing the energy barrier against ferrite nucleation at austenite grain boundaries, without influencing the thermodynamic properties of the austenite and ferrite phases, i.e. reduce the A_{f3} temperature of the steel. The notch toughness effect of boron is sensitive to variations in the applied steel deoxidation and alloying. If steel contains small amounts of dissolved oxygen and nitrogen, these elements may combine with boron to reduce the free, diffusible boron content [21].

Results confirm that the influence of boron on increasing acicular ferrite in weld metal microstructures was very small without sufficient titanium addition. The influence of titanium was also very small without sufficient levels of boron. A large volume fraction of acicular ferrite can be obtained by maintaining optimum boron and titanium contents. This compares well with work by several authors who reported that boron segregates extensively to the prior austenite grain boundaries and reduces the grain boundary energy, which increase the energy barrier to nucleation by lowering the surface free energy ratio and therefore suppress the formation of grain boundary ferrite, facilitating nucleation on oxide inclusions [2-10].

The present results show, in the range tested, that the fraction of AF present generally decreases with the addition of titanium for 0.0005% boron. A corresponding increase in FS and PF is seen. As the boron level increases to 0.0100%, an increase in titanium results in a significant increase in AF at the expense of FS and PF. The extent of this change in as-deposited microstructure with Ti-B level is consistent with earlier studies, which mainly conducted using other welding processes [1,19].

In the as-deposited regions of welds, measurements were made of the prior austenite grain size, the grain size of the equiaxed reheated zone and of the mean lath width of acicular ferrite (see Table 3). The acicular ferrite lath width and the grain size in the reheated zone was largely independent of titanium at the lower boron level. At higher boron levels for all

Appendix F

titanium levels, the grain size in the reheated zone showed refinement particularly with 0.0228% titanium. AF on the other hand showed significant refinement with only 0.0228% titanium and 0.0100% boron. The prior austenite grain size shows some scatter with changes in boron and titanium, and does not show any clear trend within the range tested.

Another important thing for this series of Ti-B compositions, Figure 6 shows a summary plot of the variation in AF as a function of weld metal T100J(°C) temperature values. Here a direct relation is seen between low temperature impact properties and AF. A higher percentage of AF gives a lower 100J temperature. Another important feature to note is that as-deposited weld metal only represents 60% of weld metal, therefore other factors must be considered. Figure 7 shows summary plot of the variation in grain size in the reheated zone (μm) as a function of weld metal T100J(°C) temperature values. It is clear from the graph that refinement in grain size of the reheated zone also contributes towards obtaining better low temperature impact properties.

Figure 2 shows that the upper-shelf values tend to decrease with titanium level whilst the lower-shelf values increase slightly for lower boron levels. The T100J values show minima of about $-45\text{ }^{\circ}\text{C}$ at 0.0005% boron and 0.0054% titanium, any further increase in titanium deteriorates T100J values. For higher boron, as titanium increases both the upper-shelf values and lower-shelf values increase significantly, and T100J values improve substantially to $-62.5\text{ }^{\circ}\text{C}$.

With boron and titanium additions the nucleation and growth of grain boundary ferrite is hindered, and the weld metal intra-granular inclusions become the primary ferrite nucleation sites. Ohkita et al.[13] measured the inclusion size distributions for weld metal containing oxygen from 100 to 300 ppm. They showed that the most frequent inclusion size is in the range 0.3-0.7 microns, and that the average size of non-metallic inclusions increases as the oxygen content of titanium and boron containing weld metal increases. This observation suggests that there is a specific range of weld metal oxygen content or inclusion size distribution, which is most favourable for acicular ferrite nucleation. Liu and Olsen [22] studied submerged arc welds containing 250-350 ppm oxygen. Their results showed that the welds which had an inclusion size distribution in the range 0.2-0.4 microns had the largest volume fraction of acicular ferrite. Results in this study shows inclusion size distribution in the range 0.4-0.5 microns which compares with Ohkita et al but little higher than the range shown by Liu and Olsen, this variation may be due to the oxygen content associated with this processes, which is in the range of 400-500ppm. It is also acknowledged that larger inclusions, of $1\mu\text{m}$ or greater diameter, have been shown to be initiation sites for cleavage fracture [23,24,25], which is the main mode of impact fracture at low temperatures.

Figure 5 shows the variation in percentage of inclusions with a diameter greater than $1\mu\text{m}$ ($N > 1\mu\text{m}$) with an increase in titanium level. This shows that the percentage $> 1\mu\text{m}$ tends to decrease with alloy level to reach relatively low values at titanium levels greater than about 0.0228%. Whilst the number density of inclusions generally increases, the mean 3D diameter of inclusions is independent of an increase in titanium levels.

The main features of the observed low temperature impact behaviour may, to a reasonable extent in the case of titanium-boron, be explained on the basis of interactions between following factors:

In as deposited weld metal:

Appendix F

- (a) the proportion of AF increasing,
- (b) the proportion of FS and PF decreasing;

and in the reheated weld metal:
refinement in grain size of the reheated zone.

AF tends to increase and FS and PF tend to decrease continually with alloy addition, and the percentage of large inclusions also tends to decrease with alloy addition. Also refinement in grain size in the reheated zone combines to give the best low temperature impact properties.

5 Conclusions

- I. Yield and tensile strengths of weld metal were nominally independent of weld Ti-B level over the range tested.
- II. Low temperature impact properties of the weld metal were best with 0.0100% B level and 0.0228% and 0.0430% titanium levels.
- III. A direct relation is seen between low temperature impact properties and AF. A higher percentage of AF gives a lower 100J temperature.
- IV. The refinement in grain size of the reheated zone contributes towards obtaining better low temperature impact properties.

6 Acknowledgments

The work reported was undertaken as part of a Research Project of the Cooperative Research Centre for Materials Welding and Joining. The Cooperative Research Centre for Materials Welding and Joining was established by and is supported under the Australian Government's Cooperative Research Centre Program.

7 References

1. Oh, D.W., Olsen, D.L. and Frost, R.H., The Influence of Boron and Titanium on Low-Carbon Steel Weld Metal, AWS Welding Journal 151-s, April 1990.
2. Tsuboi, J., and Terashima, H., Welding in the World, 21, 304 (1983).
3. Mori N., Homma H., Wakabayashi M., and Okita S., Characteristics of Mechanical Properties of Ti-B Bearing Weld Metals, IIW DOC IX-1229-82, May 1982.
4. Watanabe, I., and Kohma, T., in the Proceedings of the International Conference, "Effect of residual, impurity and microalloying elements on weldability and weld properties" The Welding Institute of London Page 51, Nov. (1983).
5. Kohno, R., Takami, T., Mori, N., and Nagano, K., The Welding Journal, 62, 373s (1983).
6. Davis, M.L.E., Pargeter, R.J., and Baily, N., Metal Construction, 15 338 (1983).
7. Watanabe, I., Suzuki, M., and Kojima, T., '80, in the Proceedings of the International Conference "Welding research in the 1980's" Welding Research Institute, Osaka, Paper B-8, October 1980.
8. Hondros, E.D., and Seah, M.P., in Physical Metallurgy, 3rd edn. (ed. R.W. Chan and P. Haasen), Amsterdam, North Holland Physics Publishing, Part I, 855 (1983).
9. Widgery, D.J., Welding Research International, 4, 54 (1974).
10. Schumann, O., Powell, G., and French, I., WTIA Australian Welding Research CRC No 1 Nov. 1994.
11. Oh, D.W., Olsen, D.L. and Frost, R.H., The Influence of Zirconium and Boron on Low-Carbon Steel Weld Metal Microstructure, Transactions of the ASME Vol. 116, February 1994.

Appendix F

12. Mori N., Homma H., Ohkita S., and Wakabayashi M., Mechanisms of notch toughness improvement in Ti-B bearing weld metals, IIW Doc. IX-1196-81k, American Council, American Welding Society, Miami, Fla. 1981.
13. Ohkita S., Homma H., Tsushima S., and Mori N., The effect of oxide inclusions on the microstructure of Ti-B containing weld metal, IIW Doc. II-1070-86, American Council, AWS, Miami, FL. 1986.
14. Australian Standard 3678 'Structural steel --- hot rolled plates, floor plates and slabs' 1990.
15. Tyagi V.K., French I.E. and Bee J.V., Welding Research Supplement, Australian Welding Journal, Vol. 43, 1998.
16. 'Guide to light microscope examination of ferritic steel weld metals' Welding in the World, 29, 160, 1991.
17. Australian Standard 1733 - Methods for the determination of grain size in metals, 1976.
18. Klucken A.O., Grong O. and Hjelen J., Materials Science and Technology, 4, 649, 1988.
19. Evans G.M., Microstructure and Properties of Ferritic Steel Welds Containing Ti and B, Welding Research Supplement, Welding Journal, pp 251-260, August, 1996.
20. Morral J.E., and Cameron T.B., Proc. Int. Symp. on Boron in Steel, Milwaukee, Wis. Pp. 19-32, 1979.
21. Bhadeshia H.K.D.H., and Svensson L.E., In Mathematical Modelling of Weld Phenomena, The Institute of Materials, London, 1993.
22. Liu, S. and Olsen, D.L., The Role of Inclusions in Controlling HSLA Steel Weld Microstructures, Welding Journal, Vol.65, No.6, pp139s, 1986.
23. Tweed J.H. and Knott J.F., "Effect of Reheating on Microstructure and Toughness of C-Mn Weld Metal", Metals Science, Vol. 17, pp 45-54, 1983.
24. Schumann G.O. and French I.E., Scripta Materialia, Vol. 36, No. 12, pp. 1443-1450, 1997.
25. Tweed J. H. and Knott J.F., Acta Metall., 35(7), 1401, 1987.

Appendix F

Table 1.
Weld metal compositions (wt %) with varying Ti-B levels.

Si	Mn	C	S	P	Ti	Al	B	O	N
0.64	1.34	0.04	0.012	0.014	0.0054	0.0133	<0.0005	0.0530	0.0047
0.58	1.26	0.05	0.011	0.013	0.0273	0.0142	<0.0005	0.0420	0.0054
0.66	1.38	0.05	0.011	0.013	0.0458	0.0111	<0.0005	0.0380	0.0037
0.67	1.44	0.04	0.013	0.015	0.0054	0.0150	0.0095	0.0390	0.0027
0.68	1.47	0.05	0.013	0.015	0.0228	0.0150	0.0112	0.0430	0.0036
0.68	1.49	0.05	0.014	0.015	0.0430	0.0147	0.0110	0.0460	0.0036

Table 2.
Weld metal tensile properties with varying Ti-B levels.

B%	Ti%	Yield Strength (MPa)	Tensile Strength (MPa)	Elongation (%)
<0.0005	0.0054	507	557	29
<0.0005	0.0273	482	565	25
<0.0005	0.0458	535	610	25
0.0095	0.0054	491	571	24
0.0112	0.0228	556	602	24
0.0110	0.0430	519	575	26

Table 3.
Acicular ferrite lath width and reheated grain size for Ti-B series.

B%	Ti%	Columnar Austenite Grain Width (μm)	Acicular Ferrite Lath Width (μm)	Grain Size of Reheated Zone (μm)
<0.0005	0.0054	135	2.86	5.13
<0.0005	0.0273	150	2.44	5.56
<0.0005	0.0458	130	2.44	5.13
0.0095	0.0054	174	2.94	4.65
0.0112	0.0228	125	1.85	4.17
0.0110	0.0430	134	2.50	4.44

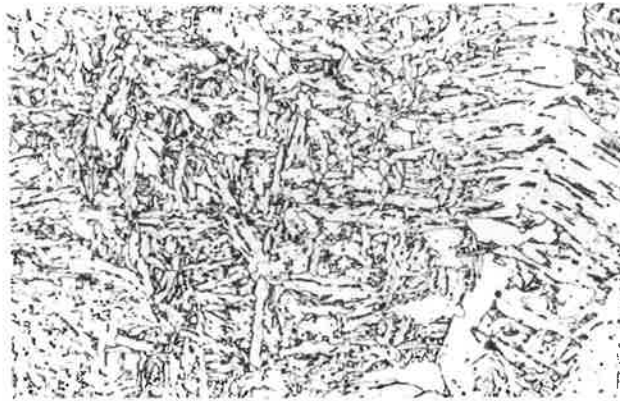
Table 4.
Number of non-metallic inclusions with varying Ti-B levels.

Weld B (%)	Weld Ti (%)	Composition (wt%)			
		SiO₂	MnO	Al₂O₃	TiO₂
<0.0005	0.0054	35	47	14	4
<0.0005	0.0273	15	48	7	30
<0.0005	0.0458	12	29	11	48
0.0095	0.0054	19	65	10	5
0.0112	0.0228	12	49	17	23
0.0110	0.0430	9	45	11	36

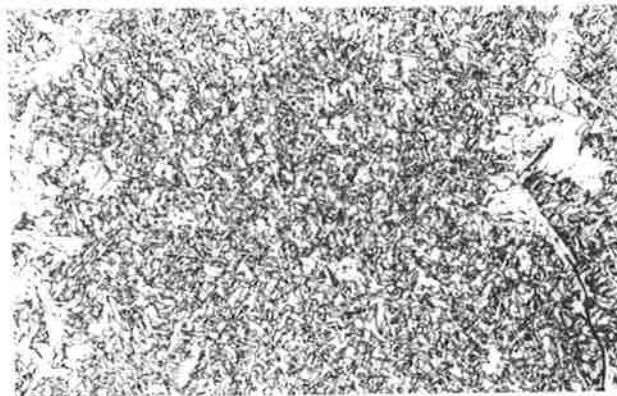
Appendix F



(a) as-deposited weld metal

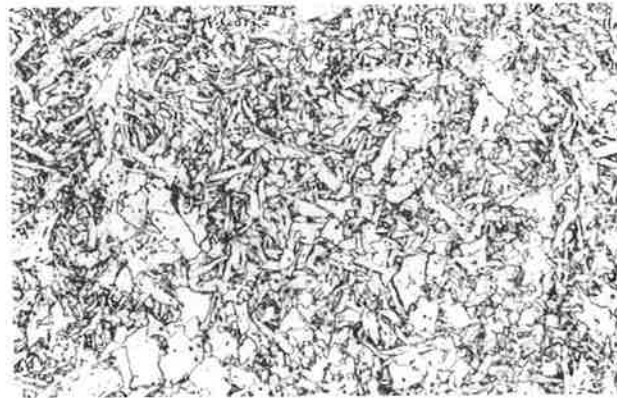


(b) as-deposited weld metal

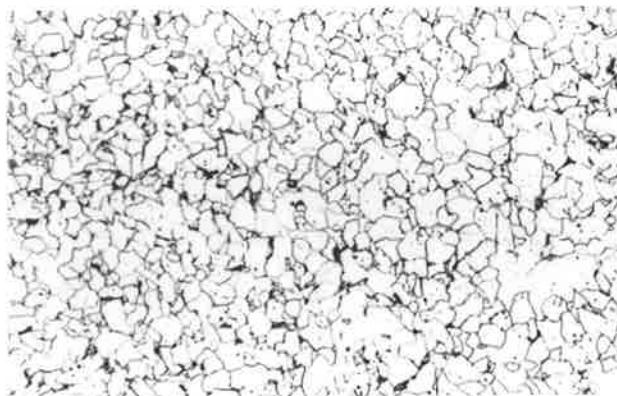


(c) as-deposited weld metal

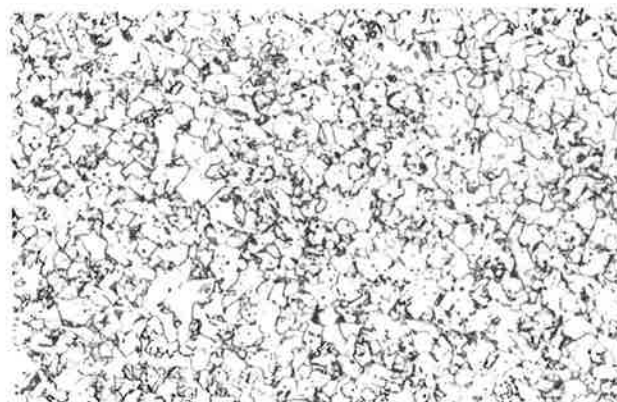
Appendix F



(d) as-deposited weld metal



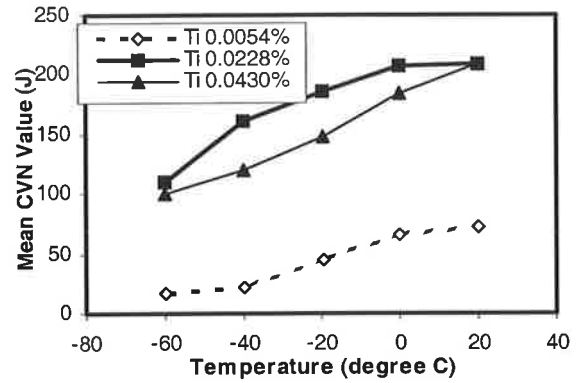
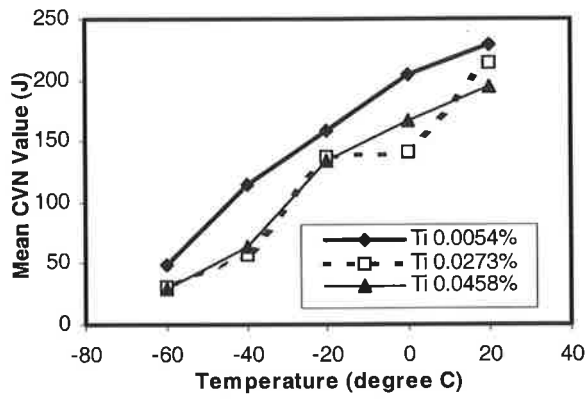
(e) re-heated weld metal



(f) re-heated weld metal

Figure 4. Photomicrographs (x500) of as-deposited and re-heated weld metal with (a) 0.0005% B and 0.0458% Ti, (b) 0.0095% B and 0.0054% Ti, (c) 0.0112% B and 0.0228% Ti, (d) 0.0110% B and 0.0430% Ti, (e) 0.0005% B and 0.0273% Ti, (f) 0.0112% B and 0.0228% Ti in weld metal.

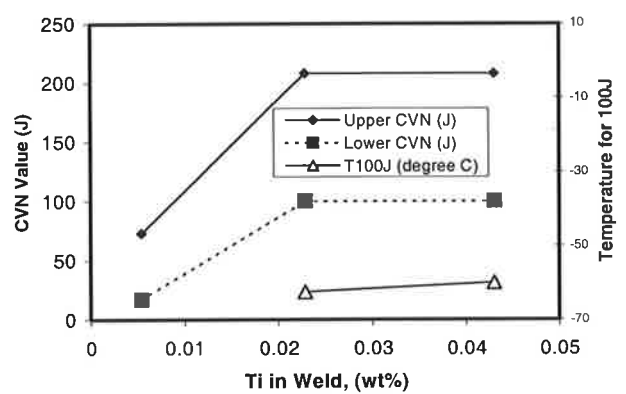
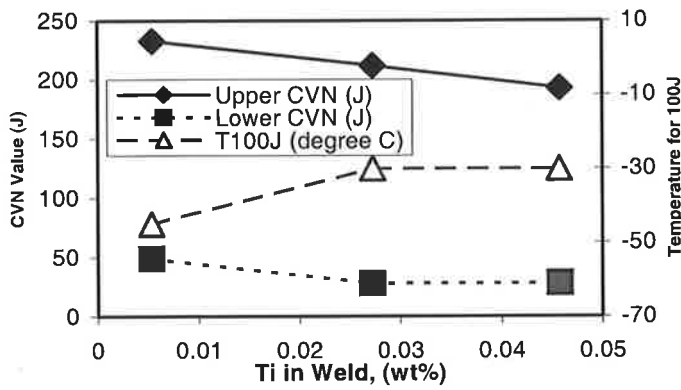
Appendix F



(a)

(b)

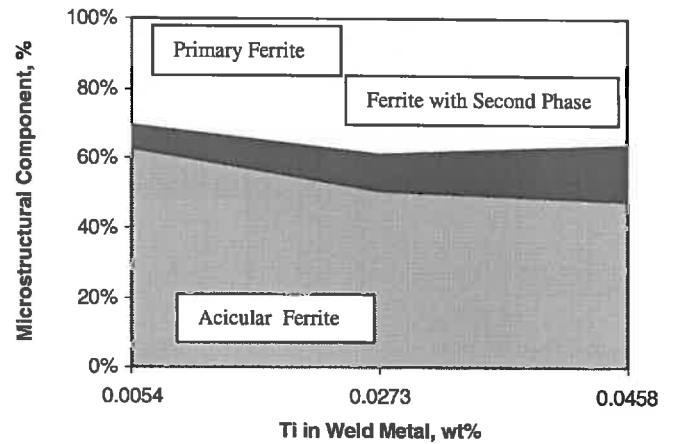
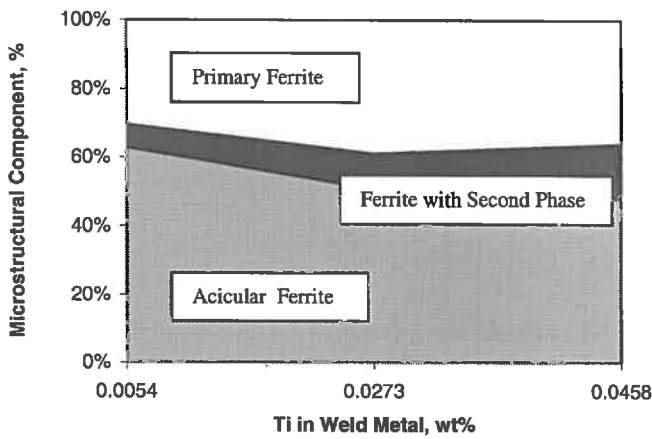
Figure 1. Mean CVN impact energy as a function of temperature for various titanium levels in weld metal (a) at 0.0005% boron and (b) at 0.0100% boron level in the weld metal.



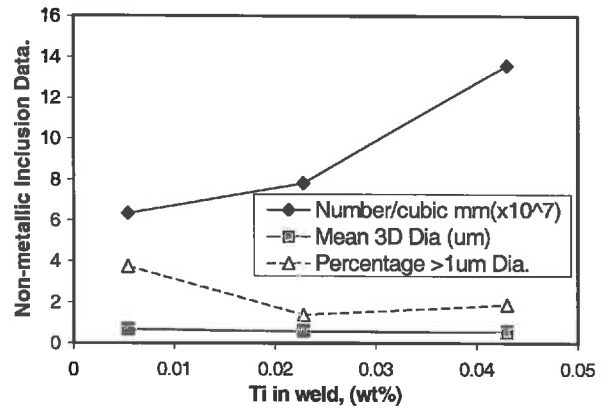
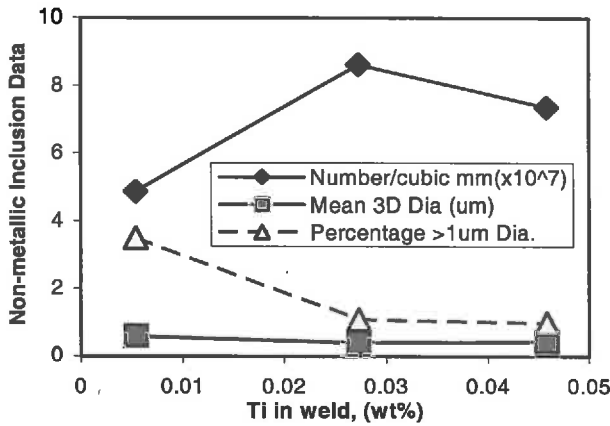
(a)

(b)

Figure 2. The upper CVN (J), lower CVN (J) and T100J(°C) values as a function of titanium contents (a) for 0.0005% boron and (b) for 0.0100% boron in the weld metal.



(a) (b)
 Figure 3. Variation of the proportions of acicular ferrite, ferrite with second phase and primary ferrite in as-deposited weld metal with varying titanium levels (a) for 0.0005% boron (b) for 0.0100% boron.



(a) (b)
 Figure 5. Variation of number of non-metallic inclusions, mean 3D diameter and percentage > 1 μm diameter with increase in titanium levels (a) for 0.0005% boron (b) for 0.0100% boron.

Appendix F

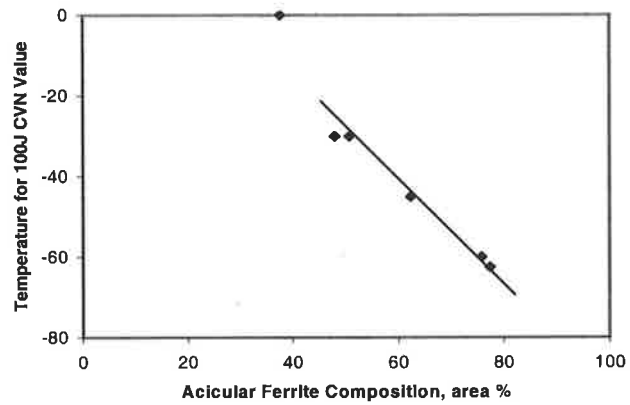


Figure 6. Summary Plot of the Variation in Acicular Ferrite as a Function of Weld Metal T100J(°C)Temperature values.

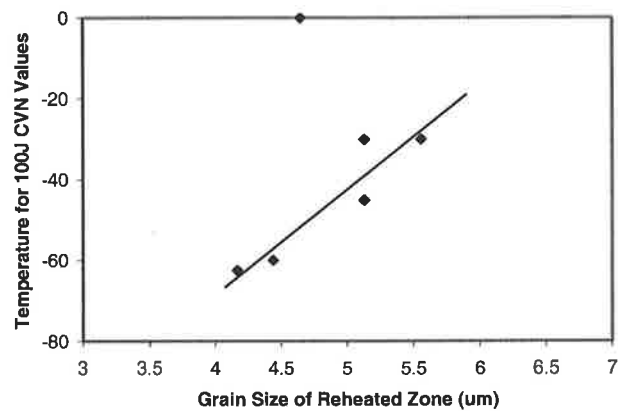


Figure 7. Summary Plot of the Variation in Grain Size in the Reheated Zone (μm) as a Function of Weld Metal T100J(°C)Temperature values.

Influence of Titanium and Aluminium on the Properties of Multi-pass Weld Metal from Gas-shielded, Metal-cored Wires

V. K. Tyagi⁽¹⁾, J.V. Bee⁽²⁾ and I. E. French⁽¹⁾

(1) CSIRO Manufacturing Science and Technology - a Core Partner of the CRC-MWJ

(2) University of Adelaide, Australia - a Core Partner of the CRC-MWJ

Abstract

A series of metal-cored wires was manufactured with varying titanium and aluminium contents calculated to give weld metal Ti and Al levels of nominally 0.005% to 0.095% and 0.013% to 0.065% respectively. Weld metal C, Mn and Si contents were kept constant. The tensile properties and Charpy-V-notch impact properties, as a function of temperature, of multi-pass weld metal from these wires have been measured. Weld metal yield and tensile strength were found to increase with increase in Ti, while little change was found with Al increase. Weld metal impact properties were found to be optimum at Ti levels of either 0.005% or 0.085%. With variation in Al, the best impact properties were obtained at the lowest level assessed, corresponding to 0.013% Al in the weld metal. Assessment of weld microstructure and non-metallic inclusion features suggested that low temperature impact properties were controlled by competing influences from ferrite morphology and non-metallic inclusions.

1. Introduction

Metal-cored wires are often used in applications which require premium weld metal mechanical properties in multi-pass welds. It is therefore important that the influence of alloying additions on mechanical properties of welds from such wires should be well understood so optimum wires can be produced for this high productivity process.

There is only limited information available in the literature regarding the influence of alloy additions in the metal-cored arc welding system¹. A previous paper² reported on the influence of Mn and Si levels on weld metal properties in this metal-cored system and concluded that the low temperature impact properties are optimum when Mn is between 1.3 and 1.6% and Si is between 0.3 and 0.6%. Abson³ studied the effect of Al on metal cored wires and observed changes in strength and microstructure. In this instance cleavage resistance changed little with the lowest Al additions, before decreasing with the highest Al addition while Al additions were generally detrimental to upper-shelf fracture toughness.

Observations from other arc welding processes indicate that acicular ferrite in as-deposited regions has a major influence on weld mechanical properties and that the formation of acicular ferrite depends on micro-alloy / de-oxidant additions, most notably aluminium and titanium⁴. Evans⁵ investigated the effects of titanium and aluminium micro-alloying on toughness for multi-pass basic flux MMA weld deposits. Ti was found to be the most effective element for enhancing the toughness of as-welded deposits. Adding Al powder when 0.0035% Ti was present indicated that toughness was degraded at all Al levels higher than 0.008%.

Non-metallic inclusions can have a beneficial or detrimental effect on the microstructure and mechanical properties of the weld metal⁶. The major beneficial effect of inclusions is the nucleation of acicular ferrite. It is also acknowledged that larger inclusions may enhance cleavage fracture by providing crack nuclei for cleavage cracking in the weld metal^{7,8,9}.

This paper reports a study of the influence of Ti and Al on the mechanical properties of weld metal from specially prepared metal-cored wires in which the major alloying/deoxidising elements, Mn and Si, were kept nominally constant at the optimum level for this system². The microstructural features of the welds have also been examined in order to better understand the relationship between alloy level and mechanical properties. The results are not only applicable to the metal-cored system but also have some applicability to the solid wire gas metal arc welding (GMAW) process since only metallic additions were made to the wires.

2. Materials and Methods

2.1 Manufacture of Special Wires

For the present investigation, special metal cored wires were manufactured. The sheath material was cold rolled mild steel of approximate composition 0.05% C, 0.22% Mn, 0.01% Si and 0.015% Al. Core ingredients used included iron powder, silicon-manganese, ferro-silicon, electrolytic manganese titanium metal and aluminium metal powders. All of these were commercial powders normally used for arc welding consumable manufacture. The wires were manufactured with a nominal core weight to total wire weight of 21% and were drawn to a final diameter of 1.6 mm.

The Mn and Si content of the wires was held constant to yield weld metal containing nominally 0.60% Si and 1.34% Mn. Different amounts of Ti and Al were added to the core to produce eight levels of Ti and six levels of Al in the deposited metals, in the ranges 0.005 to 0.095%Ti and 0.013 to 0.065% Al. In addition, the weld metal carbon content was kept constant at nominally 0.05%.

2.2 Welding Procedure

Welding was done in the flat position (1G) on parent plate material of AS Grade 250⁹ under mechanised conditions. Direct current electrode positive was used with the welding current being 300A and 30V welding voltage. Heat-input was nominally 1.5kJ/mm. The shielding gas used was Argon with 5% CO₂. Inter-pass temperature was standardised at 150 °C (see reference 2 for details).

2.3 Weld Composition

Chemical analyses of the all-weld-metal deposits were carried out with an optical emission spectrometer. The vanadium, niobium, titanium, aluminium and boron contents of the experimental welds were determined to four decimal places so that small variations could be detected. Oxygen and nitrogen levels in the weld metal were determined using a Leco TC136 analyser.

2.4 Mechanical Testing

The impact toughness of each weld metal was assessed by the Charpy-V-notch (CVN) test. Tests were carried out at -60, -40, -20, 0, 20 and 40 °C respectively in order to obtain a transition curve for each weld. Three specimens were tested at each temperature and the mean absorbed energy calculated. An all-weld-metal tensile test was carried out. The tensile specimens were heat treated at 250 °C for 16 hours for hydrogen removal, prior to testing. The details of test specimens and procedures have been given previously².

2.5 Metallography

Transverse sections were prepared and detailed examination was carried out on top beads and on the adjacent reheated zones. The volume fraction of the different micro-constituents was obtained from point counts on more than 1000 points, by using the IIW Guidelines¹¹. The prior austenite grain sizes were determined by means of the mean linear intercept technique¹² for all welds as were the lath widths of the acicular ferrite.

2.6 Study of Inclusions

The size distribution of non-metallic inclusions on polished specimens of the as-deposited weld metal was examined, using a scanning electron microscope (SEM) based automatic image analyser. The methods used were in line with those detailed in (13). In the present investigation, magnification of 10,000, accelerating voltage of 15kV, grid point spacing of 0.02 µm and working distance between 8 and 10 mm was used (see reference 2 for details).

3. Results

3.1 Weld Compositions

The chemical compositions of the all-weld-metal deposits studied are given in Table 1 for the Ti series and in Table 2 for the Al series. C, Mn and Si levels were nominally constant at 0.04 to 0.06%, 1.15 to 1.38% and 0.52 to 0.77% respectively. The levels of the remaining metallic elements were relatively low and constant throughout the series. In the titanium series, Ti was varied between 0.005 and 0.094% while in the aluminium series, Al was varied between 0.013 and 0.064%. For the Ti series, the oxygen levels in the welds decreased from 0.053 to 0.038% as Ti level increased, while for the Al series oxygen level was relatively constant and were all in the range 0.053 and 0.065%.

The nitrogen levels found in the welds of both the Ti and Al series were essentially constant. Most of the nitrogen values were in the range 0.004 and 0.008% which is considered normal for this type of weld and process. One nitrogen value however was above 0.01% and is considered high for the process.

3.2 Mechanical Properties

3.2.1 Tensile Properties

The tensile test data are presented in Figure 1 (a) and (b). For the Ti series, the measured yield strengths varied between 504 and 581 MPa, while tensile strengths varied between 547 and 610 MPa and elongations were between 22 and 30%. For the Al series, yield strengths varied between 475 and 531 MPa, while tensile strengths varied between 522 and 565 MPa and elongations were between 16 and 29%. Figure 1(a) shows that both yield and tensile strength increase approximately linearly with Ti content by about 50 MPa over the range of Ti values, while elongation tended to decrease. For the Al series, Figure 1(b) suggests yield and tensile strengths are independent of Al content over the range tested although elongation tended to decrease.

3.2.2 CVN Impact Results

The variations of mean CVN energy with test temperature for the various weld Ti and Al levels are plotted in Figure 2(a) and (b) respectively. For the Ti series, mean CVN energies at lower temperatures appear best at 0.005 and 0.085% Ti levels. For the Al series mean CVN energies across the temperature range are best at 0.0133% Al level.

For each case the upper-shelf energy (at +40 °C), the lower-shelf energy (at -60 °C) and the temperature corresponding to a CVN energy of 100J (T100J) were found. These values are plotted in Figure 3(a) and (b) against weld Ti and Al contents respectively.

Figure 3(a) shows that the upper-shelf values have considerable scatter but tend to decrease with Ti level while the lower-shelf values, except at the lowest and highest Ti levels, are independent of Ti. The T100J values, while

not showing large variations with Ti level, do show minimum value of about -45 °C at Ti contents of approximately 0.005 and 0.085%.

The variations with Al level, as plotted in Figure 3(b) show that the highest upper and lower-shelf values occur at the lowest Al while, these impact values are largely independent of Al content at all higher Al levels. Similarly the lowest T100J value occurs at the lowest Al level while T100J is independent of Al at higher Al levels. The variation of T100J is considerably larger with the weld Al level than with Ti.

3.3 Weld Metal Microstructure

Area measurements from cross-sections of welds indicated that the region of the weld from which mechanical test specimens (particularly CVN specimens) were extracted contained approximately 60% as-deposited and 40% reheated weld metal². Area fractions of acicular ferrite (AF), ferrite with second phase (FS) and primary ferrite (PF) were determined in as-deposited regions of the top layer from each weld.

Plots of the variation of percentage area of AF, FS and PF with weld Ti and Al levels are shown in Figure 4 (a) and (b) respectively. These graphs show that area of AF tends to decrease in the range from 60 to 20% with increase in Ti level. A corresponding increase in FS is seen, as PF stayed relatively unchanged. The extent of this change in as-deposited microstructure with Ti level is illustrated in Figure 5 which shows micrographs of the welds containing 0.0054 and 0.0852% Ti with 62 and 43% AF respectively.

As the Al levels are increased, AF also decreases in the range 60 to 20%. The decrease was somewhat irregular in that AF appeared to decrease rapidly with the initial increase in weld Al from the base level of 0.013%. As shown by Figure 4(b), this decrease in AF is accompanied by an increase in area of FS while PF area is fairly constant at 30%.

In addition to these measurements of area of the ferrite morphologies, measurements were also made of the prior austenite grain size, the grain size of the equiaxed reheated zone and of the mean lath width of acicular ferrite (see Tables 3 & 4). For the titanium series, the prior austenite grain size tended to decrease slightly with Ti level as did the acicular ferrite lath width while the grain size in the reheated zone was largely independent of Ti except perhaps at the highest Ti levels. For the aluminium series, both prior austenite grain size and acicular ferrite lath width were largely independent of Al level while the grain size in the reheated zone tended to increase with Al except for the highest Al level.

3.4 Non-metallic Inclusions

Figure 6 (a) & (b), show the details of the non-metallic inclusions, including number per unit volume, mean three dimensional (3D) diameter and percentage of diameter equal or larger than 1µm for each weld, as measured using the SEM with automated image analyser. For the titanium series, both

mean 3D inclusion diameter and percentage of inclusions with diameter greater than $1\mu\text{m}$ decreased with increase in weld Ti. The number density of inclusions measured tends to increase with weld Ti, with the exception of a maximum of $16 \times 10^7 / \text{mm}^3$ at about 0.08% Ti.

The inclusion data for the aluminium series (Figure 6(b)) indicates that the mean 3D inclusion diameter and the percentage of inclusions with diameter greater than $1\mu\text{m}$ tends to decrease with Al level. The number density of the inclusions, while showing some variability, appears to increase with increase in weld Al level.

4. Discussion

4.1 Weld Metal Tensile Properties

While some variability existed between measurements, the results generally showed that both yield and tensile strength increased by about 50MPa as weld Ti increased from 0.005 to 0.095% but were approximately constant as weld Al increased from 0.013 to 0.065%. The tensile properties are consistent with those for MMAW¹⁴ for which it was shown that the tensile properties increased by approximately 60MPa as weld Ti increased from essentially zero to 0.055% but by only about 30MPa as weld Al increased from zero to 0.061%.

4.2 Weld Metal Impact Properties

In general the major microstructural features present in the weld metal that may influence the impact properties are the as-deposited regions, those regions which have been reheated by subsequent welding passes and the non-metallic inclusions present. In addition, the strength level of the weld metal and grain size may affect impact properties.

Across the present series of trials with varying weld Ti and Al contents the proportion of as-deposited to reheated region was nominally constant at approximately 60:40. This is because both heat input and run placement were held constant. It was observed that there was little apparent difference in either the appearance of the reheated zones or in the measured grain sizes of the equiaxed portions of these zones between the trial welds (see Table 3 & 4). Furthermore, most investigators have concluded that the reheated regions play a minor part in determining weld impact properties^{8,15}. This is because the largely equiaxed, fine-grained structure gives a more difficult cleavage path than the coarser parts of the as-deposited regions. Attention will therefore be concentrated on the influence of the other factors on weld impact properties.

The as-deposited regions of welds have been characterised as consisting of acicular ferrite (AF), ferrite with second phase (FS) and primary ferrite (PF). Of these ferrite types, AF is widely considered to be the most beneficial to impact

properties. This is because it consists of small non-aligned grains with high angle boundaries and therefore provides a difficult path for cleavage.

The present results show, in the ranges tested, that the proportion of AF present generally decreases with the addition of either Ti or Al. It is shown that maximum AF occurs at total Al and Ti of around 0.02% with ratio of Al to Ti around 2.4, this is consistent with earlier studies which were mostly concerned with other welding processes^{14,16,17}. The present results do demonstrate some correlation between low temperature impact, as measured by the T100J value, and AF proportion at relatively low Ti or Al additions where the AF proportions are relatively high. As shown in Figure 7, this correlation occurs down to around 50%AF for Ti addition and 55%AF for Al addition, these correspond to Ti and Al levels in the welds of about 0.06 and 0.02% respectively. However, while AF decreases continually with alloy addition, the T100J values tend to be insensitive to further alloy addition or, in the case of Ti addition, to improve at some higher alloy level. This suggests that other factors are becoming important at higher alloy levels.

It is known that non-metallic inclusions play two distinct roles in weld metals. Smaller inclusions, of around 0.4 μ m in diameter, have been identified as efficient nucleation sites for AF¹⁸. Larger inclusions, of 1 μ m or greater diameter, have been shown to be initiation sites for cleavage fracture¹⁹ which is the main fracture mode of impact fracture at low temperatures.

Figure 8 shows the variation in number density of inclusions with diameter greater than 1 μ m ($N > 1\mu\text{m}$) with Ti and Al level. The $N > 1\mu\text{m}$ values were calculated from the product of overall number density and the percentage with diameter greater than 1 μ m values. This shows that $N > 1\mu\text{m}$ tends to decrease with alloy level to reach relatively low values at Ti levels between about 0.04 and 0.09% and Al levels greater than about 0.04%.

The inclusions with diameter greater than 1 μ m ($N > 1\mu\text{m}$) at low Ti and Al level will also be present in the 40% reheated region and could adversely affect T100J temperature despite the high AF content in weld metal which has not been re-austenitised. The total AF seems to vary from about 60% to 20% but taking into account that as solidified weld metal is about 60% of total weld metal, the variation in AF as a proportion of the total weld metal is 36% to 12%.

The main features of the observed low temperature impact behaviour may, to a reasonable extent, be explained on the basis of the interaction between two factors: the proportion of AF present and the number density of large inclusions. This is because, although AF tends to decrease continually with alloy addition, the number density of large inclusions also tends to decrease with alloy addition. Consequently, while low temperature impact properties may be expected to be continually degraded by lower AF levels, this effect is offset by the smaller number of the large inclusions available to nucleate the cleavage fracture.

Other factors can undoubtedly influence weld metal impact properties. Increase in weld metal strength, for example, generally has a deleterious effect on impact properties. This does not appear to be a major factor in the present case since, while the changes in impact properties are considerable, the changes in strength level are small (about 50MPa) for the Ti addition and non-existent for the Al addition.

It is worth checking if the factors identified above are also important in influencing the impact properties of the previously investigated welds in which Mn and Si levels were varied². These welds were made and tested under nominally the same conditions as the present ones. In this earlier case the premium low temperature impact properties were obtained with Mn contents between 1.3 and 1.6%, provided the Si level was less than about 0.7% while poorer impact properties were found with Mn contents less than 1.3% and high Mn and Si contents. AF proportion tended to increase continuously over the whole range of Mn values while $N_{>1\mu m}$ increased only slightly with Mn. These observations suggest that low Mn contents did not result in sufficient AF to give premium low temperature impact properties while high Mn and Si resulted in high values of both $N_{>1\mu m}$ and weld strength thus degrading the impact properties.

Conclusions

1. Yield and tensile strength increased by about 50 MPa as weld metal Ti level was increased, but were independent of increase in Al level. These changes in strength are relatively small and do not appear to have any affect on impact properties.
2. The weld metal low temperature impact properties were best at the lowest weld Al level tested and at weld Ti levels of either 0.005% (the lowest tested) or 0.085%.
3. The proportions of AF present generally decreased with the addition of either Ti or Al as did the number density of large non-metallic inclusions.
4. Low temperature impact behaviour appears to largely depend on the combination of AF proportion and number density of large inclusions in which more AF or fewer large inclusions result in improved impact properties.

Acknowledgments

The work reported herein was undertaken as part of a Research Project of the Cooperative Research Centre for Materials Welding and Joining. The Cooperative Research Centre for Materials Welding and Joining was established by and is supported under the Australian Government's Cooperative Research Centre Program.

References

- (1) V.K.Tyagi, I.E. French and J.V.Bee, Australian Welding Research Publications, WTIA, CRC No. 20, 1996.
- (2) V.K.Tyagi, I.E. French and J.V.Bee, Welding Research Supplement, Australian Welding Journal, Vol. 43, 1998.
- (3) D.J.Abson, The TWI Welding Journal, 1(1), 99, 1992.
- (4) O. Grong and D.K.Matlock, Int. Metals Reviews, 31, No. 1, 27-48, 1986.
- (5) G. M.Evans, Welding in the World, 31, (1), 12, 1993.
- (6) P.Hart, Metal Constr., 18(10), 610, 1986.
- (7) J.F.Knott, Trans. ISIJ, @!, 1981.
- (8) J.H. Tweed and J.F.Knott, "Effect of Reheating on Microstructure and Toughness of C-Mn Weld Metal", Metals Science, Vol. 17, pp 45-54, 1983.
- (9) G.O. Schumann and I.E.French, Scripta Materialia, Vol. 36, No. 12, pp. 1443-1450, 1997.
- (10) Australian Standard 3678 'Structural steel - hot rolled plates, floor plates and slabs' 1990.
- (11) 'Guide to light microscope examination of ferritic steel weld metals' Welding in the World, 29, 160, 1991.
- (12) Australian Standard 1733 - Methods for the determination of grain size in metals, 1976.
- (13) A.O.Kluken, O. Grong and J.Hjelen, Materials Science and Technology, 4, 649, 1988.
- (14) G. M. Evans and N.Bailey, "Metallurgy of Basic Weld Metal" Woodhead Publishing Ltd., 1997.
- (15) S.A.Gedeon, S.J. Rudd and J.E.M.Braid, International Conference on Pipeline Reliability, Vol 2, Paper VI-12, 1992.
- (16) A.G.Fox, and D.G.Brother, Scripta Metallurgica et Materialia, Vol.32,No.7, pp. 1061-1066, 1995.
- (17) G.L.F.Powell, and G.Herfurth, accepted Met. and Met. Trans.
- (18) F.J.Barbaro, P. Kraukis and K.E.Easterling, Materials Science and Technology, Vol. 5, pp1057-1068, Nov. 1989.
- (19) J.H. Tweed and J.F.Knott, Acta Metall., 35(7), 1401, 1987.

Appendix F

Table 1. Weld Metal Compositions (wt %) with Varying Ti Levels.

<u>Si</u>	<u>Mn</u>	<u>C</u>	<u>S</u>	<u>P</u>	<u>Ni</u>	<u>Cr</u>	<u>Mo</u>	<u>Cu</u>	<u>V</u>	<u>Nb</u>	<u>Ti</u>	<u>Al</u>	<u>B</u>	<u>O</u>	<u>N</u>
0.64	1.34	0.04	0.012	0.014	0.02	0.01	<0.01	0.01	0.0058	0.0005	0.0054	0.0133	<0.0005	0.0530	0.0047
0.55	1.30	0.05	0.008	0.015	0.02	0.01	0.01	0.010	0.0059	<0.0005	0.0124	0.0132	<0.0005	0.0450	0.0040
0.58	1.26	0.05	0.011	0.013	0.02	0.01	0.01	0.01	0.0058	<0.0005	0.0273	0.0142	<0.0005	0.0420	0.0054
0.66	1.38	0.05	0.011	0.013	0.02	0.01	0.01	0.01	0.0066	<0.0005	0.0458	0.0111	<0.0005	0.0380	0.0037
0.56	1.24	0.05	0.010	0.012	0.02	0.01	<0.01	0.02	0.01	<0.01	0.0588	0.0161	<0.0005	0.0380	0.0070
0.60	1.32	0.05	0.013	0.014	0.02	0.01	0.01	0.01	0.01	<0.01	0.0852	0.0147	<0.0005	0.0400	0.0038
0.63	1.27	0.05	0.012	0.012	0.02	0.01	0.01	0.02	0.01	<0.01	0.0910	0.0164	<0.0005	0.0400	0.0080
0.63	1.27	0.06	0.011	0.012	0.02	0.01	<0.01	0.02	0.01	<0.01	0.0940	0.0132	<0.0005	0.0430	0.0130

Table 2. Weld Metal Compositions (wt %) with Varying Al Levels.

<u>Si</u>	<u>Mn</u>	<u>C</u>	<u>S</u>	<u>P</u>	<u>Ni</u>	<u>Cr</u>	<u>Mo</u>	<u>Cu</u>	<u>V</u>	<u>Nb</u>	<u>Ti</u>	<u>Al</u>	<u>B</u>	<u>O</u>	<u>N</u>
0.64	1.34	0.04	0.012	0.014	0.02	0.01	<0.01	0.01	0.0058	0.0005	0.0054	0.0133	<0.0005	0.0530	0.0047
0.61	1.32	0.06	0.024	0.015	0.05	0.03	0.02	0.01	0.0055	<0.01	0.0060	0.0190	<0.0005	0.0580	0.0048
0.60	1.29	0.05	0.020	0.017	0.05	0.03	0.03	0.01	0.0057	<0.01	0.0049	0.0320	<0.0005	0.0650	0.0065
0.77	1.38	0.05	0.020	0.018	0.05	0.03	0.02	0.01	0.0067	<0.01	0.0058	0.0495	<0.0005	0.0530	0.0054
0.52	1.15	0.06	0.016	0.018	0.05	0.03	0.02	0.01	0.0053	<0.01	0.0050	0.0570	<0.0005	0.0580	0.0045
0.68	1.35	0.05	0.013	0.018	0.05	0.03	0.01	0.01	0.0065	<0.01	0.0058	0.0642	<0.0005	0.0580	0.0068

Appendix F

Table 3. Acicular Ferrite Lath Width and Reheated Grain Sizes for Ti Series.

<u>Ti</u> %	Columnar Austenite Grain Width (μm)	Acicular Ferrite Lath Width (μm)	Grain Size of Reheated Zone (μm)
0.0054	135	2.86	5.13
0.0124	135	2.22	5.17
0.0273	215	2.44	5.56
0.0458	130	2.44	5.13
0.0588	135	2.78	5.26
0.0852	95	2.08 *	5.41
0.0910	115	1.92 *	5.00
0.0940	110	--- **	4.76

* --- Small patches of continuous AF limited the AF count.

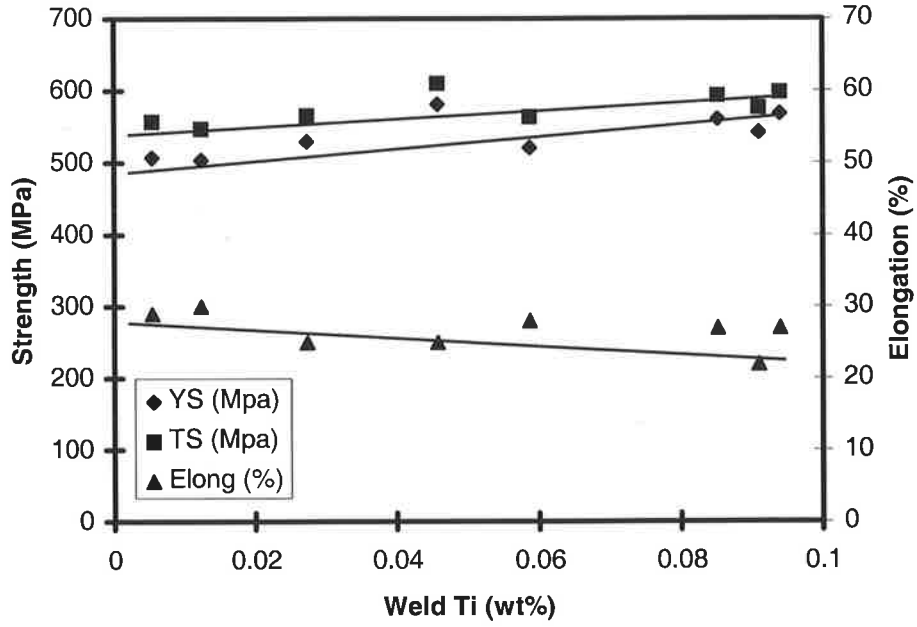
** --- Not sufficient, continuous areas of AF, for measurements.

Table 4. Acicular Ferrite Lath Width and Reheated Grain Sizes for Al Series.

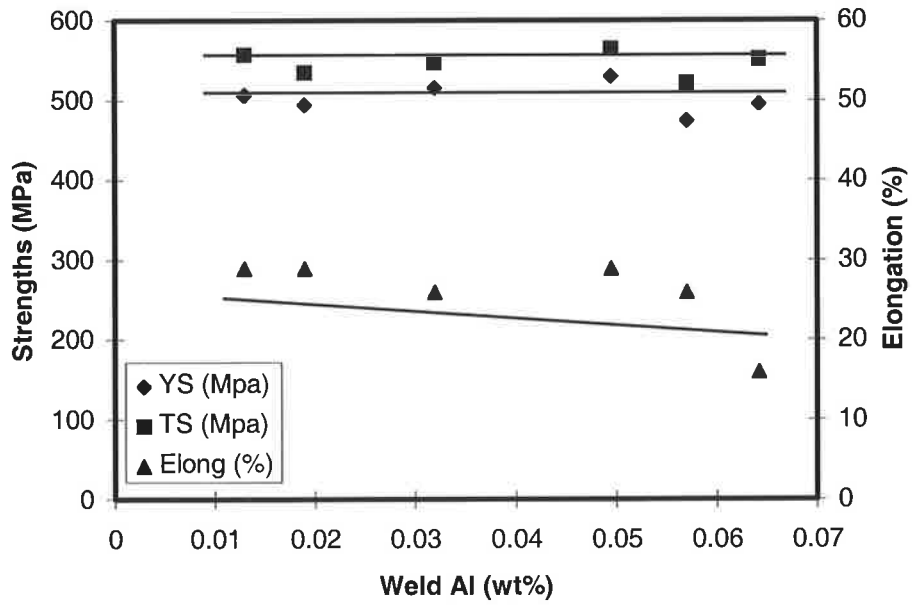
<u>Al</u> %	Columnar Austenite Grain Width (μm)	Acicular Ferrite Lath Width (μm)	Grain Size of Reheated Zone (μm)
0.0133	135	2.86	5.13
0.0190	105	2.17	6.06
0.0320	125	2.38	6.25
0.0495	140	2.44	6.67
0.0570	125	--- **	6.89
0.0642	120	2.63	5.13

** --- Not sufficient, continuous areas of AF, for measurements.

Appendix F



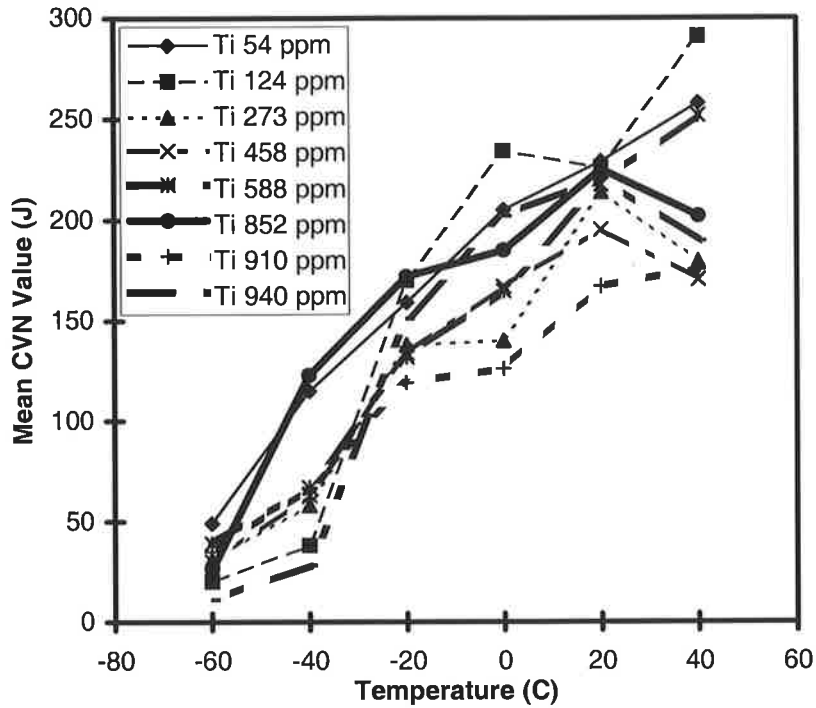
(a)



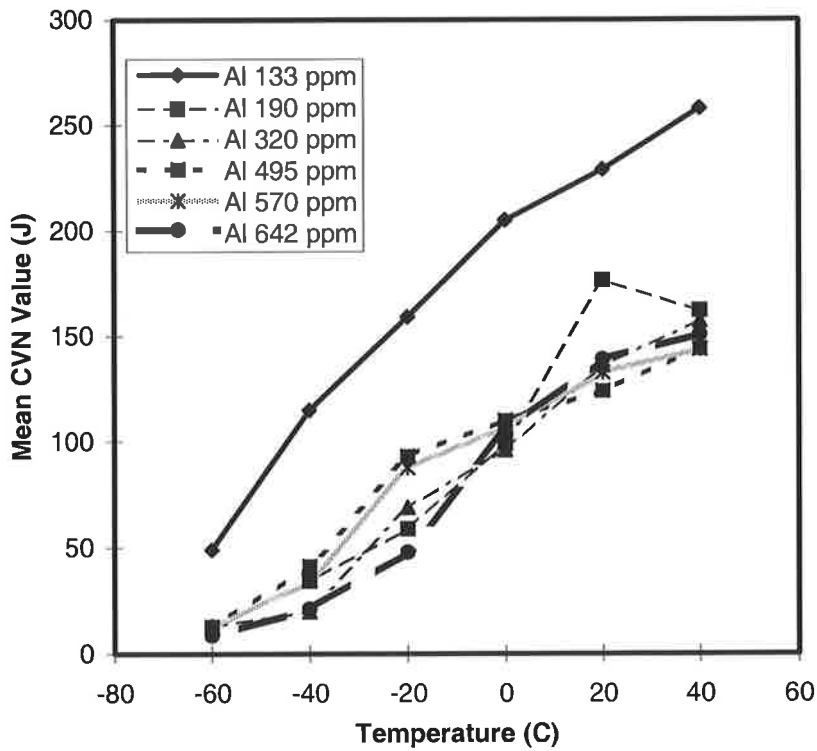
(b)

Appendix F

Figure 1 Variations in yield, tensile strength and percent elongation as a function of (a)titanium and (b)aluminium in weld metal.



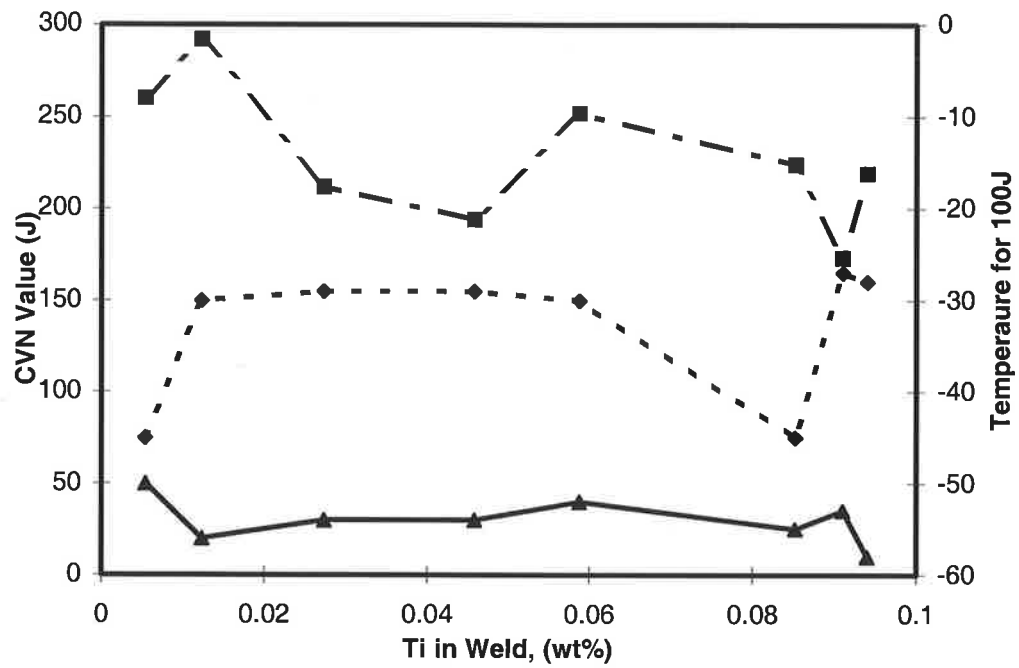
(a)



Appendix F

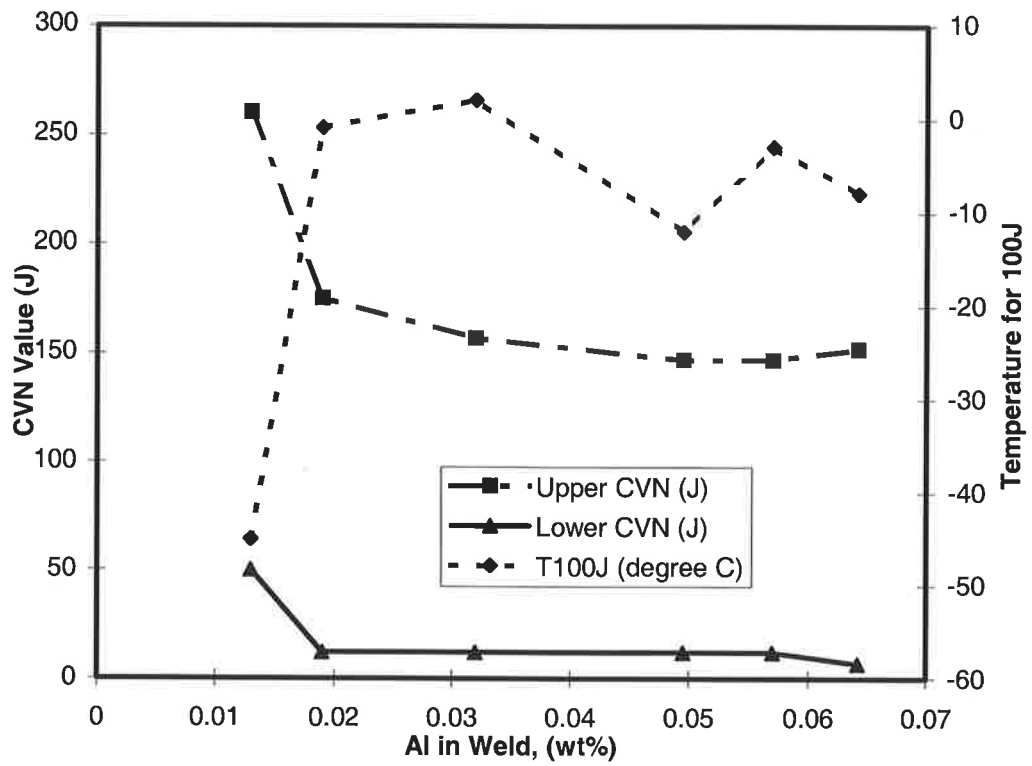
(b)

Figure 2. Mean CVN impact energy as a function of temperature (a) for the various Ti levels in weld metal (b) for the various Al levels in weld metal.



(a)

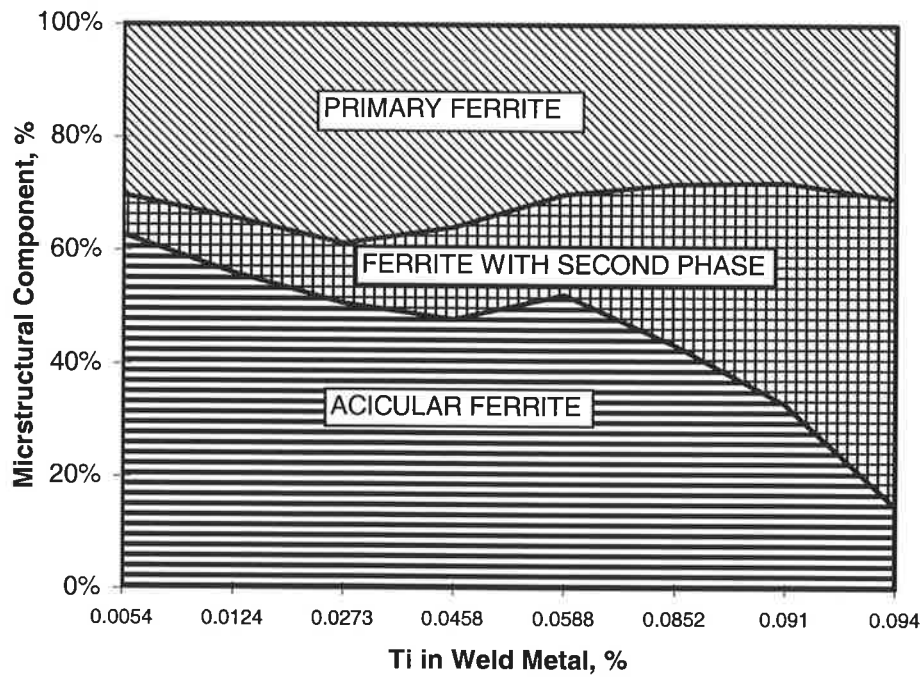
Appendix F



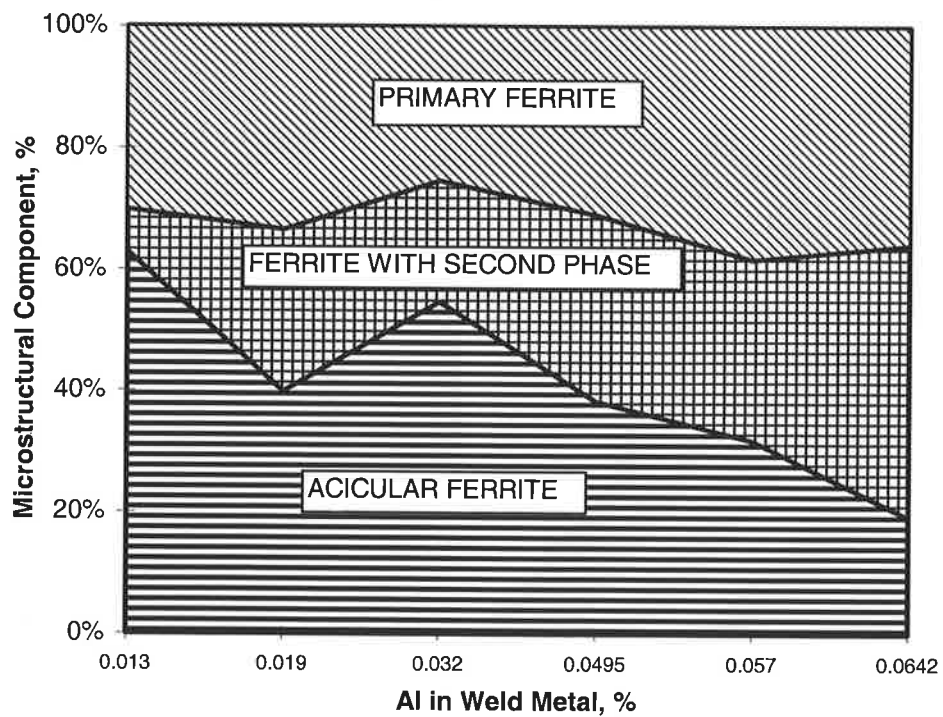
(b)

Figure 3 The upper CVN (J), lower CVN (J) and T100J($^{\circ}$ C) values as a function of (a)Ti and (b)Al contents.

Appendix F



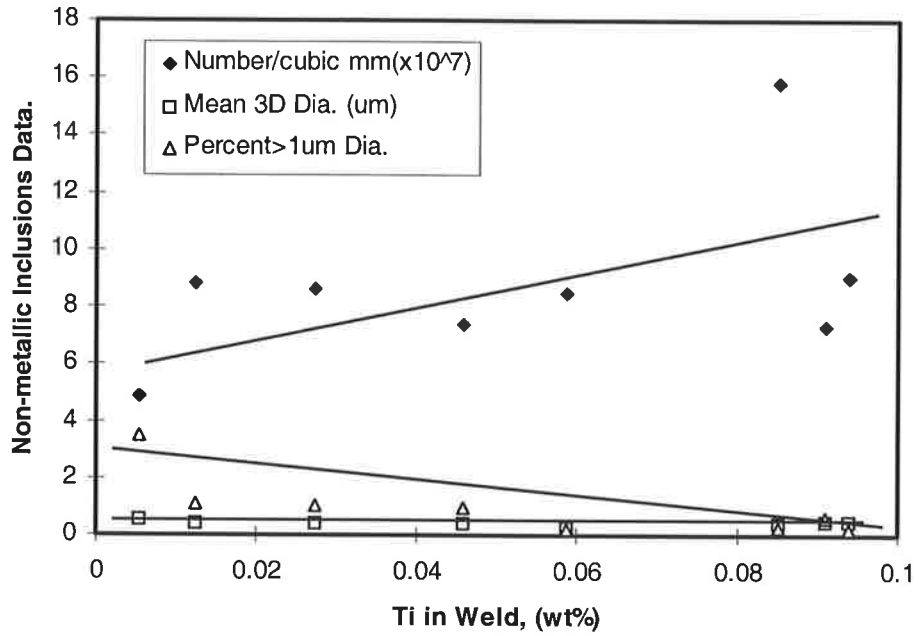
(a)



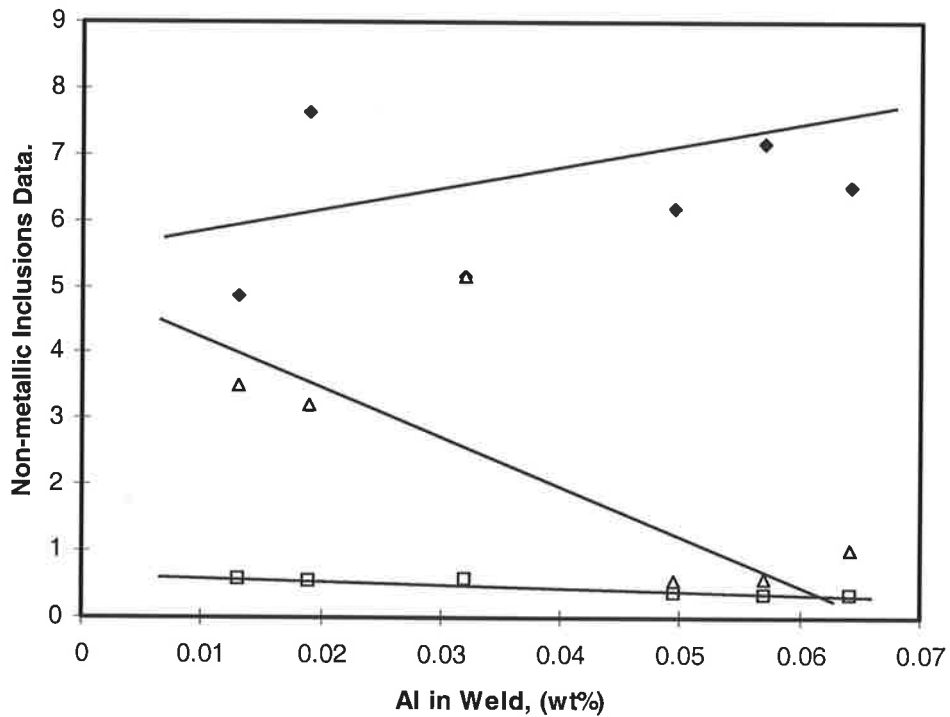
(b)

Figure 4. Variation of the proportions of acicular ferrite (AF), ferrite with second phase (FS) and primary ferrite (PF) in as-deposited weld metal (a) with varying Ti levels (b) with varying Al levels.

Appendix F



(a)



(b)

Figure 6. Variation of non-metallic inclusions Number/ mm^3 , Mean 3D diameter and Percent $> 1\mu\text{m}$ diameter with increase in (a) weld Ti level (b) weld Al level.

Appendix F

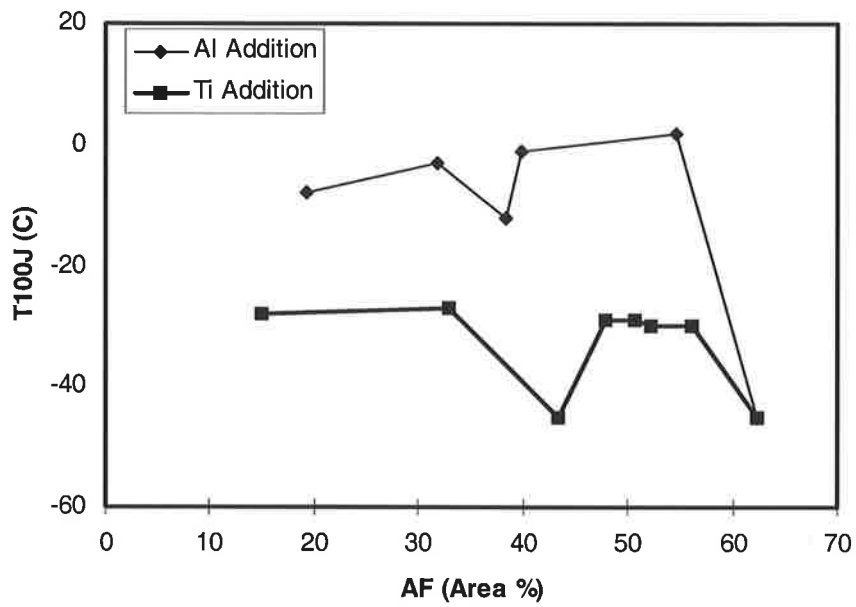
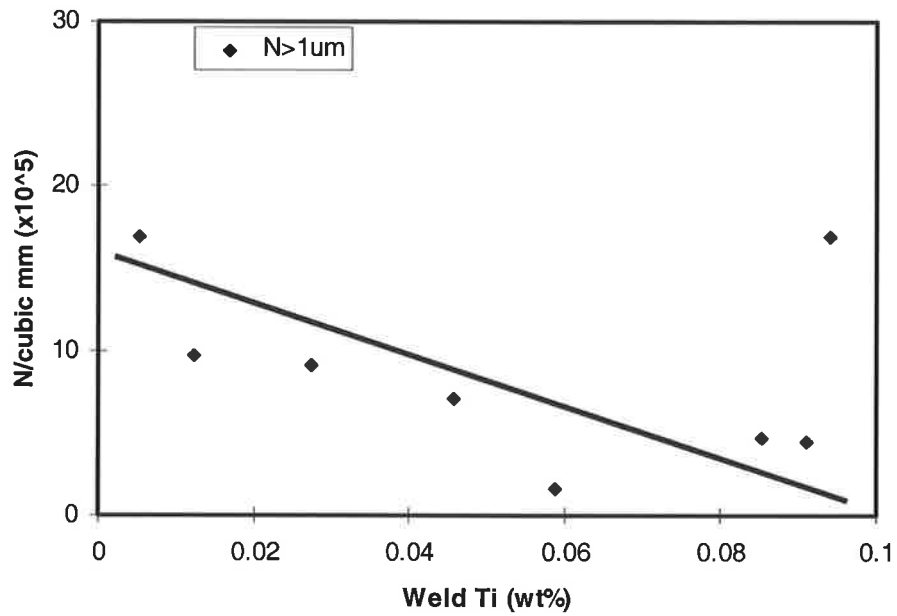
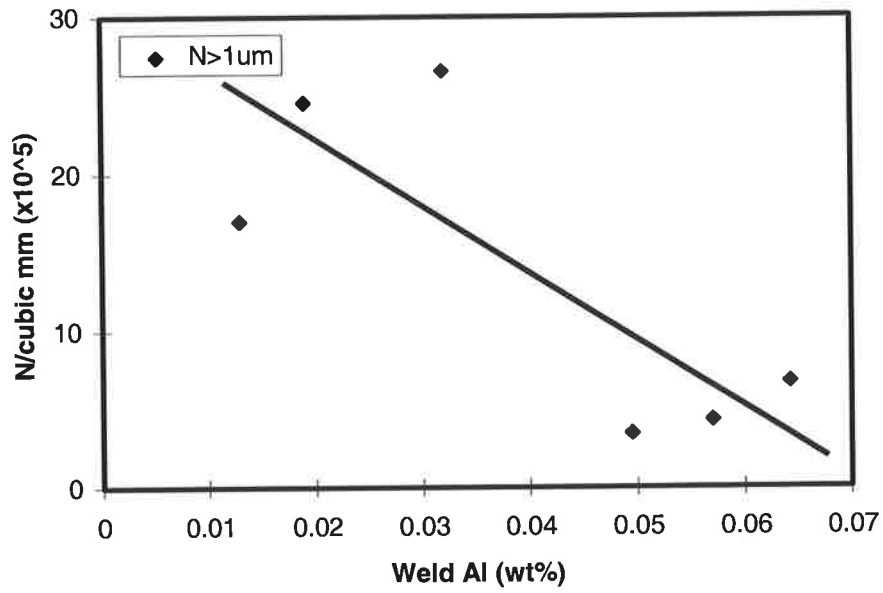


Figure 7. Effect of AF on mean CVN impact energy corresponding to T100J, for Ti and Al series of weld metal.



(a)

Appendix F



(b)

Figure 8 Number density of inclusions with Dia. > 1 μm as a function of increase in (a) Ti and (b) Al in the weld metal.